# DIRECT ANALYSIS IN REAL TIME IONIZATION FOR HIGH-RESOLUTION MASS SPECTROMETRY

By

JULIA DIANE LANEY RUMMEL

A DISSERTATION PRESENTED TO THE GRADUATE SCHOOL
OF THE UNIVERSITY OF FLORIDA IN PARTIAL FULFILLMENT
OF THE REQUIREMENTS FOR THE DEGREE OF
DOCTOR OF PHILOSOPHY

UNIVERSITY OF FLORIDA

2009

To my family and my wonderful husband

ACKNOWLEDGMENTS

I would like to express my deep appreciation to the many people who have aided me in my work and studies throughout graduate school and my education in general. First, I must thank my research advisors. I will always be grateful to Dr. David Powell for welcoming me into his lab, for patiently answering all of my questions, and for instilling in me a sense of careful independence that I surely will apply throughout the rest of my career. I am thankful to Dr. John Eyler for his wise guidance, his scientific insight, and for the freedom he gave me to explore many different areas. I am also very grateful to Dr. Eyler for allowing me to conduct studies at the FOM Institute in The Netherlands. It was a great experience that I will never forget. I'd like to thank my other committee members, Dr. Richard Yost, Dr. Joseph Delfino, and Dr. Kirk Schanze for their helpful suggestions.

Numerous other individuals directly benefitted my research. First, I am so grateful to the UF Chemistry Machine Shop and Electronics Shop. My research would not have been possible without Joe Shalosky, Todd Prox, Bryan Smith, Steve Miles, and Larry Hartley. They were responsible for fabricating every new device used in this work and were graciously willing to quickly fix/rewire any broken parts with little or no notice. I will always appreciate all of their efforts in supporting my work and will be amazed at their incredible talent. Next, I would like to thank Dr. Jos Oomens and Dr. Jeffrey Steill for their help in performing spectroscopic studies at the FOM Institute. I also greatly appreciate the contributions by Dr. Jan Szczepanski and Dr. Cesar Contreras in computing theoretical spectra for these studies and Dr. Wright "Lee" Pearson for operating the OPO laser at UF.

I would like to thank Northrop Grumman Corporation (NGC) and the Department of Homeland Security for funding my research for the last two years. Specifically, I must thank Dr. Danielle Dickinson for connecting me with NGC, for exposing me to very interesting areas of research, and for the advice and encouragement she provided. I would also like to acknowledge Dr. Douglas Henderson from NGC for his help and encouragement.

I would like to thank the Powell and Eyler groups for their friendship, helpful conversations, and useful critiques. In particular, I thank Dr. Soledad Cerutti for her impressive scientific insights, the great friendship she provided, and all of the random and interesting conversations she shared with me inside and outside of the lab. I thank Dr. Joanna Barbara for training me and for the hilarious wit she so often shared. I'd also like to acknowledge Dr. Michelle Sweeney. She was one of my earliest friends in graduate school and a great asset when it came to studying for our cumulative exams.

Last, I want to acknowledge the people who truly carried me throughout my education. I thank my parents for all of their love and support and for raising me to believe that with hard work, I could achieve my goals. I thank my grandparents for the vast wisdom they have shared and the love and constant encouragement they have always provided. I thank my sister and friends from home for always cheering me on.

Finally, I thank my husband and very best friend, Ian, for all of the love, encouragement, entertainment, and sanity he has given me throughout graduate school. It would have been very different without him.

TABLE OF CONTENTS

page

LIST OF TABLES

LIST OF FIGURES

LIST OF ABBREVIATIONS

| | |
|---|---|
| APCI | Atmospheric pressure chemical ionization |
| APGD | Atmospheric pressure glow discharge |
| APPI | Atmospheric pressure photoionization |
| ASAP | Atmospheric solids analysis probe |
| CI | Chemical ionization |
| DAPCI | Desorption atmospheric pressure chemical ionization |
| DART | Direct Analysis in Real Time |
| DBDI | Dielectric barrier discharge ionization |
| DESI | Desorption electrospray ionization |
| DIOS | Desorption ionization on porous silicon |
| EI | Electron ionization |
| FAPA | Flowing atmospheric pressure afterglow |
| FT-ICR MS | Fourier transform ion cyclotron resonance mass spectrometry |
| HPLC | High performance liquid chromatography |
| HRMS | High-resolution mass spectrometry |
| IE | Ionization energy |
| IRMPD | Infrared multiple photon dissociation |
| LTP | Low temperature plasma probe |
| MALDI | Matrix-assisted laser desorption ionization |
| PA | Proton affinity |
| PAH | Polycyclic aromatic hydrocarbon |
| PADI | Plasma-assisted desorption ionization |
| TOF-MS | Time-of-flight mass spectrometry |

Abstract of Dissertation Presented to the Graduate School
of the University of Florida in Partial Fulfillment of the
Requirements for the Degree of Doctor of Philosophy

# DIRECT ANALYSIS IN REAL TIME IONIZATION FOR HIGH-RESOLUTION MASS SPECTROMETRY

By

Julia Diane Laney Rummel

December 2009

Chair: John R. Eyler
Major: Chemistry

Direct Analysis in Real Time (DART) is an ionization method for mass spectrometry (MS) that was introduced by Cody and coworkers in 2005.[1] This source operates by passing helium or nitrogen between a high voltage needle and a counter electrode to produce an electrical discharge. Additional electrodes are present to remove all but the excited-state gas atoms/molecules. The excited species produced by the DART source may either ionize analytes directly or may interact with ambient components to create reagent ions that may ionize analyte molecules. Analytes are inserted directly into the stream of excited gas atoms or molecules that exit the DART source for desorption and ionization. Because little or no sample preparation is required and analyses are performed in ambient conditions, DART-MS offers rapid analyses of a variety of compound classes with minimal effort.

For the current work, a DART source was fabricated and interfaced to several different mass spectrometers. The source was optimized and its analytical figures of merit were determined with analytes representative of illicit drugs, explosives, pesticides, and chemical warfare agents. Sensitivity and signal stability of the mass

spectrometers were improved with the addition of a passively sampling flared inlet modification. A commercial actively sampling inlet modification was added and compared to the passive design.

The utility of the custom-built DART source was demonstrated with a number of different applications with little or no sample preparation. Analytes were sampled from a wide variety of surface types including glass, metal, soil, sand, money, food products, and more. Matrixes such as ocean water, wine, and dimethyl sulfoxide caused suppression of analyte signal, while salt content and the presence of other solvents showed little or no effect. The addition of dopants to the sampling region was explored as a method of modifying ionization characteristics and expanding DART capabilities.

The mechanistic factors governing DART sensitivity were systematically studied. With volatile compounds, proton affinity was found to be the most important determinant of sensitivity. In addition to the mechanisms previously proposed in the literature, evidence of a self-protonation mechanism was observed. A spatial variation in the mechanism of ion formation was demonstrated with polycyclic aromatic hydrocarbons. Generally, the pathways of DART ionization appeared to fall into the class of mechanisms operative in atmospheric pressure chemical ionization (charge exchange, proton transfer, etc.).

DART was coupled to several FT-ICR MS instruments. The highest resolving powers ever reported with DART-MS analyses were demonstrated. The capability of the FT-ICR MS to do extended ion trapping was exploited to conduct infrared multiple photon dissociation experiments for spectroscopic structural determination of DART-ionized molecules.

# CHAPTER 1
# INTRODUCTION

## Overview

Direct Analysis in Real Time (DART) is an ionization technique for mass spectrometry (MS) that was introduced by Cody and coworkers in 2005.[1] DART-MS is used for the analysis of samples with very little or no sample preparation for a wide range of analytes. Though its wide applicability has afforded the technique growing interest in the mass spectrometry community, a number of areas involving DART have seen little exploration. For example, the underlying mechanisms of DART ionization are not fully understood. Additionally, DART has only been applied using mass spectrometric instruments capable of low to moderate mass resolving power, thus potentially limiting the information that may be gained from a sample.

The work described in this thesis was aimed at exploring a number of facets of DART ionization. A custom-built DART source was fabricated and optimized for a diverse array of applications. The effects of analyte substrate, matrix, and surrounding environment were investigated. The mechanisms of DART were systematically studied so that the factors governing DART sensitivity could be better understood. Lastly, the custom-built DART source was coupled to ultra-high mass resolution instruments for the first time. These instruments were used to accomplish another first: a spectroscopic study of DART-ionized samples.

In the following sections, concepts relevant to this work will be discussed. First general introductions to mass spectrometry and ambient ionization will be given. Next, the current literature on the function, mechanisms, and applications of DART will be reviewed. The chapter concludes with introductions to the two high-resolution mass

spectrometry techniques used in this work: time-of-flight mass spectrometry and Fourier transform ion cyclotron resonance mass spectrometry.

**Mass Spectrometry**

Mass spectrometry is a workhorse analytical technique with widespread applicability in many areas. The technique is known for its speed, sensitivity, and selectivity.[2] Mass spectrometry is used to measure the mass-to-charge ratio (m/z) of molecules and, depending on the type of mass analyzer, may be used to determine the elemental composition and structure of a molecule. The technique can be used for compound identification, quantitation, kinetics studies, and reaction monitoring.[3-8]

A number of stages occur during a mass spectrometric analysis. As mass spectrometry is a gas-phase technique, an analyte must be volatilized prior to analysis. For analyses involving gas chromatography/mass spectrometry, this occurs long before analyte molecules reach the mass analyzer. For most other analyses, the volatilization occurs just before or during the ionization step. After ionization, analyte molecules are focused and guided through vacuum regions by way of pressure differentials and electric field manipulations with ion optics. The ion optics can include a series of plates to which electric potentials are applied such as einzel lenses or a series of RF-multipoles.[9] Eventually, the ionized analyte molecules reach a mass analyzer, which detects the ions based on their mass-to-charge ratios. A number of different types of mass analyzers are available, each with its own set of strengths and weaknesses, but only those relevant to this work will be discussed in detail later in this chapter. Also depending on the type of analyzer, structural elucidation of the analyte may be accomplished by performing fragmentation studies. Methods of effecting analyte fragmentation are discussed in Chapter 7.

**Ionization**

As this work focuses on a single ionization technique, the concept of ionization is of great importance here. A variety of methods may be employed to impart a charge to an analyte molecule. Generally, ionization techniques are classified as “hard” or “soft” based on the energy involved and the resultant ion types. Election ionization (EI) occurs under vacuum conditions and is a hard ionization technique that produces a high degree of fragmentation.[10] A softer alternative to EI that is performed under vacuum is chemical ionization.[10]

Many soft ionization techniques have been introduced in recent years, the majority of which operate at atmospheric pressure (AP). One of the most popular AP soft ionization techniques is electrospray ionization (ESI), developed by John Fenn.[11] ESI operates by passing an analyte solution through a fine tube or needle toward a mass spectrometer interface. An electric field is created by applying a high voltage to either the needle or the interface, which results in a build up of charge at the exit of the needle and the formation of a Taylor cone.[12] Charged droplets that are emitted from the Taylor cone as an aerosol undergo Rayleigh explosions and solvent evaporation as they drift toward the inlet of the mass spectrometer, eventually becoming free ionized molecules that can be mass analyzed.[13,14] A depiction of this process is given in Figure 1-1. Higher-flow ESI sources benefit from the addition of a nebulizing gas flowing axially to the sample solution.[15] If this occurs, the capillary/nebulizing gas emitter is called a nebulizer.

In 2004, the Cooks group introduced desorption electrospray ionization (DESI). DESI forms ions in a similar manner as ESI.[16] The differences in the two techniques lie in the geometry and sample introduction mechanism. Unlike ESI, where the nebulizer

is essentially aimed uninterrupted at the mass spectrometer inlet, with DESI, the nebulizer is aimed at a surface, typically at an angle. Droplets from the aerosol roll along the surface, picking up analyte molecules. Beyond this point, ionization occurs similar to ESI. DESI can be used to ionize samples with no sample preparation in the open air and, thus, is part of the growing field in mass spectrometry known as ambient ionization.[16]

The field of ambient ionization mass spectrometry has seen rapid growth in the last five years with a wide range of application areas including forensics, metabolomics, natural products, and food science.[17-20] Because of the wide applicability of this field, over twenty new techniques have been introduced since 2004. Like DESI, all of these techniques can be used to ionize samples with little or no preparation under ambient conditions. These methods are usually related to a previously published methods and involve a desorption step and an ionization step, which may occur simultaneously. To name a few, ambient sources employing laser desorption, photoionization, and chemical ionization have been developed recently.[21-26] Table 1-1 contains details on many of the ambient ionization techniques currently available. Numerous general reviews of ambient ionization techniques have been published in the last year.[27-29]

The capabilities of the different ambient ionization techniques vary greatly. All of the techniques employing the ESI ionization mechanism are capable of ionizing analytes ranging in mass from tens of Daltons (Da) to tens of kDa. The drawback in these techniques, however, is that they are generally only applicable to analytes of moderate to high polarity. The thermal desorption followed by atmospheric pressure chemical ionization (APCI) or atmospheric pressure photoionization (APPI) techniques

can typically analyze a wider range of polarities, but can only be used for analytes with masses up to about one kDa. The very newly introduced technique desorption electrospray/ metastable-induced ionization (DEMI) attempts to bridge the gap by combining the effective desorption/ionization capabilities of DESI with the applicability of DART analyze nonpolar molecules.[30]

All of the work presented in this dissertation involved the small molecule-technique, DART, which is valuable for its applicability for low to high polarity analytes and its simplicity of use. DART will be the focus of the rest of the discussion on ambient ionization techniques.

## Direct Analysis in Real Time Literature Review

### Introduction

Direct Analysis in Real Time (DART) is an ionization technique that was introduced by Cody and coworkers in 2005.[1] DART is not an entirely original idea. Similar techniques that were introduced before it include metastable atom bombardment,[43] atmospheric pressure Penning ionization,[44] and atmospheric sampling glow discharge.[45] The difference in these techniques and DART is that they were not open-air techniques; samples had to be volatilized and/or entered into a vacuum region prior to ionization.

Because it is capable of simple and rapid analyses, it is safe and free of exposed high voltages, and it has had an effective marketing campaign, DART has continuously grown in popularity since its introduction. Currently there may be more than 200 users and the number of publications involving DART-MS grows each year (Figure 1-2).[46,47] This review is intended to introduce and summarize the current work presented on or

related to DART and provide some understanding of its underlying mechanisms, its applications, and its relationship to other ambient ionization techniques.

**DART Function**

All DART sources are relatively simple in design and consist of few basic components that play very specific roles. A diagram of the latest version of the custom-built DART used in this work is presented in Figure 1-3. The first component is a gas inlet through which an inert gas, such as helium or nitrogen is introduced. The gas flows past a needle electrode and through a grounded counter electrode between which an electrical discharge is generated. The gas, now containing excited and charged species, continues down the bore of the DART source through a perforated disk electrode. This electrode serves to remove charged species from the gas stream. The gas next passes through a region surrounded by a heater and eventually exits the source through a grid electrode. The grid electrode removes remaining charged species from the gas stream and prevents signal losses due to ion-ion recombination. [1] Reported operating parameters of the DART source components are listed in Table 1-2.

Typically, DART sources are aimed at the inlet of a mass spectrometer and can be applied to any mass spectrometer with an atmospheric pressure inlet. Samples of any phase are introduced and ionized between the DART exit, or grid electrode, and the inlet of the mass spectrometer. A number of devices to improve the function of DART, such as auto-sampling devices and inlet modifications, have been fabricated but will not be discussed in detail here because they are not crucial to the operation of this ionization source.[51-54] The devices used in to improve the function of the DART source described in this dissertation included an automated sample introduction stage and two different inlet modifications, which will be discussed in Chapter 2.

## DART Mechanism

### Ionization

DART ionization originates from species created by the interaction of the reagent gas with the electrical plasma produced at the needle electrode. Debate continues on whether this is a corona or glow discharge.[48,55] In either case, electrons, radical ions, and metastable neutrals are created.[56] A photograph of the plasma generated in the custom-built DART source at UF is shown in Figure 1-3. The perforated and grid electrodes serve to remove ionized species from the stream such that only metastable gas atoms or molecules exit the DART source.[1] From this point, the ionization processes include competing reactions that are governed by analyte gas-phase basicities, acidities, ionization energies and electron affinities, and discharge gas type. Dopants present in the sampling region (added intentionally or not) can also alter ionization. These processes can be divided into two general categories: Penning ionization and chemical ionization. Gas temperature, DART exit-to-mass spectrometer distance, and electrode voltages can also heavily impact the types of ions seen.

Penning ionization[57] occurs according to the following reaction:

$$N^* + M \rightarrow N + M^{+\bullet} + e^- \quad (1.1)$$

This reaction may be possible if the analyte, M, has a lower ionization energy than the internal energy of the excited gas atom or molecule, N. The $2^3S$ state of helium is a long-lived metastable with an internal energy of 19.8 eV, which is higher than the ionization energies of most common organic molecules as well as many atmospheric gases. Odd-electron molecular ions of the volatilized (or gaseous) analyte may be directly formed in this manner. The Penning ionization mechanism may be responsible for spectra resembling those of compounds ionized by electron impact ionization.[48]

The reaction of the $2^3S$ state of helium with ambient water is very efficient.[58] Protonated water clusters are generated as seen in reactions 1.2 through 1.4.

$$He\ (2^3S) + H_2O \rightarrow He\ (1^1S) + H_2O^{+\bullet} + e^- \quad (1.2)$$

$$H_2O^+ + H_2O \rightarrow H_3O^+ + OH^- \quad (1.3)$$

$$H_3O^+ + nH_2O \rightarrow [(H_2O)_{n+1}H]^+ \quad (1.4)$$

The number of water molecules present in the clusters, n, depends on the partial pressure of water in ambient air.[59] Clusters containing as many as 14 water molecules have been observed as a result of this process.[1] Cody has also demonstrated that by lowering the bias on the potential of the RF ion guide at the entrance of a time-of-flight mass spectrometer, using a normal voltage on the grid electrode (250 V), and by positioning the DART source 1 cm from the inlet, the protonated water dimer was the base peak in an atmospheric background spectrum.[48] This specie has a proton affinity of 808 ± 6 kJ/mol and any volatilized analyte with a proton affinity greater than 808 should be able to form protonated molecules under these conditions.[60] For this reason, analytes such as naphthalene and toluene, which have proton affinities below this value, may be difficult to protonate.

Protonation is the most common path of positive mode ionization and has been reported for analyses of drugs, fungicides, flavors, and fragrances, as well as many other types of analytes.[54,61,20] Analyte molecules are said to be protonated by a simple proton-transfer between the molecules and the water clusters or according to Kebarle's water displacement mechanism summarized in reaction 1.5.[1,7,48,]

$$(H_2O)_n H^+ + M \rightarrow M(H_2O)_{n-1}H^+ + H_2O \xrightarrow{-((n-1)\,H_2O} [MH]^+ \quad (1.5)$$

This process may occur entirely in the gas phase or low-volatility analytes may ionize by reactions 1.1 or 1.2 in a chemical sputtering-type mechanism via reactive collisions of the protonated water clusters or the metastable helium atoms on the sample surface.[62]

Another route for protonation that has seen little discussion in the DART community is self-protonation. This reaction occurs according to reaction 1.6.

$$M^{+\bullet} + M \rightarrow MH^{+} + [M - H]^{\bullet} \quad (1.6)$$

This reaction is said to be ubiquitous for many classes of compounds and in many cases the rate constant for self-protonation is quite comparable to the calculated capture collision rate constant.[63] Evidence of this mechanism occurring in DART ionization was shown as a result of the with the work presented in this dissertation where deuterium adducts were observed during the analysis of deuterated anthracene (no other source of deuterium was present).[64]

Charge-exchange is another method of positive mode ionization that cannot be ignored. Also initiated by Penning ionization, analytes with ionization energies below 12.621 eV may form odd-electron molecular ions by charge-exchange with diatomic oxygen.[48] Reactions 1.7 through 1.9 illustrate this pathway.

$$He\ (2^3S) + O_2 \rightarrow O_2^{+\bullet} + He\ (1^1S) + e^- \quad (1.7)$$

$$O_2^{+\bullet} + M \rightarrow M^{+\bullet} + O_2 \quad (1.8)$$

$$O_2^{+\bullet} + M \rightarrow fragment^{+} + O_2 + R^{\bullet} \quad (1.9)$$

This phenomenon is evidenced by the presence of the $O_2^{+\bullet}$ specie observed in atmospheric pressure background spectra when the DART source is moved close to the mass spectrometer inlet and its grid electrode voltage is raised to 650 V. Additionally, Cody demonstrated that these conditions produced odd-electron ions that directly

correlated with the appearance of $O_2^{+\bullet}$ in background spectra.[48] Notably, conditions that favored the appearance of $O_2^{+\bullet}$, reduced the appearance of protonated water clusters. Table 1-3 contains information on the gas-phase ion energetics of species observed in DART background spectra.

Although nitrogen is in great abundance in the ambient atmosphere and has an ionization energy that is amenable to Penning ionization by the metastable helium atoms, $N_2^+$ is generally not observed in the background spectra. This may be because nitrogen has a Penning ionization collisional cross section that is roughly half of that of oxygen, may be the result of a fast charge-exchange between $N_2^+$ and $O_2$, or may be due to a dissociative recombination mechanism of the $N_2^+$ species.[67-69] Though reported to be low in intensity in the background spectra, $NO^+$ is known to be highly reactive and can effect hydride abstraction, oxidation, and charge-exchange when chemical ionization is performed.[48,63]

Negative mode ionization is initiated by thermal electrons interacting with ambient components, such as molecular oxygen or directly with the sample.[1] These electrons may be generated by Penning ionization (reaction 1.1) or, as Song et al. suggested, by the collisions between electrons and gas molecules in open air .[65] Electron-capture occurs as shown in reactions 1.10 and 1.11 and produces odd-electron molecular ions.

$$O_2 + e^- \rightarrow O_2^{-\bullet} \quad (1.10)$$

$$M + e^- \rightarrow M^{-\bullet} \quad (1.11)$$

If an analyte has an electron affinity greater the electron affinity of molecular oxygen (0.451 eV) or other ionized compounds, charge-exchange may occur according to reaction 1.12.

$$O_2^{-\bullet} + M \rightarrow M^{-\bullet} + O_2 \quad (1.12)$$

The products of electron-capture and charge-exchange reactions are indistinguishable as odd-electron molecular ions appear in both situations. Additionally, dissociative electron capture and dissociative charge-exchange may occur (Rxns 1.13 and 1.14).

$$AB + e^- \rightarrow A^- + B^\bullet \quad (1.13)$$

$$AB + O_2^{-\bullet} \rightarrow A^- + B^\bullet + O_2 \quad (1.14)$$

In a comparative study of DART and atmospheric pressure photoionization (APPI), Song et al. demonstrated these mechanisms occur with fullerenes, perfluorocarbons, and nitrated explosives; however, dissociative pathways are less prevalent in DART than in APPI .[65]

Gas phase acidities of analytes also play an important role in negative mode ionization. Song et al. reported that negative ion mode background spectra contain a series of low-abundance, basic anions, which they claim are products of dissociative electron transfer events or combinations of their products.[65] The more abundant negative background ions are listed in Table 1-3. Deprotonation of the analyte is possible if the analyte has a higher gas-phase acidity than these reactive species. Deprotonation has been reported with some nitrated explosives, alchohols, and organic acids.[1,65]

Numerous types of adduction reactions occur in DART ionization. In positive mode ionization, the presence of ammonia near the sampling region can induce

ammonium adduct formation that is more pronounced when analytes contain carbonyl functionalities .[48] Ammonium adducts usually appear in addition to protonated molecules and can complicate spectra. In negative mode ionization, the use of dopants is required for detection of some molecules. For example, RDX and tetryl are not detectable as molecular ions but will ionize by adduction of the chloride or nitrate ions that appear when containers of methylene chloride or nitric acid are open near the sampling region.[64] The chloride ions arise from methylene chloride (and other halogenated solvents) undergoing a dissociative electron-capture mechanism.[70] It should be noted that although dopants can enhance ionization of some molecules, their presence may suppress other ionization events. Halogenated solvent vapors can reduce the number of thermal electrons available for electron-capture by analytes. Volatile acids will also preferentially deprotonate prior to weakly acidic analytes.[70]

**Other considerations**

Harris et al. reported simulations of the fluid dynamics and ion transmission of DART.[49] Both types of simulations indicated that placing samples in the region nearest the exit of the DART source would provide the greatest sensitivities. These results were confirmed experimentally.

The desorption mechanisms operative in DART have received little discussion in the literature from a mechanistic standpoint. In the introductory DART publication, Cody et al. insinuated that thermal desorption and chemical sputtering may be operative.[1] Further evidence of the importance of the thermal desorption mechanism was presented by Smith et al. and Nilles et al.[38,50]

**Applications**

Numerous applications employing DART have been published since its

development. Most of the applications reported capitalize on the ease with which DART is operated for rapid and sensitive analyses. Recent publications by Yu et al. and Nilles et al. demonstrate that DART-MS can be used in a fashion similar to better-established techniques such as electrospray-MS for quantitation with high precision and sensitivity.[50,54] For simplicity, these reports will be divided into three categories: biological applications, forensic science and homeland security applications, and "other."

**Biological applications**

Biological analyses can be interesting and difficult because the samples are often highly complex and require extensive sample preparation. Typically, these specimens require a means of analyte extraction as well some kind of separation, such as high performance liquid chromatography, prior to mass spectrometric analysis.[71] As no preliminary extractions were performed in the following applications, these reports demonstrate the relatively low susceptibility of DART-MS to signal suppression by biological interferents. Taking a fairly obvious direction in biologicals analyses, Zhao et al. and Yu et al. both quantified pharmaceuticals in blood plasma.[54,72] In the area of microbiology, cell cultures were directly analyzed with DART MS by Banerjee et al.[73] Finally, in the area of entomology, the first DART-MS analysis of a living specimen was reported by Yew *et al*. Differences in the pheromone profiles of male and female flies and females that had or had not been successfully courted were evident in their mass spectra.[74]

**Forensic science and homeland security applications**

The subject areas where DART-MS is perhaps the most useful are forensic science and homeland security. The technique is so applicable to these areas because

it can provide analyses that are rapid, selective, and relatively non-destructive. Applications relevant to these areas have focused on the analysis of pharmaceuticals distributed in various matrices, other evidentiary materials, and chemical warfare agents. As an example of a pharmaceuticals analysis, Steiner et al. validated DART-MS as a rapid screening tool for forensic drugs analyses.[17] In a very large-scale and a smaller-scale study, Fernandez and collaborators determined that a large percentage of anti-malarial drugs originating in areas of Southeast Asia were counterfeit.[75,76] In more diverse areas of forensic science, Jones et al. demonstrated that DART-MS could be used in writing ink identification and Coates et al. used DART-MS to detect and track the disappearance of gasoline and paint thinner on cotton, nylon, and drywall.[77,78] In a series of publications relevant to homeland security, Laramée and coworkers reported using DART-MS to detect chemical warfare agents (CWAs) and explosives on various surfaces.[77-80] The group also successfully quantified CWAs in unmodified muddy water.[50]

**Other application areas**

A number of examples of DART-MS being applied to areas that do not fall into the above categories have also been discussed in the literature. These reports span a diverse array of applications ranging from synthetic chemistry to food science and consumer products. In an interesting study, Kpegba et al. used DART-MS to analyze self-assembled monolayers on gold surfaces.[81] Vaclavik and coworkers demonstrated DART-MS as a tool for rapid differentiation of olive oil grades and adulterants.[82] In response to a popular media event, Vail et al. used DART-MS to detect melamine in dog food.[83] In its own sub-category of "other," DART-MS analysis of thin layer chromatography plates has been a popular topic in the DART community. Morlock et

al. first demonstrated DART analyses of high performance thin layer chromatography plates in 2007.[84] The group has presented more applications of TLC DART since then.[85,86]

### Related Ionization Techniques

As mentioned earlier, many new ambient ionization techniques have been introduced in recent years. A number of these techniques, like DART, are driven by an atmospheric pressure electrical discharge and are dominated by chemical ionization-like processes. Six of these (including DART) may be grouped according to the type of electrical plasma generated.

### Corona discharge

Both introduced in the same year as DART, desorption atmospheric pressure chemical ionization (DAPCI) and Atmospheric-pressure Solids Analysis Probe (ASAP) produce ionizing species with a corona discharge.[25,26] DAPCI was first introduced by the Cooks group as a method of probing the ionization mechanisms of desorption electrospray ionization (DESI) and involves placing a high voltage needle in the vicinity of a sample.[26] McEwen et al. implemented a similar source by simply cutting a hole for sample introduction (on melting point tubes) into a standard APCI source.[25] Samples were volatilized by a hot stream of nitrogen prior to ionization. In both designs, reagent ions are produced by applying several kilovolts to a needle electrode to create a corona discharge.[25,26]

### Dielectric barrier discharges and RF plasmas

A particularly interesting class of ambient ionization sources generate ions by employing a dielectric barrier discharge or RF plasma. The following sources produce low-temperature plasmas generated by applying alternating polarity high voltages

(several kilovolts) to electrodes that are separated by a dielectric barrier. In 2007, Na et al. first introduced the dielectric barrier discharge ionization (DBDI) source.[34] DBDI utilizes a glass slide where samples are placed as a dielectric barrier between a hollow needle electrode through which an inert gas is introduced and a counter electrode.[87] In 2008, Harper et al. presented the "low temperature plasma probe" (LTP), a more versatile probe version of DBDI.[37] Though not technically a dielectric barrier discharge the plasma-assisted desorption ionization (PADI) source, by Ratcliffe et al., is very similar in design and function to the LTP probe.[88] The two-tube design of PADI allows users to perform gas mixing *in situ* inside the source if desired.[88] In all three sources, samples are ionized by direct interaction with the low-temperature plasmas.

**Glow discharges**

The ambient ionization source most similar to DART is flowing atmospheric pressure afterglow (FAPA).[55] This technique was first called an atmospheric pressure glow discharge, or APGD, by the Hieftje group in 2006 and adapted to mass spectrometry in 2008.[36,89] FAPA employs a pin-to-plane DC atmospheric pressure glow discharge with an operating potential of around 500V. An APGD source (the Hieftje group had not changed the name when this source was made) fabricated for studies in the Powell lab at UF is diagrammed in Figure 1-5. DART is also suggested to be based on a pin-to-plane glow discharge; however, several kilovolts are typically applied to the discharge needle.[1] As with DART, the gas primarily used for FAPA is helium. One important difference between FAPA and DART is that with FAPA, samples are introduced directly into the glow discharge, not downstream of it as with DART.[55] This may result in additional fragmentation that may be useful in structural elucidation but can complicate spectra. Numerous other glow discharge-based techniques have been

reported in recent years, but are beyond the scope of this discussion.

### DART Literature Review Concluding Remarks

In this literature review an overview of the theory and applications involving DART were given and some related techniques were described. Although the mechanism of DART ionization is still not fully understood, as Chapter 5 demonstrates, it is clear that atmospheric pressure chemical ionization processes dominate. Literature searches into the mechanism studies performed with other ionization techniques that eventually effect chemical ionization, such as atmospheric pressure photoionization, may also provide readers with a better understanding the processes governing DART ionization.[70]

Instances of DART-MS applications continue to surface in a very diverse range of areas. As its popularity continues to grow due to its rapidity and ease of use, the DART methodology will continue to move from the proof-of-concept stage into the mainstream in many areas, as it has already done in the area of forensic science with illicit drugs analyses.[17]

## High-Resolution Mass Spectrometry

All of the work discussed in this dissertation was performed with high-resolution mass spectrometers. Mass resolution is defined as the minimum mass difference between two mass spectral peaks so that the valley between the peaks is a specified fraction of the height of the smaller peak.[90] In practice, mass resolution is $\Delta m_{50\%}$, meaning the width of a peak at half of its maximum. The mass resolving capabilities of a mass spectrometer are usually described with mass resolving power. It incorporates the mass of the ion(s) in question into the calculation ($m/\Delta m_{50\%}$).[90] Resolving power

may be expressed in terms of two mass spectral peaks or one peak. Figure 1-6 demonstrates mass resolution and mass resolving power.

Instruments are said to be “high resolution” if they are capable of resolving powers greater than 10,000.[91] Many orthogonal-acceleration (*oa*) time-of-flight (TOF) instruments fall into this category— the *oa*-TOF in the Powell lab at UF is capable of achieving resolving powers of 18,000. As many questions still cannot be answered with this level of resolving power, instruments such as FT- ICR mass spectrometers that are capable of resolving powers in the hundreds of thousands (depending on the field strength of instrument’s magnet and the molecular weight of the ion of interest) can be appropriately described as “ultrahigh-resolution.” Other examples of instruments capable of very high resolving powers are the Orbitrap ($m/\Delta m_{50\%}$ near 200,000) and multiple-pass TOF instruments (a mass resolving power of 350,000 was reported with $N_2^+$).[92,90]

An obvious advantage of high-resolution mass spectrometry (HRMS) is the ability to distinguish multiple components all of a single nominal mass, as may be present in complex samples. In some situations, chromatographic separation can negate the need for HRMS by physically separating components, reducing the likelihood that more than one component will be mass analyzed at any given time. Exact masses may be inferred in these cases, with an assumption that a mass spectrometric peak contains only one component and careful mass calibration with internal standards. Fragmentation patterns, such as those achieved with electron ionization, are extremely useful in analyte identification.[10] Generally, ambient ionization methods like DART do not have the advantages of preliminary separation or additional structural information

from fragmentation and must rely on the precision and accuracy of the mass analyzer to which they are attached for compound identification.

As alluded to above, another advantage of HRMS is the high mass accuracy it achieves. HRMS instruments such as those used for FT-ICR MS can achieve low-ppm to ppb mass accuracies.[93] With the exact mass of an unknown determined, an elemental composition can be assigned and the unknown's identity may be narrowed to a few possibilities. Evaluation of the isotope pattern and knowledge of the sample origin and can often assist in establishing a positive identification.[94]

In the following sections, a brief overview of the high-resolution mass spectrometers used in this work will be given. The first type of HRMS discussed is oa-TOF, which was used most often. Next, FT-ICR MS will be covered because three different FT-ICR instruments were used in this research.

**Time-of-Flight Mass Spectrometry Overview**

Time-of-flight (TOF) mass spectrometry employs the simplest of the mass analyzers. In its most basic form, ions are pulsed through a field-free (no magnetic or electric field) flight tube and their flight time, or time required to traverse the tube, is measured.[2] As all ions should have the same kinetic energy upon entering the tube, their flight time will be proportional to the square root of their mass-to-charge (m/z) ratio. This relationship is described by equation 1-1, where *m* is the mass of the ion (kg), *z* is the number of charges on the ion, *d* is the drift distance (m), *V* is the accelerating potential of the electric field (V), and *e* is the elementary charge (C).[95]

$$t = d\sqrt{\frac{m}{2zeV}} \qquad (1\text{-}1)$$

From equation 1-1, the relationship between resolving power (m/ m) and time can be shown:

$$\frac{m}{\Delta m} = \frac{t}{2\Delta t} \tag{1-2}$$

As flight time is directly proportional to distance, the resolving power achieved by TOF instruments is dependent on the length of the flight tube and the number of passes made by the ions being mass analyzed (two in the case of the TOF used in this work).

Spatial, temporal, and velocity dispersions in an ion population broaden the ion arrival time to the detector and limit the resolving power of the instrument.[96] To overcome this problem, most new TOF mass spectrometers are equipped with a reflectron. The reflectron, also called an ion mirror, consists of a series of ion lenses that retard, reflect, and refocus traveling ions into discreet packets, yielding a reduction in the spread of times that ions of a given m/z will reach the detector.[97]

The TOF used in this work is designed so that the flight tube is positioned perpendicular to the initial trajectory of the ion. A diagram of the ion optics and flight tube of this instrument is shown in Figure 1-7. An instrument with this geometry is known as an orthogonal acceleration TOF, or *oa*-TOF. With *oa*- TOF, a nearly parallel beam of ions is pulsed at a right angle into the flight tube, refocused by the ion mirrors in the reflectron, and sent to the detector. Prior to the pulse, the ion beam's average velocity in the direction of the flight tube (or in the opposite direction) is zero.[98] The result is resolving powers greater than 18,000 for low masses. With internal calibration, this instrument can achieve mass accuracies of 2 ppm or better.

**Fourier Transform Ion Cyclotron Resonance Mass Spectrometry Overview**

Fourier transform ion cyclotron resonance mass spectrometry (FT-ICR MS) offers the best resolving powers and mass accuracies of any broadband mass analysis technique.[100] The fundamental operating principle of FT-ICR MS is the motion of an ion in a magnetic field (depicted in Figure 1-8). In practice, ions are transported to and electrostatically trapped in a cell (the ICR cell) that is located in the bore of a either a permanent or a superconducting magnet with field strengths typically from 1 to 14.5 Tesla.[101] Also called Penning traps, diagrams of a cubic ICR cell (the earliest design) and a cylindrical ICR cell are given in Figure 1-9. Regardless of the geometry, all ICR cells consist of sets of plates responsible for trapping the ions, exciting the ions, and detecting the ions.[102]

Inside the ICR cell, ions are subjected to the Lorentz force, that is perpendicular to the magnetic field causing them to travel in a circular path, or cyclotron motion.[100] The path of an ion with respect to a magnetic field, B, is depicted in Figure 1-8. Next, ions are excited with a broadband RF frequency chirp, which creates coherent packets of ions ( with ions of a single m/z) that continue in the cyclotron motion in a larger radius than before. At this larger radius, the ions induce a current on opposing detection plates in the cell, called an image current. This image current is detected as a frequency-dependent voltage, and many frequencies are simultaneously detected for all m/z packets of ions. For this reason, FT-ICR MS has the benefit of broadband detection and the multiplex advantage.[90] The detected transient is processed with a fast Fourier transform. Because the frequency is known to be inversely proportional to

the m/z of an ion, this time domain signal is easily converted to a mass-to-charge signal and a mass spectrum is generated. The cyclotron frequency, *f,* of an ion can be related to the magnetic field strength, B, the ion's mass, and the ion's charge with the following equation (a rearrangement is also shown to demonstrate how m/z is determined):

$$f = \frac{ezB}{2\pi m} \quad \Rightarrow \quad \frac{m}{z} = \frac{eB}{2\pi f} \tag{1-3}$$

If the pressure in the ICR cell is sufficiently low and collisions are limited, the ions can be nondestructively detected over a long period of time. As the number of detection events and collected data points increases, the resolving power also increases. Therefore, the resolving power can be improved by increasing the time over which signal is collected (the length of the transient) or by increasing the speed at which the ion packet travels. Lower m/z ions travel at higher speeds, thus having higher frequencies and are better resolved than higher m/z ions. As indicated in equation 1-3, the cyclotron frequency is proportional to the magnetic field strength. Equation 1-4 demonstrates the factors affecting resolving power, R, where *T* is the length of the transient and f is the cyclotron frequency. A substitution with the mass, charge, and magnetic field strength from equation 1-4 demonstrates how resolving power is related to magnetic field strength.

$$R = \frac{Tf}{2} = \frac{TezB}{2\pi m} \tag{1-4}$$

Equation 1-4 shows that as the magnetic field strength increases, the potential resolving power also increases. Figure 1-10 demonstrates how the resolving power varies as the magnetic field strength is increased. Scientists at the National High Magnetic Field Laboratory continue to increase their ability to resolve more and more

components by building FT-ICR MS instruments with larger and larger magnets. With their 14.5 T FT-ICR MS, resolving powers of 800,000 were demonstrated and approximately 50,000 components were resolved between 340 and 1500 Da in a mass spectral analysis of a crude oil sample.[103]

In addition to its superior resolving power and mass accuracy, FT-ICR MS can be used for tandem-in-time mass spectrometry experiments. The extended trapping times possible with FT-ICR MS allow ions to be isolated and manipulated with a number of dissociation methods. An introduction to the dissociation techniques used in this work, sustained off-resonance irradiation-collision induced dissociation and infrared multiple photon dissociation, will be given in Chapter 7.

### High-Resolution Mass Spectrometry Discussion Conclusions

The advantages of coupling a DART source with high-resolution mass spectrometers are easily understood. The ability of HRMS to distinguish many components in a single mass unit window compensates for the absence of a preliminary separation, as is usually the case with DART-MS analyses. The high mass accuracy of HRMS allows unambiguous identification of unknowns. Time-of-flight mass spectrometers are generally simpler to operate, easier to maintain (they do not have cryogenically-cooled magnets), and of lower-cost than FT-ICR MS instruments and are ideal for routine analyses. When resolving powers in the hundreds of thousands are desired, as will be demonstrated in Chapter 6, FT-ICR MS instruments are a better option.

## Scope of Thesis

In the following chapters, new contributions to the field of DART mass spectrometry will be described. First, the implementation of a custom-built DART

source comparable to the commercial version will be discussed. Numerous examples of the applicability of this DART source will be given. The effects of analyte substrate, matrix, and surrounding environment will be explored. The coupling of DART to the ultrahigh-resolution technique, FT-ICR MS, will be discussed. Last, a novel infrared multiple photon dissociation spectroscopic study taking advantage of the ease with which DART ionizes molecules and the trapping and tandem-MS capabilities of FT-ICR MS will be presented.

Table 1-1. Some currently available ambient ionization techniques.

| Name of Ionization Technique | Acronym | Ionization Method | Desorption Method | Date |
|---|---|---|---|---|
| Desorption Electrospray Ionization[16] | DESI | ESI | Spray | 2004 |
| Surface Sampling Probe[31] | SSP | ESI | Spray | 2004 |
| Direct Analysis in Real Time[1] | DART | APCI | Thermal | 2005 |
| Ambient Solid Analysis Probe [25] | APCI | APCI | Thermal | 2005 |
| Electrospray Laser Desorption/Ionization[21] | ELDI | ESI | Laser | 2005 |
| Desorption atmospheric pressure chemical ionization[32] | DAPCI | APCI | Thermal | 2005 |
| MALDI* Assisted Electrospray Ionization[22] | MALD ESI | MALDI/ ESI | Laser | 2006 |
| Desorption Sonic Spray Ionization[33] | DeSSI | | Momentum | 2006 |
| Dielectric Barrier Discharge Ionization[34] | DBDI | APCI | Sputtering | 2007 |
| Neutral Desorption Extractive Electrospray Ionization[35] | ND-EESI | ESI | Momentum | 2007 |
| Laser Ablation Electrospray Ionization[23] | LAESI | ESI | Laser | 2007 |
| Desorption Atmospheric Pressure Photoionization[24] | DAPPI | PI | Spray/ Thermal | 2007 |
| Atmospheric Pressure Glow Discharge or Flowing Atmospheric Pressure Afterglow[36] | APGD or FAPA | APCI | Thermal | 2008 |
| Low Temperature Plasma Probe[37] | LTP | APCI | Sputtering | 2008 |
| Easy Ambient Sonic Spray Ionization[38] | EASI | | Spray | 2008 |
| Liquid Microjunction Surface Sampling Probe/Electrospray Ionization[39] | LMSSP/ ESI | ESI | Solvent Flow | 2008 |
| Laser Ablation Flowing Atmospheric Pressure Afterglow[40] | LA/ FAPA | APCI | Laser | 2008 |
| Infrared Laser Desorption Electrospray Ionization[41] | IR-LADESI | MALDI/ ESI | Laser | 2008 |
| Secondary Electrospray Ionization [42] | SESI | ESI | Spray | 2009 |
| Desorption Electrospray/Metastable-Induced Ionization[30] | DEMI | ESI/APCI | Spray/ Thermal | 2009 |

Table 1-2. Reported DART settings[1,38,48-50]

| Electrode Settings | | Gas Settings | |
|---|---|---|---|
| Setting | Voltage | Setting | Value |
| Discharge Electrode | 1-5 kV | Gas Type | He, $N_2$ |
| Ring Electrode | 100-200V | Flow Rate | 1-7 L/min |

Table 1-3. Gas-phase ion energetics of possible reagent species involved in DART ionization[48, 65,66]

| Reagent | Ionization Energy (eV) | Proton Affinity (kJ/mol) | Reagent Ion |
|---|---|---|---|
| Water | 12.621 | 691 | $H_3O^+$ , $[H_2O]_nH^+$ |
| Oxygen | 12.0697 | 421 | $O_2^+$, $O_2^-$ |
| Ammonia | 10.070 | 853.6 | $NH_4^+$ |
| Nitric Oxide* | 9.264 | 531.8 | $NO^+$ |
| Nitrogen Dioxide* | 11.5 | N/A | $NO_2^-$ |
| Carbon Dioxide** | 13.777 | 540.5 | $CO_3^-$, $HCO_3^-$, $HCO_4^-$ |

* Species likely formed from reaction of oxygen and nitrogen
**Ionic species likely formed from reactions of water, carbon dioxide, and/or oxygen.

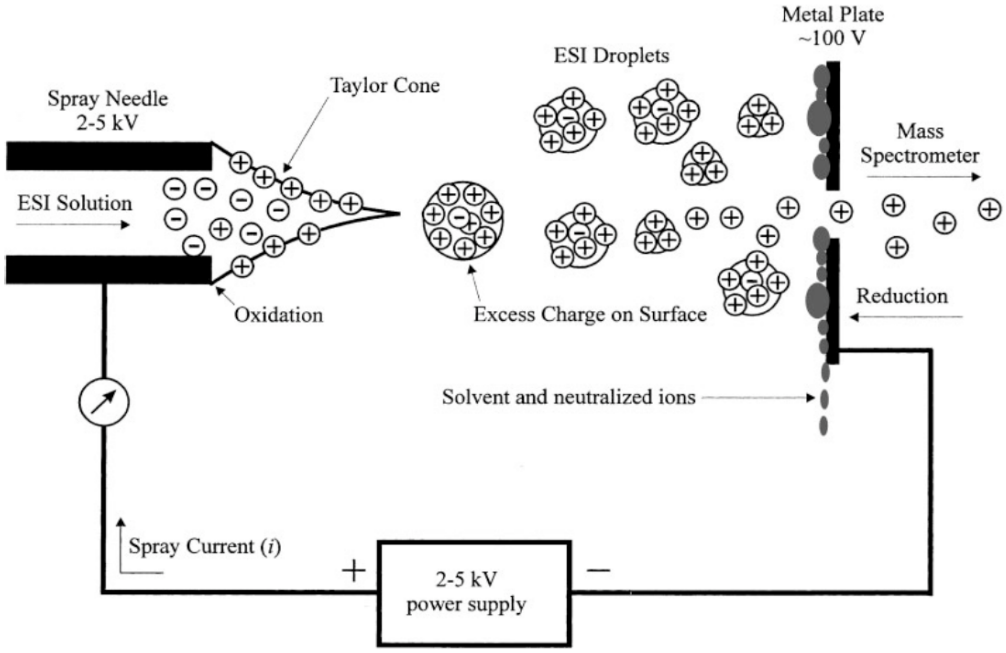


Figure 1-1. Schematic of the electrospray ionization process. The analyte solution is pumped through a needle or transfer line. A high voltage is applied either to the needle (shown above) or the mass spectrometer inlet, creating a field that results in the formation of Taylor cone and a spray of charged droplets. Reprinted with permission from John Wiley and Sons, Inc. from Cech, N.B.; Enke, C.G. *Mass Spectrom. Rev.* **2001,** *20,* 364.

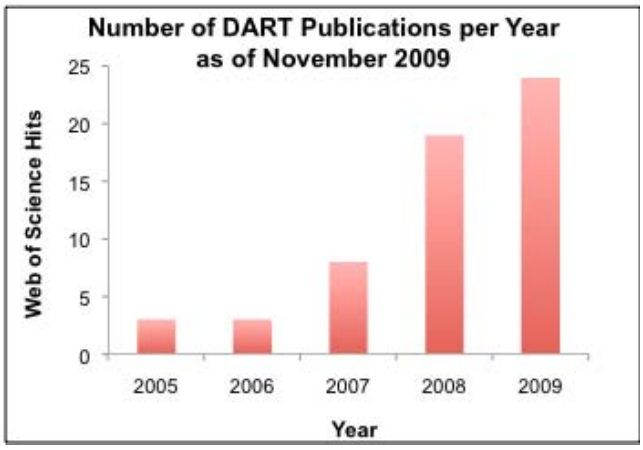


Figure 1-2. Number of DART publications per year since 2005. This data is based on a Web of Science search for "DART Mass Spectrometry."

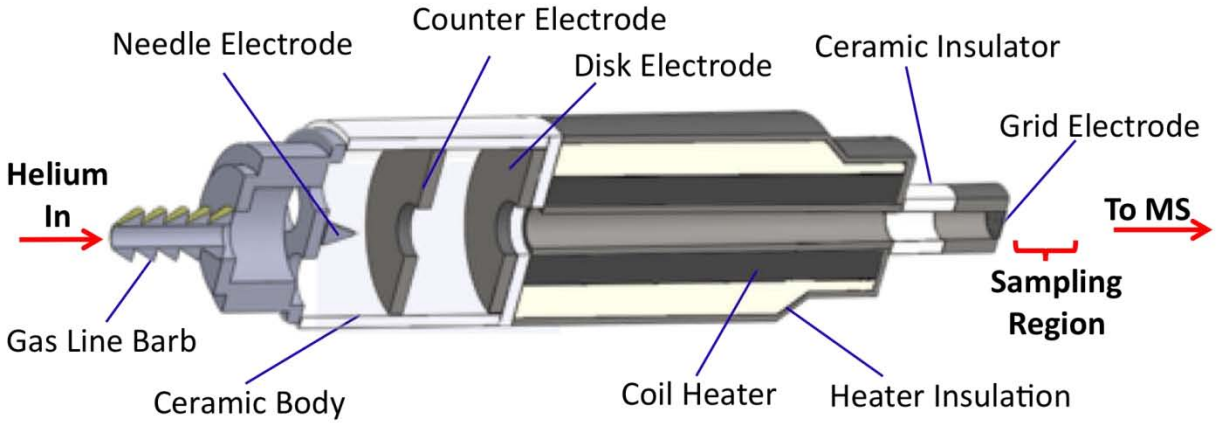


Figure 1-3. Schematic diagram of the latest version of the custom-built DART source used at the University of Florida.

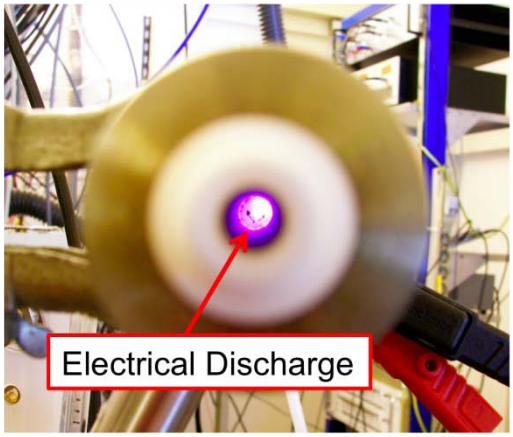


Figure 1-4. Photograph of the electrical discharge produced in a DART source. Note: the grid electrode was removed to take this picture.

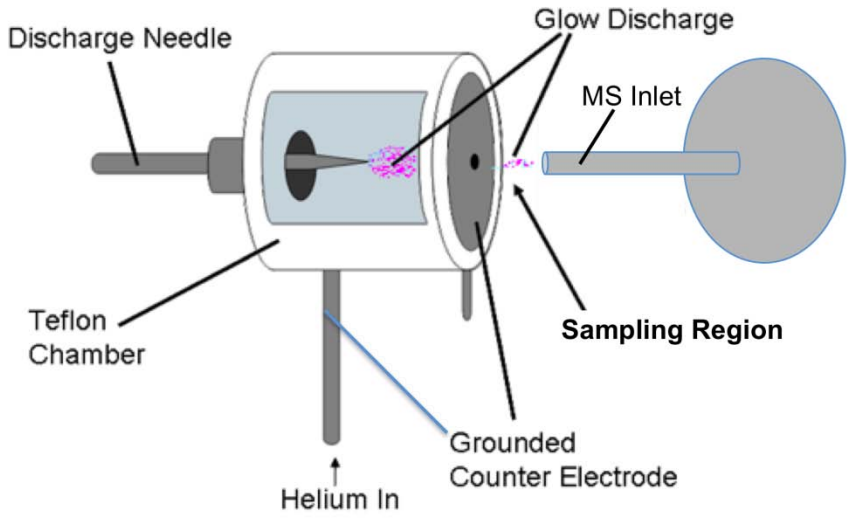


Figure 1-5. Diagram of an atmospheric pressure glow discharge source. This source was fabricated at UF. Analytes are placed directly into the plasma for desorption and ionization.

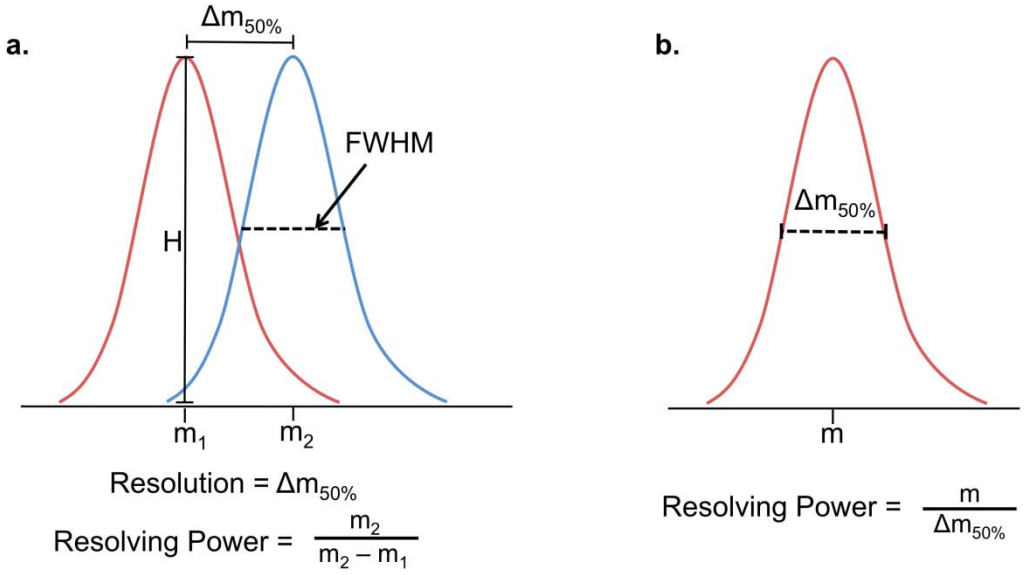


Figure 1-6. Demonstration of mass resolution and resolving power. Two equal-height mass spectral peaks, $m_1$ and $m_2$, in (a.) demonstrate resolution and resolving power. Note: FWHM stands for full width at half-maximum. The two-peak calculation of resolving power is given in (a.). The single-peak calculation of resolving power is given in (b.).[90]

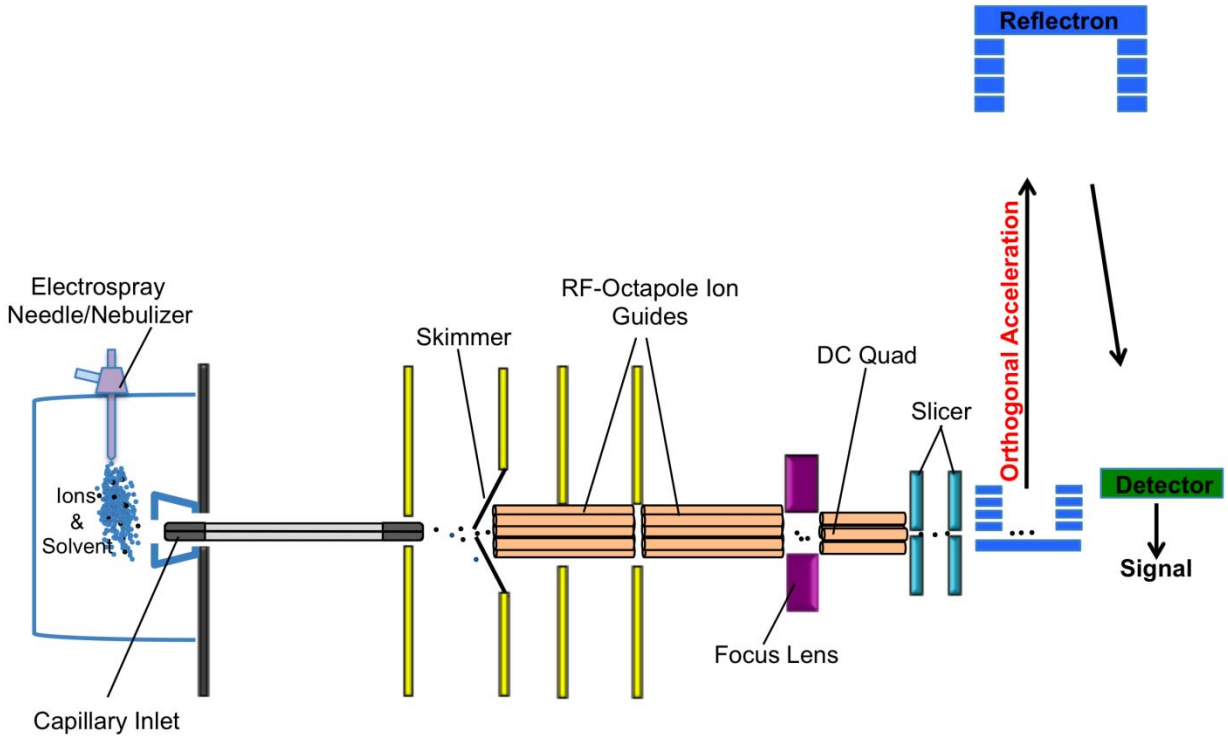


Figure 1-7. Diagram of the ion optics and ion trajectory of the Agilent 6210 Time-of-Flight mass spectrometer. This diagram was adapted from a figure in the Agilent "Instrument and Software Overview" training module.[99]

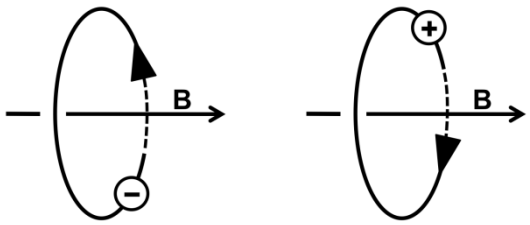


Figure 1-8. Motion of charged particles in a magnetic field, B. Negative ions follow the "right hand rule" and travel counter clockwise to the field lines directed as shown. Positive ions travel in a clockwise motion relative to the field lines directed as shown.

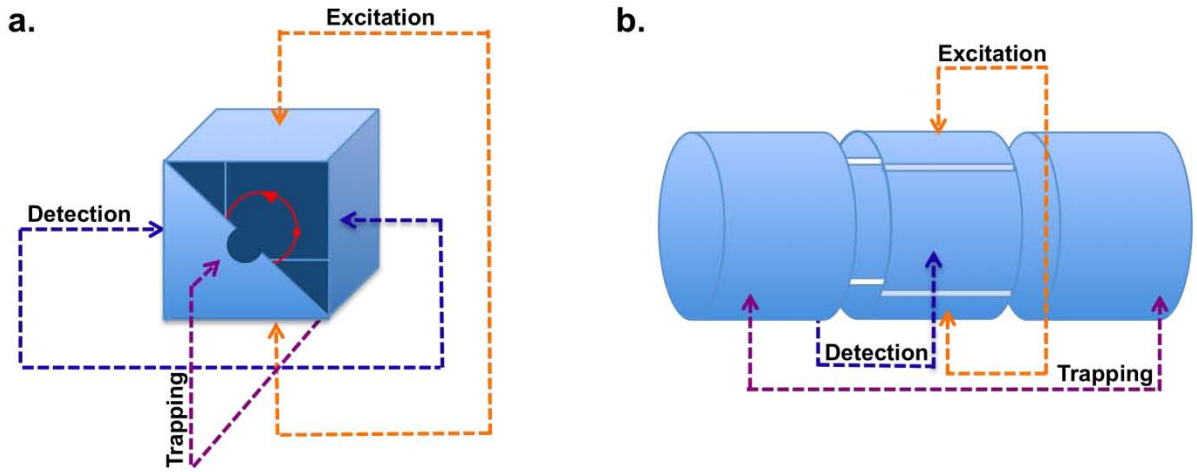


Figure 1-9. FT-ICR MS cell designs. Both the (a.) cubic and (b.) cylindrical cell designs consist of plates responsible for trapping, excitation, and detection. A cut-away region in the cubic cell (a.) depicts the path of ions when inside it.[102]

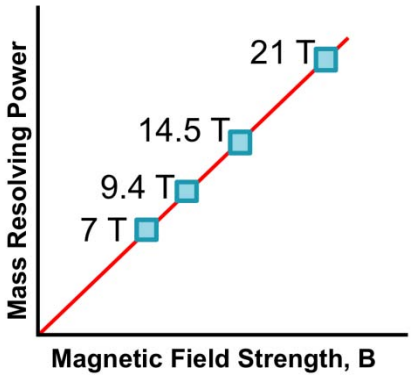


Figure 1-10. Relationship between magnetic field strength and the achievable resolving power of an FT-ICR MS. Figure adapted from report by Marshall et al.[101]

# CHAPTER 2
# IMPLEMENTATION OF A CUSTOM-BUILT DART SOURCE

## Introduction

Initial studies in this work involved the implementation of a custom-built DART source. This source was designed after the description given by Cody et al. in 2005.[1] A schematic diagram of the DART source in its earliest form is given in Figure 2-1. This ionization source was machined entirely by the UF Chemistry Department Machine Shop and the power supply/control box was assembled by the UF Chemistry Department Electronics Shop. The assembly and optimization of this DART source will be discussed in the following sections as well as a comparison of two different mass spectrometer inlet modifications for facilitating ion transport.

Numerous parameters were optimized with this DART source. Some of the parameters, particularly the electrode voltages and gas flow rate, were adjusted to maximize the production of metastable helium atoms that initiate all ionization processes. Optimal settings for these parameters are independent of the analyte. Other parameters, such as the gas temperature, required optimization for each analyte. It should be noted that many steps were taken and tests performed to create a DART source that performed optimally. Only the tests/actions that directly impacted the function of this DART source or have been discussed in the literature will be addressed here.

## Experimental

### Chemicals and Reagents

HPLC grade methanol was purchased from Burdick and Jackson (Muskegon, MI) and used without further purification. Dodecylamine was purchased from Sigma Aldrich

(St. Louis, MO) and was used undiluted. Caffeine, spiperone, 2,6-dinitrotoluene, and 1,3-dinitrobenzene were also purchased from Sigma Aldrich (St. Louis, MO) and were dissolved in methanol (caffeine and spiperone) or acetonitrile (2,4-dinitrotoluene and 1,3-dinitrobenzene). Dimethyl methylphosphonate and diisopropyl methylphosphonate were purchased from Alfa Aesar (Ward Hill, MA) and dissolved in methanol. Dimethoate and methamidophos were donated by Northrop Grumman Corporation (Baltimore, MD) and prepared in methanol. Fentanyl citrate (1 mg/mL) was purchased from Supelco (Bellefonte, PA) and was diluted with methanol.

**Instrumentation**

**DART source**

As shown in Figure 2-1, the DART source consists of a gas inlet, a tungsten needle electrode of dimensions 1.2 mm base x 3 mm height, a grounded counter electrode, a ring electrode, a copper heating block, and a grid exit electrode. The source was approximately eight inches long and less than two inches wide. A Dwyer Visi-Float® flow meter, model VFB-65-BV (Dwyer Instruments Inc., Michigan City, IN), was used to monitor the helium flow rates. All electrodes were powered by Emco 15 Watt HV modules, models H50P, H15P, and H20N (Emco High Voltage Corp., Sutter Creek, CA).

Initially, the DART source was heated with a nickel-plated copper heating block into which four ¼ inch Watlow Firerod® cartridge heaters, model E1A53 (Watlow Electric Manufacturing Co., St. Louis, MO) were inserted. The temperature inside the heating block was monitored with a thermocouple and controlled with a 1/16 DIN Micromega® Autotune PID Temperature/Process Controller, model number CN77332 (Omega Engineering Inc., Stamford, CT). Later, gas heating was accomplished with an

insulated coil heater removed from the APPI source that was sold with the Agilent TOF used in this work (Agilent Technologies Wilmington, DE). This heater was powered by the TOF electronics and its temperature was controlled and monitored with the Agilent MassHunter software responsible for controlling the TOF.

To prevent arcing between the needle electrode and the grounded counter electrode, a 31 MΩ resistor was placed in series with the high voltage cable and the needle electrode. The needle electrode voltages reported in this document were the values measured by the power supply and read prior to the resistor. A flared capillary extender that was used to interface the DART to the mass spectrometer inlet for most implementation studies will be discussed in detail later in this chapter. Unless otherwise stated, the source parameters used were as follows: needle electrode +3 kV, ring electrode +100 V, grid electrode +250 V, heating block temperature 100-450$^{o}$C (depending on sample), and gas flow-rate 3 L/min. When one setting was varied, the other settings were kept as listed.

**Optical studies design**

Optical detection studies were performed with an Ocean Optics S2000 Fiber Optic UV/Visible Spectrophotometer (Ocean Optics, Dunnedin, FL) to observe and optimize the plasma generated by the DART source. The spectrophotometer was equipped with a fiber optic for receiving signals and a detector composed of an array of 2048 charged-coupled devices. The device was interfaced to a Toshiba laptop computer via a SD500 analog-to-digital converter and USB cables for data collection. Spectra were collected for 210 ms per acquisition with 10 acquisitions averaged per spectrum. All data points are an average of 3 spectra. The wavelengths 389 and 587 nm were identified as strong helium emission bands and were monitored as parameters

of the DART were varied.

All of the optical studies were performed in a “dark box,” which consisted of a 21 x 15.5 x 21 in. filing cabinet with its drawers removed that was covered with a thick piece of black corduroy to block ambient light. The optical spectrometer was equipped with a flexible fiber optic for receiving light signals. Two sampling configurations were tested; first with the lead of the fiber optic aimed directly down the bore of the DART source and next with the lead positioned orthogonal to the exit of the DART source. The two configurations are diagramed in Figure 2-2. Optical signals were only detectable with the DART and fiber optic in the first configuration and it was used for all optical experiments. A typical optical emission spectrum obtained with the first configuration is given in Figure 2-3.

**Mass spectrometer**

An Agilent 6210 time-of-flight (Agilent Technologies, Wilmington DE.) mass spectrometer (TOF) was used for all experiments in this chapter. Tuning and mass calibration with the instrument’s autotune function were performed approximately every two days using an electrospray ionization (ESI) source and the ESI Tuning Mixture (Agilent Technologies, Wilmington DE.). The commercial atmospheric pressure photoionization source sold with the Agilent TOF was partially installed (the source was powered and its cables and identification magnet were connected to the mass spectrometer) to enable the safety interlock attached to the source inlet region of the TOF. By doing so, the high voltage capillary inlet of the TOF could be exposed and interfaced with the DART source. A voltage of -1000 V was typically applied to the capillary.

**Sample introduction**

Samples were only introduced and analyzed during the studies employing the TOF-MS as a detector. The tapered ends of glass pipettes were coated in melted dodecylamine and mounted between the DART source and the mass spectrometer inlet for analysis after the dodecylamine had solidified to test the following parameters: gas flow rate, high voltage, disk electrode voltage, and grid electrode voltage. Because large fluctuations were observed in the signals achieved depending on sample position, a single dodecylamine sample was held in place for the duration of an experiment. By operating the DART source with unheated helium, the dodecylamine sample remained relatively unchanged throughout the experiment. All data points given in the graphs that present trends in protonated dodecylamine signal are averages of approximately 30 seconds of mass spectrometric measurements.

Later in the work, a motorized stage was fabricated to eliminate the poor reproducibility in sample placement that occurred when doing things by hand. Pictured in Figure 2-4, the stage was equipped with a motor and a sample tray for automatically passing samples between the DART source exit and the TOF inlet. Holes 1 cm deep were drilled in the sample tray so that either melting point tubes or posts could be mounted upright in a row. For most of the studies, glass posts approximately 6 cm long and 2 mm in diameter with one end cut and fired to create a smooth, flat surface were used to transport samples into the DART gas stream. For most analyses, droplets of sample solution were deposited on the ends of the glass rods and allowed to dry. Samples were moved through the sampling region at a rate of approximately 1 mm/sec.

## Results and Discussion

### DART Optimization

#### Flow rate tests

Initially, the helium flow through the DART source was modified by adjusting the head pressure with the gas cylinder regulator. The flaw in this setup was that the flow rate was unknown and, thus, could not be compared to rates presented in the literature. To circumvent this problem, a flow meter was purchased and used in all of the experiments in this work. To test its effects, the helium flow rate was ramped from approximately 0.5 L/min to 4 L/min. The light output of the electrical plasma continually increased with the flow rate both with and without the presence of the 32 MΩ resistor As shown in Figure 2-5 a. the plasma light intensity of the selected helium emission lines increased through the limit of the flow meter. The fact that no maximum in optical signal was achieved was unimportant because the mass spectrometer gave errors at flow rates above 3 L/min and would stop generating spectra due to overpressure of the vacuum system. The response of solid dodecylamine as a function of flow rate is given in Figure 2-5 b. Each of the three plots in the graph represent the responses of a single dodecylamine sample as the flow rate was varied. A flow rate of 3 L/min was used for the rest of the optimization studies.

#### High voltage tests

The effect of the high voltage was tested by ramping the discharge needle voltage from 0 to 4.8 kV. The results of these studies are plotted in Figure 2-6. A maximum in both optical and mass spectrometric signal intensity was observed with voltages of 3 to 3.5 kV. Upon visual inspection, the electrical discharge at the needle electrode, which was shaped like a band connecting the needle and counter electrode,

was observed to increase in brightness and gradually narrow as the voltage was increased. At approximately 3.5 kV, the combination of plasma intensity and width produced the greatest signals. Beyond that point, the band-shaped plasma became so narrow that the apparent brightness and metastable production decreased, resulting in lower signals observed both optically and with the mass spectrometer.

**Disk and grid electrode tests**

In a similar manner to the discharge needle tests, the optical and mass spectrometric outputs were monitored as the voltages of the disk and grid electrodes were ramped. The optical and mass spectrometric responses are given in Figure 2-7. Demonstrating that the applied voltages had no effect on the nature of the plasma, no significant changes in light output were detected as a function of disk or grid voltage (Figure 2-7 a. and c.). Similar results were observed with the TOF when the voltage of the disk electrode was varied. Though the abundance of protonated dodecylamine did fluctuate as the voltage was adjusted, the pattern of variation was never reproducible from one trial to the next. The grid electrode, to which typically 250 V was applied, was suspected to be reducing the observable effects of the disk electrode. However, no effect was seen from the disk electrode when the grid electrode was left unpowered. To be consistent with the original DART publication, 100 V was typically applied to the disk electrode for the rest of the work reported in this document.

While investigating the effect of grid voltage using the TOF as a detector, larger signals for protonated dodecylamine were achieved between 200 and 400 V with a maximum typically occurring at 250 V (Figure 2-7 d.). These values were consistent with those reported in the first DART publication from 2005.[1] A voltage of 250 V was typically applied throughout the rest of the work in this dissertation.

## Other Considerations

### Gas temperature

The effect of gas temperature on analyte detection has been demonstrated in numerous reports.[38, 49,50] Similar effects were noticed while performing experiments for this research as well. The thermal desorption of an analyte is dependent on its boiling point and an analyte's boiling point is dependent on its chemical structure and polarity. Figure 2-8 demonstrates the effect of analyte structure on its volatility with methamidophos (MW = 141 Da) and fentanyl (MW = 336). If sensitivity is a concern, the gas temperature should be chosen based on the intended analyte as shown here. Interestingly, dodecylamine, a simple 12-carbon alkyl chain terminated with a primary amine with a molecular weight of 185 Da (greater than methamidophos), can be analyzed at room temperature; though higher temperatures do enhance its detection. As it will be demonstrated in the discussion of DART analyses of thin layer chromatography plates in Chapter 3, analyte substrate can also play an important role in determining the correct temperature for the DART gas stream.

### Sample placement

A correlation between the closeness of a sample to the DART source and sensitivity was observed on many occasions. Initially, this was assumed to be caused by a decrease in thermal desorption due to the drop in temperature. Harris et al. predicted with calculations and showed experimentally that the gas temperature decreases linearly as the distance from the DART source is increased.[49] In the same document, however, fluid dynamic simulations predicted a loss in sensitivity due to a sub-optimal particle trajectory as the sample-to-DART distance was increased. With these things in mind, dodecylamine was tested at various distances (Figure 2-9 a.) with

the DART left unheated. As plotted in Figure 2-9 b., the signal abundance of dodecylamine sharply declined as the distance was increased. These data showed that even when gas temperature was not a factor, detection was dependent on sample placement. A likely explanation for this is that the rapidly moving excited gas atoms and reagent ions disperse and dilute more and more as they travel farther from the DART source exit. As a result, the region closest to the DART source exit is the best location for sample placement.

### Inlet Modifications

#### Flared capillary extender description and introduction

As previously mentioned, a device referred to as a flared capillary extender was used to interface the DART source to the TOF instrument discussed above and to other mass spectrometers as well. Diagrammed in Figure 2-10, this device was inspired by work of the Bruce group and was employed to improve ion transport.[104] In its earliest form, the flared capillary extender consisted of three parts. Positioned closest to the DART source was a stainless steel funnel that tapered from 1 cm i.d. at its widest point to 0.5 mm i.d. at its narrowest point. Past its most tapered point, attached to the funnel was a sleeve that fit over a 5 cm capillary extender that consisted of a 4 cm long, 0.5 mm i.d. stainless steel ion transfer tube affixed to a ¼ in. i.d. sleeve for attachment to the capillary inlet of the TOF. This capillary extender was included with the atmospheric pressure matrix-assisted laser desorption ionization source sold with the TOF. Inside the capillary extender was a gold-coated canted coil spring responsible for securing the capillary extender to the capillary inlet of the TOF. After some time, the original capillary extender was replaced with one fabricated by the UF Machine Shop that had a shorter (1 cm long) transfer tube.

By passively guiding the DART gas stream and analyte ions into the mass spectrometer, the average signal abundance was increased and fluctuations in the abundance were decreased. Representative extracted ion chromatograms (EICs) taken with a stationary dodecylamine sample are given in Figure 2-11. The approximate average signal abundance in each EIC is marked with a dashed line. With the addition of the flared capillary extender, the protonated dodecylamine signal variability was decreased and the signal-to-noise ratio was improved by a factor of 2.5.

**Vapur® description and introduction**

In the summer of 2008, IonSense (Saugus, MA), the company that produces the commercial DART sources, provided an inlet modification known as a Vapur® for experiments at UF. Diagramed in Figure 2-12, the Vapur® consists of a ceramic tube protruding from a metal chamber that fits around the MS inlet. Attached to the metal chamber is a vacuum connection to which a Vacuubrand (Wertheim, Germany) MZ4 diaphragm pump is connected. By reducing the pressure between the sampling region and the mass spectrometer inlet, the Vapur® actively pulls gas and ions into it and toward the mass spectrometer inlet. After being aspirated into the Vapur®, ions are electrostatically guided into the mass spectrometer inlet and the neutral gas atoms or molecules are pumped away with the diaphragm pump.

A device called a “drying gas diverter” was fabricated and attached to the Vapur® to reduce background ions (see Figure 2-13). The capillary inlet of the TOF used in this work is heated by an axial flow of nitrogen called the drying gas. Because the nitrogen is heated to 300 °C, it desorbs contaminants from the tubing and fittings around the capillary inlet. With other API sources, such as electrospray, this is not a problem because the hot gas can flow away from the inlet. Unfortunately, with the unmodified

Vapur® installed, this drying gas was allowed to remain in close proximity to the entrance of the capillary inlet. Consequently, the reactive species produced by the DART source ionized these contaminants, creating a very high background. To remedy this problem, a polyetheretherketone (PEEK) drying gas diverter was machined to fit between the Vapur® and the inlet of the TOF. With the aid of several o-rings, the device created a seal between the region of the capillary heated by the drying gas and the interior of the Vapur® chamber. Holes cut into the device allowed the drying gas to be diverted away from the opening of the capillary and significantly reduced background contamination previously seen with the Vapur®. A comparison of the path of the drying gas with and without the diverter is given in Figure 2-13. The differences in background signals before and after the diverter was added will be presented in the "Background comparison" section appearing later in this chapter.

To dampen the noise generated by the diaphragm pump, a wooden "quiet cabinet" was constructed. Pictured in Figure 2-14, the quiet cabinet consists of a wooden cabinet 2 x 2 x 2 ft. with fans installed on opposite sides, one blowing in and the other blowing out. Foam and insulation material are inserted along the sides and door of the cabinet. Wheels (not shown) are connected to the bottom of the cabinet for easy transport.

### Comparison of Inlet Modifications

Most commercial DART sources were sold interfaced to a mass spectrometer via a skimmer cone to the atmosphere. This setup probably adversely affects the sensitivity of a DART-interfaced instrument because the DART gas stream, reagent ions, and the analyte are deflected away from the entrance to the mass spectrometer. To improve ion transmission and sensitivity, the flared capillary extender and Vapur®

were employed. In the following studies, the two designs were compared for ease of optimization, ion signal variability, the presence of background noise, and analytical figures of merit.

**Inlet Modification Optimizations**

The inlet modifications were first compared based on the ease with which they could be optimized and the time it would take for one to become operational with each inlet. Several steps were required to optimize each of the inlet designs. Unless stated otherwise, 1 to 10 ppm caffeine (based on instrument response, which varied from day to day) was used in all of the studies described below. As will be obvious from the descriptions of the studies performed for each inlet modification, optimization of the flared capillary extender was much less involved and took considerably less time.

**Flared capillary extender optimization**

The optimization studies required for the flared capillary extender were fairly simple. If one were intending to rapidly become operational with a DART source, this might be the best option.

**Flare angle.** In order to determine the best flare angle, four different flared attachments were fabricated. The attachments had angles of 15°, 30°, 45°, and 60° relative to normal. This optimization required the most time of the studies with the flared capillary extender because a new flared attachment was fabricated for each angle. After receiving the attachments, the optimization was simple and, as demonstrated in Figure 2-15 a., all of the flare angles greater than or equal to 30° provided good but similar signal abundances.

**Helium flow rate and DART-to-flare distance.** The optimization of the helium flow rate was previously described and is plotted in Figure 2-5. The last parameter to

be optimized with the flare was the DART-to-flare distance. To perform this test, the DART source was positioned various distances from the flare. In all cases, the sample-to-DART distance was held constant at approximately 1 mm. As Figure 2-15 b. demonstrates, the greatest signal abundances were achieved with distances of 2.5 to 3 cm. A distance of 2.5 cm was chosen for future experiments because it yielded less variation in signal abundance. This concluded the optimization of the flared capillary extender.

**Vapur® optimization**

It was far more involved to optimize the Vapur®. First, the same types of tests required for the flare, e.g. gas flow rate, DART position, etc., were also necessary for the Vapur®. Additionally, the optimal length of the ceramic tube and its position were tested. Most of these tests were complicated by the need to determine the correct pumping speed. Unfortunately, the optimal pumping speed varied based on the gas flow rate and the tube position. This meant that a variety of pumping speeds had to be tested for each new flow rate or tube position, thus extending the time required to optimize the Vapur®. It should be noted that the order in which the tests are discussed here is not necessarily related to their chronological order of being performed.

**Ceramic tube length and DART-to-Vapur® distance.** The simplest Vapur® optimization studies to perform involved the ceramic tube length and DART-to-Vapur® distance. To optimize the tube length, caffeine samples were analyzed with various lengths of ceramic tubes inserted into the Vapur®. Shown in Figure 2-16 a., the abundance of protonated caffeine continually increased as the length of the tube was increased, though the 15.8 cm tube demonstrated significantly increased fluctuation in signal. Longer tubes were not tested because significant changes in the DART

source/power supply setup would be necessary to accommodate the extra length and because no longer tubes were on hand. A decision was made to use 14.6 cm tubes in future studies. The DART-to-Vapur distance was also tested, with the best signals occurring when the DART source exit was 0.5 cm from the opening of the ceramic tube (Figure 2-16 b.).

**Ceramic tube-to-capillary distance and helium flow rate.** Of great importance to signal abundance and stability was the pumping speed of the diaphragm pump attached to the Vapur®. As previously mentioned, the optimal speed was dependent on both the position of the ceramic tube relative to the capillary inlet and the helium flow rate. In each of the following tests, the speed was varied by adjusting a needle valve attached to the pump. The effect of the speed was monitored with the analyzer pressure readout in the TOF operating software.

Inside the metal enclosure of the Vapur® is a gap between the end of the ceramic tube and the capillary inlet of the mass spectrometer. The length of this gap, i.e. ceramic tube-to-capillary distance, was varied from 0 to 6 mm. At each distance, the diaphragm pump speed was varied so that a range of analyzer pressures was detected. Figure 2-17 a. through c. shows the responses of protonated caffeine with the gap distances 2 to 6 mm and a range of analyzer pressures. Gap distances shorter than 2 mm produced drastically lower signal abundances and are not shown here. It may be noted that a smaller range of pressures is reported for the 4 mm and 6 mm gaps than the 2mm gap. This is because the pressure was more difficult to control with the wider gaps and the highest pressure obtainable was approximately $3 \times 10^{-7}$ torr. The gap distance of 2 mm yielded the best results and was used for all future studies.

Flow rates ranging from 1 to 4 L/min were tested to determine the optimal value. At each flow rate, the diaphragm pump speed was varied over a range of analyzer pressures. As demonstrated in Figure 2-17 d. through f., no flow rate between 2 and 4 L/min provided significantly better results. Though not shown here, 1 L/min was insufficient for adequate detection of protonated caffeine. These results demonstrated that the Vapur® could operate with one third less helium than the flared capillary extender. This was considered advantageous because helium is costly and is rapidly consumed during DART-MS analyses.

**Background Ions**

The second criterion by which the inlet modifications were compared was their levels of background ions. The industrial solvent 2-(2-ethoxyethoxy)ethanol was detected with all configurations of the inlet modifications. Its structure is given in Figure 2-18 a. The ions at m/z 119, 135, and 152 Da correspond to the $[M - (H_2O) + H]^+$, $[M + H]^+$, and $[M+NH_4]^+$ species, respectively, and were most abundant in each background spectrum. The flared capillary extender typically yielded maximum background ion abundances below 2000 counts (Figure 2-18 b). Background abundances of this level are much lower than what is typically seen with an electrospray source installed on the same TOF instrument.

Used as delivered, very high background signals were detected with the Vapur®. Figure 2-18 c. demonstrates that the background ions were about 30 times greater in abundance than those detected with the flared capillary extender. These large contaminant peaks were introduced by the TOF drying gas. Upon addition of the drying gas diverter and six o-rings snuggly fitting around the capillary extender (refer to Figure 2-13 b.) background ions were reduced to levels comparable to those observed with the

flared capillary extender. A background ion spectrum with the drying gas diverter installed is given in Figure 2-18 d. The two inlet modifications were concluded to be equivalent in background ion detection.

**Signal Abundance and Variation**

**Signal abundance.** The next metrics used to compare the two inlet modifications were signal abundance and signal variation. The signal abundances achieved by the two inlet modifications can easily be compared by either viewing extracted ion chromatograms (EICs) or by examining the mass spectra obtained. Each peak in the EICs represents a caffeine sample introduced into the sampling region with the moving stage. As shown in Figure 2-19 a. and b., the EIC obtained with the Vapur® contains peaks that are roughly five times greater than those observed with the flared capillary extender. Examination of protonated caffeine in the corresponding mass spectra (Figure 2-19 c. and d.) yields the same result.

**Signal variation.** The same data can be used to evaluate signal variation. By examining the EICs of caffeine obtained with each inlet modification (Figure 2-19 a. and b.), similar levels of fluctuation in peak size and height are observed. To better understand the degree of signal variation obtained with each modification, one should also view the mass spectra acquired (Figure 2-19 c. and d.). Aside from overall signal abundance, the major difference in the two mass spectra given is that background ions are present in the spectrum acquired with the flared capillary extender but not with the Vapur®. Though performed with both spectra, the background subtraction performed with the Vapur® was more effective. This means the blank used for background subtraction with the Vapur® was more representative than that used with the flared capillary extender. This result indicates that the abundances of the background ions

changed less from one acquisition to the next with the Vapur® than they did with the flared capillary extender. With this information, one may conclude that less overall signal variation occurs with the Vapur® than with the flared capillary extender. A likely explanation for the fluctuation observed with in the EICs is that the samples were not being introduced in an entirely uniform manner because of small changes in sample position in the stage (samples wobbled in their holder). Subsequent figures of merit studies were performed with internal standards to minimize the effects of the fluctuation in signal.

**Figures of Merit**

The final area where the inlet modifications were compared was their analytical figures of merit. To do so, calibration curves were generated for compounds representative of illicit drugs, pesticides, explosives, and nerve agent simulants (Figure 2-20). Calibration sensitivities, linear ranges, and limits of detection were determined for all of the analytes. Internal standards (ISs) were used in these studies to reduce the effects of the sample-to-sample variability caused by the inconsistencies in sample introduction. The ISs were similar to the target analytes in ionization characteristics and volatility. The target analyte-to-IS EIC peak area ratios were plotted for each quantity of analyte introduced. The curves generated with the flared capillary extender will also be discussed in Chapter 4 in a study comparing different sample substrates.

Similar figures of merit were achieved for both devices and are presented in Table 2-1. Because the slopes were in terms of peak ratios, very similar values were obtained for both the Vapur® and the flared capillary extender, with neither modification consistently yielding better calibration sensitivities. Linear ranges were calculated by subtracting the limit of detection from the highest sample quantity where the calibration

curve was still considered linear ($R^2 > 0.99$) assuming the line was linear through the LOD. Again, the modifications achieved similar results, both with linear ranges of two to four orders of magnitude. The Vapur® did, however, consistently achieve lower limits of detection (LOD) than the flared capillary extender. LOD was calculated with the equation below[105]:

$$LOD = 3\sigma_{Blank}/ m \quad (2\text{-}1)$$

In equation 2-1, $\sigma_{Blank}$ is defined as the standard deviation of the blank and *m* is the slope of the calibration curve. Better LOD values were obtained with the Vapur® because it provides more stable signals (both with samples and blanks), thus resulting in smaller values of $\sigma_{Blank}$ and overall lower LODs than the flared capillary extender. It should be noted that the limits of detection presented here with both modifications are similar to those reported with the commercially available DART source.

**Inlet Modification Comparison Conclusions**

In comparing the flared capillary extender with the Vapur®, one can see advantages and disadvantages to both inlets. The major advantage of the flared capillary extender is its simplicity. This characteristic affords the user the ability to rapidly setup and become functional with the DART source. A disadvantage of this inlet modification is the need to custom-machine a flared attachment that will fit the inlet of the mass spectrometer in use. Fortunately, two of the mass spectrometers used in this research have extremely similar source region designs and identical capillary inlets.

The Vapur® also presents a number of advantages. First and perhaps most importantly, lower limits of detection can be achieved with the Vapur because of the improved signal stability it provides. Next, the Vapur® reduces costs by requiring less helium to be passed through the DART source. Last, though not discussed above, the

additional pumping provided by the Vapur® reduces the gas load on the source region of the mass spectrometer to which it is interfaced. This is particularly important with the Agilent TOF used in this work because it completely halts spectral acquisition if a high pressure error occurs. After such an event, the instrument may display fairly different signal intensities and mass calibration, which can be highly detrimental in a long day of experimentation. If run with the proper diaphragm pumping speed, high vacuum errors never occur with the Vapur®. Some disadvantages of the Vapur® include a far more complicated setup and optimization, more delicate parts (particularly the ceramic tubes), and increased laboratory ambient noise levels caused by the diaphragm pump. It may be concluded that once all optimization studies are finished and measures are taken to reduce audible noise, the Vapur® provides somewhat better results than the flared capillary extender.

## General Conclusion

Many steps were taken in constructing and optimizing the custom-built source used here. Though small changes may be made depending on the application or experiment, the lessons learned and results from the optimization studies performed in this chapter were applied in the majority of the work presented throughout this dissertation. Though not a major theme of this chapter, the work presented here demonstrates that a comparable DART source may be produced with far less money than one must spend to purchase a commercial DART source (less than $1000 versus $75,000). The user also has options in how the DART source is interfaced to their instrument, either with a simple flared capillary or a more complicated Vapur®. Again, however, a cost is paid ($1200 for the Vapur® flange plus $3750 for a diaphragm pump) for the somewhat better results of the Vapur®.

Table 2-1. Comparison of the flared capillary extender and Vapur® figures of merit.

| Compound | Flared Capillary Extender | | | Vapur | | |
|---|---|---|---|---|---|---|
| | Slope ($ng^{-1}$) | Linear Range[a] | LOD[b] (pg) | Slope ($ng^{-1}$) | Linear Range[a] | LOD[b] (pg) |
| Fentanyl | 0.88 | 1.3 | 19 | 1.12 | 3.6 | 0.81 |
| Dimethoate | 1.45 | 4.8 | 8.8 | 1.99 | 4.3 | 0.88 |
| 2,4-DNT[c] | 0.28 | 2.3 | 224 | 0.42 | 2.6 | 147 |
| DMMP[d] | 0.58 | 3.6 | 30.2 | 0.28 | 2.6 | 5.2 |

a. Linear range is expressed in orders of magnitude
b. Abbreviation for limit of detection
c. Abbreviation for dinitrotoluene
d. Abbreviation for dimethyl methylphosphonate

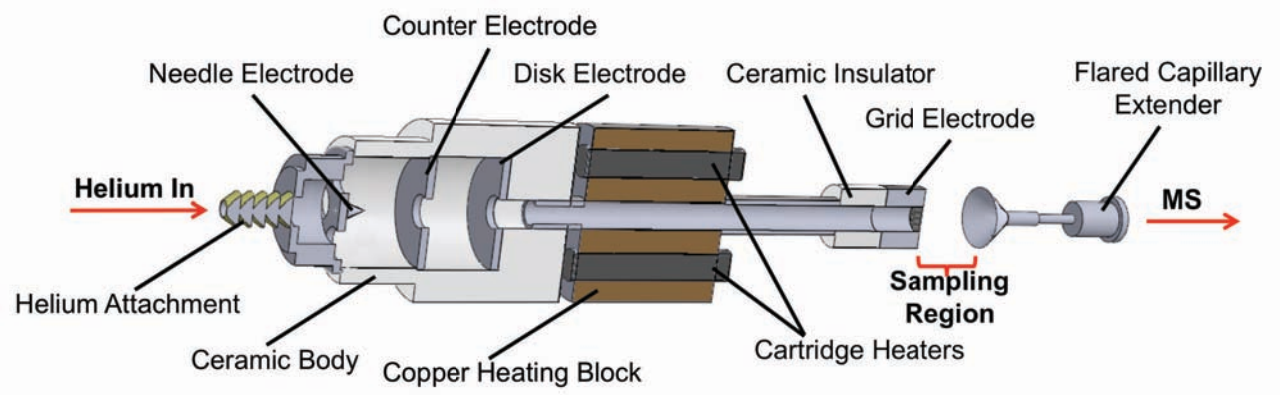


Figure 2-1. Cutaway diagram of the custom-built DART source.

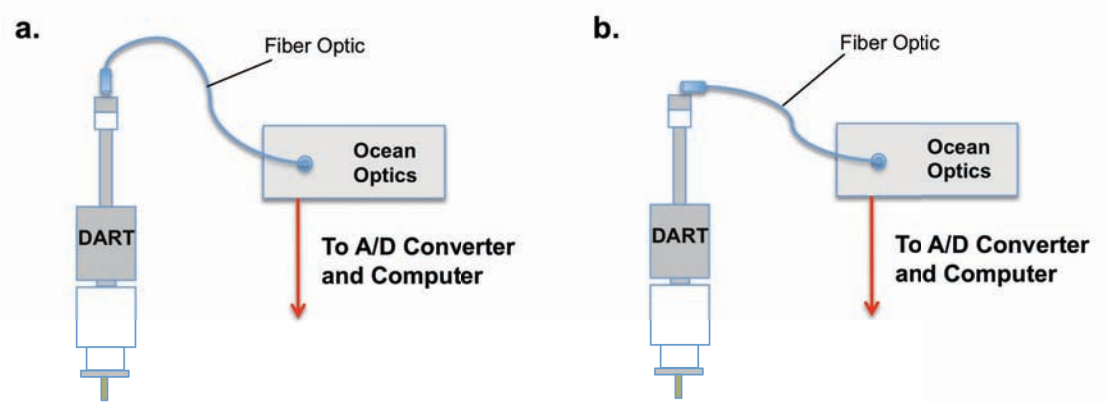


Figure 2-2. Possible configurations of DART source with fiber optic probe. The fiber optic is aimed (a.) down the bore of the DART source or (b.) orthogonal to bore of DART source.

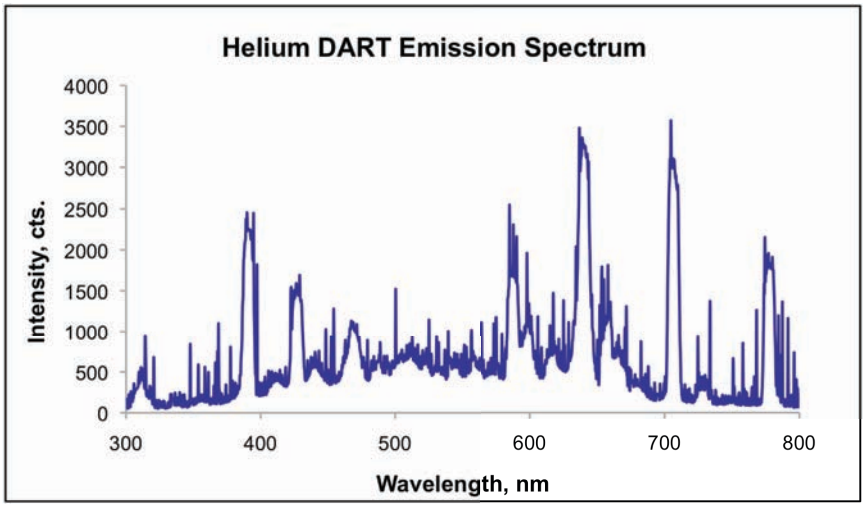


Figure 2-3. Helium DART emission spectrum. This spectrum was collected using the configuration shown in Figure 2-2 a.

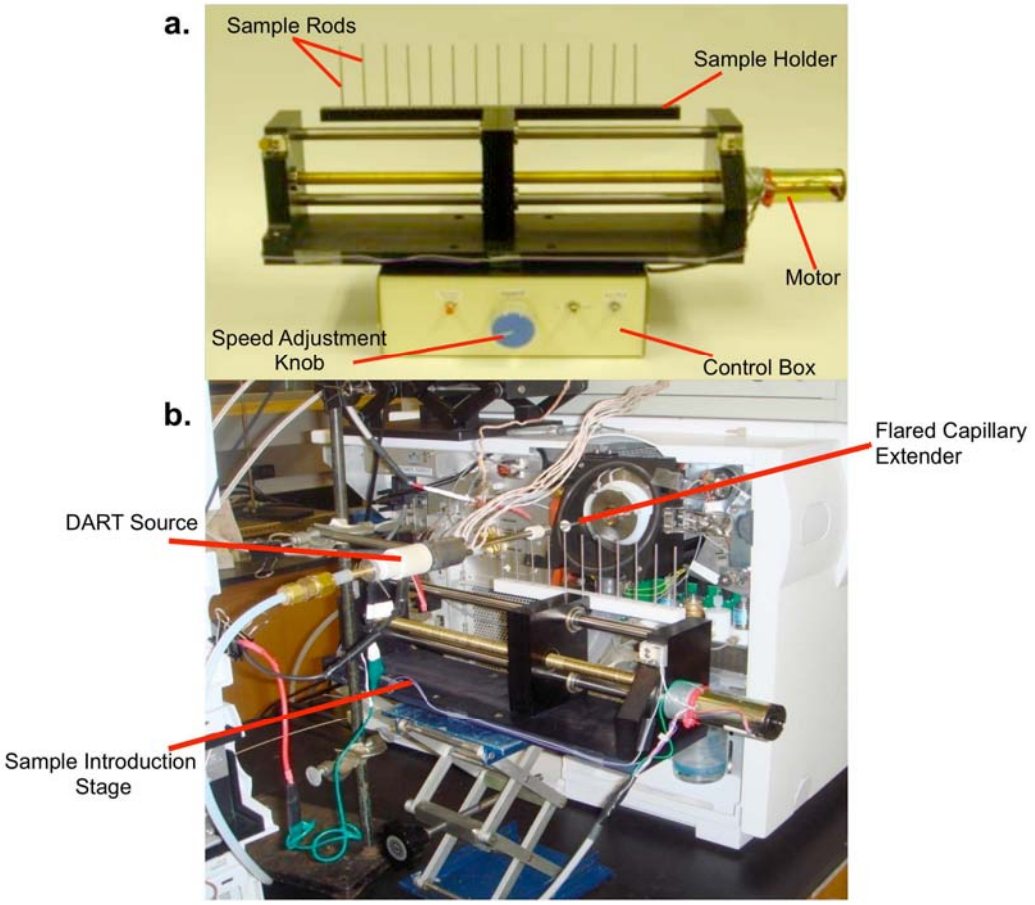


Figure 2-4. Pictures of the motorized sample introduction stage. The stage is shown (a.) with metal sample rods inserted into the sample tray and (b.) in position with the instrument.

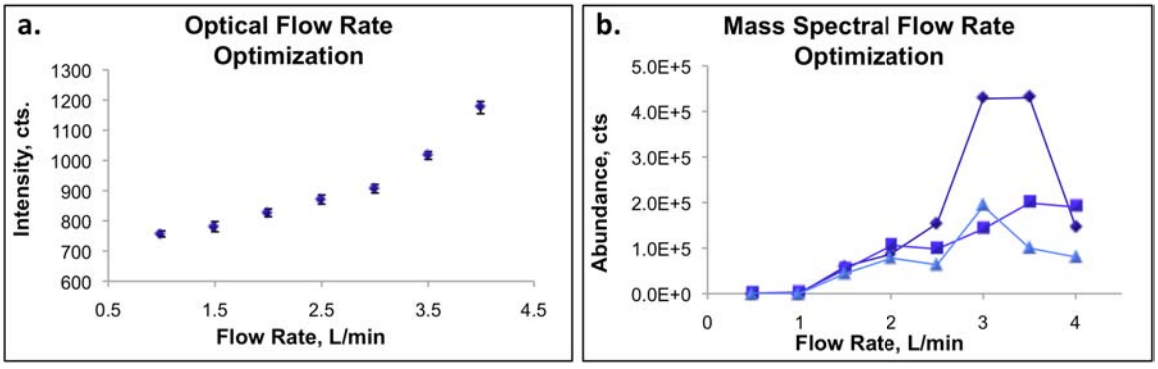


Figure 2-5. Gas flow rate optimization performed (a.) optically and (b.) with the mass spectrometer. Each plot in (b.) represents the responses of a single dodecylamine sample.

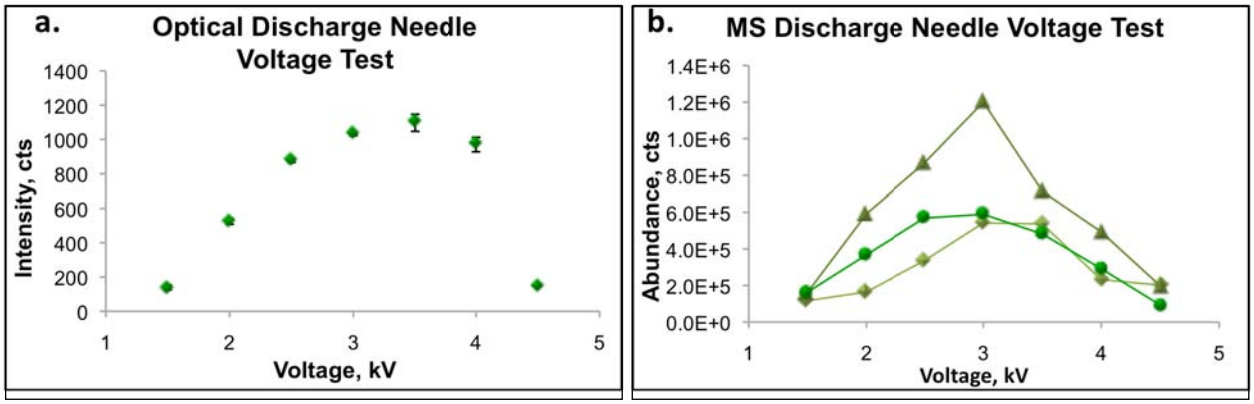


Figure 2-6. Discharge needle voltage optimization performed (a.) optically and (b.) with the mass spectrometer. Each plot in b. represents the responses of a single dodecylamine sample.

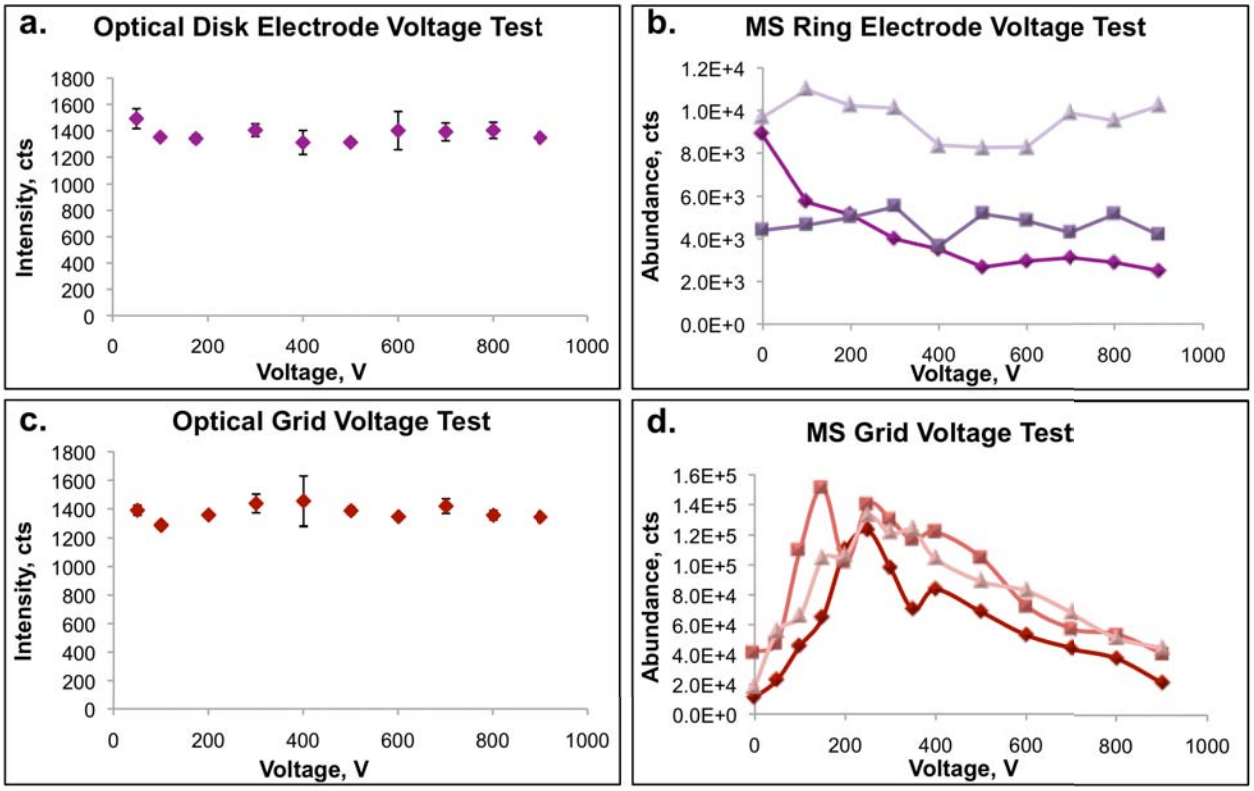


Figure 2-7. Disk and grid electrode optimizations performed (a. and c.) optically and (b. and d.) with the mass spectrometer. Each plot in b. and d. represents the responses of a single dodecylamine sample.

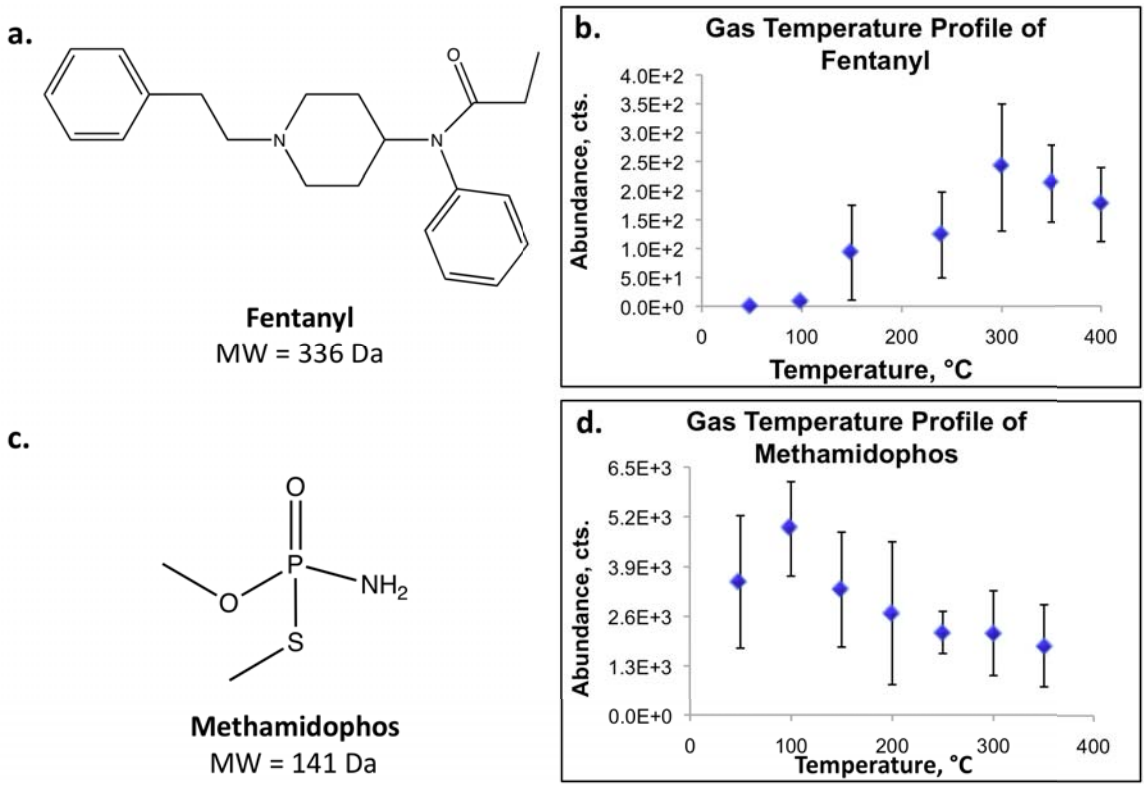


Figure 2-8. Effect of gas temperature on analyte detection. Fentanyl (a.), is optimally analyzed at a higher temperature than methamidophos (c.) as indicated by their temperature profiles (b. and d., respectively).

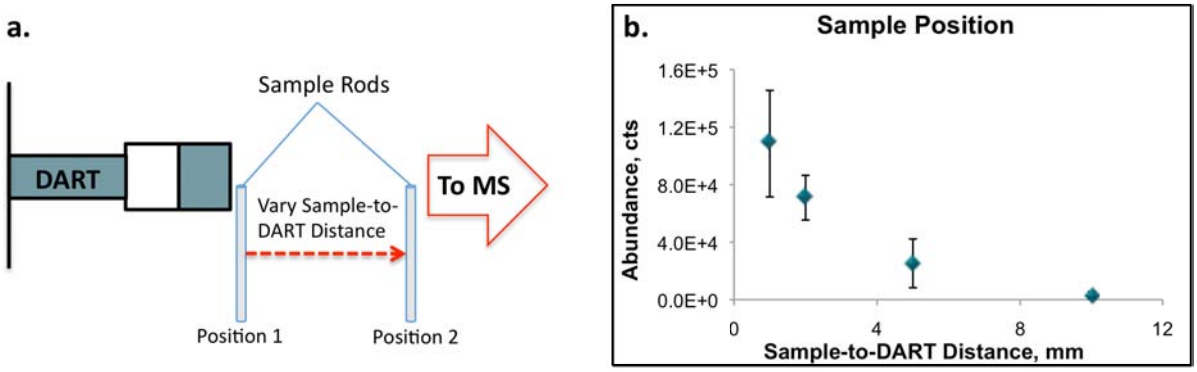


Figure 2-9. Diagram and results of sample positioning study. A diagram of how the sample placement was adjusted is presented (a.) as well as the response of dodecylamine as a function ion sample distance (b.).

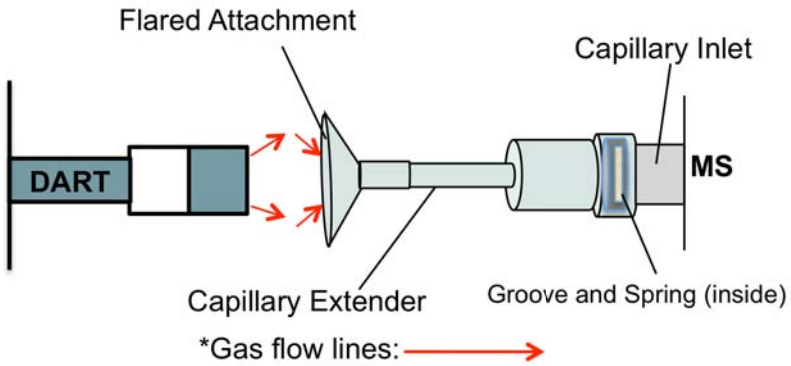


Figure 2-10. Diagram of flared capillary extender with end of DART source. The red arrows depict gas flow lines. A section of the extender is cut away to show the canted coil spring.

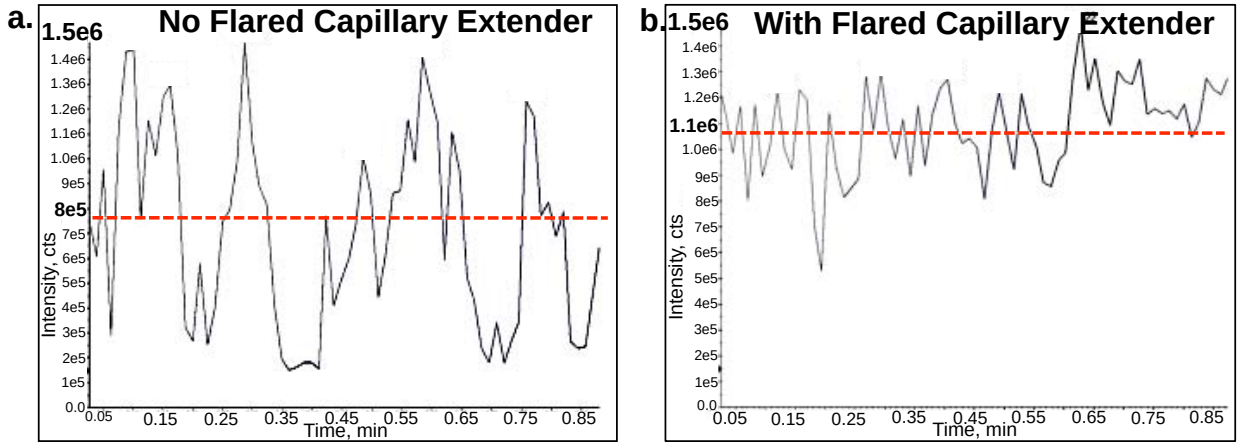


Figure 2-11. Extracted ion chromatograms of dodecylamine (a.) without and (b.) with the flared capillary extender.

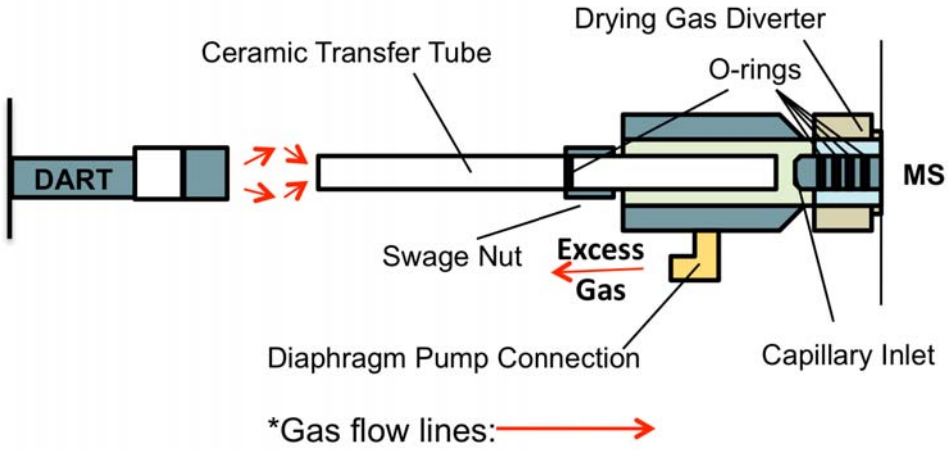


Figure 2-12. Diagram of the Vapur ® interfaced to the DART source with red arrows depicting DART gas flow lines. The drying gas flow lines will be shown in Figure 2-13.

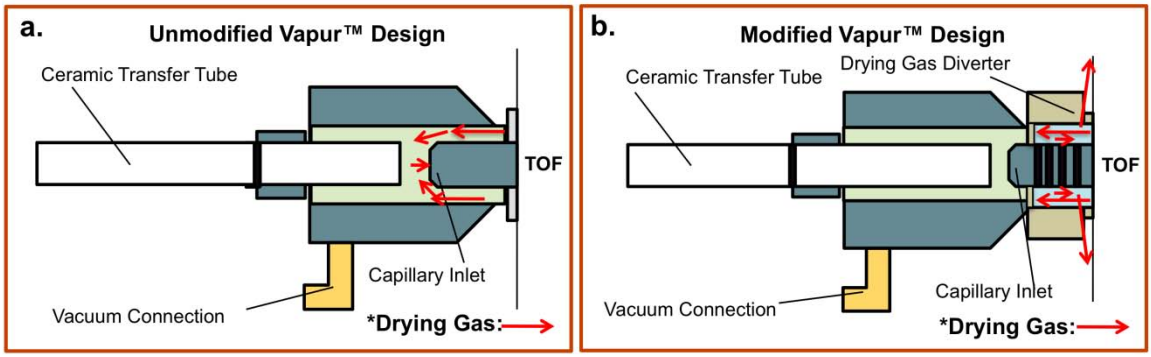


Figure 2-13. Diagram of Vapur® without and with the drying gas diverter. Red arrows represent the flow of drying gas from the TOF.

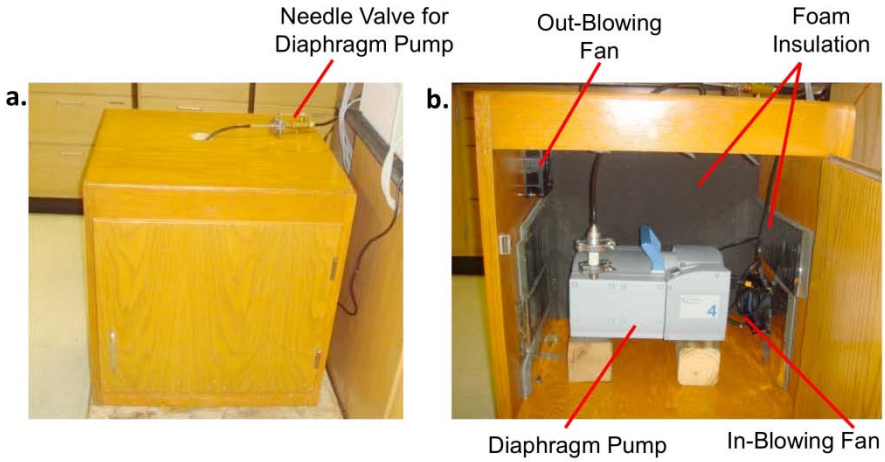


Figure 2-14. Photographs of the quiet cabinet (a.) closed and (b.) open, displaying the diaphragm pump.

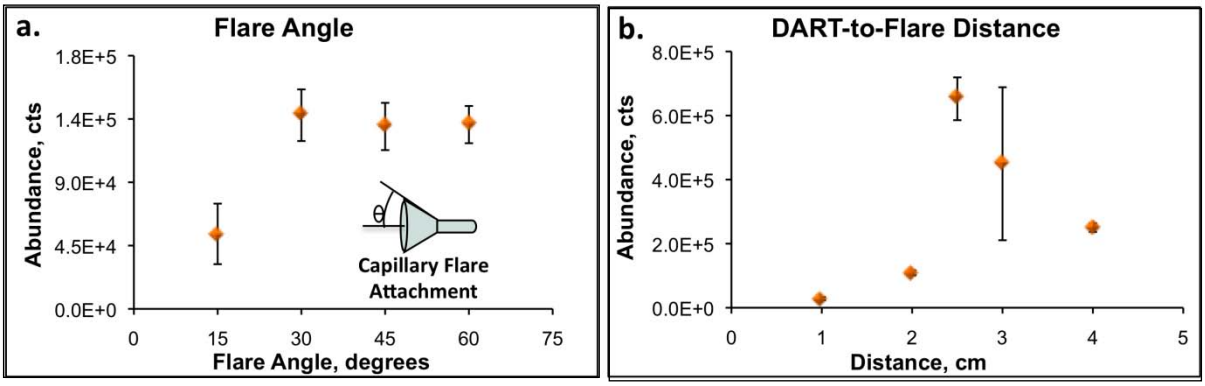


Figure 2-15. Flared capillary extender optimization studies. The studies were used to optimize (a.) flare angle and (b.) DART-to-flare distance.

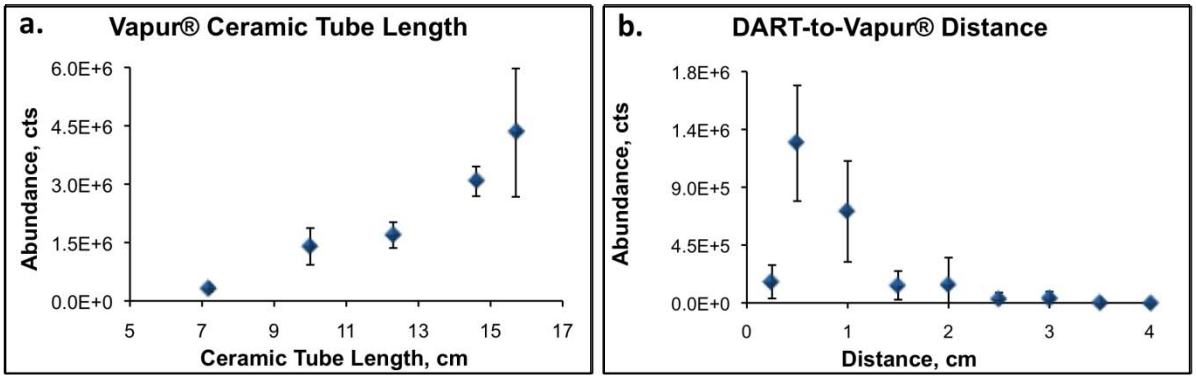


Figure 2-16. Less complicated Vapur® optimization studies. The signal abundances of 10 ng caffeine samples were plotted as a function of (a.) the ceramic tube length and (b.) the DART-to-Vapur® distance.

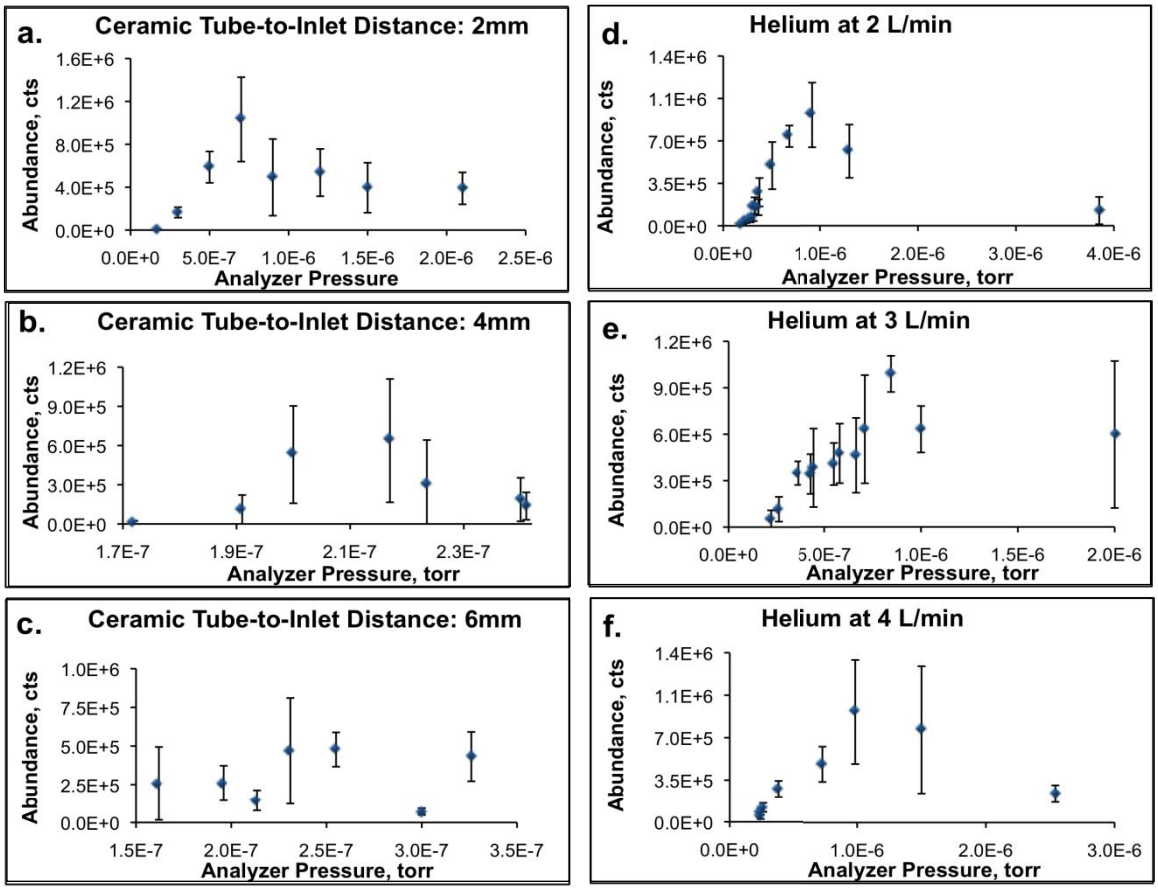


Figure 2-17. Additional Vapur® optimization studies. The signal abundance of 10 ng caffeine samples was monitored as a function of (a.-c.) tube to inlet distances and (d.-f.) the helium flow rate.

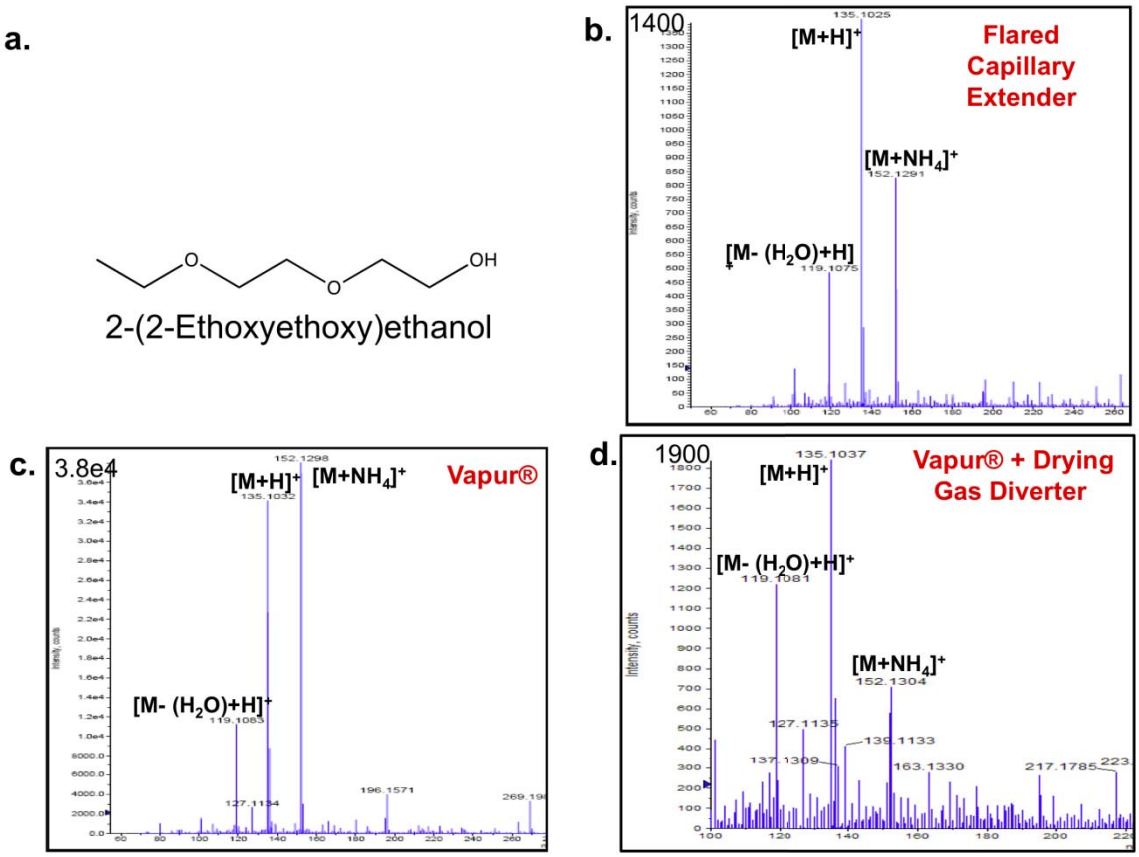


Figure 2-18. (a.) Primary contaminant in the DART-MS background and comparison of background spectra of the (b.) flared capillary extender and Vapur® (c.) without and (d.) with the drying gas diverter.

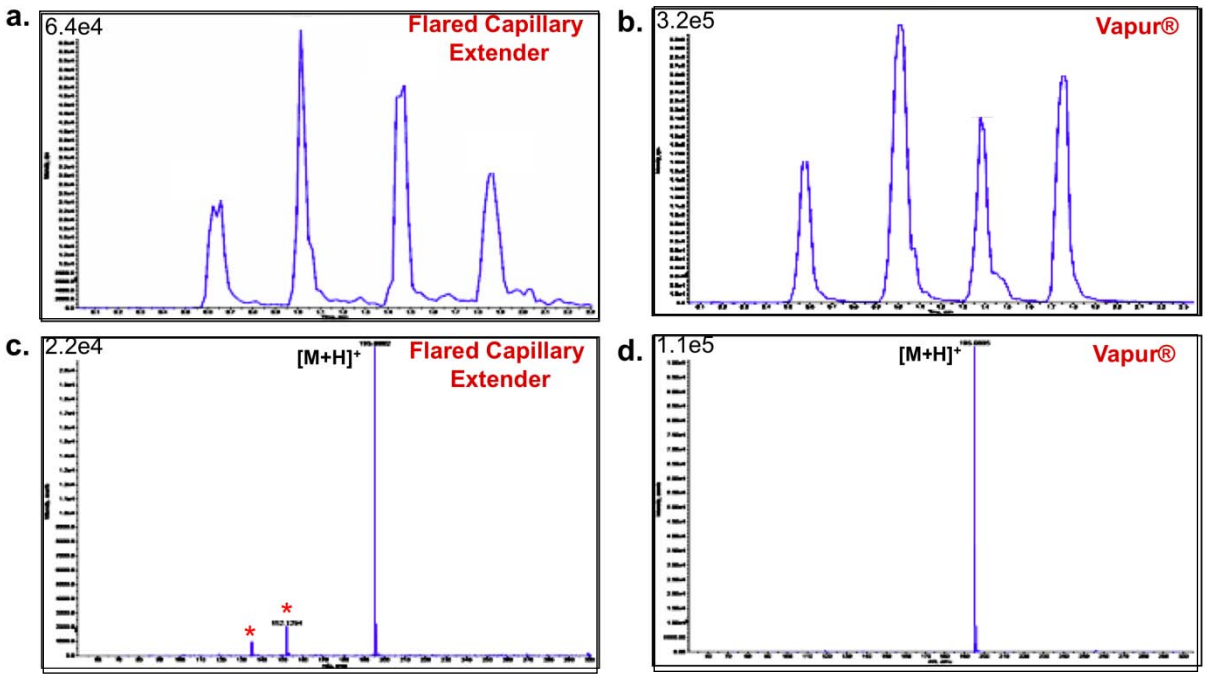


Figure 2-19. Comparisons of signal variation and signal abundance using the Vapur® and flared capillary extender. Extracted ion chromatograms of separate 1 ng caffeine samples are plotted in a. and b. Mass spectra of 1 ng caffeine samples are plotted in c. and d. Background ions are marked with (*).

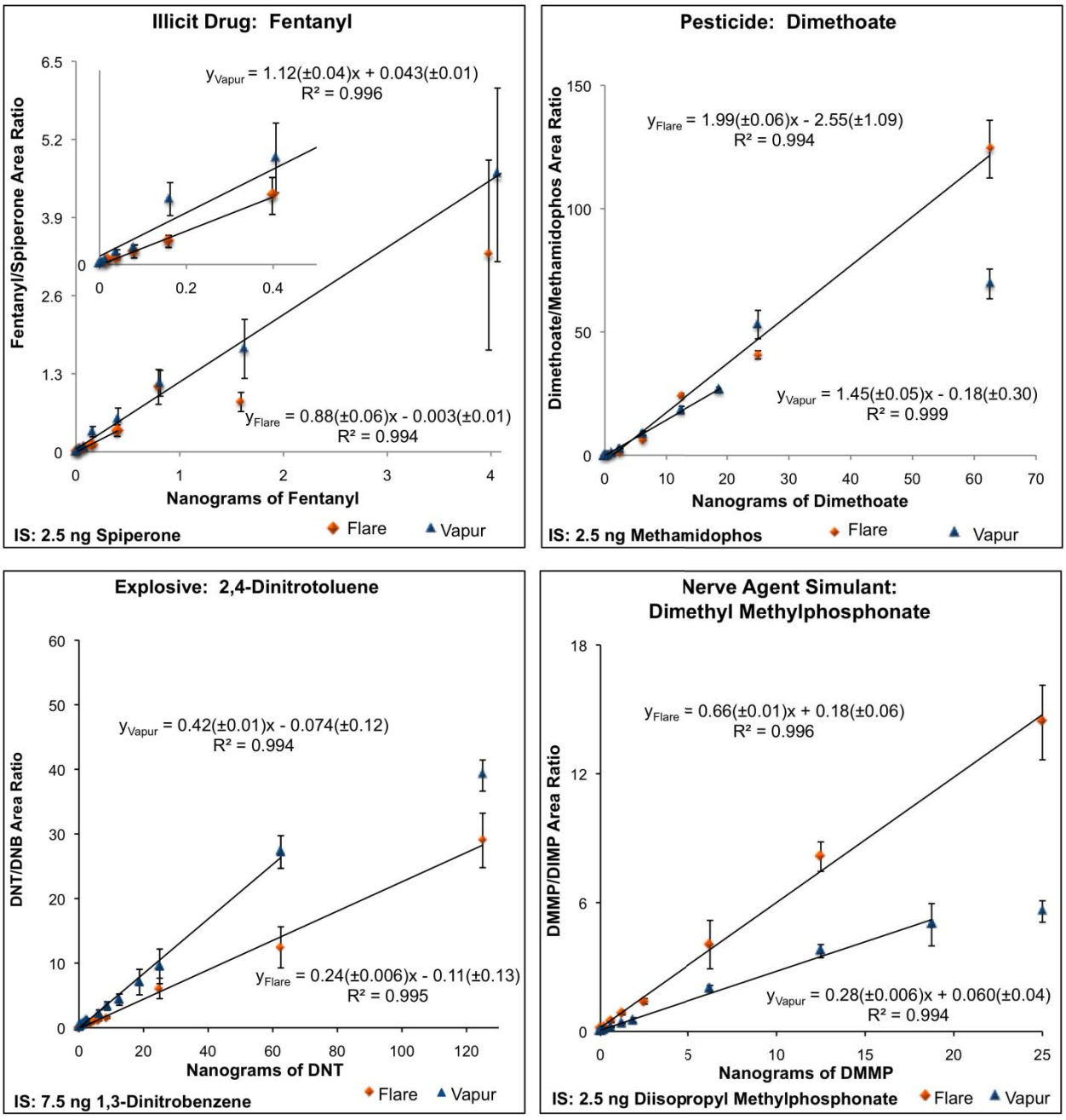


Figure 2-20. Calibration curves generated to compare figures of merit of the flared capillary extender and the Vapur®. Trend lines are not drawn through data points that were past the linear region of the curve.

# CHAPTER 3
# SELECTED APPLICATIONS

## Introduction

One of the greatest benefits of DART as an ionization technique is its versatility. Not only can it ionize compounds from a wide variety of surfaces, but it can be used to examine many different classes of compounds with a wide range of polarities. Figure 3-1 presents compound classes and groups that have been detected with the custom-built DART sourced described in Chapter 2. While many of these compound classes were purchased from chemical companies, several were synthesized by students in the UF Chemistry Department. The structures included in the chalcones group were synthesized by students in the UF undergraduate organic chemistry teaching labs. This experiment aptly demonstrated both the directness (absolutely no sample preparation was done) and rapidity of analyses by DART-MS. With the aid of Dr. Soledad Cerutti processing the data, approximately 250 chalcone samples were analyzed in a little over 4 hours.

In addition to analyzing many different compound types, a number of applications were performed with either “real” samples that originated from somewhere other than a chemical company or were performed with reaction mixtures to demonstrate the potential utility of DART-MS to the synthetic chemists in the UF Chemistry Department. Much of the work presented here was done as proof-of-concept, demonstrating the general applicability of DART-MS. These selected applications also demonstrate that the custom-built DART source is capable of the same types of analyses as a commercial version. Additional attention will be paid to studies involving the analysis of

thin layer chromatography plates and detection of nicotine from fingerprints with DART-MS.

## Experimental

### Instrumentation

The Agilent 6210 TOF (Agilent Technologies, Wilmington, DE) was used for all TLC plate studies. Its setup and usage are described in Chapter 2. The custom-built DART source and flared capillary extender described in Chapter 2 were also employed in this work.

### Chemicals and Materials

HPLC grade methanol was purchased from Burdick and Jackson (Muskegon, MI). HPLC grade methylene chloride and ACS grade hexane and ethyl acetate were purchased from Fisher Scientific (Fair Lawn, NJ). All solvents were used without further purification. Theophylline and caffeine were purchased from Sigma Aldrich (St. Louis, MO). Goodies Powder was purchased from a local grocery store. Cyclam and a reaction mixture containing diethyl 2-(dodecylamino)terephthalate were synthesized by Ian Rummel of the UF Chemistry Department. All TLC experiments were performed with Whatman 20 x 20 cm “Aluminum-backed Flexible Silica TLC Plates” with $UV_{254}$ indicator (catalog no. 4420222) cut to sizes ranging from 0.5 x 1 cm to 3 x 6 cm.

### Thin Layer Chromatography Plates

Thin layer chromatography (TLC) separates multi-component solutions into “spots” that vary according to the compound’s retention times. When solution components are known or suspected, as is often the case in fields like forensic science or food science, TLC spots can be identified by comparing the spot positions, related to the retention times, to the retention times of known materials. Synthetic chemists,

however, often face the challenge of separating materials from solutions that contain multiple unknown components for which no standards are available, making it difficult to ascertain the nature of the resulting TLC spots. In this situation, additional analytical techniques are required to ascertain the nature of the TLC spots. As demonstrated in the following paragraphs, DART-MS can be used to rapidly identify unknowns from TLC plates with a high degree of certainty. Very shortly after this work was completed but prior to publishing, Morlock et al. reported DART analyses of high performance TLC plates.[84]

**Explanation and Method**

At least two different methods have been presented for analyzing TLC plates with DART. Morlock et al. were able to analyze compounds from TLC plates by mounting the plates in a holder and tilting them 160° so that an exposed edge (cut into an eluted sample spot) could be introduced into the sampling region of a commercial DART source.[84] Kusai et al. employed a glycerol matrix to enhance detection of compounds from TLC plates.[106]

Presented here is a somewhat simpler method that employs a higher gas temperature than typically used in DART-MS analyses of small molecules. A number of different sampling geometries were tested, but the best results were achieved by horizontally positioning the plates against the end of the DART source (diagrammed in Figure 3-2). In this configuration, both the top and the bottom of the plate were exposed to the hot gas, which was thought to enhance thermal desorption. The glycerol method was also attempted here, but was dismissed because of the very high background ion count it produced.

Samples were deposited on the TLC plates 1 μL at a time, with 5 – 10 μL being deposited in total. Some TLC plates were incubated in chambers with varying amounts of ethyl acetate and hexane and others were spotted and analyzed without incubation. Eluted samples were visualized with a UV lamp and marked with a pencil. Sample spots were cut from the TLC plates in roughly 0.5 x 1.5 cm strips with DART sampling occurring across the short side of the strip.

**Heating effects**

As mentioned above, one of the most important factors in detecting analytes in this study was the gas temperature. Deposited on nonporous substrates such as glass, organic molecules with masses below 200 Da are typically desorbed with DART gas temperatures below 250 °C. Dodecylamine, as discussed in Chapter 2, does not require heating for DART-MS analyses. However, as demonstrated in Figure 3-3, additional heating is required for desorption from TLC plates. Appreciable protonated dodecylamine signal was not detected until the gas temperature was raised to 300 °C and drastic improvement was observed by raising the temperature above 400 °C.

This disparity in required gas temperatures in TLC plates versus smooth samples is not surprising. With smooth sample holders such as glass, very little interaction occurs between the analyte and its substrate. The porous TLC substrate offers an increased surface area allowing additional van der Waals interactions as well as other intermolecular attractions depending on the stationary phase to occur.

**Storage effects**

Though testing a TLC plate immediately after a separation is achieved is ideal, there are no doubt times when this is not convenient. To test the effects of storage time and, consequently, exposure to air, TLC plates were analyzed within minutes of

preparation and one month later. The month-old plate was stored in a drawer uncovered. As Figure 3-4 demonstrates, little change was observed between the spectrum of a freshly prepared caffeine-loaded TLC plate and that of a month-old plate. A fragment of caffeine at m/z 138 was observed with both of the plates, but it was likely formed by thermal degradation rather than exposure to air.

**Mixtures**

**Goody's Powder.** As an example of a commercial pharmaceutical product separated with TLC and analyzed with DART-MS, Goody's Powder was tested. The active ingredients of this over-the-counter pain medication are acetaminophen, aspirin, and caffeine. After incubation, three spots were visualized with a UV light. Of those, one was identified as caffeine and another was identified as acetaminophen. The mass spectrum of the second spot is given in Figure 3-5. With internal mass calibration using the phthalate fragment at m/z 149, sub-ppm mass accuracy was achieved with the protonated acetaminophen. The exact mass of this and all other compounds identified with accurate mass are given in Table 3-1. No ions other than the expected background ions were detected in the third spot. If this spot contained aspirin (a.k.a. acetylsalicylic acid), detection in positive mode would be unlikely because the compound would probably deprotonate to form a negative ion. Unfortunately, the instrument was not operable in negative mode when this test was done.

**Synthetic reaction mixture.** To prove the technique could be used in a capacity beneficial to synthetic chemists, a TLC plate used to separate components of a reaction mixture was analyzed. With exposure to UV light, eight different components fluoresced. After direct analysis of each of the spots, the sixth was found to contain the desired product, diethyl 2-(dodecylamino) terephthalate. A photograph of the TLC plate

and the mass spectrum corresponding to the sixth spot are given in Figure 3-6. This study provided information on the purity of the sample and allowed the researcher to better estimate when the desired product would elute during a large-scale preparative column separation of the reaction mixture.

**Whole TLC plate analysis.** Ideally, DART-MS could be used to analyze TLC plates with no prior visualization step (typically with a UV lamp). As a proof of concept, a TLC plate lane was spotted with caffeine, theophylline, cyclam, and adenine at various positions. For analysis, the TLC plate was slowly slid between the DART source and the capillary. Because the motorized stage was not yet built, this was done by hand. A total ion chromatogram (TIC) and the extracted ion chromatograms for each of the compounds are shown in Figure 3-7. Though varying degrees of sensitivity and fragmentation were observed, each analyte was detected. Cyclam was detected with the lowest signal-to-noise ratios, which could have resulted from improper sample positioning. A moving sample introduction stage equipped with a device for mounting TLC plates could reduce this effect and generally reduce the “hands-on time” by the operator. By knowing the rate at which the samples were introduced and the starting position, correlation between chromatogram peaks and location on the plate would be trivial.

**TLC Plates Study Conclusion**

A method has been presented for the analysis of thin layer chromatography plates using the custom-built DART source. A high gas temperature was demonstrated to effectively desorb the analytes used in this study. Though probably compound-dependent, analysis of fresh and old TLC plates produced similar results. With internal mass calibration, compounds from TLC-separated mixtures were successfully

indentified with accurate mass. These studies proved that, like the commercial system, the custom-built DART source is capable of desorbing and ionizing analytes from TLC plates.

### Nicotine Detection from a Smoker's Fingerprints

The goal of another proof-of-concept study was to use DART-MS to determine if a person had been smoking without testing his or her blood or urine. Though one method would be to test the breath of a person, it was decided that a better demonstration of DART as a surface ionization technique would be to test skin excretions. Fingerprints were thought to be an ideal source of skin excretions because they could be obtained in a completely non-invasive manner, preserved for later use if required, and could be analyzed without exposing the test subject to the 250 °C helium exiting the DART source.

The smoker who participated in this study was an interesting candidate because he typically handles machinery and industrial lubricants, which could contribute significantly to the "matrix" of the fingerprints. It should be noted that the smoker's participation in this study was completely voluntary and that the smoker was not required to smoke any additional cigarettes than he would have smoked in a normal day. No incisions or bodily fluids were taken for this study. Fingerprint collection was achieved by rolling a glass pipette between a smoker's index finger and thumb. No additional sample preparation was performed. Samples were directly analyzed by inserting the print-loaded area of the pipette into the gas stream of the DART source. Analyses were performed after smoking with and without hand washing.

## Fingerprint Analysis

### Fingerprints immediately after smoking

**No hand washing.** The first sample was taken moments after the smoker had smoked a cigarette prior to washing his hands. As shown in Figure 3-8, protonated nicotine was detected in low abundance. In much greater abundance were several peaks attributed to known industrial solvents or phthalates (industrial plasticizers). As will be demonstrated in Chapter 5, DART ionization is a competitive process. The presence of the many contaminants on the smoker's fingers may have caused some signal suppression when this mass spectrum was acquired.

**Hand washing prior to smoking a cigarette.** To solve the problem of the contamination observed above, the smoker washed his hands immediately prior to his next cigarette. Shown in Figure 3-9, a slightly larger nicotine signal was detected and the previously observed contaminants were greatly reduced with this combination of hand washing and smoking. The protonated nicotine peak observed here had better signal-to-noise than in the last spectrum and better mass accuracy (0.6 ppm error versus 6.1 ppm error in the previous spectrum).

**Hand washing after cigarette.** To determine if the nicotine observed above was excreted from the smoker's fingers or transferred directly from the cigarettes, the smoker washed his hands immediately after smoking but prior to sample collection. Upon analysis of the finger prints, no nicotine was detected (Figure 3-10). Only the contaminants shown in the previous spectrum were detected here. The series of peaks from 200 to 300 Da were suspected to come from soap used for the hand washing.

### Fingerprints twenty minutes after smoking

Approximately 20 minutes after the previous spectrum was acquired, additional fingerprints were collected. Some differences were observed between this spectrum (Figure 3-11) and the one acquired 20 minutes prior (Figure 3-10). First, the relative distributions of a number of the background ions changed. An explanation for this could be that the sample introduction was slightly different. If the fingerprint-coated pipette was held closer to the DART source, it would have been exposed to higher temperatures, which could promote desorption of the larger-mass contaminants. The more important difference between the two spectra was that a low-abundance nicotine peak was observed. As the smoker had not smoked a cigarette in 20 minutes and had limited his interaction with the items he typically handles, the detected nicotine was probably excreted from his fingers.

### Fingerprint Study Conclusions

A method for detecting nicotine from the fingerprints of a smoker was presented. With various combinations of smoking and hand-washing, varying nicotine signals were detected. As expected, the signal-to-noise ratio of protonated nicotine was affected by the presence of contaminants like machine lubricants. Hand-washing completely depleted the nicotine signal, but weak signals attributed to nicotine were regained after 20 minutes and were suspected to be the result of skin excretions. This proof-of-concept study demonstrated the utility of DART-MS in the analysis of components from fingerprints. This study should be repeated on fingerprints distributed on surfaces, first directly analyzed from glass slides and later analyzed from collected prints. One might take the direction described by Benton et al. of doping fingerprint dust with sorbent

materials, followed by DART-MS analysis.[107] It would also be very interesting to perform the same analyses using other pharmaceuticals or illicit drugs.

## Miscellaneous Applications

### Food Products

An area where DART-MS may see increased application in coming years is the food industry. Two examples are DART analyses of food products are given in Figure 3-12. The first spectrum was obtained by directly analyzing melted Dove dark chocolate with DART-MS. The primary alkaloid produced by cocoa beans, theobromine, and the listed ingredient, vanillin, were detected. Though caffeine detection was also expected, the overly abundant peak seen in this spectrum was suspected to originate from sample carry-over instead of the chocolate. The other spectrum in Figure 3-12 demonstrates that both the protonated molecule and the proton-bound dimer of limonene can be detected when directly analyzing orange peels. The dimerization demonstrates how highly concentrated the limonene is on the peel's surface. Interestingly, limonene was not detected when the flesh of the same orange was analyzed by DART-MS (not shown).

### Pharmaceuticals

The subject area where DART-MS has seen the most utility thus far is pharmaceuticals analysis. Drugs are often very good candidates for DART-MS analysis because they tend to be small molecules (less than 1000 Da) that possess functionalities amenable to DART ionization (amines, carbonyls, phenyl groups, etc.). Two examples of pharmaceuticals analyzed with the custom-built DART source are presented in Figure 3-13. In the first spectrum, an Excedrin Tension Headache tablet with its outer coating removed was positioned between the DART source and the mass

spectrometer. By doing so, the two active ingredients (caffeine and acetaminophen) were detected as protonated molecules as well as a proton-bound adduct of the two compounds. The twenty-dollar bill spectrum is a reproduction of the most famous DART-MS analysis. With no special sample preparation, the edge of a twenty-dollar bill was inserted into the DART gas stream. Confirmed with accurate mass, cocaine and nicotine were detected in high abundance. The presence of cocaine was not surprising as it has been detected on currency in a number of studies employing various analytical methodologies.[108-113]

**Flavors and Fragrances**

With DART-MS, one can rapidly see that pure vanilla extract and imitation vanilla purchased from a grocery store are different. Figure 3-14 contains spectra obtained by directly analyzing pure vanilla extract, imitation vanilla extract, Mexican vanilla extract, and, for comparison purposes, a vanilla-scented Little Tree air freshener. Peak identifications were based on exact masses. Of the four spectra, only the pure vanilla extract and the Mexican vanilla displayed a peak identified as protonated vanillin (sometimes called “methylvanillin”). It is not surprising that the synthetic vanilla flavoring, ethylvanillin, appeared in the spectra of the imitation vanilla and the air freshener. However, as ethylvanillin does not occur naturally, it was suspicious that the Mexican vanilla also contained the compound. The ethylvanillin detected in the Mexican vanilla could not be attributed to carry-over because it was analyzed in an entirely different week than the other samples, after the mass spectrometer inlet was cleaned several times. This indicated that the Mexican vanilla extract was artificially flavored. Ammoniated and deprotonated species of a simple sugar (either glucose or

fructose) were detected in the vanilla extract and imitation vanilla but not in the unsweetened Mexican vanilla or the air freshener.

## General Conclusion

Several different applications of the custom-built DART-MS have been presented in this chapter. Almost no sample preparation was done in any of the above studies, demonstrating the utility of DART as a rapid screening technique. However, making DART-MS more than just a screening technique, highly specific information was obtained and identifications were made with a high degree of certainty because the DART source was combined with high resolution-mass spectrometry (i.e. the TOF used in this work). These studies demonstrated that the custom-built DART source can be used in the same ways as the commercial DART source and that, like the commercial version, it can be applied to analyses in a wide variety of areas.

Table 3-1. Compounds of interest exact masses[a]

| | Ion Specie | | | |
|---|---|---|---|---|
| Compound | [M+H]+ | [M+NH4]+ | [M-H]+ | [2M+H]+ |
| Vanillin | 153.0546 | | | |
| Ethyl vanillin | 167.0703 | | | |
| Glucose or Fructose | | 198.0972 | 179.055 | |
| Limonene | 137.1325 | | | 273.2577 |
| Caffeine | 195.0877 | | | |
| Theobromine | 181.072 | | | |
| Nicotine | 163.123 | | | |
| Cocaine | 304.1543 | | | |
| Acetaminophen | 152.0706 | | | |

a. All masses are numbers represent mass-to-charge ratios, expressed in terms of Da.

| | |
|---|---|
| Pharmaceuticals | 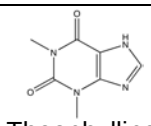 Theophylline 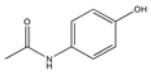 Acetaminophen 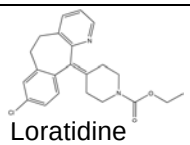 Loratidine 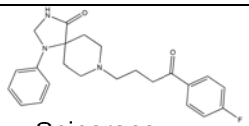 Spiperone |
| Polycyclic Aromatic Hydrocarbons |  Anthracene  Chrysene 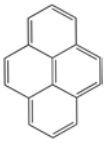 Pyrene 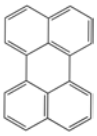 Perylene  Rubrene |
| Organometallics and Coordination Complexes | 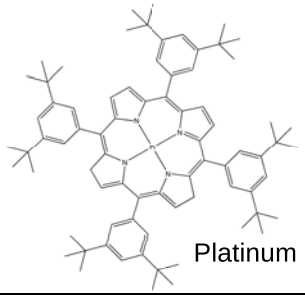 Platinum Oligomer 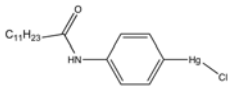 (4-dodecanamidophenyl) mercury(II) chloride |
| Pesticides | 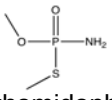 Methamidophos 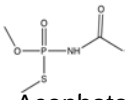 Acephate 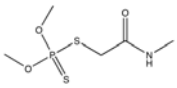 Dimethoate 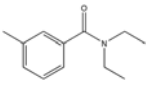 DEET |
| Chemical Warfare Agent Simulants | 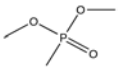 Dimethyl methylphosphonate 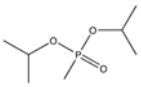 Diisopropyl methylphosphonate 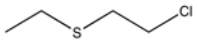 2-Chloroethylethylsulfide |
| Explosives | 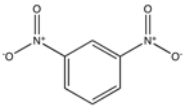 1,3-Dinitrobenzene 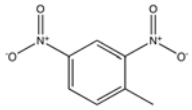 2,4-Dinitrotoluene 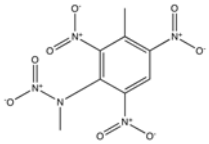 Tetryl 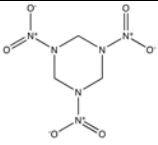 RDX |
| Flavors and Fragrances | 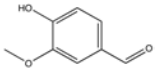 Vanillin 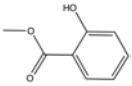 Methyl Salicylate 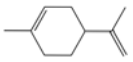 Limonene 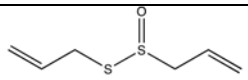 Allicin |
| Toxic Industrial Compounds | 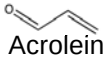 Acrolein 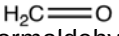 Formaldehyde 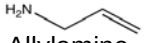 Allylamine |
| Compounds of Biological Relevance: Nucleotide Bases, Amino Acids, Carbohydrates, Metabolites | 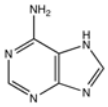 Adenine 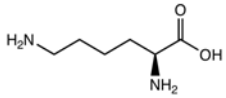 Lysine 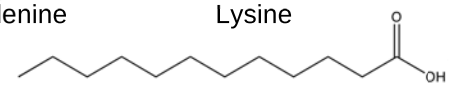 Lauric Acid 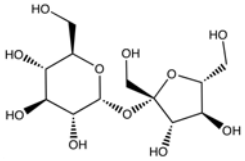 Sucrose 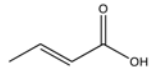 Crotonic Acid |
| Chalcones and Related Compounds | 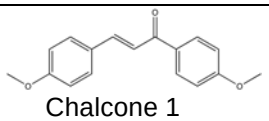 Chalcone 1 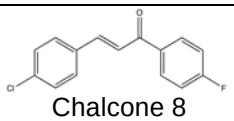 Chalcone 8 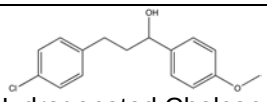 Hydrogenated Chalcone 5 |

Figure 3-1. Compound classes/groups analyzed by DART and example structures.

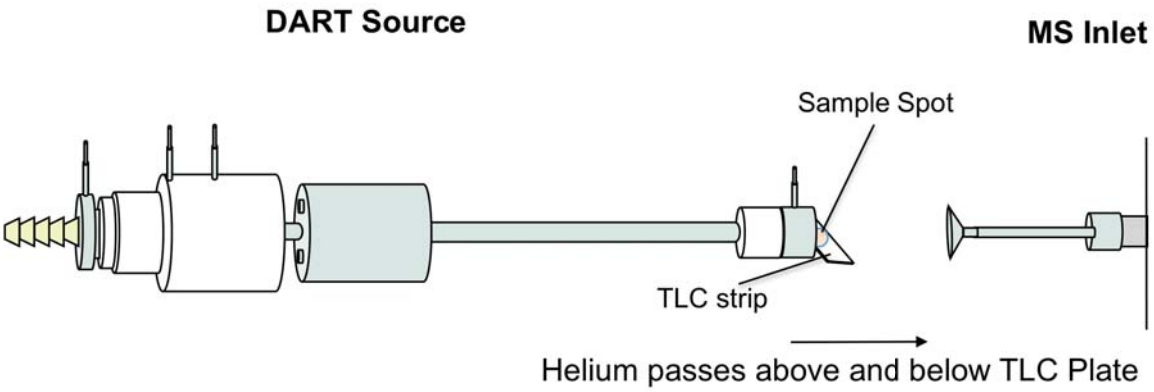


Figure 3-2. Diagram of the TLC plate sampling configuration.

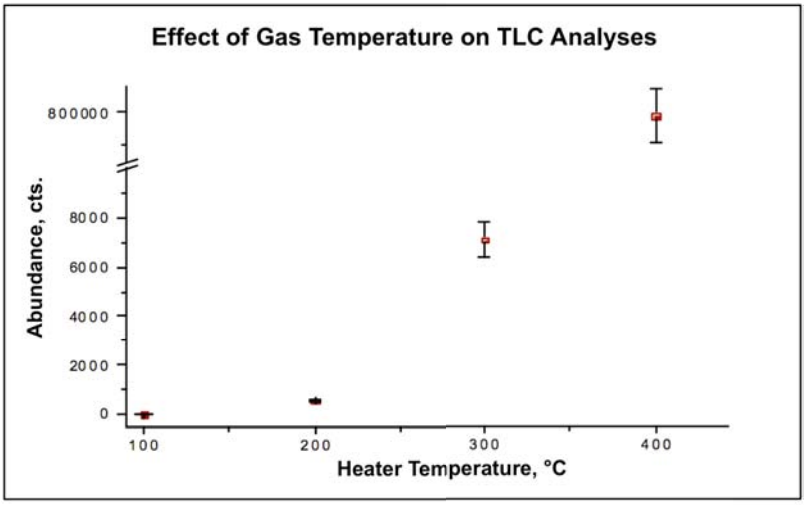


Figure 3-3. Effects of gas heater temperature on TLC plate analyses. Responses of protonated dodecylamine are given.

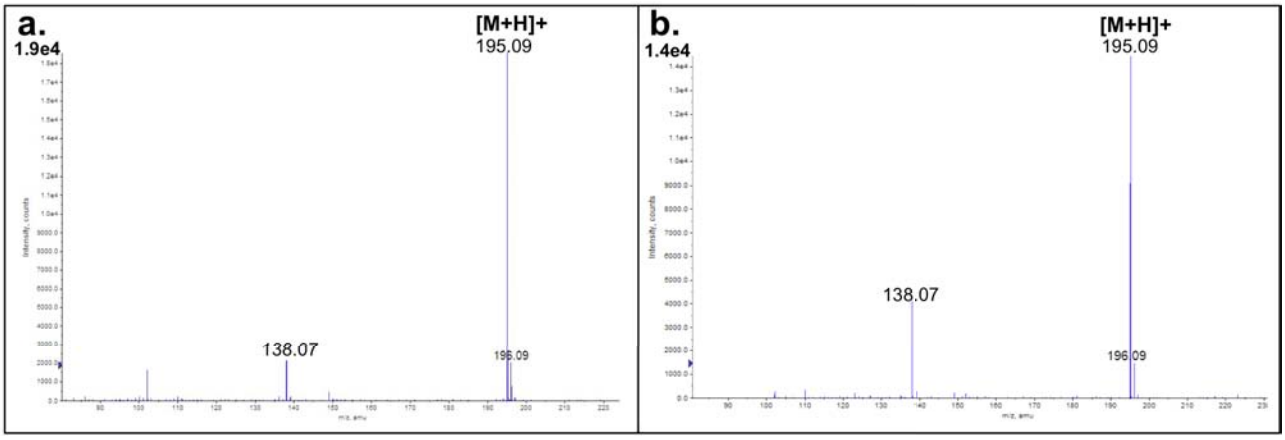


Figure 3-4. Effects of extended TLC plate storage. Spectra of a (a.) fresh TLC plate and a (b.) month-old TLC plate containing caffeine are presented.

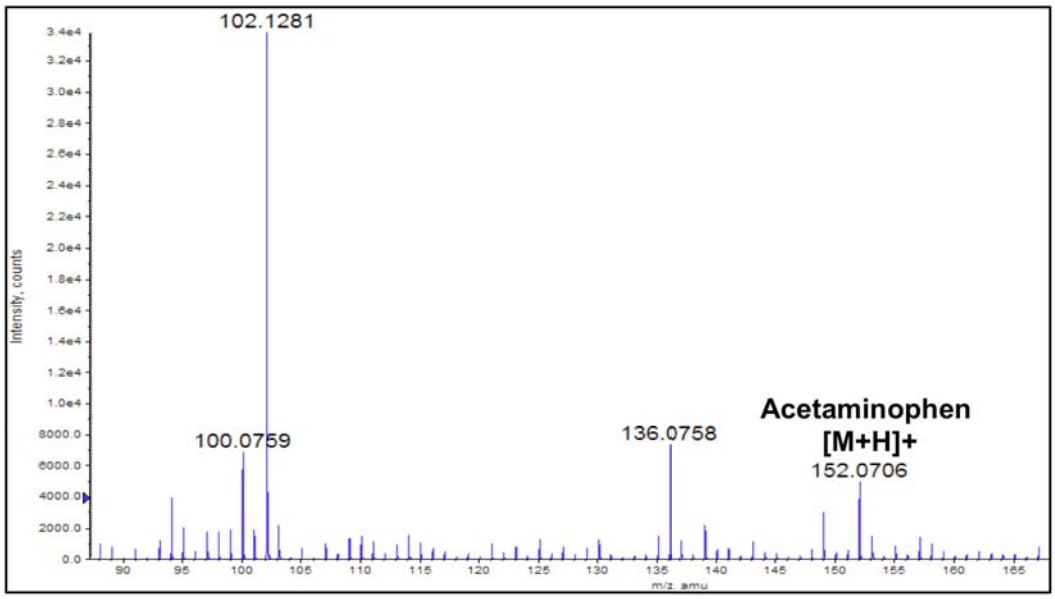


Figure 3-5. DART-MS analysis of the second spot from a Goodies Powder-loaded TLC plate.

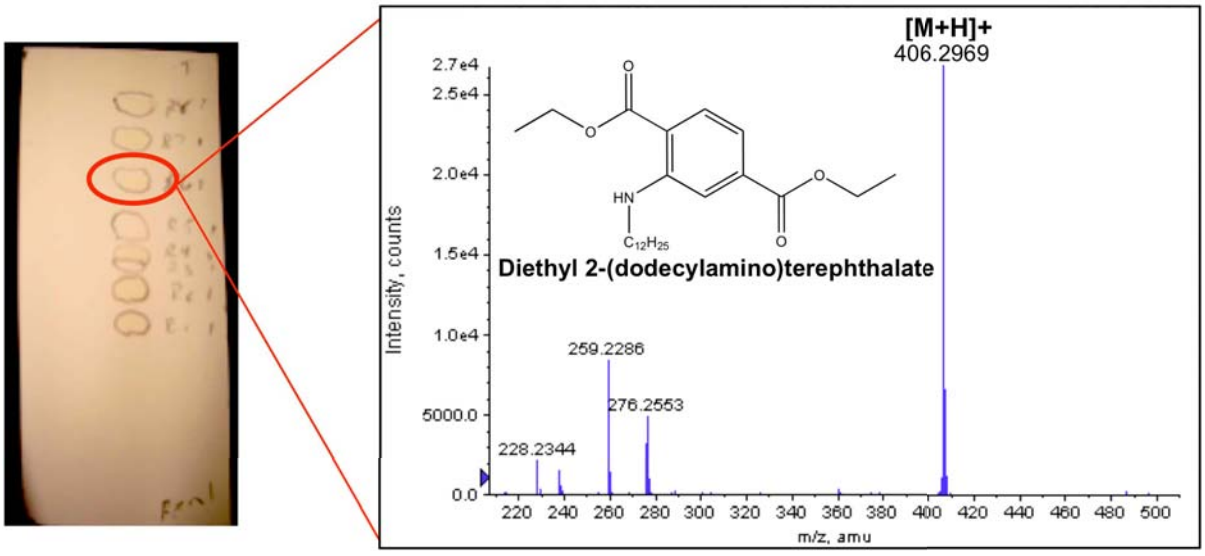


Figure 3-6. Photograph of TLC separation of synthetic organic reaction mixture and corresponding mass spectrum.

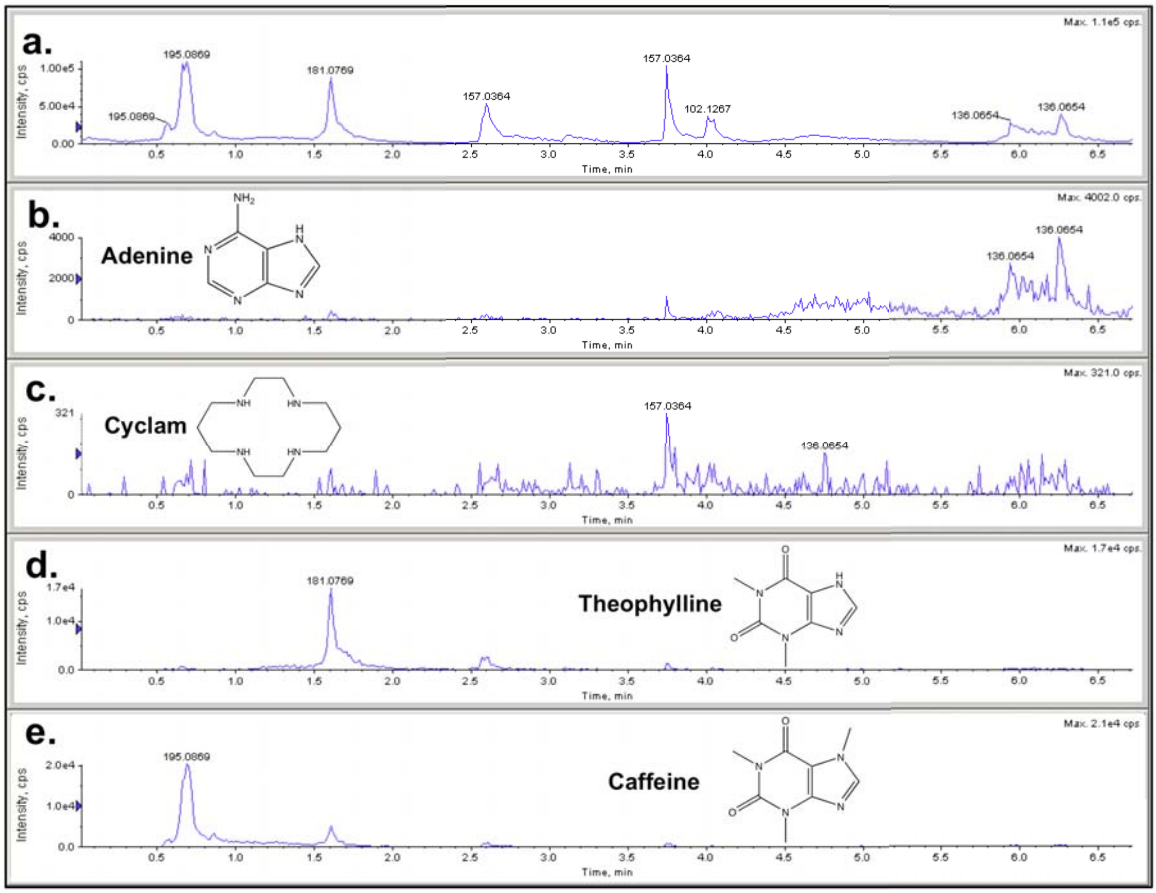


Figure 3-7. Whole TLC plate analysis by DART-MS. The total ion chromatogram (a.) and corresponding extracted ion chromatograms of (b.) adenine, (c.) cyclam, (d.) theophylline, and (e.) caffeine are presented.

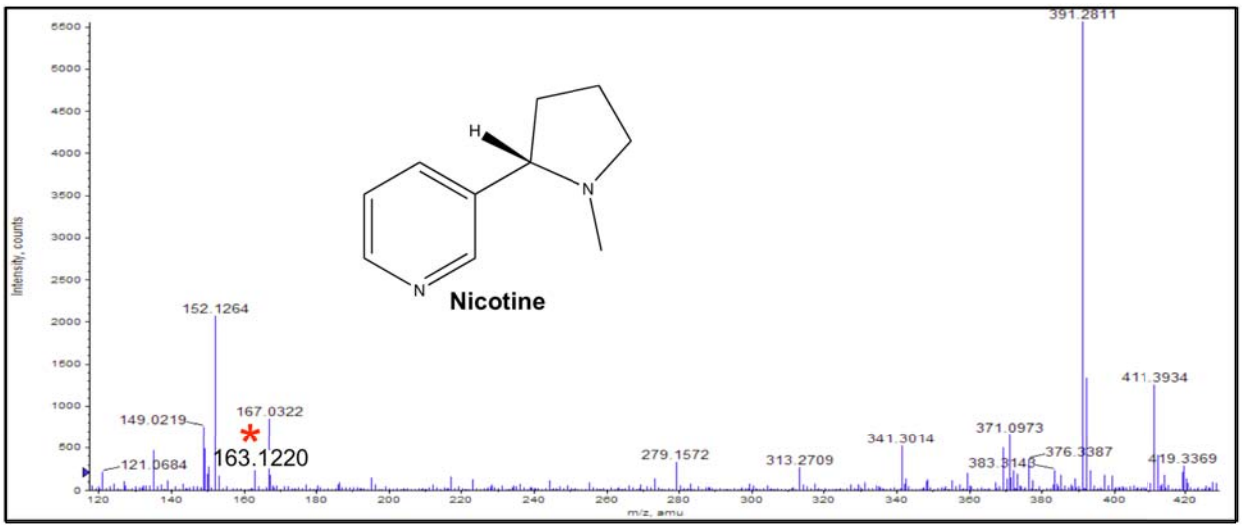


Figure 3-8. Spectrum of smoker's fingerprint after cigarette but before washing hands. Protonated nicotine is marked with (*).

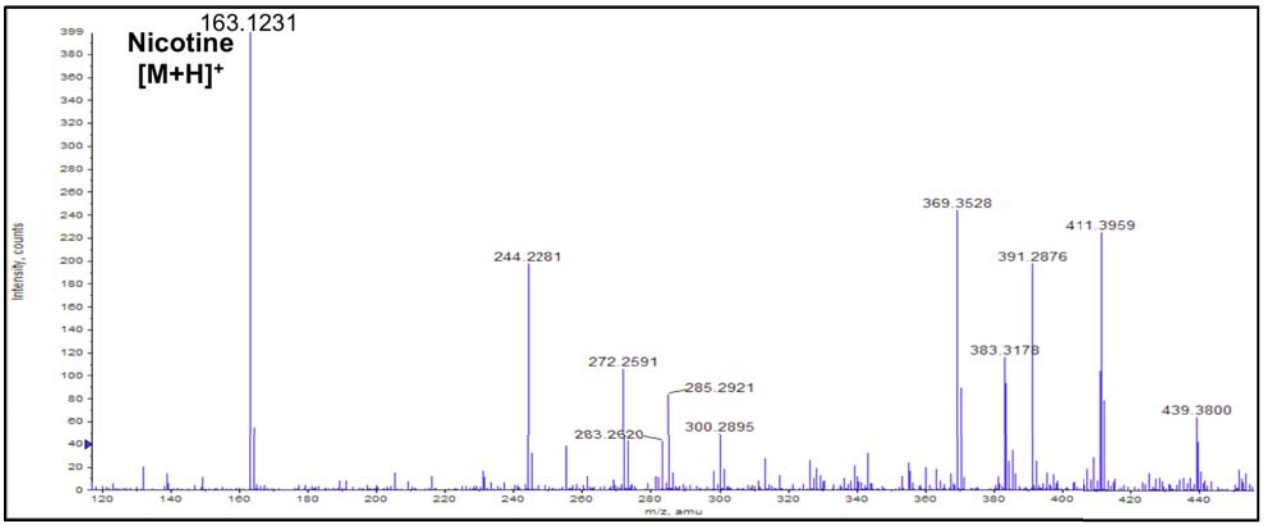


Figure 3-9. Spectrum of smoker's fingerprint after cigarette, hands washed before.

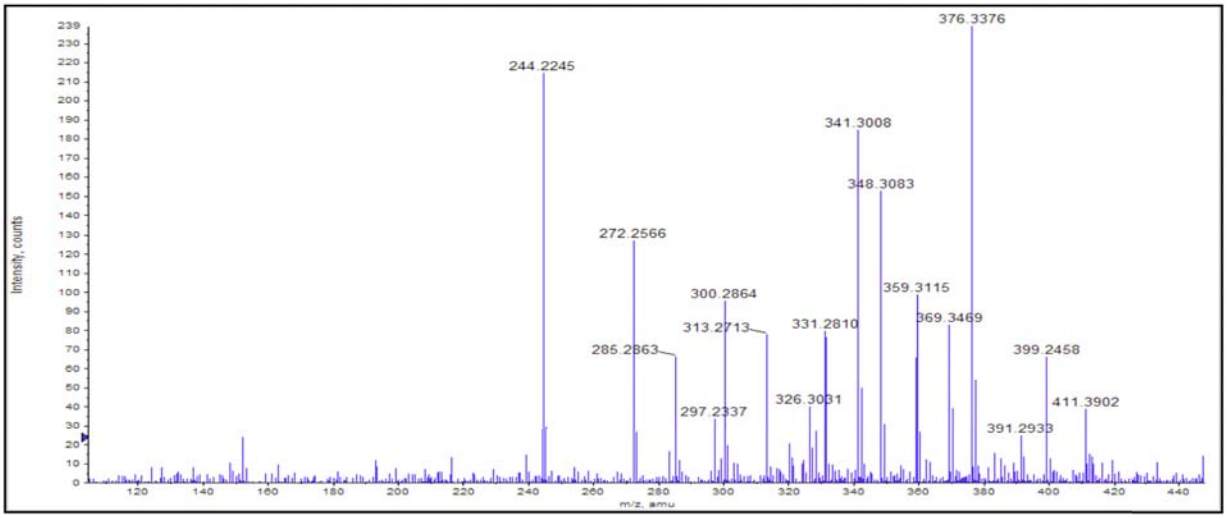


Figure 3-10. Spectrum of smoker's fingerprint after cigarette, hands washed afterward.

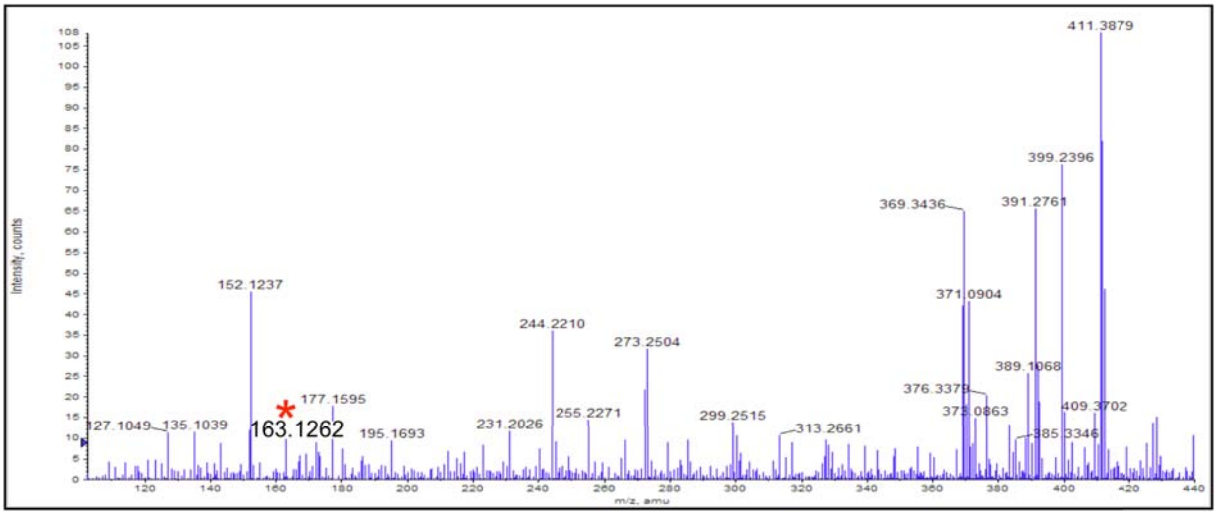


Figure 3-11. Spectrum of smoker's fingerprint 20 minutes after cigarette. Protonated nicotine is marked with (*).

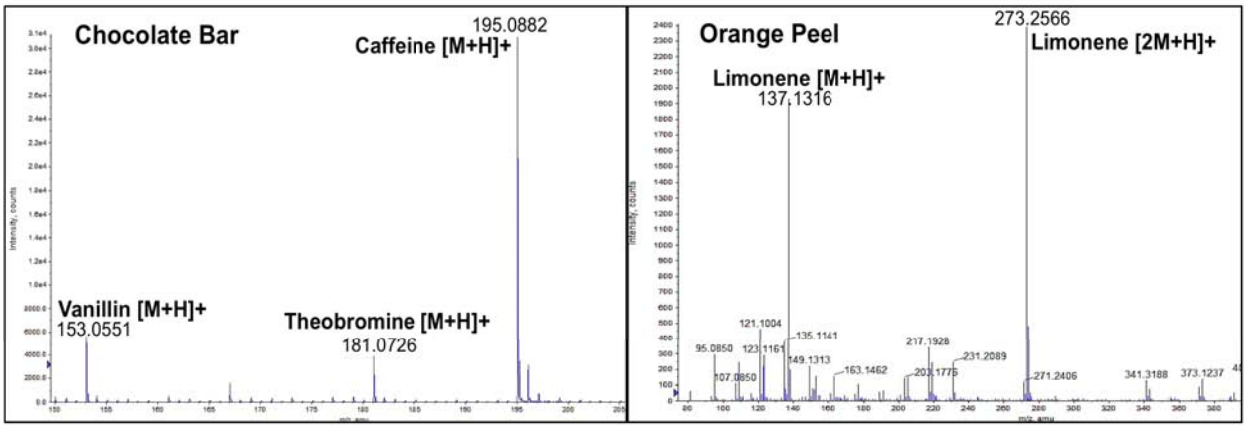


Figure 3-12. Examples of DART-MS analyses of food products. Mass spectra acquired by analyzing melted chocolate bar and an orange peel are presented.

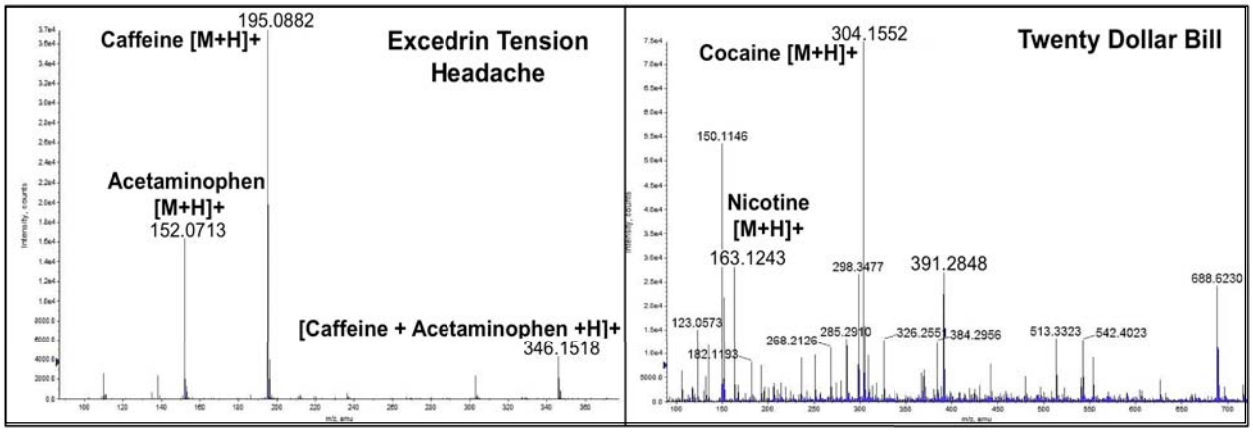


Figure 3-13. Examples of DART-MS analyses of pharmaceuticals. Mass spectra from the analysis of a pain reliever and a twenty-dollar bill are presented.

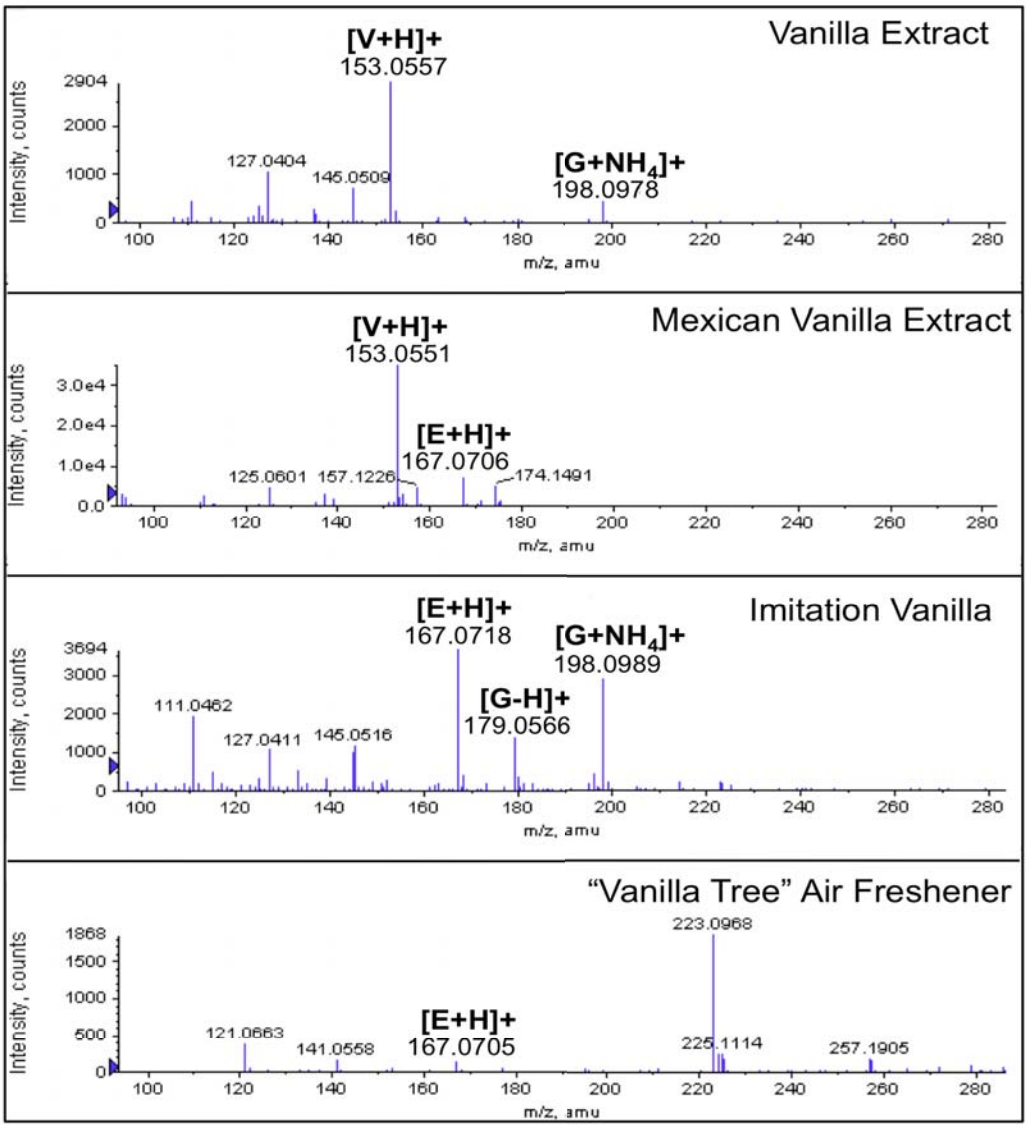


Figure 3-14. Examples of DART-MS analyses of different vanilla flavorings and a vanilla air freshener. Note: "V" stands for vanillin, "E" stands for elthylvanillin, and "G" stands for glucose or fructose.

# CHAPTER 4
# SUBSTRATE EFFECTS

## Introduction

An important consideration in developing analytical methods is the analyte matrix. Many analytical methods incorporate several preparative steps for extracting, purifying, and pre-concentrating samples prior to the actual analysis. Often described as their greatest advantage, ambient ionization techniques like DART can be performed with a minimal number of preparative actions (sometimes none). However, when little or no sample preparation is done, the technique must overcome numerous obstacles that may hinder the analysis including the means by which the sample is introduced and the presence of compounds that can compete for ionization. In the following sections, the effects of analyte substrate surface, material, and matrix in DART analysis will be discussed. Included in this discussion are examples of how the ambient environment might affect and effect ionization of analyte molecules.

## Experimental

### Instrumental

The Agilent 6210 TOF mass spectrometer was used for all TLC plate studies. Its setup and usage are described in Chapter 2. The custom-built DART source described in Chapter 2 was applied to all of the studies presented here. The flared capillary extender was used for all cases except the signal suppression studies. The Vapur® modified the TOF inlet throughout the suppression studies. The gas temperature was varied according to application and will be specified in the discussion of each study. The motorized stage described in Chapter 2 was used for sample introduction for all data that are plotted on an Excel graph.

### Chemicals and Materials

HPLC grade methanol, acetonitrile, water, and isopropanol were purchased from Burdick and Jackson (Muskegon, MI). Methylene chloride (HPLC grade), hexane, ethyl acetate, dimethyl sulfoxide, ammonium hydroxide, nitric acid, sodium chloride, sodium acetate, and ammonium acetate were purchased from Fisher Scientific (Fair Lawn, NJ). All solvents were used without further purification. Glycerol was purchased from Mallinckrodt (St. Louis, MO). Caffeine, spiperone, 2,6-dinitrotoluene, 1,3-dinitrobenzene were purchased from Sigma Aldrich (St. Louis, MO) and were dissolved in methanol (caffeine and spiperone) or acetonitrile (2,4-dinitrotoluene, 1,3-dinitrobenzene). Dimethyl methylphosphonate and diisopropyl methylphosphonate were purchased from Alfa Aesar (Ward Hill, MA) and dissolved in methanol. Dimethoate and methamidophos were donated by Northrop Grumman Corporation (Baltimore, MD) and prepared in methanol. The “Nitroaromatics and Nitramine Explosives in Drinking Water” mixture (Catalog no. 33900) was purchased from Restek (Bellefonte, PA) and diluted in acetonitrile. Deuterated water was purchased from Cambridge Isotope Laboratories (Andover, MA). Ocean water was collected from the Canaveral National Seashore (Titusville, FL). “Cab Cube” cabernet sauvignon was purchased from a local Target store.

## Surface Effects

### Explanation and Method

It was demonstrated with thin layer chromatography plates in Chapter 3 that surface morphology can play a role in the desorption of an analyte during DART-MS analysis. The influences of substrate and surfaces were studied with the following compounds: fentanyl, dimethyl methylphosphonate (“DMMP”), 2,4-dinitrotoluene

("DNT"), and dimethoate. These analytes were chosen because they are of Department of Homeland Security interest, representing an illicit drug, a nerve agent simulant, an explosive, and a pesticide. In addition to determining the effects of surface on analyte detection, a goal of these studies was to determine the analytical figures of merit of this DART source.

Calibration curves were generated to evaluate the sensitivity (calibration curve slope), limit of detection, and linearity for each of the analytes. Internal standards (IS) that were similar to the analytes in volatility and ionization properties were used to reduce signal variability and responses were reported in terms of analyte-to-IS extracted ion chromatogram peak area ratios. Six replicates were analyzed for each data-point. All four analytes were tested on smooth glass and smooth metal surfaces. The liquid analyte, DMMP, was also tested on rough glass and rough metal surfaces. Preliminary tests with solid analytes indicated that sampling from the rough surfaces resulted in a 10x reduction in signal abundance and a decision was made to forego generation of calibration curves with dimethoate, fentanyl, and DNT on rough surfaces for the sake of time. Information on the target analytes along with their selected internal standards and DART gas temperatures are presented in Table 4-1.

**Substrate preparation and sample introduction.** Glass and stainless steel rods with diameters of approximately 2 mm were obtained from the UF Chemistry Glass and Machine Shops. The rods were cut to lengths of 6.5 cm. From their respective cutting processes, the ends of the glass rods possessed rough surfaces and the metal rods possessed smooth surfaces. Measures were taken to obtain smooth and rough surfaces of both substrate types. To create smooth glass surfaces, half of the glass

rods were held in a Bunsen Burner flame for a short period of time until their ends were smooth but not rounded. To create rough metal surfaces, the metal rods were sanded by the Machine Shop. The ends of all of the "rough" rods appeared to have been sandblasted with a homogenous granular surface (no long striations were visible). All "smooth" rods' ends were smooth (no obvious markings) and flat (no rounding from the flaming process).

The rods were inserted into the tray of the sample introduction stage as described in Chapter 2 and samples were deposited onto the flat ends facing upward prior to analysis. Samples were "driven" in front of the DART source with the stage motor operated at its maximum rate and then stopped. A camera aimed from above the DART source sampling region and a video monitor were used to monitor the position of the sample posts so that all samples could be brought to the same location for analysis. Analyte responses were monitored with the real-time chromatograms plotted by the Agilent TOF operating software while each sample rested in front of the DART source. Samples were driven out of the sampling region after their analyte responses returned to the baseline. Sample rods were soaked with methanol or acetonitrile and heated with the DART gas between analyses for cleaning. All analytes except DMMP were allowed to dry prior to analysis. DMMP was immediately analyzed to prevent sample losses due to evaporation.

**Results and Discussion**

The calibration curves generated with analyte and each substrate are presented in Figure 4-1. The figures of merit for each analyte/substrate combination are listed in Table 4-2. The limit of detection was calculated according to the following equation:[105]

$$LOD = 3\sigma_{Blank} / m. \quad (4\text{-}1)$$

In equation 4-1, $\sigma_{Blank}$ is the standard deviation of the blank and *m* is the slope of the calibration curve. Linear ranges were calculated by subtracting the limit of detection from the highest sample quantity where the calibration curve was still considered linear ($R^2 > 0.99$) assuming linearity through the LOD.

Based on the preliminary tests, smooth surfaces were determined to be better for analysis of the solid analytes (DNT, dimethoate, and fentanyl) than rough surfaces. The rough surfaces were not disregarded for DMMP because it is a liquid and more volatile than the other compounds. The added surface area of the rough surfaces was hypothesized to provide better control of the thermal desorption of DMMP. This would perhaps allow more DMMP to be desorbed while the sample was positioned correctly between the DART source and the inlet of the mass spectrometer and not earlier in the process of moving the sample into the DART stream. When a comparison was done, however, very little difference in any of the figures of merit was seen between the two surface morphologies or the two material types. This at least indicated that the rough surface did not hinder the analysis of the semi-volatile liquid, DMMP.

Though differences in the figures of merit were detected for dimethoate, fentanyl, and DNT on glass and metal, neither glass nor metal rods consistently produced better results. Slightly calibration better slopes with both substrates were achieved with dimethoate than with fentanyl, but the limits of detection were similar for both compounds because the background levels at m/z 230 (dimethoate $[M+H]^+$) were higher and more variable than those at m/z 337 (fentanyl $[M+H]^+$). The dramatically worse results obtained with DNT may have resulted from less efficient negative ion formation by DART. Another contributor is the poorer sensitivity of the TOF when run in negative

mode. Additionally, the $^{13}C$ isotope of the largest background contaminant, suspected to be deprotonated glucose, had the same nominal mass as the $[M-H]^-$ ion of DNT. This compound increased both the abundance and variation in blank measurements. The reduction in sensitivity due to instrument problems and background contributions seems especially possible when considering that Song et al. reported an LOD of about 4.5 pg for nitroaromatic explosives with negative mode DART-MS using a JEOL TOF.[65]

### Conclusion from Surface Effects Studies

The surface studies showed little difference between glass and metal substrates for the three compounds that are solids at room temperature. For DMMP, a semi-volatile liquid, detection was independent of the surface material and morphology (this statement is limited to “smooth” versus “rough” surfaces and does not include “porous” surfaces). These similarities are actually a good testament to the versatility of DART and its utility in the analysis of analytes from different substrate surfaces. The other goal of this study, to establish the analytical figures of merit for this technique, was accomplished for four different model compounds. The results of the analytes forming positive ions (fentanyl, dimethoate, and DMMP) reported in Table 4-2 are similar to those reported for the commercial DART source.[50,54,72]

## Alternative Surfaces

### Explanation and Method

As was demonstrated in Chapters 1 and 2, the greatest advantage of DART-MS is the ability to introduce and analyze samples directly. Substrates such as pharmaceutical tablets and plant material lend themselves to fairly simple introduction because they either can fit directly into the sampling region or small segments can easily be excised and placed into the DART gas stream. In applications where

pesticide analysis is required or in the event of a chemical warfare attack, the analytes of interest may be distributed over a large area and sample substrates may include sand, soil, concrete, or other materials in the immediate vicinity. In an effort to explore detection from alternative media, target analytes were spiked onto sand, soil, concrete, cotton swabs, aluminum foil, and more. Target analytes in these studies included pesticides, illicit drugs, nerve agent simulants, volatile organic compounds, metabolites, and explosives. In the following paragraphs, the analysis of dimethoate, a pesticide, and dimethyl methylphosphonate, a nerve agent simulant, from a number of alternative media will be described. Because of the anticipated real-world variability of the surfaces in question, the purpose of these studies was to establish the feasibility of direct detection from the various surfaces rather than to establish a detailed set of figures of merit.

**Sample Preparation and Analysis**

**Sand and soil samples.** Sample solutions, 1 mg/mL in concentration, were auto-pipetted into samples of sand or soil for a final “concentration” of 50 ppm (w/w). To better distribute the analyte, the pipette tip used for sample deposition was used to stir the sand/soil. Samples were allowed to dry after thorough distribution. To retrieve the analytes from the soil/sand matrix, a cotton swab wet with methanol was stirred throughout the mixture until it appeared to be coated. After they had dried, the swabs were shaken and blown briefly to assure that no sand or soil particles could fall off. Immediately prior to analysis, the sample-loaded swabs were rewetted with 150 µL of methanol and introduced by hand into the DART gas stream. The DART heater was set to 350 °C for sand samples and 450 °C for soil samples.

**Concrete samples**. Sample solutions in 1 mg/mL concentrations were deposited onto chunks of concrete in 10 µL aliquots and allowed to dry. Immediately prior to analysis, 10 µL of glycerol was deposited on top of the sample-loaded area. The DART source was tilted 10° downward to sample from the glycerol-covered concrete (diagramed in Figure 4-2) for analysis.

**Activated carbon.** For vapor collection, pure solid or liquid samples were placed in open 1.5 mL Eppendorf tubes that were allowed to stand upright inside 30 mL scintillation vials. Resting in the bottom of the scintillation vials was a thin layer of activated carbon (20 mg). For sample collection, the scintillation vials were closed and incubated at room temperature for 30 minutes (DMMP) to 8 hours (dimethoate).

Approximately a quarter of the activated carbon was loaded between the two mesh pieces of the sample holder for direct analysis as pictured in Figure 4-3. The hollow sample holder consists of an outer brass section into which two pieces of stainless steel mesh are placed. Another brass section screws into the outer brass section to hold the pieces of mesh in place. The sample-loaded brass holder was inserted between the DART source and the mass spectrometer inlet for analysis, allowing the DART gas stream to pass through it (Figure 4-4).

## Results and Discussion

**Sand and soil.** Spectra acquired with dimethoate-loaded sand, soil, and concrete samples are shown in Figure 4-5. As mentioned above, elevated gas temperatures (450 °C vs. 350 °C for sand) were required to detect samples from soil. This was attributed to the increased porosity of the soil compared to sand that led to an increase in sample adsorption. Results with DMMP (and many of the other compounds tested) were comparable but are not displayed. The signal-to-noise ratios presented

here are not ideal, but these data demonstrate that DART-MS can be used to analyze sand and soil. With further optimization of the sample retrieval and introduction, these spectra could probably be improved and levels lower than 50 ppm (w/w) could be detected. Similar results were observed when the sand and soil samples were analyzed in the holder designed for sorbent analyses.

**Concrete.** A mass spectrum of dimethoate analyzed from concrete is presented in Figure 4-6 a. To detect analyte molecules from concrete it was necessary to apply a liquid matrix to the area suspected to contain the analyte molecules. The glycerol matrix was suspected to dissolve the analytes from the concrete surface prior to exposure to the hot DART gas stream, thus less heating was required for analyte desorption than with dry concrete. It is also possible that analyte molecules were desorbed from the surface from the sheer force of the rapid-moving helium atoms passing over it. Detection of dimethoate and many of the other compounds tested was not possible without both the glycerol matrix and a gas temperature of 450 °C. The disadvantage of using the liquid matrix addition technique in DART analysis is that signal suppression will occur if the analyte has a lower proton affinity than the matrix. For example, if any of the analytes used in this study had proton affinities lower than 874.8 kJ/mol (the proton affinity of glycerol), suppression would be very likely.[66] Background subtraction using a glycerol blank improved the quality of the spectra obtained by this method. A comparison of dimethoate mass spectra with and without background subtraction is presented in Figure 4-6.

Because of the shape of the concrete samples and the normally tight geometry of the sampling region, it was necessary to tilt the DART source downward approximately

10° toward the samples (refer to Figure 4-2). Now all new commercial DART sources are equipped with movable stages for adjusting the sampling geometry.[114] Again, the signal-to-noise values detected were less than desirable, but these experiments did demonstrate that DART-MS could be used to detect analytes from concrete.

**Activated carbon.** A mass spectrum displaying protonated dimethoate analyzed from activated carbon is presented in Figure 4-7 a. It should be noted that the activated carbon never came into contact with the dimethoate sample bed, but instead was exposed to dimethoate vapors in a closed chamber for 8 hours. When the more-volatile DMMP was incubated with activated carbon for just 30 minutes, an intense signal of the protonated DMMP molecule and its proton-bound dimer were detected, Figure 4-6 b. Additional ammoniated-DMMP species were also observed. These results demonstrate that analytes may be detected from sorbent materials. Instead of loading exposed sorbent into a sample holder, an action that may promote sample carry-over, it is easy to envision pre-made “sorbent packs” that could be hung in a room to monitor air purity or worn on clothing to monitor the presence of nerve agents. After exposure for a given time, the packs could be analyzed by DART-MS.

**Conclusions Regarding Alternative Substrates**

Although different operating conditions and some instrumental modifications were required for each, the ability to perform DART-MS analyses from sand, soil, concrete, and sorbent materials was demonstrated. As indicated by the varying degrees of success, further development and optimization studies would be required to establish these methods for routine analyses.

## Suppression Studies

As discussed in Chapter 1, DART is among several ionization techniques considered to be governed by a mechanism akin to atmospheric pressure chemical ionization (APCI). Being an APCI technique, various competing chemical reactions can occur among analyte molecules, contaminants, and reagent ions during DART ionization. Depending on the ionization characteristics of the substances involved, varying proportions of the desired target analyte ions may be observed. Signal suppression is said to have occurred if, for example, fewer analyte molecules are protonated because a higher-proton affinity contaminant is present and competing for available protons. This phenomenon will be discussed further in Chapter 5. Other effects may also cause apparent ion suppression, such as a decrease in analyte desorption due matrix components.

In the following studies, the target analytes caffeine and methamidophos were combined with various matrices to observe suppression. Their structures are presented in Figure 4-8. Caffeine and methamidophos were chosen for this study because they are small molecules known to both desorb and ionize well by DART and because they are representative of the types of analytes typically analyzed with DART-MS (drugs, pesticides, etc.). Caffeine and methamidophos solutions were combined with matrix solutions for final target analyte concentrations of 5 ppm each. Three categories of "matrices" were tested here: salt, solvent, and "real" matrices. Sample solutions were deposited in 0.5 µL aliquots and allowed to dry before analysis. Four replicates were analyzed for each data-point. Sums of the different ion species responses (protonated molecule abundance plus ammoniated molecule abundances) of each analyte are plotted. All analyses were performed with the gas heater set to 250 °C.

## Salt Matrices

**Explanation and method.** The suppressive effect of inorganic salts has been discussed in studies involving matrix-assisted laser desorption ionization (MALDI), surface-assisted laser desorption ionization (SALDI), and electrospray ionization (ESI).[115-118] With DART, the presence of salts co-crystallized with the analytes was suspected to reduce analyte volatility either by physical submersion in the salt matrix (with a resultant difficulty in desorption) or by ion pair formation. To determine if the presence of salts has an effect on DART detection, solutions of 5ppm caffeine and methamidophos were combined with varying quantities of sodium chloride (NaCl), sodium acetate ("NaAc"), and ammonium acetate ("AmAc").

**Results and discussion.** The responses of caffeine and methamidophos relative to their average unspiked (no additives) responses are plotted as a function of salt concentration in Figure 4-9. Variation was observed in the responses of both analytes. Somewhat unexpectedly, only NaAc appeared to impact the response of caffeine, but not methamidophos. As no suppression was observed with NaCl or AmAc with methamidophos, this effect was disregarded. Because no discernable trend was detected with the non-volatile NaCl, it was concluded that the presence of salts at these levels (up to 25 mg/mL) does not reduce analyte volatility.

The only salt that appeared to affect the response of both analytes was ammonium acetate. With both methamidophos and caffeine, significant improvements in signal were achieved with an AmAc concentration of 12.5 mg/mL. The response of methamidophos further improved with 25 mg/mL, but did not with caffeine. Upon plotting the ammoniated and protonated species of methamidophos separately, a more pronounced effect was seen with the ammoniated ion than with the protonated specie

(Figure 4-10). These data indicate that the observed signal enhancement was due to a dopant effect, which will be discussed later in this chapter. This was not the case for caffeine because ammonium-adducted ions were not observed.

**Solvent Matrices**

**Explanation and method.** Non-conductive solvents are known to suppress signal in electrospray ionization (ESI).[119] Because it does not rely on an electric field gradient or a conductive nebulizer for ionization, DART ionization should be unaffected by solvent conductivity. However, as the solvent can effectively be considered a contaminant competing with the analyte for ionization, its composition is of concern. In the following studies, the effects of various solvents were tested. The analytes dissolved only in methanol were considered unspiked. Other solvents commonly used in ESI were tested, including isopropanol and acetonitrile. To determine if conductivity was important, hexane was combined with the analytes.

A solvent with a moderate proton affinity (PA), ethyl acetate (PA = 835.7 kJ/mol), and a solvent with a higher proton affinity, dimethyl sulfoxide ("DMSO", PA = 884.4 kJ/mol), were tested to evaluate their competitive effects.[66] Table 4-3 presents the proton affinities and boiling points of the solvent matrices applied here. To assure solvent presence during the desorption/ionization event, samples were not allowed to dry prior to analysis and instead were deposited onto the glass rods immediately before introduction into the DART gas stream.

**Results and discussion.** The responses of caffeine and methamidophos relative to their average unspiked (no additives) responses are plotted as a function of added solvent percentage in Figure 4-11. With concentrations up to 10 percent, none of the solvents except for DMSO produced a significant reduction in analyte signal. The

responses of both caffeine and methamidophos were reduced significantly with 50 percent hexane. This effect was not attributed to solvent conductivity but rather poor sample deposition. It was considerably more difficult to consistently aspirate and dispense equal volumes using the auto-pipette with this concentration of hexane and visibly less volume was deposited onto the sample rods at this point in the experiment.

The most dramatic effects were observed with a DMSO-spiked matrix. A significant decrease in signal was observed with a DMSO concentration of 1 percent with both caffeine and methamidophos. The analyte signals were nearly depleted with 10 percent DMSO. At 50 percent (not plotted), the signal abundances of caffeine and methamidophos were too low to be recorded by the data analysis software. Two characteristics of DMSO may have affected the responses of caffeine and methamidophos. First, because of its high proton affinity, DMSO could better compete for protons than the other solvents. Second, DMSO has a much higher boiling point than the other compounds. Though the DART gas was heated to 250 °C, a temperature that should have been adequate for volatilization of any of the solvents, DMSO would have taken longer to desorb than the other solvents. This could have also reduced the thermal desorption rate of caffeine and methamidophos. The high proton affinity and low volatility of DMSO combined to create very poor sampling conditions for caffeine and methamidophos.

**“Real” Matrices**

**Explanation and method.** The final set of matrices tested was intended to mimic “real” samples, which are often complex and require some kind of preparation. Ocean water, urine, and wine are examples of matrices that may cause problems due to their high salt content and/or presence of other compounds. Additionally, these

matrices hold relevance in commonly studied areas including environmental science, biological/metabolomics, and food science and will all likely be interrogated with DART-MS in the near future. In the same manner as the salt and solvent suppression studies, the real matrices were combined in varying amounts with the caffeine and methamidophos solutions. The samples were deposited onto glass rods, allowed to dry, and introduced into the sampling region for analysis.

**Results and discussion.** The responses of caffeine and methamidophos relative to their average unspiked responses are plotted as a function of added real matrix percentage in Figure 4-12. All three matrices eventually caused reduction in the signals of caffeine and methamidophos. Above all, the urine was expected to cause the most dramatic reductions because of both its high salt content (the results in the salt suppression study disprove this idea) and because of its high content of urea, which has a proton affinity of 873.5 kJ/mol.[120] The spectrum of urine in Figure 4-13 demonstrates that urea was so concentrated in the sample that it readily formed abundant proton-bound dimers. Interestingly, combined with 1 percent wine, an increase in methamidophos abundance was observed. This was suspected to be due to either instrumental variation of the TOF being used for this study or resultant of some kind of controlled release of the analyte molecules from their wine substrate that may have been absent with the less complicated matrices. This effect was not retained when the wine concentration was increased to 10 percent.

The experiments with these three matrices demonstrated that DART-MS is subject to signal suppression. At only 10 percent of added matrix, significant reductions in caffeine and methamidophos signal abundances were detected. One can infer the

sort of results that would be attained if caffeine or methamidophos were analyzed by DART-MS in matrices made up of 100 percent ocean water, urine, or wine. It is obvious from these data that a preliminary extraction may be necessary in various “real world” situations. Thus, a limitation of DART-MS has been presented.

### Conclusions from Suppression Studies

These studies provided information on DART’s resistance and susceptibility to matrix suppression. Unlike other ionization techniques, DART showed no susceptibility to salt suppression and no dependence on solution conductivity. In cases where ocean water, urine, and wine are analyzed, the “directness” of DART may be limited by the need for a pre-purification to reduce signal suppression.

## Atmospheric Effects

Another area that can heavily influence the analytical responses of DART-MS is the ambient environment. Unmodified, this environment consists of air, water vapor (humidity), and the hot gas exiting the DART source. Though generally adequate for analyzing many types of molecules, occasionally it may be useful to modify the air with an additional compound, or dopant, to improve detection. Presented below are a few examples of how the detection of certain analytes may be altered with the addition of a dopant. In the first two examples, this was accomplished by opening containers of the dopant-producing liquids in the vicinity of the DART source and sampling region. In the last example, a cotton swab soaked in the dopant of choice was inserted into the sampling region along with the analyte. The gas temperatures ranged from 250 to 350 °C for the three studies.

**Ammonium Hydroxide**

In positive ion mode, the most common ions other than protonated species are ammoniated species. These adducts are suggested to be formed from interaction with ambient ammonium that has escaped from open containers of ammonium hydroxide.[1] Figure 4-14 gives a comparison of mass spectra collected with 250 pg of methamidophos before and after a container of ammonium hydroxide was opened near the source region. Because of low instrumental sensitivity at the time of analysis, methamidophos signals in both spectra were low. However, with the addition of ammonium vapor, an ammoniated methamidophos ion was detected, the abundance of the protonated methamidophos molecule was increased, and the noise was generally reduced.

The ammonium adduct was expected and in many cases can be used to enhance sensitivity of an analyte. Ammonium adducts of oxygen-containing compounds are commonly observed with chemical ionization when ammonia was used as a reagent gas.[121] As is probably the case with methamidophos, if an analyte has a proton affinity greater than ammonia (PA = 853.6 kJ/mol), the molecule can also receive protons from the ammonium ions.[66] For this reason, the abundance of the protonated molecule also increased. The reduction in noise was less expected but can be explained by suppression. If the compounds responsible for making up the observed background have lower proton affinities than ammonia, their ionization (protonation) could be suppressed.

**Methylene Chloride and Nitric Acid**

The negative ion work in this research has primarily focused on the detection of nitroaromatic explosives. For example, calibration curves generated with 2,4-

dinitrotoluene (“DNT”) and 1,3-dinitrobenzene (“DNB”) were presented earlier in this chapter. Little effort was required to detect the deprotonated DNT or the electron-attached DNB ions. However, when the explosives hexahydro-1,3,5-trinitro-1,3,5-triazine (a.k.a. RDX) and tetryl were analyzed, as demonstrated with the Restek explosives mixture in Figure 4-15 a., they were not detected in an unmodified ambient environment. The spectrum in Figure 4-15 b. shows the Restek explosives mixture analyzed in negative ion mode with both methylene chloride and nitric acid containers open near the DART source. When only a container of methylene chloride was opened near the sampling region, chloride-adducted RDX ions were detected. Upon opening a container of nitric acid near the DART source, nitrate adducts were detected with both RDX and tetryl. As discussed in the DART Mechanisms section of Chapter 1, the addition of halogenated solvents and volatile acids may enhance detection or they may reduce sensitivity. The electronegative halogenated solvent vapors may preferentially capture thermal electrons, which could reduce the detection of compounds such as DNB. The acids may preferentially donate protons and reduce the formation of $[M-H]^-$ ions, such as those formed by DNT.

**Deuterium Oxide**

Another way one may modify the ambient environment about the DART source is with the addition of deuterium oxide ($D_2O$). This is compound is not a dopant in same sense as the compounds discussed above, but it is certainly capable of modifying the ions formed during a DART-MS analysis. Figure 4-16 presents spectra of cyclam analyzed without and with a $D_2O$-soaked cotton swab held in the DART gas stream. In the presence of an H/D exchange reagent, such as $D_2O$, exposed protons bound to nitrogen or oxygen may exchange with deuterium atoms. With four exchangeable

protons, the ion distribution of cyclam drastically changed in the presence of $D_2O$ (Figure 4-16 b.). Vail et al. have used the H-D exchange process to characterize the structures of unknowns.[83]

**Atmospheric Effects Study Conclusions**

As demonstrated above, the addition of dopants can dramatically modify the ionization processes that occur with DART. All of the dopants presented above have benefits and drawbacks. In positive ion mode, ammonium can enhance detection of analytes or it can compete for available protons and suppress ionization. In negative ion mode, methylene chloride and nitric acid allow detection of RDX and tetryl, but they can also suppress ionization of analytes that form $M^-$ and $[M-H]^-$ species. Finally, the addition of $D_2O$ can provide information useful in structural elucidation but it can also greatly complicate spectra.

## General Summary

The effects of analyte substrate, matrix, and surrounding environment were explored in this chapter. Little difference was seen between molecules desorbed from glass or metal, but substrate roughness was important in the analysis of solids. The ability to analyze alternative substrates such as sand, soil, and concrete was established. Some of the governing factors in matrix suppression included matrix volatility and proton affinity. Finally, the importance of ambient gas composition in ionization properties was demonstrated.

Table 4-1. Analyte names and experimental information for figures of merit studies with various substrates.

| Calibration Compound | Molecular Weight (Da) | Internal Standard ("IS") | Amount of IS on Substrate (ng) | Gas Temperature (°C) |
|---|---|---|---|---|
| Fentanyl | 336.4705 | Spiperone | 2.5 | 350 |
| Dimethoate | 225.2574 | Methamidophos | 2.5 | 250 |
| 2,4-DNT[a] | 182.1335 | 1,3-DNB[b] | 7.5 | 330 |
| DMMP[c] | 124.0755 | DIMP[d] | 2.5 | 100 |

a. Abbreviation for dinitrotoluene
b. Abbreviation for dinitrobenzene
c. Abbreviation for dimethyl methylphosphonate
d. Abbreviation for diisopropyl methylphosphonate

Table 4-2. Results from figures of merit studies with various substrates.

| Compound and Substrate | Slope ($ng^{-1}$) | Linear Range[a] | LOD[b] (pg) |
|---|---|---|---|
| Fentanyl-Smooth Glass | 0.877 | 1.3 | 19 |
| Fentanyl-Smooth Metal | 1.17 | 2.7 | 7.7 |
| Dimethoate-Smooth Glass | 1.98 | 3.9 | 8.8 |
| Dimethoate-Smooth Metal | 1.83 | 2.8 | 28.9 |
| 2,4-DNT[c]-Smooth Glass | 0.227 | 2.3 | 305 |
| 2,4-DNT[c]-Smooth Metal | 0.316 | 2.0 | 565 |
| DMMP[d]-Smooth Glass | 0.642 | 2.9 | 34.1 |
| DMMP[d]-Smooth Metal | 0.524 | 2.9 | 38 |
| DMMP[d]Rough Glass | 0.659 | 2.6 | 30.2 |
| DMMP[d]-Rough Metal | 0.568 | 2.9 | 35.1 |

e. Linear range is expressed in orders of magnitude
f. Abbreviation for limit of detection
g. Abbreviation for dinitrotoluene
h. Abbreviation for dimethyl methylphosphonate

Table 4-3. Solvents used in solvent suppression studies.[66]

| Solvent | Proton Affinity, kJ/mol | Boiling Point, °C |
|---|---|---|
| Acetonitrile | 779.2 | 81.7 |
| Isopropanol | 793.0 | 82.4 |
| Hexane | N/A | 68.8 |
| Ethyl Acetate | 835.7 | 77.1 |
| Dimethyl Sulfoxide | 884.4 | 190.9 |

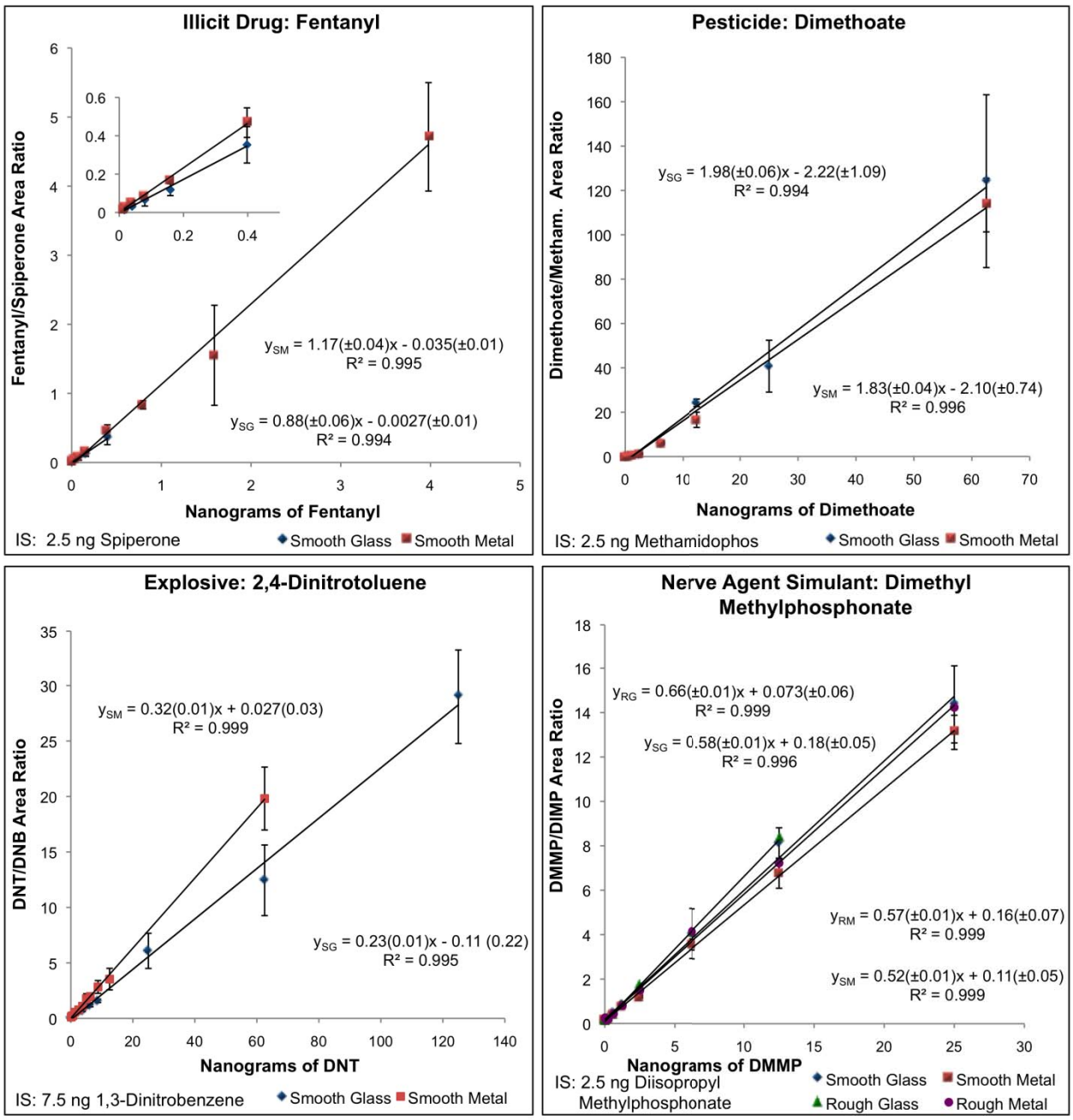


Figure 4-1. Calibration curves generated for substrate effects studies. Note: smooth glass is abbreviated as “SG”, smooth metal is abbreviated as “SM”, rough glass is abbreviated as “RG”, rough metal is abbreviated as “RM”, and internal standard is abbreviated as “IS”. See Table 4-2 for compound abbreviations.

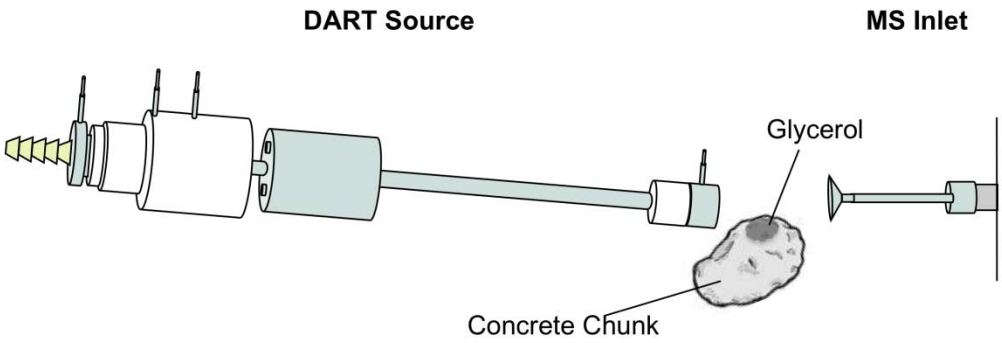


Figure 4-2. Diagram of the DART source tilted 10° for concrete sample analysis.

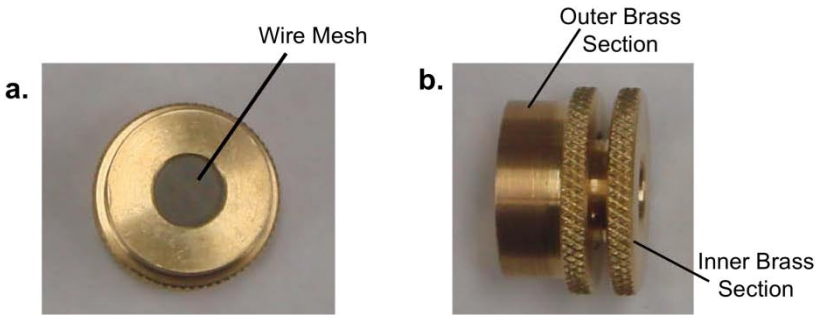


Figure 4-3. Photographs of the sample holder used for activated carbon analysis. The holder is shown from (a.) the front and (b.) the side.

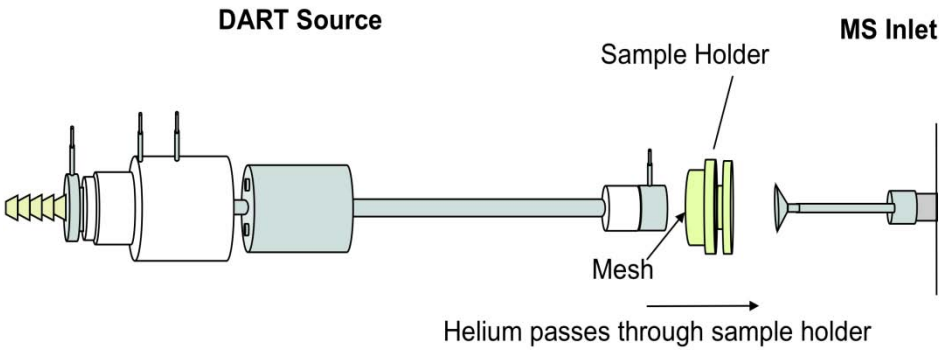


Figure 4-4. Diagram of the DART sampling configuration using the sample holder for activated carbon analysis.

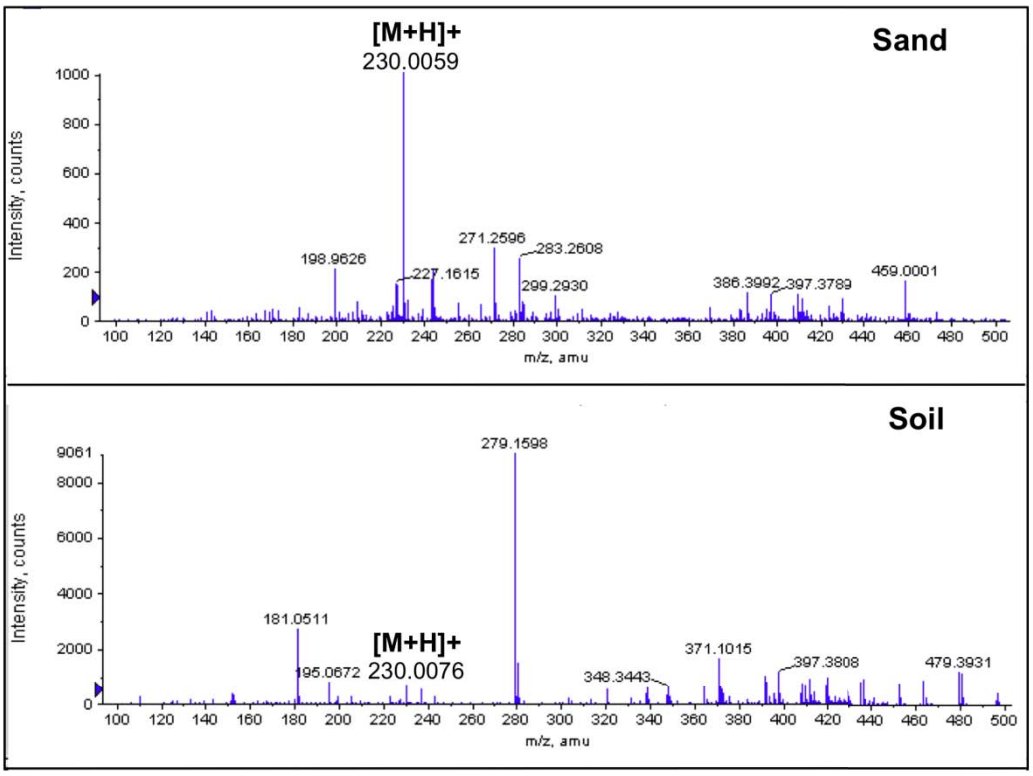


Figure 4-5. Dimethoate analyzed from sand and soil.

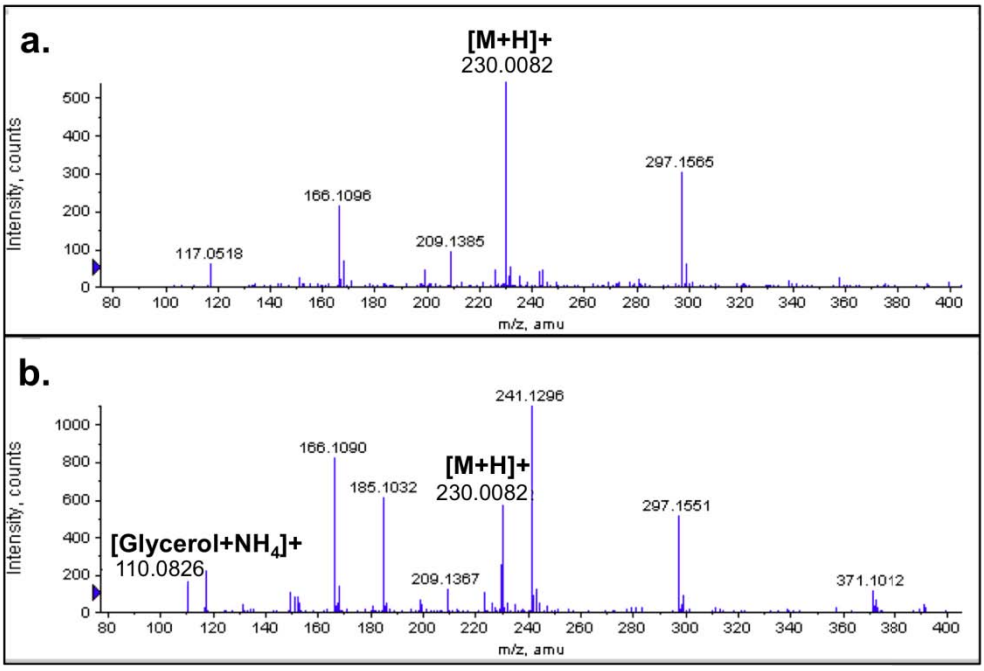


Figure 4-6. Dimethoate analyzed from concrete with a glycerol matrix. Mass spectra are presented (a.) with and (b.) without background subtraction.

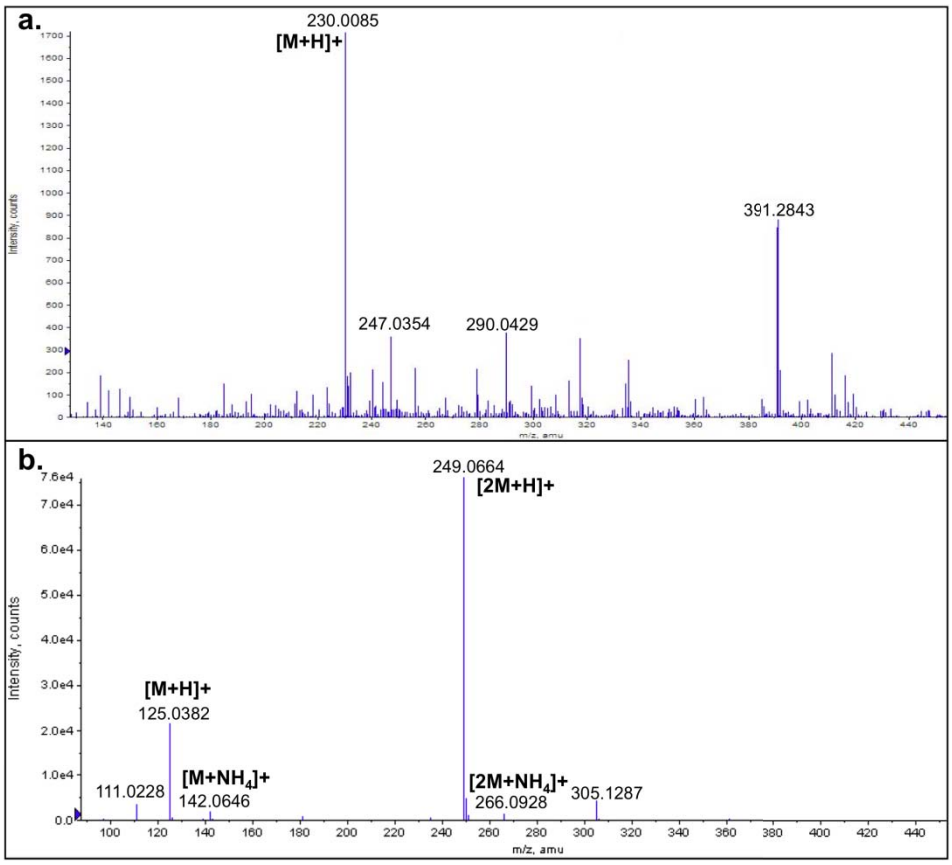


Figure 4-7. Spectra of compounds analyzed from activated carbon. Dimethoate (a.) was incubated with the activated carbon for 8 hours. DMMP (b) was incubated for only 30 minutes.

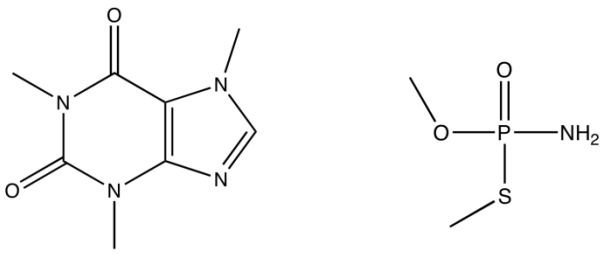


Caffeine Methamidophos

Figure 4-8. Structures of caffeine and methamidophos, compounds used for suppression studies.

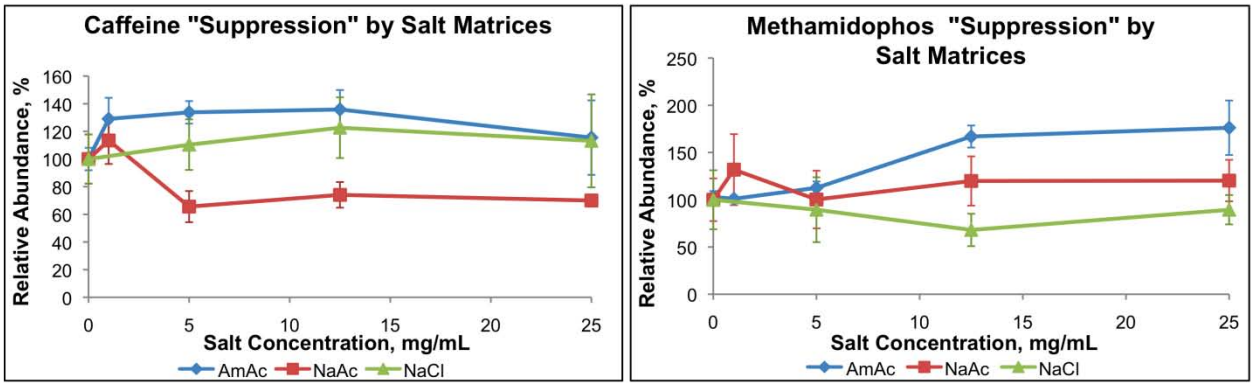


Figure 4-9. Results from salt suppression tests. Spiked analyte responses are plotted relative to their unspiked responses as a function of salt concentration. "AmAc" refers to ammonium acetate, "NaAc" refers to sodium acetate and "NaCl" refers to sodium chloride.

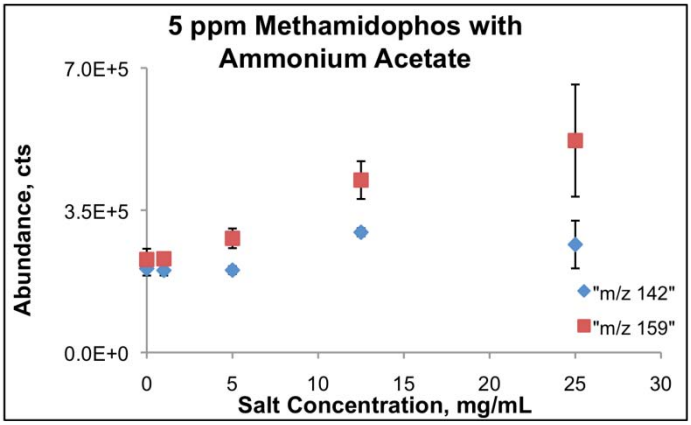


Figure 4-10. Variation in methamidophos signal with ammonium acetate concentration. The protonated specie had an m/z of 142 (blue) and the ammoniated specie had an m/z of 159 (red).

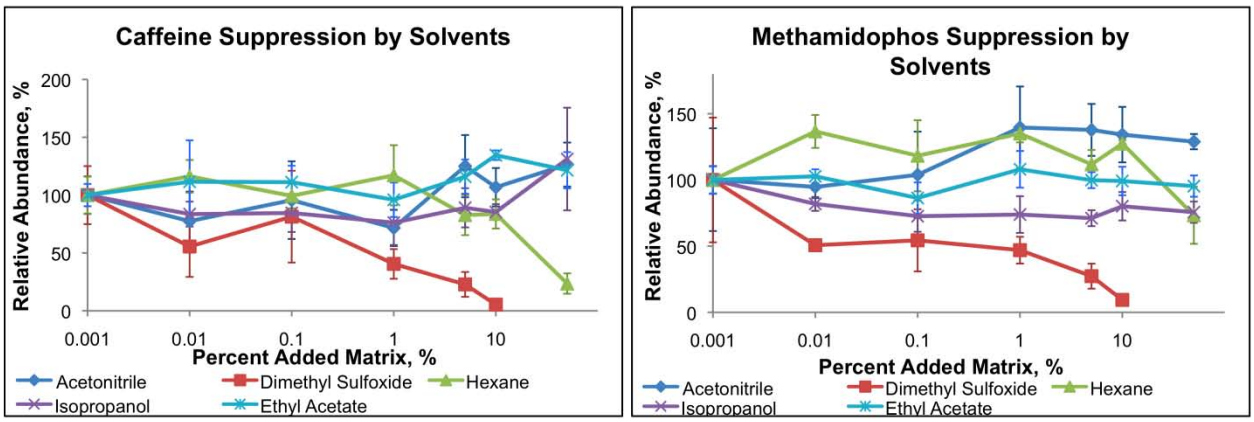


Figure 4-11. Results from solvent suppression tests. Spiked analyte responses are plotted relative to their unspiked responses as a function of added solvent percentage.

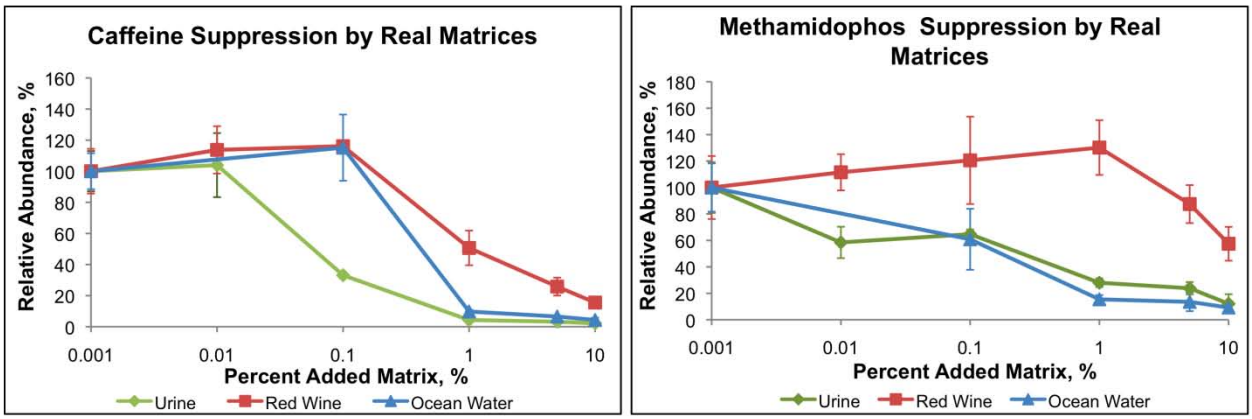


Figure 4-12. Results from “real” matrix suppression tests. Spiked analyte responses are plotted relative to their unspiked responses as a function of added matrix percentage. Real matrices include urine, red wine, and ocean water.

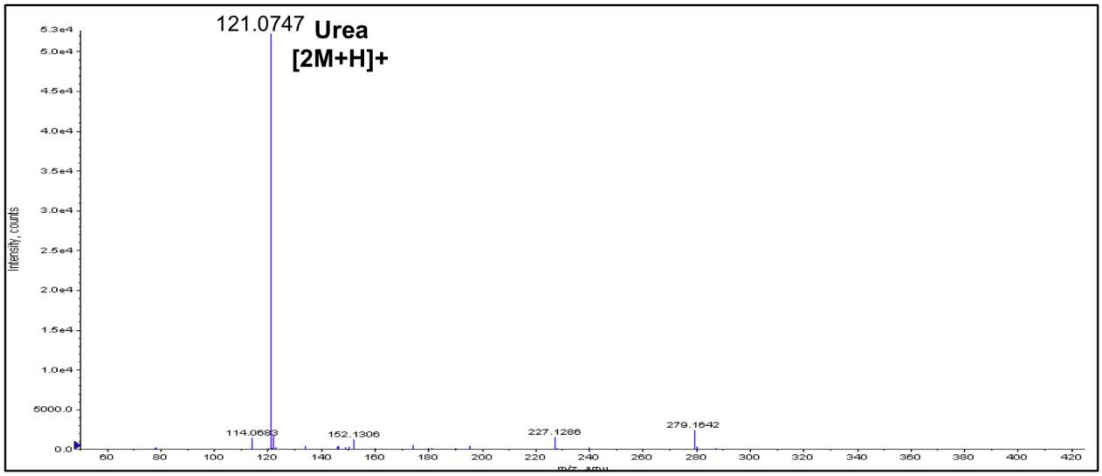


Figure 4-13. Mass spectrum of urine.

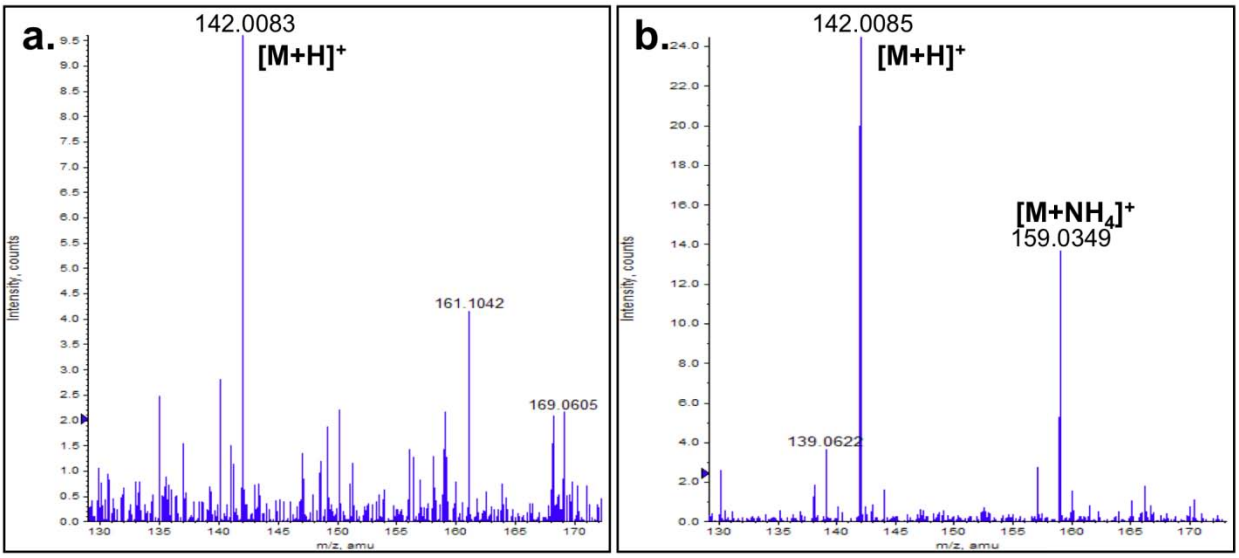


Figure 4-14. Comparison of methamidophos mass spectra acquired (a.) without and (b.) with a container of ammonium hydroxide open near the sampling region.

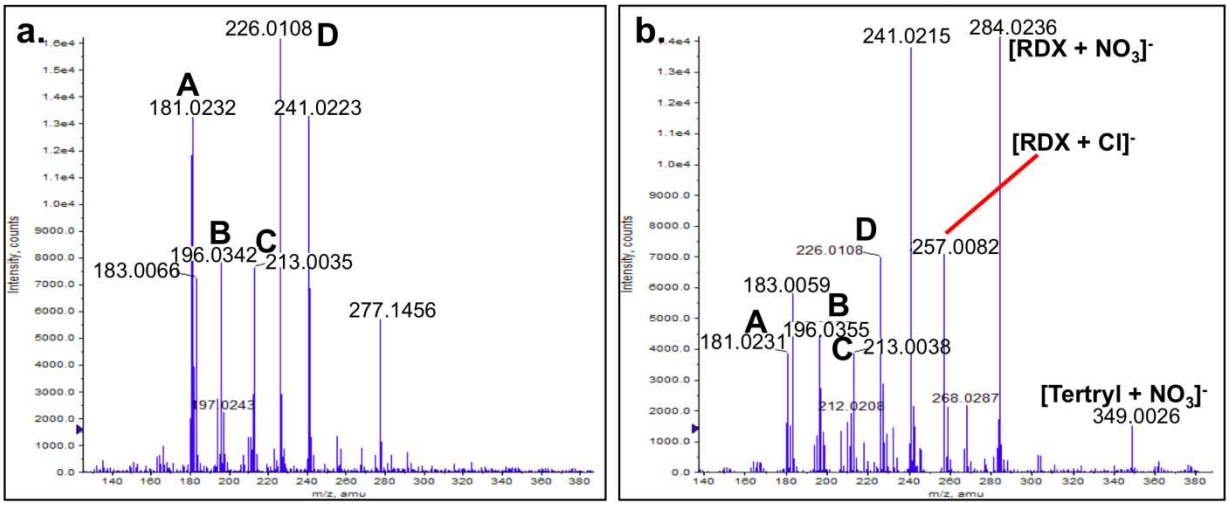


Figure 4-15. Negative ion mode DART-MS spectra of the "Nitroaromatics and Nitramine Explosives in Drinking Water" mixture analyzed (a.) without dopants and (b.) with containers of methylene chloride and nitric acid open near the sampling region. Other peaks are identified: A is dinitrotoluene (isomer is unknown), B is amino-4,6-dinitrotoluene, C is trinitrobenzene, and D is trinitrotoluene.

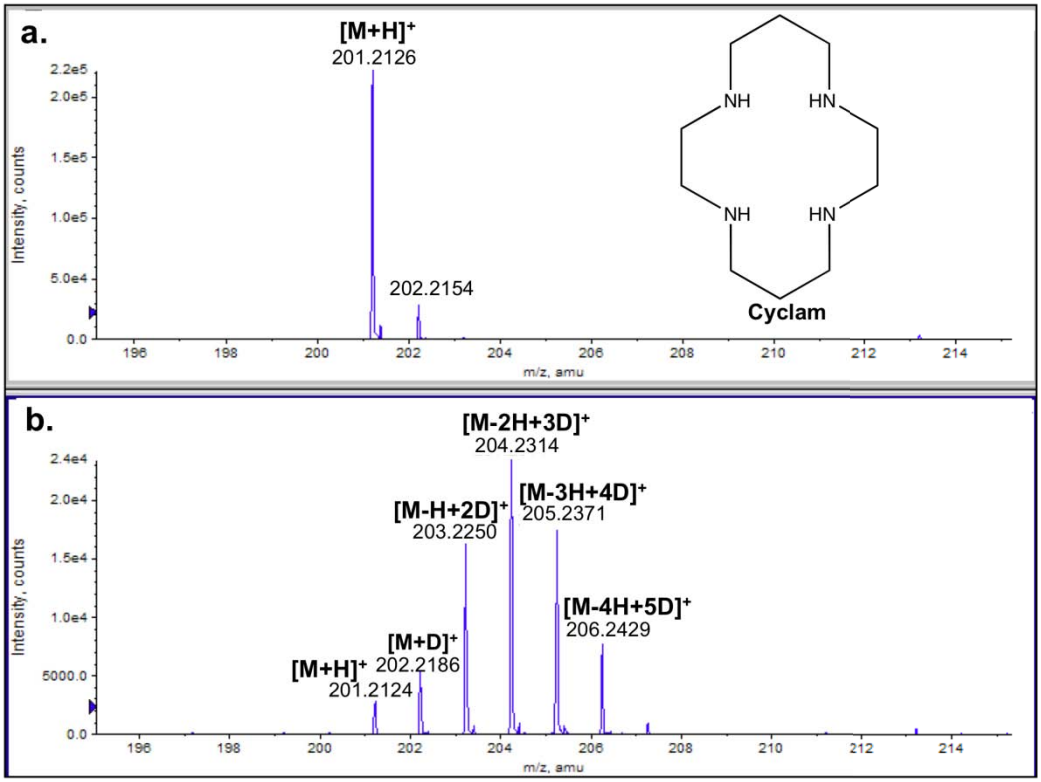


Figure 4-16. Comparison of cyclam mass spectra acquired (a.) without and (b.) with deuterium oxide present in the source sampling region. In the deuterium-exchanged spectrum (b.), each D before the M in a peak label represents an exchanged deuterium.

# CHAPTER 5
# STUDIES OF THE POSITIVE ION FORMATION MECHANISMS OF HELIUM DART

## Introduction

In recent years, there have been many reports of the use of Direct Analysis in Real Time (DART) ionization in a wide array of applications. The ionization mechanisms of DART, however, have not been fully delineated, though suggestions have been made by Cody et al. and others.[1,48,65] This chapter presents experiments carried out to further elucidate the mechanism of DART ionization. Because detailed discussion is given in Chapter 1, only a brief overview of the DART ionization mechanism will be given here. DART ionization originates from the interaction of an analyte with species created in a gaseous electric discharge where electrons, radical ions, and metastable neutrals are generated.[56] Ionized species are removed from the gas stream so that only metastable gas atoms or molecules exit the DART source.[1] From this point, the ionization processes include competing reactions that are governed by analyte gas phase basicities and acidities, ionization energies, electron affinities, discharge gas type, and dopants present in the sampling region (added intentionally or not).

Most reported applications of DART have employed helium as the discharge gas. The electrical discharge in the helium produces electronically excited $He(2^3S)$ atoms with an electronic energy of 19.8 eV. $He(2^3S)$ is sufficiently energetic to directly ionize most organic compounds via Penning ionization to form radical cations (reaction 5.1).[66]

$$He(2^3S) + M \rightarrow He(1^1S) + M^{+\bullet} + e^- \qquad (5.1)$$

The energetic $He(2^3S)$ atoms have also been shown to react with background gases (e.g. $H_2O$, $O_2$) generating a variety of reagent ions that may further react with and

ionize the sample.[48] In the original DART publication, Cody et al. observed a background of positively charged water clusters up to 14-mers that may be produced by sequential reactions as summarized below .[1]

$$He(2^3S) + nH_2O \rightarrow [(H_2O)_{n-1}H]^+ + OH^- + He(1^1S) \quad (5.2)$$

Analyte molecules are most commonly protonated during DART ionization and this is thought to occur via gas-phase proton transfer from the protonated water clusters formed as indicated in reaction 5-2.[1] The proton affinity (PA) of water is 691 kJ/mol and the PA of its dimers is considerably higher, 808 kJ/mol. [60,122] The PAs of larger ionized water clusters are even greater.[123] For the proton transfer mechanism to be operative the PA of the analyte must be greater than that of the ionizing reagent. As $[M+H]^+$ ions are often observed in positive-mode DART-MS, the PA of an analyte should play an important role in governing whether it will be ionized by protonation.

In this work, mechanistic studies were directed toward understanding the factors that govern the formation of positively charged compounds in DART analyses. First, low-mass background ions were monitored to examine the similarity between those seen with a commercial DART source and with the custom-built source and to examine their variation as a function of gas temperature, the position of the DART source, and grid electrode voltage. Next, a series of experiments were performed to systematically study the effects of analyte and competing analyte PAs and analyte volatility. These experiments included analyte sensitivity monitoring as a function of the analyte's PA and as a function of the PAs of possible ionization suppressors. Competition experiments between pairs of analytes with different PAs were also carried out to observe suppression. To determine if a competitive desorption mechanism might be

operative during DART analyses, competition experiments between pairs of analytes with different boiling points were performed. Another set of experiments was conducted to demonstrate and determine the spatial variation in DART ionization mechanisms. Lastly, efforts that involved enclosing the sampling region were made to observe the Penning ionization mechanism.

## Experimental

### Chemicals and Reagents

HPLC grade methanol was purchased from Burdick and Jackson (Muskegon, MI). Methylene chloride was purchased from Fisher Scientific (Fair Lawn, NJ). All solvents were used without further purification. Aniline, cyclohexanone, benzaldehyde, 2,5 dimethylpyrrole, 1-methyl-2-pyrrolidionone, piperazine, 2,6-lutidine, and triethylamine were purchased from Sigma Aldrich (Milwaukee, WI) and diluted in methanol. Polycyclic aromatic hydrocarbons (PAHs) including anthracene, 1,2-benzanthracene, biphenylene, chrysene, naphthacene, perylene, and triphenylene were purchased from Sigma Aldrich (Milwaukee, WI) and were dissolved in methylene chloride. Deuterated water was purchased from Cambridge Isotope Laboratories (Andover, MA). Deuterated anthracene was purchased from Isotec (Miamisburg, OH) and was dissolved in methylene chloride. Helium, nitrogen (research grade and UHP), air, and liquid nitrogen were purchased from Airgas (Gainesville, FL).

### Instrumentation

#### Mass spectrometer and DART source

The Agilent 6210 time-of-flight (Agilent Technologies, Wilmington, DE) mass spectrometer (TOF) discussed in Chapter 2 was used for all experiments. Though normally operated at 250 $V_{p-p}$, the RF-only transfer octapole ion guide was operated at

65 $V_{p-p}$ to enable detection of low-mass background ions.

The custom-built DART source described in Chapter 2 was used in these studies and operated as described. The DART source was heated with a heater removed from an Agilent atmospheric pressure photoionization source. The Vapur® inlet modification was used to interface the DART source to the TOF inlet as described in Chapter 2.

**Sample Introduction and Experimental Design**

**Background ion monitoring**

No samples were introduced when the low-mass background ions were monitored. To establish similarity between it and the commercial DART source, the custom-built DART source was operated with normal voltages and a normal helium flow rate (see Chapter 2) with its heater was set to 200 °C. Spectra were acquired for two minutes at a time for this experiment.

Additionally, the background ions were monitored as the following operating parameters were varied: DART-to-ceramic tube (of the Vapur® interface) distance, temperature, and grid electrode voltage. In the distance experiment, the gas temperature was held constant at 200 °C. In the temperature experiment, the DART-to-ceramic tube distance was maintained at 7.5 mm. Both the temperature and distance were held constant as the grid electrode voltage was varied. For these experiments, signal was averaged for 30 seconds to generate a mass spectrum and 3 spectra were averaged for each data point.

**Studies related to sample proton affinity**

Several different experiments were conducted to study the effects of analyte PA and the PAs of other compounds competing for ionization. Unless otherwise stated, the following conditions were used in all of the PA studies. The DART heater was set to

225 °C. The motorized stage and glass posts described in Chapter 2 were used to introduce samples into the DART source the sampling region at a rate of approximately 1 mm/sec. Immediately before analysis, samples from Table 5-1 were deposited in 0.5 to 1 µL aliquots onto the tops of the glass posts and introduced into the DART gas stream. In all cases, the analytes from Table 5-1 were introduced without drying to prevent sample losses from evaporation. Four replicates were run for each data point in all of the PA studies.

**Calibration curves.** To determine sensitivity as a function of analyte proton affinity, analytes from Table 5-1 were introduced in concentrations of 6.25, 12.5 and 25 µM. Three separate calibration curves were generated for each analyte and their slopes were averaged for sensitivity determinations.

To determine if the presence of a competing reagent with a different proton affinity could cause a general reduction in the sensitivity of a given analyte, possible suppression agents were added to the calibrant solutions of aniline, 1-methyl-2-pyrrolidinone, and 2,5-dimethylpyrrole. The concentration of the suppression agent in all samples was 25 µM. Calibration curves of aniline (at concentrations of 6.25, 12.5, and 25 µM) were generated with the following suppression agents: cyclohexanone, 2,5-dimethylpyrrole, and 2,6-lutidine. Calibration curves of 2-methyl-1-pyrrolidinone (at concentrations of 6.25, 12.5, and 25 µM) were generated with the following suppression agents: 2,5-dimethylpyrrole, piperazine, and triethylamine. Calibration curves of 2,5-dimethylpyrrole (at concentrations of 6.25, 12.5, and 25 µM) were generated with the following suppression agents: aniline, 1-methyl-2-pyrrolidinone, and 2,6-lutidine. The

slope of each compound's three-point "competitive" calibration curve was tracked as the type of spiked compound (and proton affinity) was changed.

**Competition experiments.** Analytes were introduced alone and paired with other "competitor" compounds from Table 5-1 to determine if any PA-based competition would occur. First, equimolar competition experiments were conducted with each compound present at a concentration of 25 μM. Next, unequal molar competition experiments were carried out with the target analytes aniline, 2,5-dimethylpyrrole, and 2,6-lutidine in 5 μM concentrations. The target analytes were introduced with competitors from Table 1 with both higher and lower proton affinities. The competitor-to-target analyte molar ratios used included 0:1, 1:1, 10:1, 50:1, and 100:1.

**Studies related to sample boiling point**

Analytes from Table 5-2 were run alone and in pairs to determine if a competitive desorption mechanism could occur. Solutions of compounds from Table 5-2 were deposited in 0.5 μL droplets onto glass rods just before introduction into the sampling region. The following sample types were analyzed: aniline alone, anthracene alone, 4-fluorobenzamide alone, aniline with 4-fluorobenzamide, and aniline with anthracene. Aniline was run alone twice because the tests occurred over two days. All solutions had 25 μM analyte concentrations. Data points were taken for each compound and the mixtures at gas temperatures between 100 and 400 °C, a range extending from below the boiling point of aniline to above the boiling points of anthracene and 4-fluorobenzamide. The proton affinities and boiling points of these compounds are given in Table 5-2.

**Mechanism mapping experiments**

Mechanism mapping experiments were conducted to demonstrate and determine the spatial distribution of ionization mechanisms that occur as the distance between the DART source exit and the sample is varied (explained further in the Results and Discussion Section). A deuterated water ($D_2O$)-humidified controlled environment glass chamber was fabricated to perform these studies; it is shown in Figure 5-1 connected to the DART source and the Vapur® inlet modification. The chamber was equipped with a row of holes spaced approximately 4 mm apart for sample introduction at different distances from the DART source. A vaporizer designed to mimic a gas chromatograph inlet was used to introduce $D_2O$ vapor through the hole at the bottom of the chamber. It was equipped with a septum through which an electrospray transfer line was inserted and a gas connection to provide unidirectional flow of $D_2O$ vapor toward its exit. $D_2O$ was introduced into the vaporizer at a flow rate of 25 µL/min and a low flow (less than 0.5 L/min) of nitrogen was used to guide the vapor into the chamber. All openings of the glass chamber but the sample hole in use were sealed with Teflon® tape during the experiments.

Glass melting point tubes were dipped into 100 ppm to 1 mg/mL solutions of the PAHs in Table 5-3, allowed to dry, and introduced into the sampling holes of the glass chamber by hand. Samples were held in place for approximately 3 seconds. Alternating sampling holes starting at the one closest to the DART source were used for mapping.

**Enclosed sampling region experiments**

It was understood that in order to observe the Penning ionization mechanism (and formation of $M^{+\bullet}$ ions) for many high-PA analytes, the sampling region needed to be enclosed to prevent exposure to advantitious water. This was first done by inserting a 1

in. length of Teflon® tubing (1/8 in. i.d.) with a hole for sample introduction cut into it between the DART and the Vapur ® ceramic tube. The hot helium passing through the tube was believed to eliminate moisture and prevent proton-transfer from protonated water clusters. A diagram of this design is presented in Figure 5-2.

A second enclosure was created with a cut 1-mL autopipette tip placed between the DART source and the Vapur®, diagrammed in Figure 5-3. A 1.5 mm diameter hole was cut into the pipette tip for introduction of "external gases," such as air, ultra-high purity nitrogen, and additional helium. An electrospray transfer line was inserted into a much smaller hole (less than 0.5 mm diameter) for sample introduction. Injections of 1 to 2 µL of neat compounds followed by multiple 8 to 10 µL injections of air were introduced into the pipette enclosure via this line. Samples were vaporized and ionized inside the enclosure.

## Results and Discussion

### Background Ion Monitoring

### Establishment of source similarity

In a recent publication, Cody discussed background ions observed with the commercial DART source.[48] These include a series of protonated water clusters, $NO^{+\bullet}$, and $O_2^{+\bullet}$. As shown in Figure 5-4, these same background ions were also observed with the custom-built DART source employed in this work. It should be noted that the relative distribution of these ions can be tailored as the operator desires by adjusting the transfer optics of the mass spectrometer. The similarity of background ions and ions observed in the analyses of various compounds in this work to those observed with a commercial DART source led to the belief that the custom-built source in this work is

adequately similar to the commercial version to perform mechanism studies that may be related to either source design.

An important series of ions that has received almost no discussion in the literature are the ammoniated water clusters observed in this spectrum. We have also observed these clusters using both helium and nitrogen with a commercial DART source. Recent *ab initio* quantum chemistry calculations performed by scientists at ENSO, Inc. using GAMESS and ACES II/ACES III software packages indicated that these species have relatively high PAs.[124-126] The PA of $[H_2O + NH_4]^+$ was computed to be 905.4 kJ/mol and the PAs of larger clusters increased as a function of the number of water molecules included. PAs of this magnitude could play a major role suppressing the proton transfer reactions that should ionize lower-PA analytes and adversely affect sensitivity.

**Background ion monitoring with DART parameter variation**

**Temperature variation.** Figure 5-5 contains plots of identified water clusters as a function of gas temperature. Both the absolute and relative abundances are plotted to give perspective of the overall amounts and relative amounts of the different species.

A couple of observations can be made from these plots. First, a slight decrease in abundance of the ammoniated water clusters was observed as a function of gas temperature, implying that their presence is not (or only mildly) temperature dependent. Second, the protonated water clusters continuously increased in abundance through 400 °C. This result implied that their formation was temperature dependent, which is somewhat counter intuitive if one considers that solvent (water molecules) evaporation should increase with increasing temperatures.

**DART-to Vapur® distance variation.** Plots of the changes in water cluster abundances as a function of DART-to-Vapur® distance are given in Figure 5-6. A distance of 15 mm produced the overall greatest response both in terms of absolute abundance and relative abundance. This result, however, is not consistent with the DART-to-Vapur® distance studies reported in Chapter 2, which indicated that the greatest analyte sensitivities were achieved with a distance of 5 mm. Though the absolute abundances of all species decreased when distances were greater than 20 mm, the relative abundances of all ammoniated species generally increased or leveled off (at 20 mm) as the distance was increased. A possible explanation is that detection of the ammoniated species was less affected by the general decrease in temperature in the sampling region (especially nearest the Vapur®) as the distance was increased. This explanation is consistent with results from the study presented in the previous section on temperature variation.

**Grid electrode voltage variation.** Plots of the changes in water cluster abundances as a function grid electrode voltage are given in Figure 5-7. Though there were some differences in the relative amounts of the different species, the absolute abundances of the all water clusters varied in approximately the same manner as the grid voltage was changed. All of the water clusters decreased in abundance as the voltage was raised through 500 V followed by a plateau in abundance variation beyond that point. This indicates that the changes seen were a function of ion transmission and not ionization mechanism. Harris et al. reported that higher grid voltages could result in greater ion velocities that caused a distortion in ion trajectory (away from the inlet) and hindered detection.[49] A similar effect was observed with the water clusters in this study.

**Proton Affinity Studies**

A number of studies were performed to demonstrate the relationship between an analyte's PA and its sensitivity and detectability. These studies addressed the impact of PA on sensitivity and the competition for available protons that may occur between analytes with differing PAs. The compounds listed in Table 5-1 were used in these studies and were chosen for their diversity in PA and their similarity in volatility. The analyte boiling points were considered acceptable if they were below 250 $^{\circ}$C and within the temperature range easily attained by the DART source heater.

**Calibration curves for sensitivity determinations**

**Unspiked calibrant solutions**. Short calibration curves were generated to track DART sensitivity as a function of analyte PA. Example calibration curves generated for 1-methyl-2-pyrrolidinone are shown in Figure 5-8 a. Curves were also generated for aniline, benzaldehyde, 2,5-dimethyl pyrrole, 2,6-lutidine, and triethylamine. As seen in Figure 5-8 b., DART sensitivity steadily increases as the PA of the analyte is increased. These data demonstrate that proton transfer is a dominant mechanism in DART ionization.

**Spiked calibrant solutions.** Short calibration curves generated from calibrant solutions with added suppression agents were generated to determine if sensitivity could be altered by the presence of another compound. The variation in sensitivities of aniline, 2,5-dimethyl pyrrole, and 1-methyl-2-pyrrolidinone are shown in Figure 5-9 a. through c. Below each of the sensitivity plots are the intensities of the spiking agents as the concentrations of the calibrants were varied in Figure 5-9 d. through f.

The sensitivities of aniline and 2,5-dimethylpyrrole decreased significantly as a function of the suppression agents' PA. The sensitivities when 1-methyl-2-pyrrolidinone

was paired with higher PA suppression agents were lower than when it was with a lower-PA agent. However, its sensitivity did not change significantly between the two higher PA agents, even though their proton affinities are separated by nearly 40 kJ/mol. Likewise, some of the responses from the spiking agents show a slight decrease in intensity, but the changes were not significant with the target analyte concentrations used. These data indicate that the sensitivity (change in signal versus changes in concentration) of these analytes was affected by the presence of higher PA compounds. Competition between analytes of varying proton affinities will be further explored in the next section.

**Equimolar proton affinity competition experiments**

Gas-phase proton transfer from Penning-ionized protonated water clusters is the only pathway for protonation that has been proposed in the literature. If this is indeed the only means of protonation, the assertion that there is a finite number of protons available for donation should be true.[1,65] To test this hypothesis and the competitive nature of compounds with differing PAs, equimolar amounts of the target analytes were allowed to "compete" for available protons and, thus, ionization. The responses of the target analytes were monitored as a function of the PA of the competing compounds.

Results from selected competition experiments are shown in Figure 5-10. No discernable trend was detected. Competing compounds with both higher and lower PAs affected the ionization of the target analyte in the same manner. An observation from these results is that similar amounts of compounds with varying PAs have little effect on each other's signal intensities at the concentrations measured. This can be considered an advantage of this ionization technique. One explanation for this may be that there was no interaction between the analytes and their competitors. This would be

dependent on the number densities and collisional cross-sections of the molecules involved. If the number density of the ionized water clusters or other ionizing media was sufficiently high, then analytes in these relative amounts could be ionized free of interference. Similar results were seen when samples were volatilized prior to ionization.

**Unequal-molar proton affinity competition experiments**

Due to the absence of suppression seen in the equimolar PA competition experiments, greater concentrations of suppression agents, or "competitors", were used to effectively reduce the ionization of the target analytes. By increasing the concentration of the competitors, the likelihood of the target analyte interacting with the competitor or being in closer proximity to effectively compete for ionizing protons was increased. Target analytes aniline, 2,5-dimethylpyrrole, and 2,6-lutidine in 5 μM concentrations were introduced with varying amounts of competitors from Table 5-1 with both higher and lower proton affinities. The spiked target analyte response relative to that of the unspiked target analyte response was tracked as a function of the competitor-to-target analyte ratio.

The results of these studies are given in Figure 5-11. In all cases, the lower PA-competitor compound caused no significant suppression of the target analyte. Also, in all cases a 10:1 or greater ratio of higher PA-competitor produced significant suppression of the target analyte. These data indicated that the presence of a higher quantity of a competing compound does not suppress ionization of the target analyte unless the competitor has a higher PA than the target analyte.

**Boiling Point Effects**

In the conjunction with the work presented in this dissertation and in several other cases, thermal desorption has been demonstrated to be the dominant mechanism for the transport of analytes into the vapor phase during DART-MS analyses.[38,50,127] For this reason, analyte volatility can play a major role in the sensitivity of a given compound. All DART sources are equipped with adjustable gas heaters that make desorption of high boiling point compounds, such as explosives, possible.

Pairs of compounds with nearly the same proton affinity but very different boiling points were analyzed separately (to establish a "baseline") and simultaneously to determine if there might be competition between the molecules while in (or just entering) the gas phase. Data were taken for each compound and the mixtures at temperatures between 100 and 400 °C in order to sample at temperatures less than and greater than the boiling points of each of the compounds in a mixture. As shown in Figure 5-12, similar responses were observed for all of the analytes with or without a competitor.

These data highlighted the importance of using an appropriate temperature setting for all components in a sample, which may be a difficult task depending on the complexity of the sample. At temperatures significantly below their boiling point, compounds such as anthracene and 4-fluorobenzamide appeared to be suppressed. It can be concluded from these data that analyte boiling point is less important to DART sensitivity than proton affinity as long as there is sufficient analyte vapor.

**Mapping Experiments**

Figure 5-13 demonstrates that both molecular ions ($M^{+\bullet}$) and protonated molecules ($[M+H]^+$) are formed during DART-MS analyses of polycyclic aromatic hydrocarbons. Additionally, it has been shown that the relative abundance ratio of the

species varies as a function of the distance from the exit of the DART source to the sample (DART-to-sample distance).[64] At first glance, this appears to be only a competition between Penning ionization or charge-exchange involving ionized ambient components, which result in the formation of the molecular ion, and proton transfer by the mechanisms discussed above (protons are donated from protonated water clusters).

An alternative route for protonation that has seen almost no discussion in the DART community is self-protonation, as represented in reaction 5-3.

$$M^{+\bullet} + M \rightarrow MH^{+} + [M - H]^{\bullet} \qquad (5\text{-}3)$$

This reaction is said to be ubiquitous for many classes of compounds and in many cases the rate constant for self-protonation is comparable to the calculated capture collision rate constant.[63] Evidence for this mechanism occurring in DART ionization is shown in Figure 5-14 where deuterium adducts were observed during the analysis of deuterated anthracene. No other source of deuterium was present during this study.

By creating a $D_2O$-humidified environment around the sampling region, efforts were made to delineate the source of protons (protonated water clusters vs. analyte molecules) and the spatial distribution of the operative ionization mechanisms. With this configuration, it was postulated that observed protonation was the result of analyte-to-analyte proton transfer, whereas observed deuteration was resultant of deuterium donation from deuterated $D_2O$ clusters, i.e. $[(D_2O)_n+D]^+$ species. The environment was considered to be adequately saturated with $D_2O$ when the background ion dioctylphthalate was deuterated. Dioctylphthalate (structure shown in Figure 5-15 (a.) was considered a good litmus for the degree of deuteration because it has no

exchangeable protons, meaning all adducted deuterium ions were known to result from a transfer from the $[(D_2O)_n+D]^+$ species. Its spectra without and with a $D_2O$ enviroment are shown in Figures 5-15 (b.) and (c.), respectively. The PAHs used in this study, along with their gas-phase ion energetics, are listed in Table 5-3.

Figure 5-16 demonstrates the change in the ion distribution that was detected at each DART-to-sample distance with 1,2-benzanthracene. Both the protonated and deuterated species increased relative to the molecular ion up to a 20 mm distance, where the abundances of the two ions were nearly equal. Similar responses were obtained with all of the PAHs tested and the molecular ion-to-deuterated molecule ratio for each PAH is plotted against the DART-to-sample distance in Figure 5-17. All of the PAHs tested showed an increase in deuteration as the DART-to-sample distance was increased. Sampling at the 20 mm position was performed in addition to the alternating sample introduction holes in the chamber for all of the PAHs because there appeared to be an inflection point between regions of low deuteration and higher deuteration at this distance.

As this behavior was exhibited with all of the PAHs, a few observations may be made. First, these data demonstrate that three mechanisms occur during ionization of these molecules: Penning ionization/charge-exchange with ionized ambient components, self-protonation, and gas-phase proton (or in this case deuterium) transfer from ionized water clusters. Under normal circumstances where analyses are performed in ambient conditions, the relative contribution of the latter two mechanisms is unknown. It should also be noted that it was possible to observe molecular ions here because PAHs have relatively low ionization energies and losses of charge by charge-

exchange processes are unlikely. Second, from the point closest to the DART source to a distance of less than 20 mm, ionization via interaction with ambient water clusters is not the dominant mechanism—it was not until after 20 mm that this became true.

**Enclosed Sampling Region Experiments**

As part of a series of experiments originally designed to demonstrate Penning ionization with DART, the sampling region was enclosed to prevent interference from protonated water clusters. Using the Teflon® enclosure, background levels were tracked as the voltage of the DART grid electrode was varied with the source in the following configurations: open, closed but with the hole open, and completely closed (hole blocked with glass rod). Average total currents of 20-second scans are plotted in Figure 5-18. The levels seen when voltage was applied in the closed configurations demonstrate that the species responsible for protonation were not originating from the helium. Several of the compounds were analyzed with the source in its open and closed configuration and in all cases sample signals were completely depleted upon closing the source (results not shown). These results led to the hypothesis that either Penning ionization was not occurring in the closed configuration or that ion charge was being lost prior to the analytes reaching the mass analyzer. Unfortunately, the method of closing the source (with a small-bore Teflon® tube that did not fit well between the DART source and the Vapur® ceramic tube) left doubt in the validity of these possible conclusions.

Next, the pipette tip enclosure was used to both create a better seal and to allow more open space inside the enclosure. Experiments were conducted with the source in a closed configuration as shown in Figure 5-3 and in an open configuration, where the DART source was placed 5 mm from the large end of the pipette tip.

**2-Octanone test**

The analyte 2-octanone has an ionization energy of 9.75 eV, which is below the internal energy of the metastable helium atoms (19.8 eV) that are responsible for Penning ionization. It also has a lower ionization energy than molecular oxygen (12.07 eV) and should be able to undergo charge exchange with ionized oxygen. Despite these facts, 2-octonone signals were only detected when the source was in an open configuration. To determine if the loss of ion signal was caused by decreased ion transfer or via another mechanism, water and air were introduced into the enclosure to induce ionization. Ion signals were only detected when air was added. A total ion chromatogram and corresponding mass spectra from an analysis of 2-octanone with periodic air introduction are shown in Figure 5-19. Ion signal was reproducibly detected when air was introduced into the enclosure but not when only water was introduced. Ions exhibiting proton-adduction were detected despite there being little or no source of water for protonated water cluster formation.

**Additional compounds**

Additional compounds were tested in a manner similar to that described above for 2-octanone and additional gases were introduced as the “external gas”. The first set of experiments was performed to demonstrate that the effects seen were not unique to 2-octanone. The TICs from enclosed-source experiments with benzaldehyde, 2,6-lutidine, triethylamine, and hexafluorobenzene are shown in Figure 5-20. The three analytes with proton affinities above that of water and the water dimer were ionized when air was introduced. However, no expected ions were observed with hexafluorobenzene. Though this molecule has a PA that makes it unlikely to protonate,

hexafluorobenzene should be able to Penning ionize or undergo charge transfer from ionized molecular oxygen or nitrogen.

**Additional gases**

In Figure 5-21, the TICs from enclosed-source analyses of 2-octanone using purified air, ultra-high purity nitrogen, and helium as external gases are given. Ionization was observed with 2-octanone when purified air and nitrogen were added but not when helium was introduced. The same results were seen with benzaldehyde, 2,6-lutidine, and triethylamine. When only helium was introduced as the external gas, Penning ionization of all of the molecules should have been observed. Instead no ion signal was detected. It should be noted the presence of the electrical plasma at the needle electrode was confirmed by measuring its current (it was the same as the current measured when ions were detected) and by visually observing it with the addition of a window to the gas lines. Because Penning ionization was not observed, one may conclude that another ambient constituent is required to allow ion detection. Since the nitrogen alone as the external gas allowed ion detection, water and oxygen were shown to be unnecessary.

Neither the purified air nor the ultra-high purity nitrogen reduced the amount of protonation that occurred (mass spectra not shown). Though with the purified air, one may argue that the cold trap did not effectively eliminate water vapor, if any water vapor was present in the ultra-high purity (99.999% pure) nitrogen, it was so low in abundance that water clusters were not detected. A likely conclusion to be drawn from these results is that the molecules were undergoing self-protonation upon excitation or after charge-exchange with another ambient component. Again, although Penning ionization or charge exchange should have been possible, hexafluorobenzene was not detected

with any of the gases used. Unlike the other analytes employed in these studies, hexafluorobenzene has no protons available for self-protonation.

## Ionization Mechanism Conclusions

The positive-mode ionization mechanism studies performed in this work demonstrated that several different pathways contribute to the DART ionization process. These mechanisms and the means by which they were observed are discussed below.

### Dominant Mechanism 1: Gas-Phase Proton Transfer

Though the proton affinity experiments did not provide information on the source of the proton-donating species, they did demonstrate that gas-phase proton transfer is a dominant mechanism in positive-mode DART ionization. Sensitivity with or without competition from another analyte was heavily dependent on analyte proton affinity. The boiling point study reaffirmed this conclusion, because a volatility-based competitive relationship was never observed.

During the mapping studies three different types of ions were observed for most of the PAHs involved: molecular ions, protonated ions, and deuterated ions. The first of these were expected because PAHs have been known to form molecular ions in Powell laboratory for some time.[11] The last was also expected because the samples were analyzed in a $D_2O$-humidified environment. A more rapid increase in deuteration was observed for samples positioned farther than 20 mm from the DART source exit. At points closer than this distance, self-protonation was demonstrated. The formation of protonated molecules in the closed source configuration, which should have been devoid of water vapor, also supports this conclusion.

<u>Demonstrated Proton-Transfer Avenues:</u>

1. Proton-transfer with water clusters: $M + [(H_2O)_n + H]^+ \rightarrow [M+H]^+ + nH_2O$

2. Self-protonation: $M^{+\bullet} + M \rightarrow MH^{+} + [M - H]^{\bullet}$

**Dominant Mechanism 2: Molecular Ion Formation**

Seven different polycyclic aromatic hydrocarbons in the mapping experiments formed molecular ions. Knowledge of how Penning ionization produces ions, the ionization energies of the various analytes involved, and the energy of the metastable helium produced by a DART source dictate that Penning ionization should be possible with DART ionization. However, Penning-ionized molecules were not detected in the enclosed source studies when, again, this pathway should have been possible. It was not until nitrogen or air was added that any ions were seen.

Results from these experiments indicate that something other than Penning ionization allowed molecular ions to be detected. The other options for molecular ion formation are charge-exchange or photoionization. The latter seems unlikely because samples are ionized several inches from any light source. It is entirely possible that the energetic metastable species produced by the DART source immediately react with ambient components upon exiting and produce the mentioned charge-exchange agents. The absence of any type of detectable ionization when helium was added as an external gas was most perplexing, but further supported the conclusion that ionized ambient components are responsible for molecular ion formation.

Demonstrated Molecular Ion Formation Avenues:

1. Charge-exchange: $M + CE^{+\bullet} \rightarrow M^{+\bullet} + CE$ *CE=charge exchange agent

**General Conclusion**

Through a series of experiments, the mechanism of ionization of DART was systematically studied. The impact of proton affinity (both of the analyte and other compounds in its vicinity) on analyte sensitivity and detectability was demonstrated.

## General Conclusion

Through a series of experiments, the mechanism of ionization of DART was systematically studied. The impact of proton affinity (both of the analyte and other compounds in its vicinity) on analyte sensitivity and detectability was demonstrated. Progress was made in this endeavor with the observation of pathways that had seen little or no discussion in the literature for positive-mode DART, such as charge-exchange and self-protonation. Additionally, the source-enclosure experiments exposed the fact that DART ionization may not be as simple as previously discussed in the literature and that something other than Penning ionization may be responsible for the production of ions with helium DART. In all cases, the pathways of DART ionization appeared to be firmly rooted in atmospheric pressure chemical ionization.

Table 5-1. Target analytes for proton affinity studies.[66]

| Compound | Molecular Weight (g/mol) | Proton Affinity (kJ/mol) | Boiling Point (°C) |
|---|---|---|---|
| Cyclohexanone | 98.1430 | 841.0 | 155 |
| Aniline | 93.1265 | 882.5 | 181 |
| 2,5-Dimethylpyrrole | 95.1424 | 918.7 | 165 |
| 1-Methyl-2-Pyrrolidinone | 99.1311 | 923.5 | 202 |
| Piperazine | 86.1357 | 943.7 | 147 |
| 2,6-Lutidine | 107.1531 | 963.0 | 161 |
| Triethylamine | 101.1900 | 981.8 | 89 |

Table 5-2. Compounds used in boiling point competitions.

| Compound | Structure | Proton Affinity (kJ/mol) | Boiling Point (°C) |
|---|---|---|---|
| Aniline | 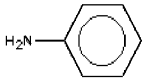 | 882 | 181 |
| Anthracene | 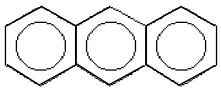 | 877.3 | 340 |
| 4-Fluorobenzamide | 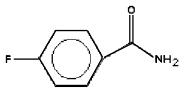 | 877.2 | ~290* |

*Value is estimated based on the melting points and boiling points of similar compounds.

Table 5-3. Polycyclic aromatic hydrocarbons used in mapping study.[66]

| PAH Name | Proton Affinity, kJ/mol | Ionization Energy, eV |
|---|---|---|
| Anthracene | 877.3 | 7.72 |
| 1,2-Benzanthracene | 861 | 7.45 |
| Biphenylene | 848.2 | 7.58 |
| Chrysene | 840 | 7.6 |
| Naphthacene | 905.5 | 6.97 |
| Perylene | 888.6 | 6.96 |

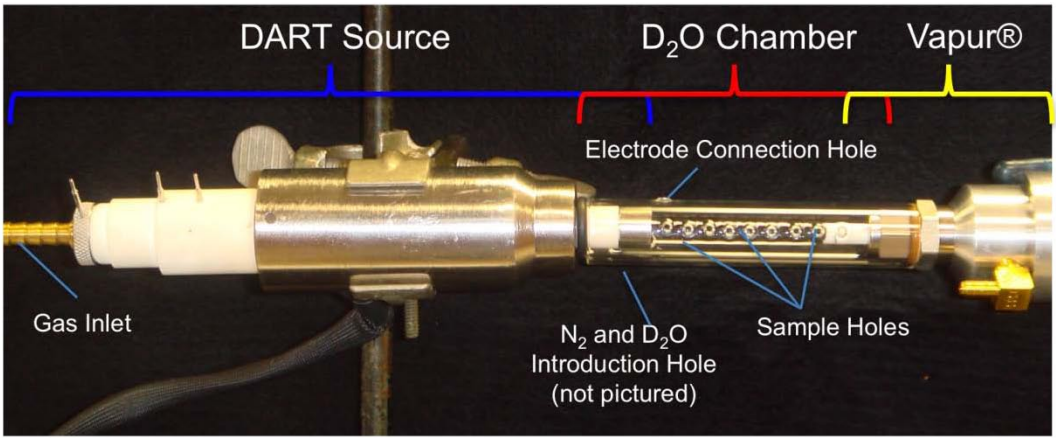


Figure 5-1. Photograph of custom-built DART source interfaced to a glass chamber. The glass chamber tube was used to create a deuterium oxide environment around the UF DART sampling region. Holes were covered with Teflon® tape (not shown) to prevent contamination with ambient water vapor.

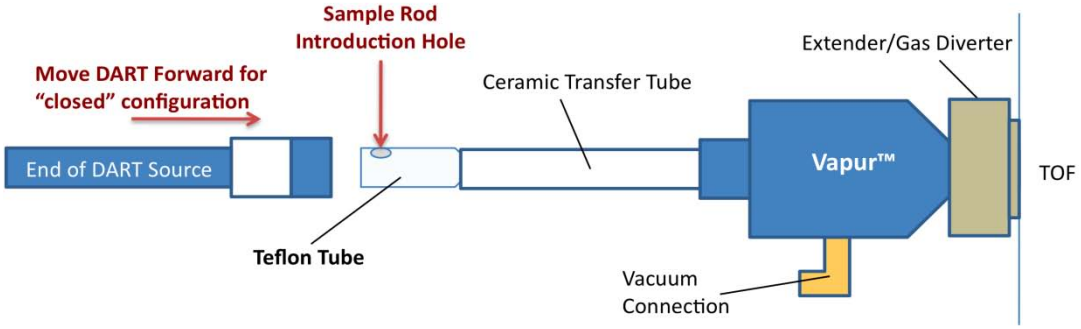


Figure 5-2. A schematic diagram of the sampling region with possibility of being closed is shown. The DART source was pressed against the end of the Teflon® tube to create a closed configuration.

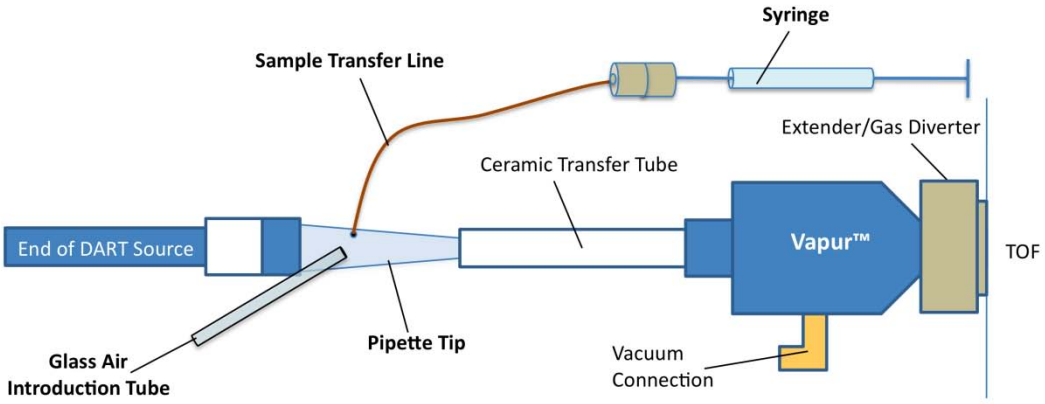


Figure 5-3. Final closed-source configuration. A pipette tip was used to make a connection between the DART source and the Vapur®.

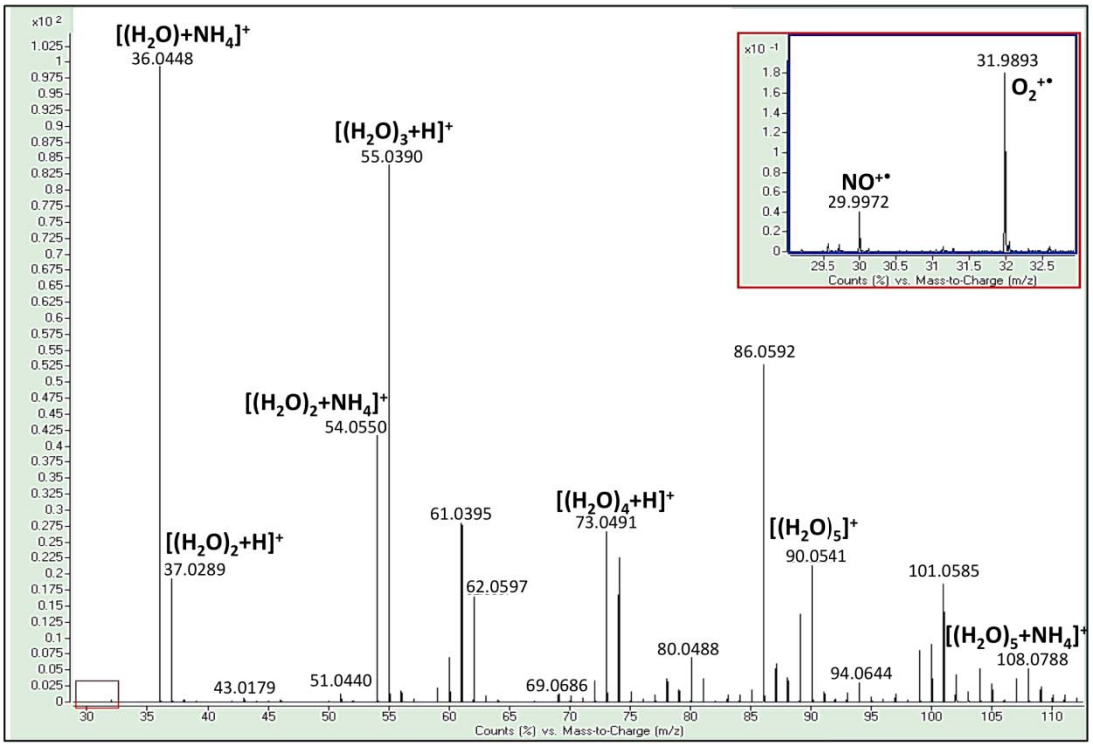


Figure 5-4. Background ion spectrum from the custom-built DART source. The inset is zoomed in on the masses ranging from 29 to 33 Da.

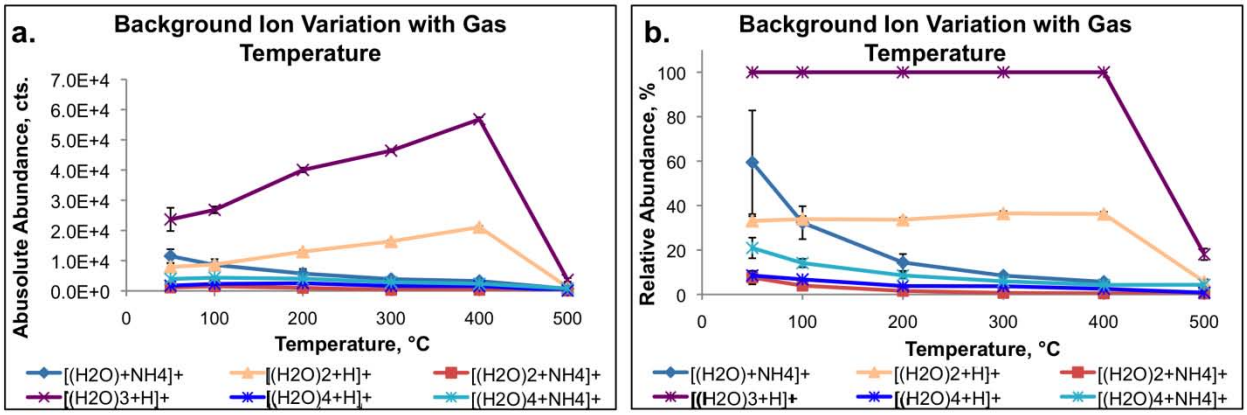


Figure 5-5. Variation of background water clusters with gas temperature expressed in terms of (a.) absolute abundance and (b.) relative abundance.

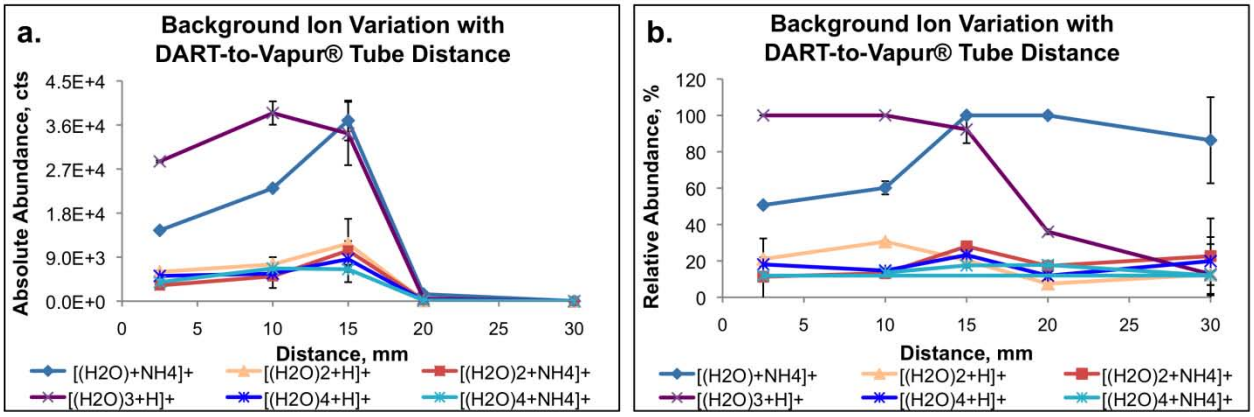


Figure 5-6. Variation of background water clusters with DART-to-Vapur® ceramic tube distance expressed in terms of (a.) absolute abundance and (b.) relative abundance.

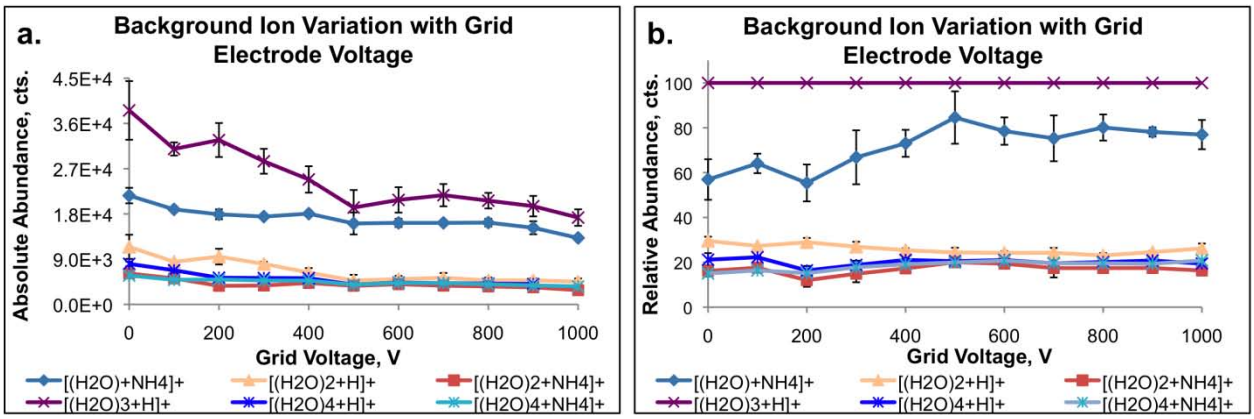


Figure 5-7. Variation of background water clusters with grid electrode voltage expressed in terms of (a.) absolute abundance and (b.) relative abundance.

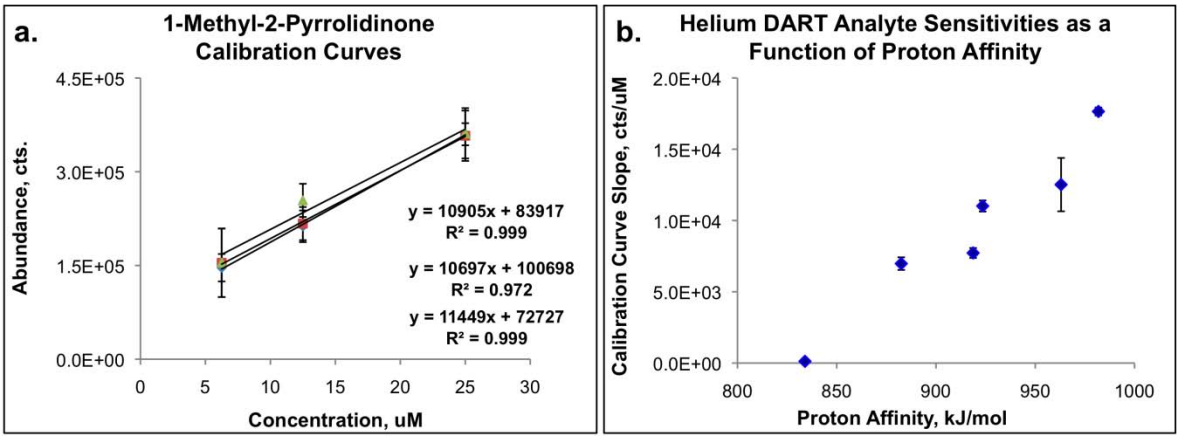


Figure 5-8. Short calibration curves and proton affinity sensitivity plots. Plots of 1-methyl-2-pyrrolidinone are given as an example of the three-point calibration curves of generated for sensitivity determination in (a.). The average sensitivities of all of the analytes are plotted in (b.) as a function of their PA.

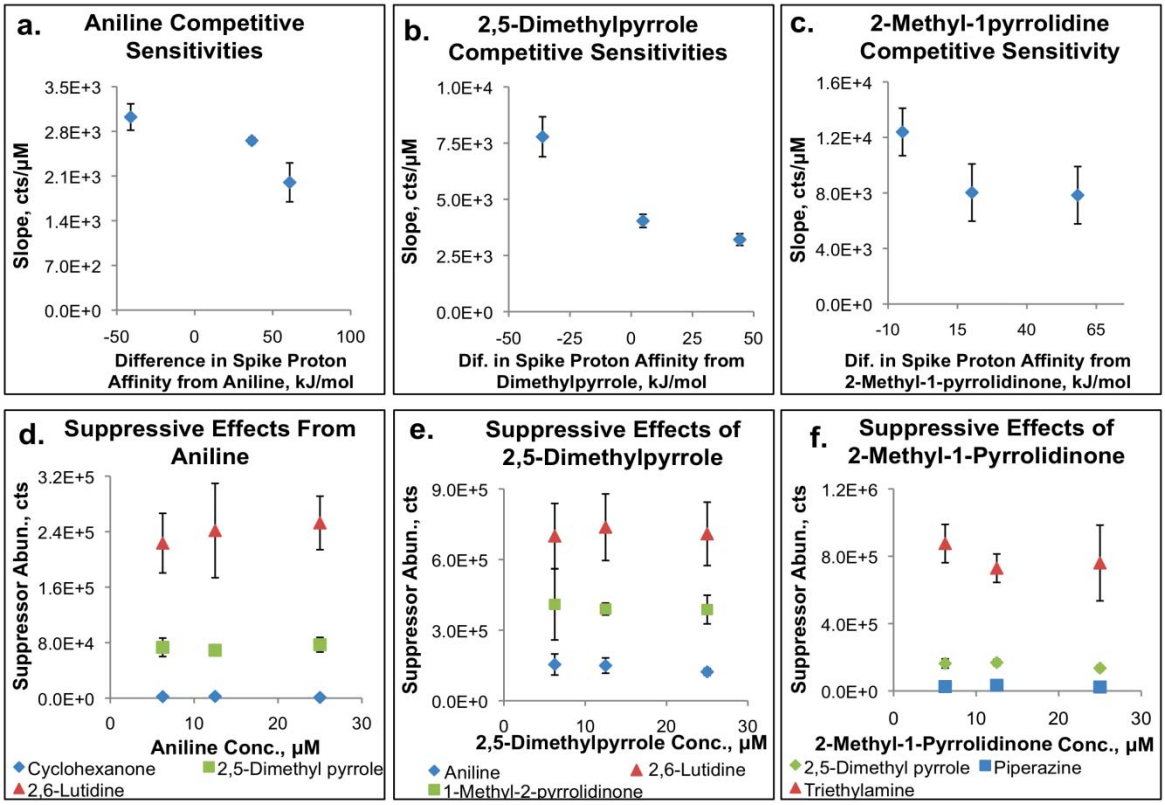


Figure 5-9. Competitive sensitivities plots. The changes in sensitivities of (a.) aniline, (b.) 2,5-dimethylpyrrole, and (c.) 2-methyl-1-pyrrolidine are shown. The change in signal of each of the spiked compounds as the concentration of the named analyte changes are shown in (d.) through (f.).

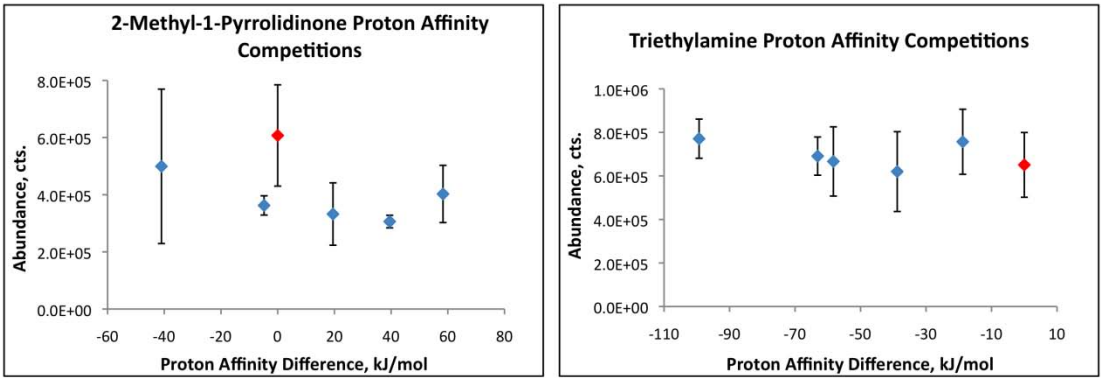


Figure 5-10. Example results of equimolar proton affinity competition experiments performed with 2-methyl-1-pyrrolidinone and triethylamine. Abundances of the target analytes are plotted against the difference in proton affinities of the target vs. that of the competitors. The red dots represent the response of the unspiked analyte. Note: Proton Affinity Difference = $PA_{Competitor} - PA_{Target}$.

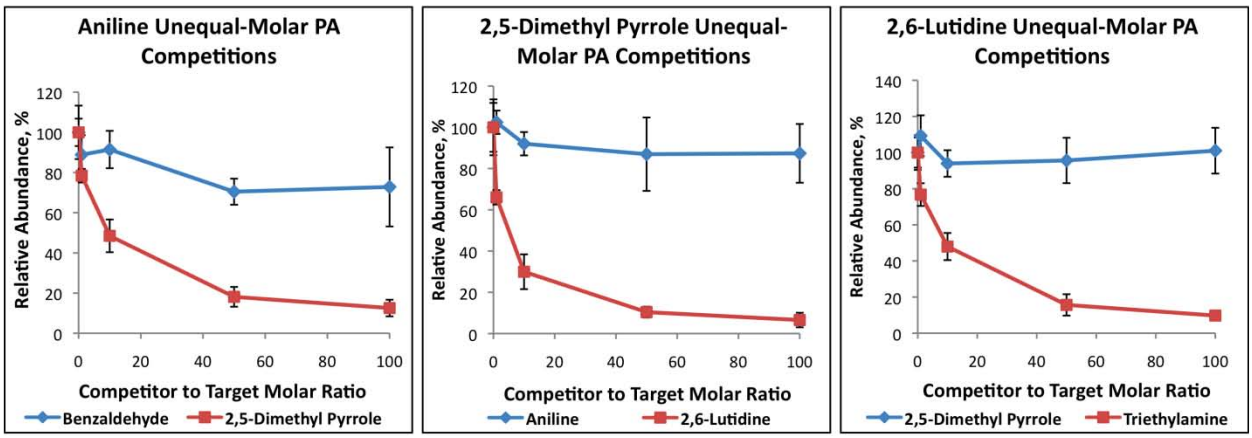


Figure 5-11. Results of unequal-molar proton affinity competitions performed with aniline, 2,5-dimethylpyrrole, and 2,6-lutidine. The abundances of the target analytes spiked with a competing compound are plotted relative to the average unspiked target analyte signal abundances. Competitions between the analyte and competitors with lower proton affinities are plotted in blue and the competitions with a higher-proton affinity competitor are plotted in red.

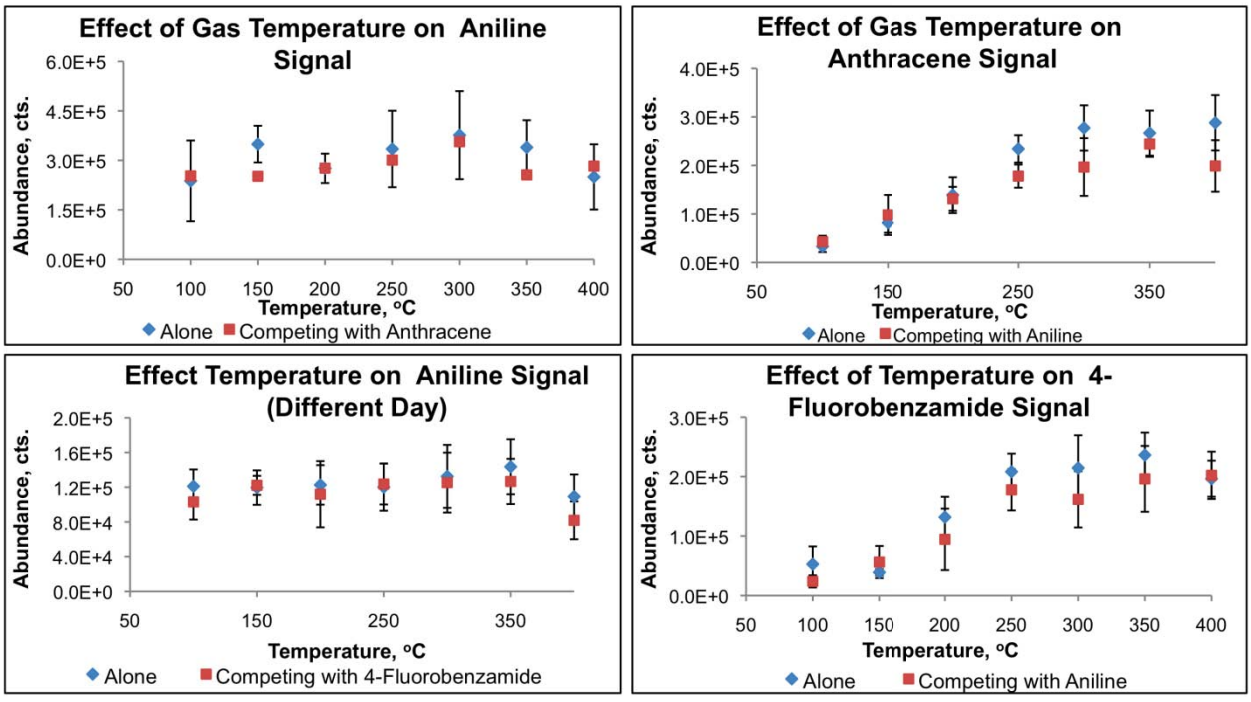


Figure 5-12. Analyte responses as a function of gas temperature during boiling point studies. The signal abundances of aniline, anthracene, and 4-fluorobenzamide are plotted as a function of gas temperature. Blue data points represent the named analyte analyzed alone and red data points represent the named analytes in competition.

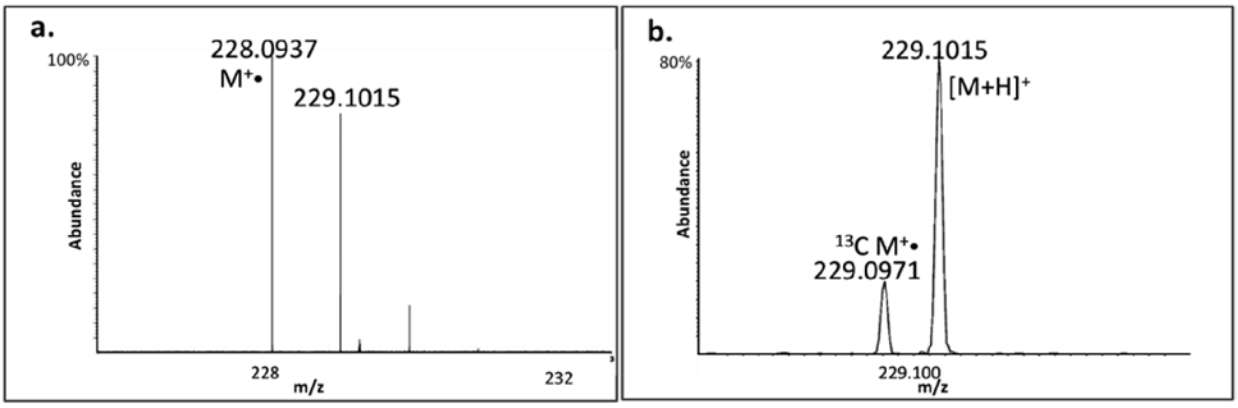


Figure 5-13. Spectra of 1,2-benzanthracene acquired with a 9.4 T Fourier transform ion cyclotron resonance mass spectrometer. These data (full spectrum in a. and zoomed-in in b.) demonstrate that both the molecular ion and the protonated molecule are produced during DART ionization.

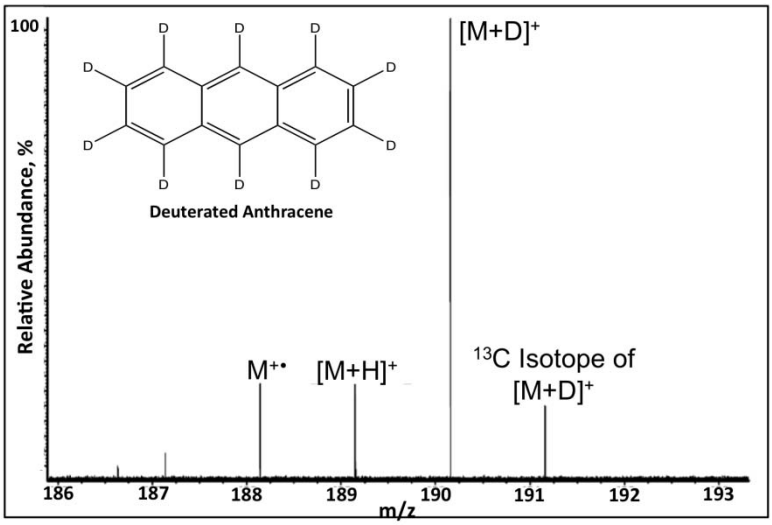


Figure 5-14. Spectrum of deuterated anthracene ionized by DART. The types of ions observed included a molecular ion, a protonated molecule, and a deuterated molecule.

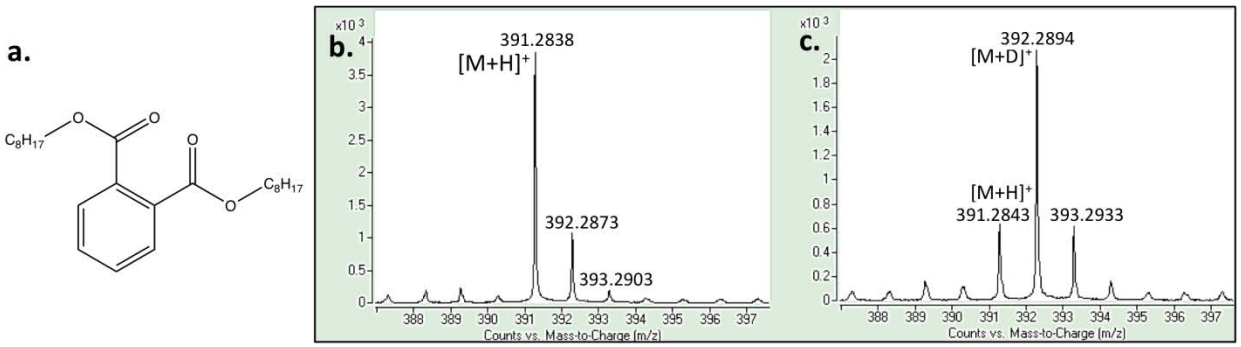


Figure 5-15. Structure and mass spectra of dioctylphthalate. As seen above in (a.), dioctylphalate has no exchangeable protons. The isotope distribution of dioctylphthalate may be seen (b.) when there is no deuterium oxide introduced (c.) and when the chamber is saturated with $D_2O$ humidity. Note: although this was the highest degree of deuteration that was ever seen for dioctylphalate; it was seen very consistently throughout experiments.

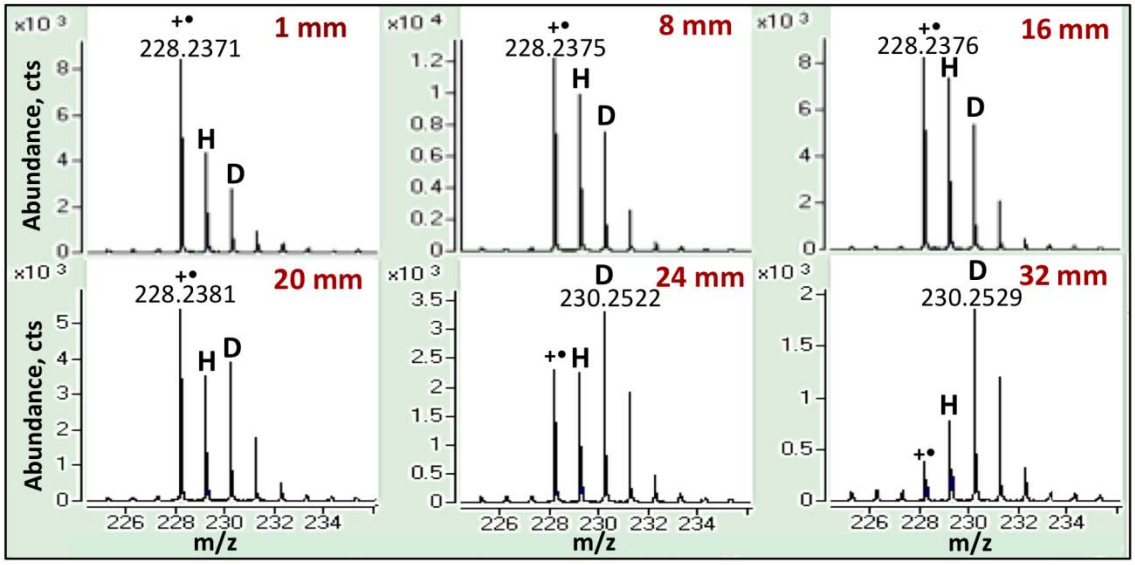


Figure 5-16. Variation in 1,2-benzanthracene ion distribution as a function of distance. Mass spectra of 1,2-benzanthracene at varying distances from the DART source are presented.

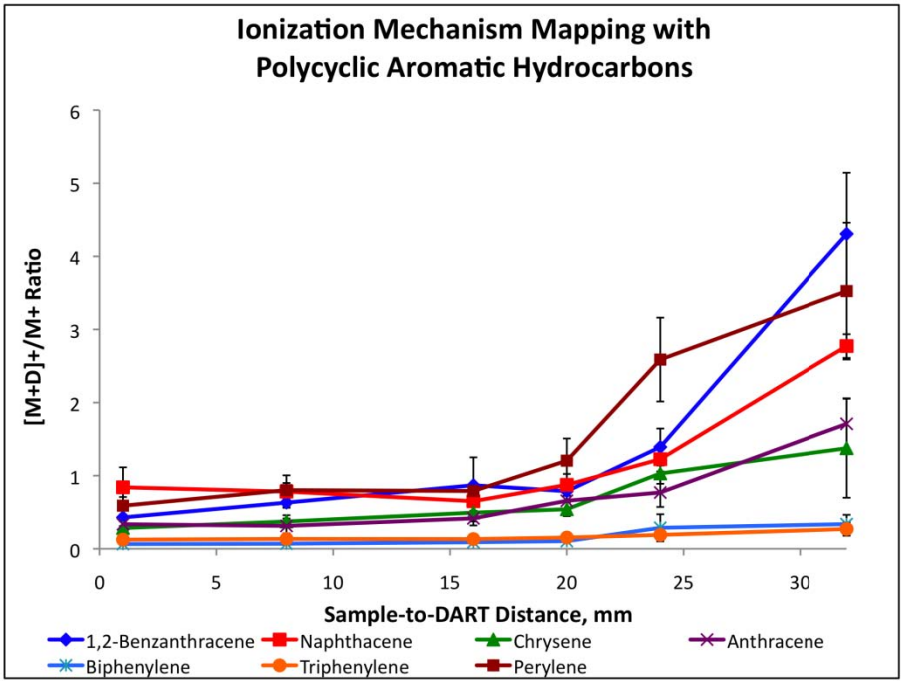


Figure 5-17**.** Variation in PAH isotope distribution as a function of distance. The deuterated molecule-to-molecular ion ratios of seven PAHs are plotted as the sample-to-DART distance was varied.

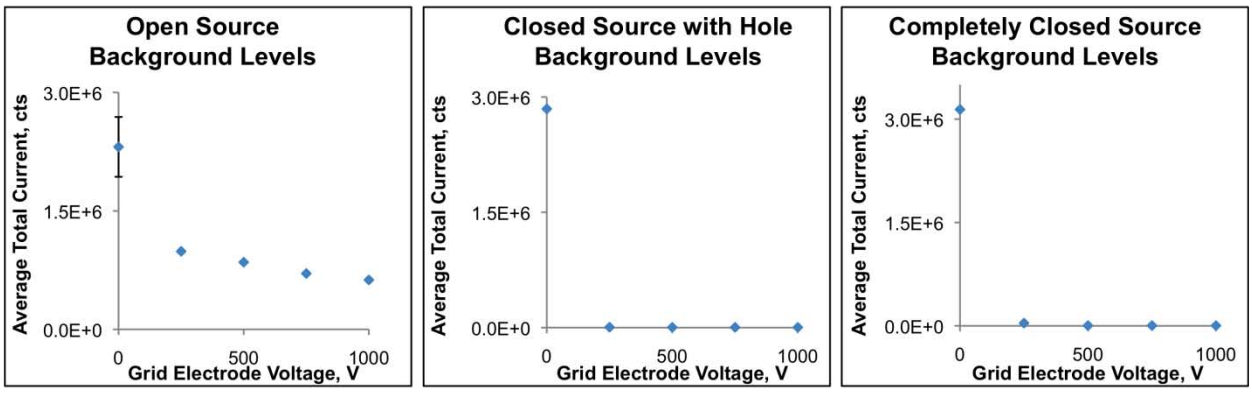


Figure 5-18. Background ion currents as a function of grid voltage. Background currents for the three different source configurations with the Teflon® tube enclosure are shown.

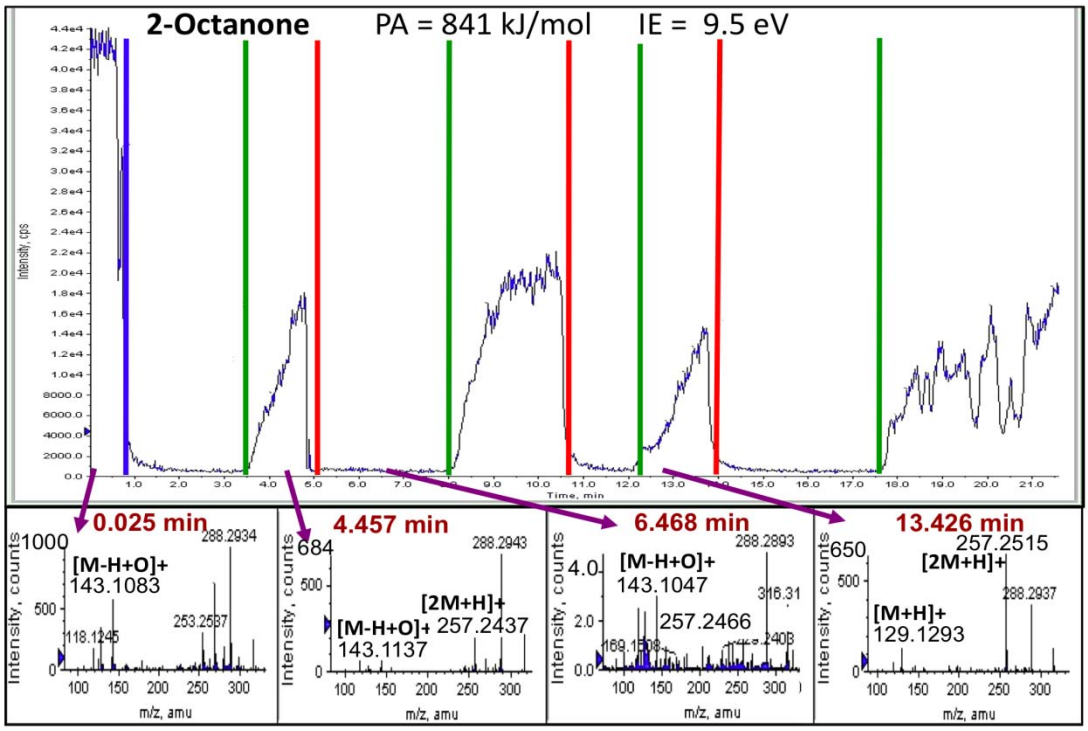


Figure 5-19. Total ion chromatogram (TIC) and extracted mass spectra from an analysis of 2-octanone inside the sampling region enclosure. Arrows are drawn from the regions of the TIC from which the mass spectra were extracted. The blue line indicates the time when the source was moved into the closed configuration, green lines represent when air was allowed to flow into the enclosure, and red lines denote when the airflow was stopped.

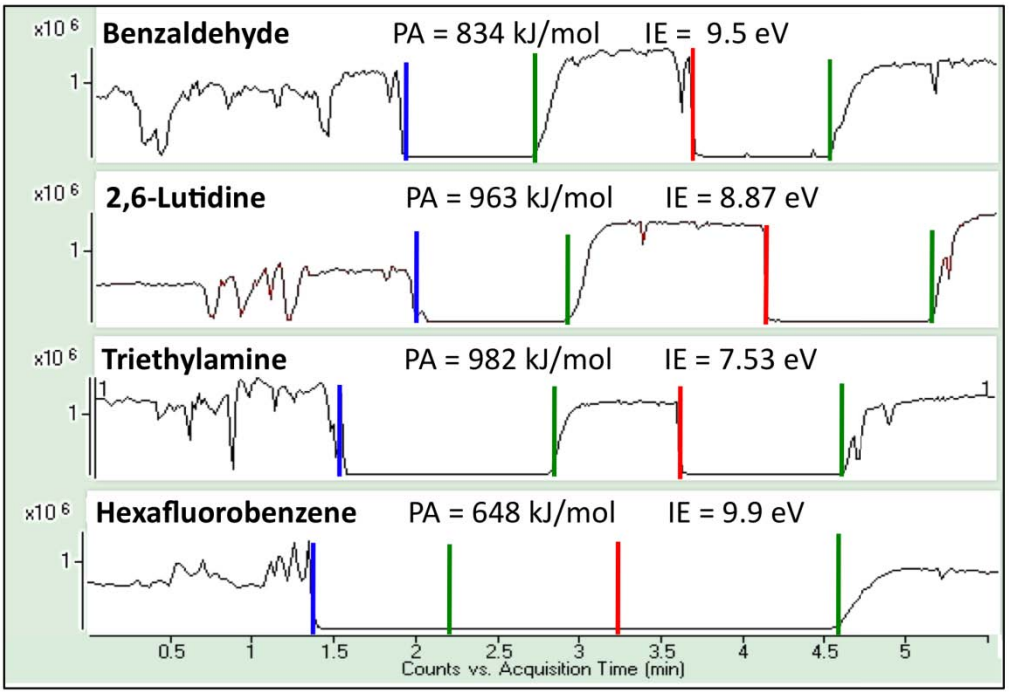


Figure 5-20. Total ion chromatograms of compounds analyzed in the source enclosure with periodic air introduction. Blue lines indicate when the source was closed. Green lines indicate when the air was turned on. Red lines indicate when the air is turned off.

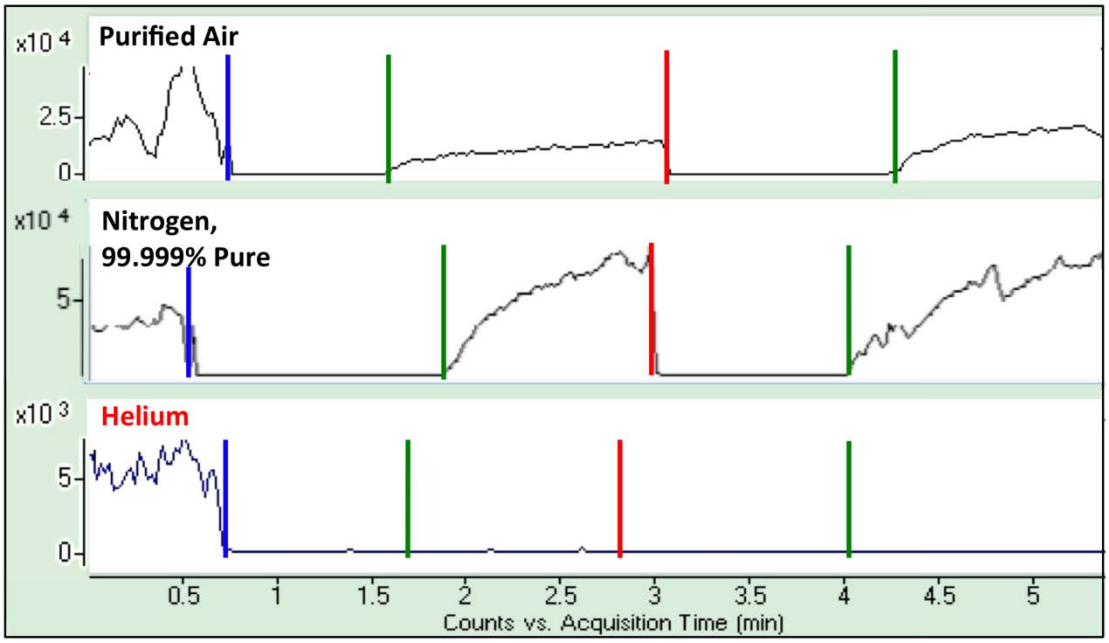


Figure 5-21. Total ion chromatograms of 2-octonone analyses in the enclosure with purified air, ultra-pure nitrogen, and helium introduced. Blue lines indicate when the source was closed. Green lines indicate when the external gas flow was began. Red lines indicate when the external gas flow was ended.

# CHAPTER 6
# THE COUPLING OF DART TO FT-ICR MASS SPECTROMETERS FOR ULTRAHIGH-RESOLUTION MASS ANALYSIS

## Introduction

To date, DART sources have been interfaced only to mass analyzers of low to moderate resolving power. Fourier transform ion cyclotron resonance mass spectrometry (FT-ICR MS) is uniquely advantageous over other mass analyzers because it provides higher resolving power and higher mass accuracy, and can isolate and observe ions for extended periods.[100] FT-ICR MS is thus well suited for analysis of complex mixtures containing multiple ions of the same nominal mass, as well as for tandem mass spectrometry. Combining ambient ionization methods such as DART with FT-ICR MS can provide an approach for analyses that are rapid, highly selective, and information-rich.

This chapter presents the first coupling of a DART source, custom-built at the University of Florida, with two FT-ICR mass spectrometers.

## Experimental

### Chemicals and Reagents

HPLC grade methanol was purchased from Burdick and Jackson (Muskegon, MI). Methylene chloride was purchased from Fisher Scientific (Fair Lawn, NJ). Both solvents were used without further purification. Polycyclic aromatic hydrocarbons (PAHs) 1,2-benzanthracene and 9,10-diphenylanthracene were purchased from Aldrich (Milwaukee, WI) and were dissolved in methylene chloride at 100 ppm (w/v) and dried on glass pipettes. Theophylline and bergamottin were purchased from Sigma Aldrich (St. Louis, MO) and dissolved in methanol at 10 ppm (w/v). Diisopropyl methylphosphonate (“DIMP”) was purchased from Alfa Aesar (Ward Hill, MA) and

vapors from an open container of it were introduced into the sampling region. A crude oil sample, NIST Standard Reference Material 2722, a heavy, sweet (low sulfur) crude oil, obtained from the National Institute of Standards and Technology (Gaithersburg, MD), was analyzed with no dilution. Fresh ruby red grapefruit (*citrus paradisi*) and habanero peppers (*capsicum chinense*) were purchased from a local grocery store and washed with tap water.

**Mass Analyzers**

**4.7 T FT-ICR MS.** The first FT-ICR MS instrument to which this ionization source was interfaced was a Bruker Daltonics (Billerica, MA) BioApex II 4.7 T FT-ICR MS. Daily tuning of ion focusing optics and mass calibration were performed with electrospray ionization (ESI) with ESI Tuning Mix (Agilent Technologies, Wilmington, DE). A voltage of -3500 to -4000 V was applied to the entrance electrode of the glass capillary for ESI (the spray needle was held at ground potential). After tuning, in preparation for the DART analyses, the capillary voltage was dropped to -1100 V and the hexapole accumulation period was raised from 0.5-1 second to 2-4 seconds depending on the sample. All other parameters were left unchanged.

**9.4 T FT-ICR MS.** A custom-built FT-ICR mass spectrometer equipped with a 22 cm horizontal room temperature bore 9.4 Tesla magnet (Oxford Corp., Oxney Mead, UK) controlled by a modular ICR data station (MIDAS)[128] provided the highest reported resolving power achieved with DART ionization. Ions passed through a heated metal capillary into an RF-only octapole, then through a quadrupole to a second octapole where they were accumulated for 1-2 seconds. Helium gas in the accumulation octapole served to collisionally cool the ions prior to transfer through a 200 cm rf-only octapole ion guide into a Penning ion trap (10 cm i.d. x 30 cm long).[129] Ions were

excited to their cyclotron radius by broadband frequency sweep (chirp) excitation.

**TOF-MS.** An Agilent 6210 TOF (Wilmington, DE) instrument was used for comparatively lower resolution studies at the University of Florida. The orthogonal geometry of the flight tube enables mass resolving power up to 18,000. Sampling with 2 GHz analog-to-digital (A/D) conversion at the detector allows mass resolving power up to approximately 6,000 at the lowest tune mass (118 Da), while sampling with 4 GHz A/D conversion allows mass resolving power above 10,000. Tuning and mass calibration with the instrument's autotune function were performed approximately every two days by use of ESI and the Agilent ESI Tuning Mixture.

### Custom-Built DART Source

The DART source described in Chapter 2 was used in this work. The copper heating block into which four Watlow Firerod® cartridge heaters were inserted was used for heating the gas. The heater was monitored and controlled with a Micromega temperature controller. Unless otherwise stated, the source parameters were as follows: needle electrode: +3 kV, ring electrode: +100 V, grid electrode: +250 V, heating block temperature: 100-450 °C (depending on sample), and gas flow-rate: 3 L/min. The source was aimed directly into the inlet of each of the three mass spectrometers from a distance of approximately ~2.5 cm. The DART source was interfaced to all three mass spectrometers with a 30° flared capillary extender (refer to Chapter 2 for more information).

## Results and Discussion

### Resolution Comparison of a TOF and an FT-ICR Mass Spectrometer

Although a ten-scan DART-FT-ICR mass spectrum takes about 30 seconds to acquire, the method is nevertheless attractive for reliable identification of multi-

component samples with a higher degree of specificity than the use of instruments capable of lower resolving powers. Figure 6-1 shows mass spectra obtained simultaneously for solid theophylline ([M+H]+ = 181.0720 Da) and DIMP ([M+H]+ = 181.0988 Da) vapors with DART-TOF (Figs. 6-1 a. and 6-1 b.) and DART-FT-ICR MS (Fig. 6-1 c.). With 2 GHz A/D conversion, the TOF-MS was unable to achieve the mass resolving power of 6,700 required to separate these peaks and instead one broad peak with a mass that is approximately the mean of the two masses was observed (Figure 6-1 a.). For 4 GHz A/D conversion, the TOF-MS displayed peaks for the protonated molecules with resolving power, $m/\Delta m_{50\%} \approx 10{,}000$ (Figure 6-1 b.). Although not baseline-resolved, the mass errors of the observed peaks were ł̶e̶s̶s̶ than 10 ppm. Figure 6-1 c. shows that the 4.7 T FT-ICR MS easily achieved baseline resolution for these species. The resolving power for the theophylline and DIMP protonated molecules was ~71,000 and ~62,000, respectively, with mass errors of 5.5 ppm and 2.8 ppm. FT-ICR MS demonstrated improved mass accuracy and far superior resolving power than TOF-MS.

**Polycyclic Aromatic Hydrocarbon Studies**

Both molecular radical cations and protonated molecules may be observed with DART-ionized PAHs. To resolve $M^{+\bullet}$ containing one $^{13}C$ from monoisotopic $[M+H]^+$, a resolving power of 51,000 for 1,2-benzanthracene and 74,000 for 9,10-diphenylanthracene is required. The 9.4 T FT-ICR MS displays resolving power greater than 300,000 for both analytes (Figure 6-2 b. and 6-2 d.). The 4.7 T FT-ICR MS resolved $M^{+\bullet}$ containing one $^{13}C$ from monoisotopic $[M+H]^+$ of 1,2-benzanthracene with $m/\Delta m_{50\%} \approx 60{,}000$ (Figure 6-2 c.), but failed to resolve the analogous peaks for 9,10-diphenylanthracene (Figure 6-2 f.). Where the species were resolved, comparable

mass accuracies (3.5 ppm or less) were observed with both instruments for the two ion types (Figure 6-2 b. and 6-2 c.), although improvement may be possible with instrumental calibration. Differences in the apparent distributions of the 1,2-benzanthracene and 9,10-diphenylanthracene isotopes (Figure 6-2 a. and 6-2 d.) can be attributed to the differences in the relative abundances of the two ion types.

The 4.7 T FT-ICR MS can produce resolving power greater than 100,000 for most ions below 1000 Da.[100] The sub-60,000 resolving power seen in Figure 6-2 c. and 6-2 f. may result from the increased pressure in the analyzer cell caused by the DART gas flowing into the mass spectrometer. In this situation, collisions with background gas atoms could damp the transient response signal and reduce the resolving power. However, the effect could also be attributed to a number of other factors including space charging, imperfections in the excitation conditions, and ion cloud irregularities.

As demonstrated by the 4.7 T FT-ICR mass spectra in Figure 6-3, varying the distance between the sample and the inlet allows one to observe different types of ions from PAH molecules. When a 1,2-benzanthracene sample deposited on a glass pipette was placed less than 1 mm from the exit of the DART source, the primary ionization mechanism appeared to be either direct Penning ionization or charge transfer with molecular oxygen, and an odd-electron molecular ion was produced. When the sample was positioned 5 mm from the exit, a mixture of molecular ions and protonated molecules was seen. Finally, when the sample was 40 mm from the source, only protonated species were observed. This experiment was the first demonstration that there are at least two mechanisms by which PAH molecules may ionize with DART and presents an interesting direction one may take in performing DART mechanism studies.

Chapter 5 showed that similar behavior was also observed with several other PAH molecules.

**"Real" Samples**

Due to its ultrahigh mass resolving power and accurate mass capability, FT-ICR MS presents an enhanced utility for the analysis of unknown species. As for TOFMS, a wide range of samples from a variety of matrices may be analyzed by DART-FT-ICR MS. To date, drug tablets, food items, cigarettes, gaseous samples, pesticides, and chemical warfare simulants have been analyzed; the only difference in the experimental design was that the sample was held in place in front of the FT-ICR inlet longer than for the TOFMS. Three examples of the utility of accurate-mass/high resolution DART-FT-ICR MS for the analysis of two simple food products and a complex crude oil sample are presented below.

**Grapefruit**

By direct analysis from a pipette inserted into the flesh of grapefruit, the spectrum in Figure 6-4 was obtained with the 4.7 T FT-ICR MS. A nearby opened container of ammonium hydroxide resulted in ammonium adducts for some simple carbohydrates. Based on their accurate masses, some of those masses are likely due to fructose and glucosan (i.e., a polysaccharide that yields glucose on hydrolysis) which have been previously observed in grapefruit.[130] Because the isomer types of these masses are unknown, the identifications of fructose and glucosan are tentative. Bergamottin (calculated $[M+H]^+$ = 339.1591 Da), which has been identified as a cytochrome P450 inhibitor and is the cause of grapefruit consumption related-pharmacokinetic interactions was also observed in low abundance.[131] The identification of bergamottin was further confirmed by analysis of a pure standard (not shown). The resolving powers achieved

for the low-abundance ions such as ammoniated fructose and protonated bergamottin were ~30,000 and ~20,000.

**Pepper**

Direct analysis of the vein of a habanero pepper revealed a protonated molecule and a proton-bound dimer of capsaicin (Figure 6-5). The added trapping that occurs with the 4.7T FT-ICR MS both in the hexapole, where ions are first accumulated, and in the analyzer cell increases the likelihood of ion-ion and ion-molecule interactions and the formation of proton-bound dimers. This increased propensity for dimer formation has also been observed with dilute solutions of mass standards such as caffeine and the pesticide methamidophos. Based on its accurate mass, m/z 322 likely resulted from oxidation of capsaicin (calculated $[M+O+H]^+$ = 322.2013 Da). The resolving power for the protonated capsaicin was ~50,000.

**Crude oil**

By use of a syringe pump for introduction directly into the heated gas stream exiting the DART source, NIST Heavy Sweet crude oil could be analyzed continuously and for a very long time. With 100 scans summed, a distribution of hydrocarbons that is characteristic of crude oil samples was observed by 4.7 T FT-ICR MS (Figure 6-6). Because it is a standard reference material, the NIST Heavy Sweet crude oil was expected to contain species ranging from 200-900 Da. With DART ionization, only the volatile, low-molecular weight species in this sample were detected. Changes in the heating of the DART source, syringe positioning, or crude oil flow rate could extend the upper mass limit by improving analyte desorption.

Even taking into account the limited mass range, the mass spectrum obtained was less complex than those reported in other studies of crude oil based on other ionization

techniques.[132] One reason is the limited mass resolution of the 4.7 T FT-ICR MS. As the inset in Figure 6-7 reveals, many poorly resolved clusters of peaks appear throughout the spectrum. Although the sample is clearly complex, unambiguous identification of most of the components was impossible. Dramatically better results have been reported with a 9.4 T FT-ICR MS.[132] The present mass spectral simplicity may also result from the competitive nature of DART ionization; once in the gas phase, the most easily ionized species will dominate. For example, the ionization of species with low proton affinity may be suppressed entirely by the presence of species with higher proton affinity. Use of dopants, such as ammonium hydroxide, in the sampling region may facilitate ionization of a broader range of analytes.

The combination of DART with the 4.7 T FT-ICR MS was less successful than desired for this crude oil sample. Improved results can probably be achieved with a higher-resolving power instrument and sample-specific DART source optimization.

## Conclusions

A custom-built direct analysis in real time ionization source was successfully coupled to each of two different Fourier transform ion cyclotron resonance mass spectrometers for the first time. It should be noted that a compact DART source, such as the one discussed in this work, is advantageous because it can easily be adapted to any mass spectrometer with an atmospheric pressure inlet. This design makes this device easily transportable and provides a wide range of options for source and sample positioning.

The superior resolving power of FT-ICR MS was demonstrated by comparing mass spectra of the isobaric species DIMP and theophylline. Although TOFMS offers faster analysis, it may not be able to resolve isobaric masses in complex samples. By

analyzing different PAH molecules, the highest mass resolving power yet reported for DART ionization was achieved. A spatial variation in the ionization mechanisms that occur between the DART source and the mass spectrometer was noted for the first time (this work occurred prior to the work reported in Chapter 5). Mass spectra of several analyte types analyzed by DART-FT-ICR MS were also reported, demonstrating that this technique may be useful for a wide variety of applications.

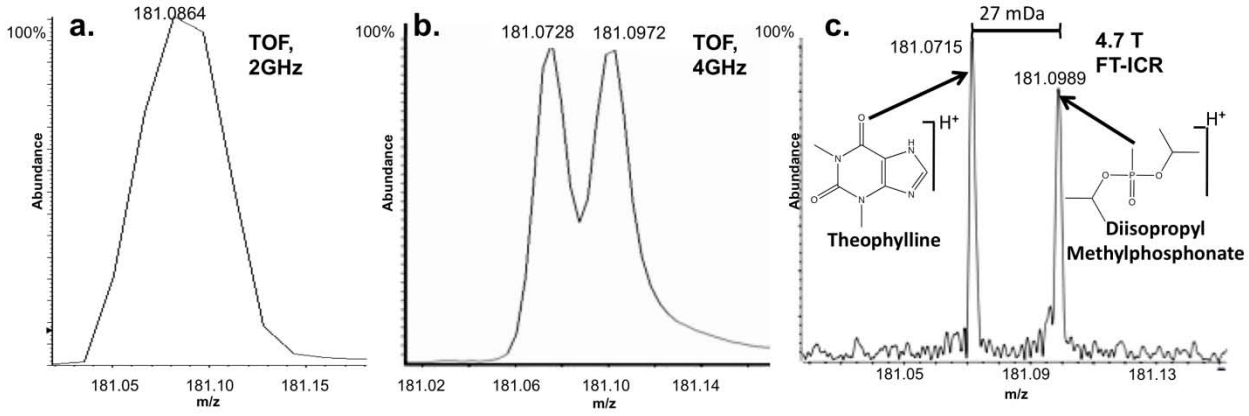


Figure 6-1. Mass spectra of solid theophylline (calculated $[M+H]^+$ = 181.0720 Da) and DIMP (calculated $[M+H]^+$ = 181.0988 Da) vapor analyzed by (a) TOFMS with 2 GHz A/D conversion, (b) TOFMS with 4 GHz A/D conversion, and (c) 4.7 T FT-ICR MS. Each peak obtained with the 4 GHz TOF exhibited $m/\Delta m_{50\%} \approx 10{,}000$ and mass errors below 10 ppm. The resolving power achieved with the 4.7 T FT-ICR MS was ~70,000 with mass errors of 5.5 ppm or less.

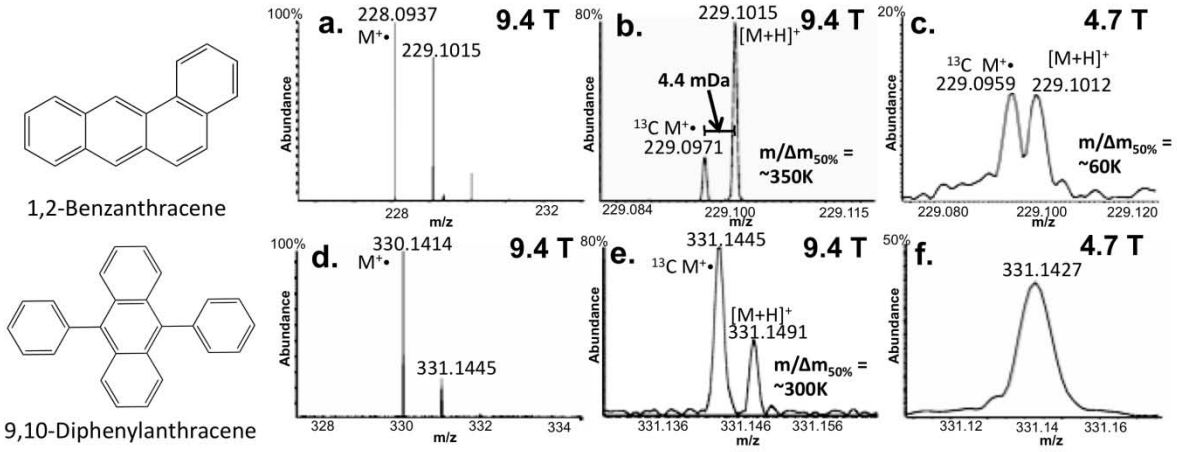


Figure 6-2. Mass spectra of 1,2-benzanthracene and 9,10-diphenylanthracene acquired by 9.4 T FT-ICR MS and 4.7 T FT-ICR MS. Ultrahigh resolution is demonstrated by the separation of the molecular ion containing one $^{13}C$ and protonated monoisotopic 1,2-benzanthracene analyzed by 9.4 T FT-ICR MS (a.), mass scale-expanded in (b.) and 4.7 T FT-ICR MS (c.). Greater resolving power is required to distinguish the molecular ion containing one $^{13}C$ and protonated monoisotopic 9,10-diphenylanthracene, which is possible with 9.4 T FT-ICR MS (d., mass scale-expanded in e.) but not with 4.7 T FT-ICR MS (f.).

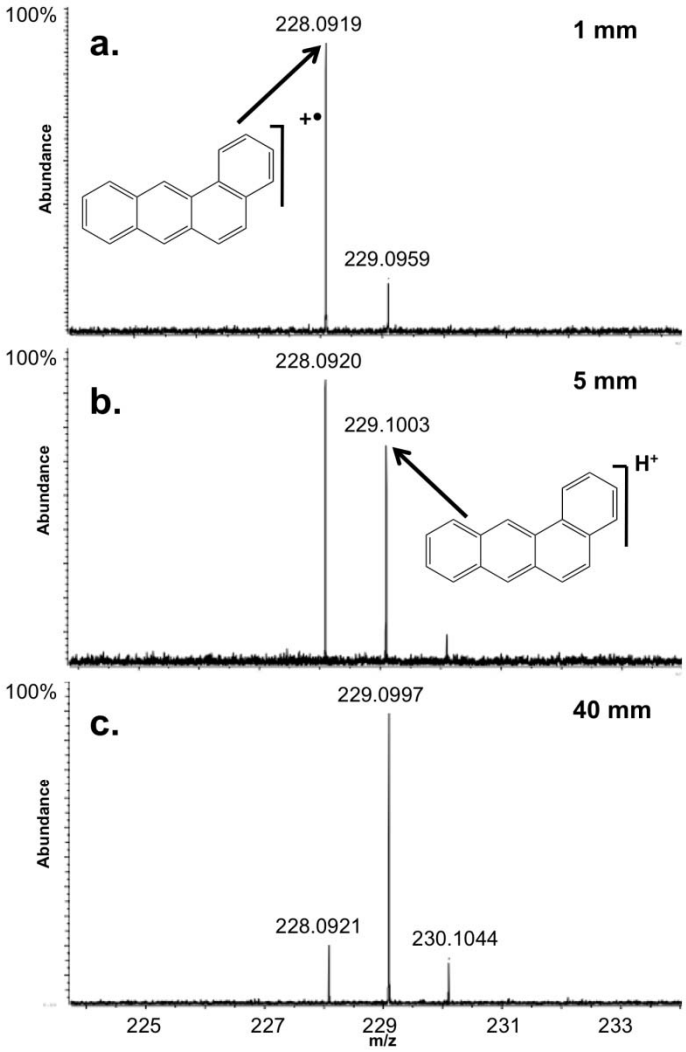


Figure 6-3. 1,2-Benzanthracene mass spectra acquired by 4.7 T FT-ICR MS. Differences in the relative abundances of $M^{+\bullet}$ and $[M+H]^+$ ions from 1,2-benzanthracene are seen when the sample is placed (a.) 1 mm, (b.) 5 mm, and (c.) 40 mm from the exit of the DART source.

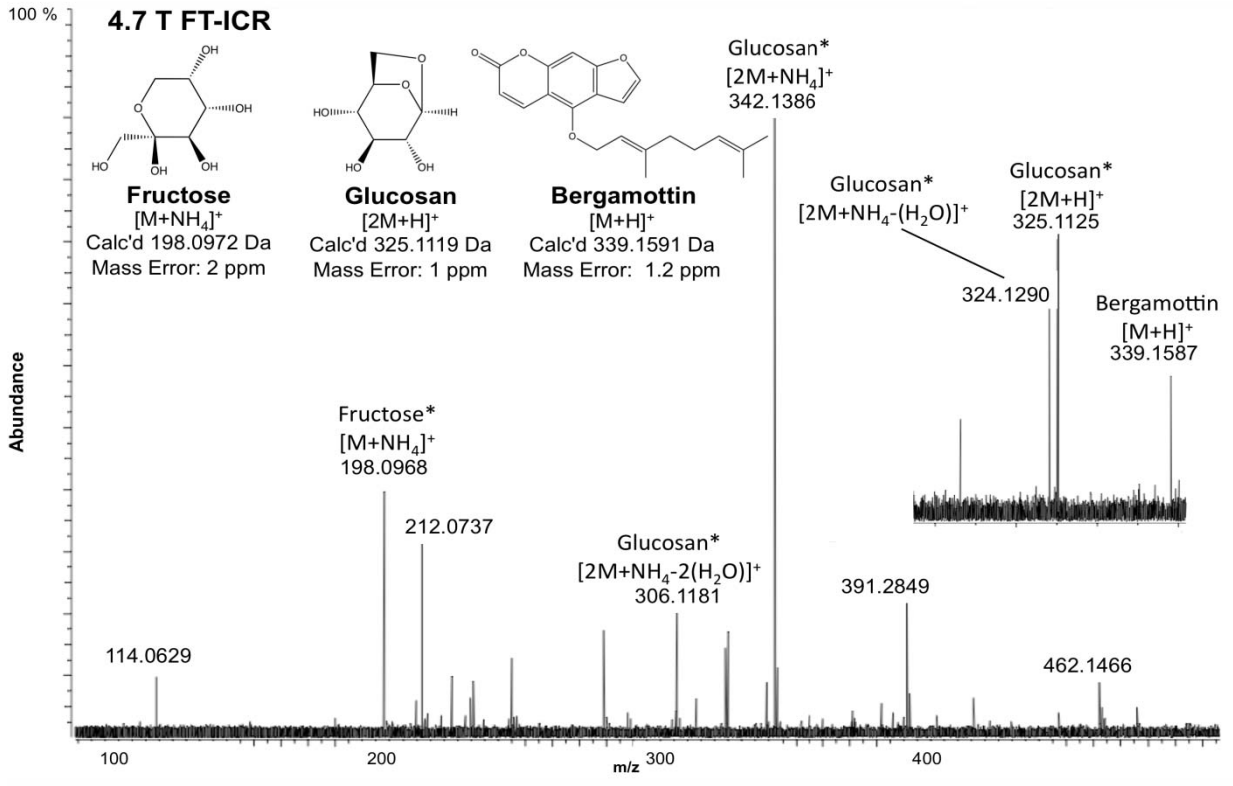


Figure 6-4. 4.7 T FT-ICR mass spectrum from grapefruit flesh deposited on a glass pipette. Protonated bergamottin (calculated $[M+H]^+$ = 339.1591 Da) was observed in low abundance. Tentative identifications are marked with asterisks and include ammoniated fructose (calculated $[M+NH_4]^+$ = 198.0972 Da) and several species of glucosan (calculated $[2M+H]^+$ = 325.1129 Da; $[2M+NH_4]^+$ = 342.1395 Da; $[2M+NH_4\text{-}H_2O]^+$= 324.1289 Da; and $[2M+NH_4\text{-}2(H_2O)]^+$ = 306.1183 Da).

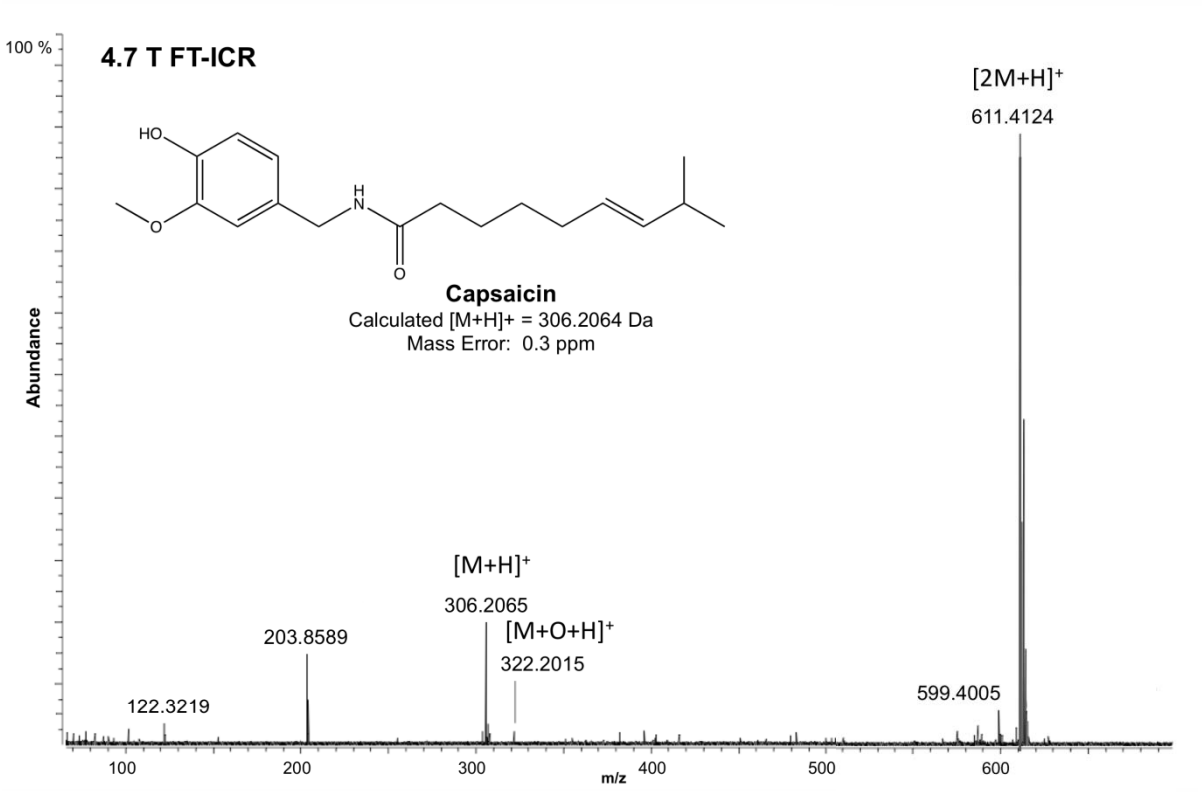


Figure 6-5. 4.7 T FT-ICR mass spectrum acquired by directly introducing a section of habanero pepper into the DART stream. Both the protonated capsaicin (theoretical [M+H]+ = 306.2064) and its proton-bound dimer (theoretical [2M+H]+ = 611.4055) are observed as well as an oxidation product of capsaicin (theoretical [M+O+H]+ = 322.2013).

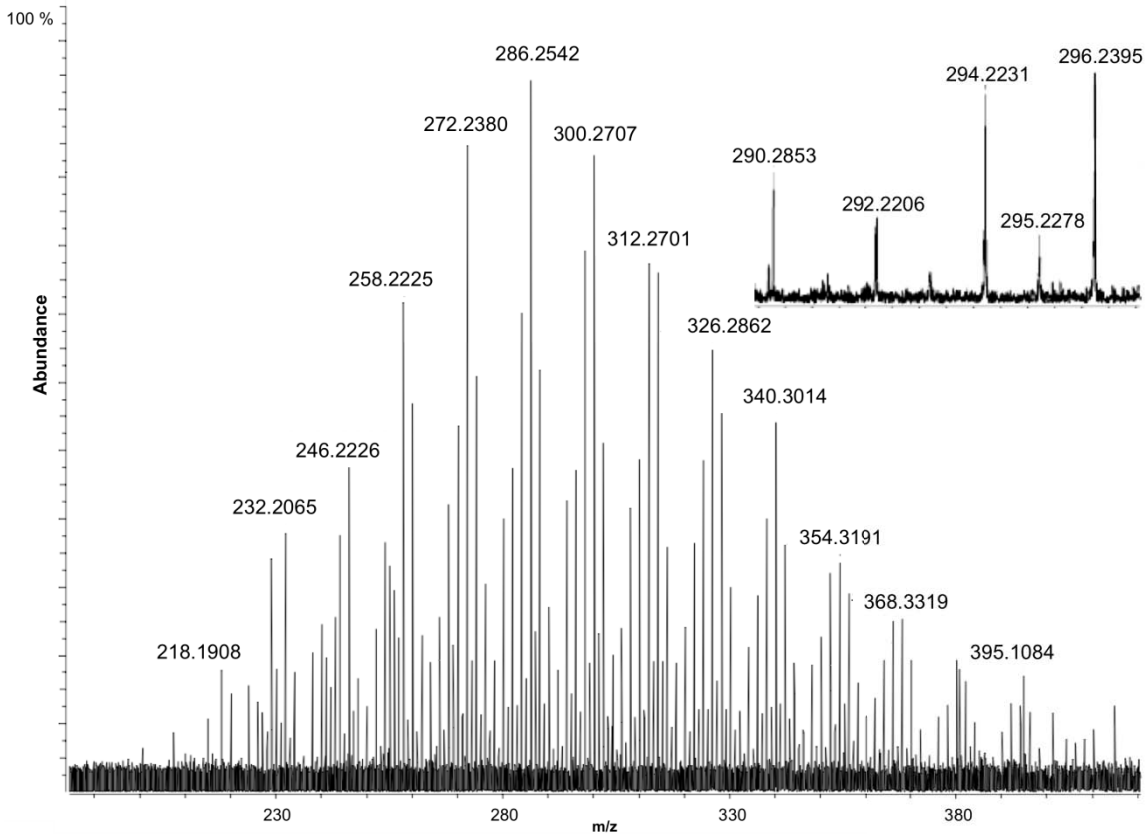


Figure 6-6. Spectrum obtained by introducing NIST heavy sweet crude oil with a syringe pump into the DART gas stream using the 4.7 T FT-ICR MS. The inset shows a representative section of masses containing several clusters of species and demonstrates the complexity of this sample.

# CHAPTER 7
# STRUCTURAL ELUCIDATION OF DART-IONIZED NERVE AGENT SIMULANTS WITH INFRARED MULTIPLE PHOTON DISSOCIATION SPECTROSCOPY

## Introduction

Compound identification with DART-MS is usually accomplished by measurement of analytes' exact masses.[133-135] Though H/D exchange was applied in one report, typically any structural elucidation in DART-MS experiments has been gained by performing source collision induced dissociation (CID)[17,83] Source-CID is induced by increasing the electric field gradient between the capillary exit and the skimmer in the first vacuum stage of a mass spectrometer. As the pressure is relatively high (up to about 1 torr) at this point in the mass spectrometer, many collisions occur between the analyte ions and the background gas molecules, causing the internal energy of the ions to increase to their dissociation threshold.[136] Though the dissociation can be tuned to some degree by varying the voltages of the capillary and skimmer, source-CID remains nonspecific because the ion of interest is not mass-selected prior to fragmentation.[137-139] When multi-component mixtures are analyzed without prior separation, as is the case with DART-MS, source-CID can create very complicated mass spectra that are difficult to interpret.

Mass spectrometers capable of tandem-in-space or tandem-in-time experiments may be used to selectively isolate and fragment parent ions of interest. Two fragmentation methods that may be employed in the cell region the 4.7 T FT-ICR MS at UF are sustained-off resonance irradiation-collision induced dissociation (SORI-CID) and infrared multiple photon dissociation (IRMPD).[140-144] With SORI-CID, the pressure inside the cell is raised to allow more collisions and the ion of interest is excited to a frequency offset from its cyclotron frequency. In this process, the selected ions

alternately increase and decrease in cyclotron radius (and kinetic energy) and undergo many collisions.[145] A slow internal energy buildup in the molecule eventually leads to dissociation.

The dissociation method focused on in the work reported in this chapter is IRMPD. This technique is performed by directing an infrared (IR) laser beam into the cell of a mass spectrometer to irradiate trapped ions. After absorbing each photon, the mass-selected ions undergo a process known as intramolecular vibrational energy redistribution (IVR) and the absorbed energy is distributed throughout the other vibrational modes of the molecules.[140-142,146] Because the initial absorbing mode returns to ground state after IVR, the process can be repeated with one wavelength until dissociation occurs.[140] This process is depicted in Figure 7-1. IRMPD is advantageous as a method of dissociation because it can be performed without raising the pressure of the analyzer cell region (and not sacrificing mass resolving power) and because it is wavelength-dependent and can be used to gain spectroscopic (and thus structural) information.

In the work discussed here, IRMPD action spectroscopy was performed on DART-ionized molecules with both the Free Electron Laser for Infrared Experiments (FELIX)[147] at the FOM Institute for Plasma Physics Rijnhuizen in Nieuwegein, The Netherlands and an optical parametric oscillator (OPO) laser at UF. Photons are generated in FELIX by oscillating free electrons through a series of oppositely poled magnets known as an undulator (Figure 7-2).[147] The spacing of the magnets in the undulator and the energy of the electrons dictate the wavelength of the light exiting the laser. The radiation exiting FELIX is composed of 30 to 50 mJ macropulses, each of

which is composed of hundreds of micropulses spaced 1 ns apart.[147] FELIX is operated with 5 or 10 macropulses being generated per second (i.e. 5 or 10 Hz). The great advantage of FELIX is that it can be tuned over a very wide range of wavelengths (approximately 5 to 250 μm).

OPO lasers generate different wavelengths of light by "pumping" a beam of light generated by another laser into a nonlinear optical crystal.[148] The pump beam is converted into two lower frequency waves by means of nonlinear optical interaction with the crystal. The outputted wavelengths may be tuned by directing the pump laser through different positions of the crystal, a.k.a. poling periods, and/or by varying the temperature of the crystal.

Infrared multiple photon dissociation spectra were generated for dimethyl methylphosphonate ("DMMP") and diisopropyl methylphosphonate ("DIMP") with the goal of elucidating the position of protonation on the two compounds (structures are given in Figure 7-3). Based on their structures, it is most likely that protonation will occur either on the phosphonyl oxygen atom of these molecules or one of the singly-bonded oxygen atoms. These compounds have been widely used to mimic the chemical and physical properties of the class of chemical warfare agents known as "G agents" such as sarin and tabin without the associated toxological properties.[149-152] As demonstrated in the previous chapters of this dissertation, DMMP and DIMP are readily ionized by DART. Making them ideal for a study coupling DART and IRMPD spectroscopy, these compounds are semi-volatile liquids that can be used in large quantities for long periods of time without contaminating the source region of a mass spectrometer because the hot DART gas continually cleans whatever surface it strikes.

Density functional theory calculations were performed to compute theoretical IR spectra of the DIMP and DMMP with the protons in each possible position.

## Experimental

### Chemicals and Reagents

Dimethyl methylphosphonate (DMMP) and diisopropyl methylphosphonate (DIMP) were purchased from Alfa Aesar (Ward Hill, MA) and dissolved in methanol in concentrations of 100 ppm to 1 mg/ml depending on instrument stability. Arginine, 18-crown-6, methanol, and water were supplied by the Molecular Dynamics group at the FOM Institute for all experiments in their facility. Arginine and 18-crown-6 were dissolved in 1:1 mixtures of water and methanol in 1 mM concentrations. HPLC grade methanol was purchased from Burdick and Jackson (Muskegon, MI) and used without purification for all experiments at UF.

### Instrumentation

#### Custom-built DART source

The custom-built DART source discussed in Chapter 2 was used in this work. The power supplies discussed in Chapter 2 were used to power the electrodes of the source for the experiments at UF. The relatively small size of this DART source made it simple to transport (on flights to Europe) and to couple to any mass spectrometer with an atmospheric pressure inlet. Heating was done with an insulated coil heater removed from an Agilent atmospheric pressure photoionization source. The heater was powered with variable AC transformers typically operated to at 20-30 percent of their maximum power.

At the FOM Institute, a high voltage power supply normally used with the electrospray ionization source was used to power the needle electrode and the counter

electrode was grounded. Another power supply was used to apply potential to the grid electrode. Because no significant changes in ionization have been seen at UF when varying the voltage of the ring electrode no voltage was applied during these studies. Unless otherwise stated, the DART source parameters used were as follows. The needle electrode was set to 3 kV. The grid electrode was set to +250 V. The gas heater temperatures ranged from 100 to 200$^{o}$C. The helium flow rate was held at 2.5 L/min.

**Infrared lasers**

Preliminary dissociation of the proton-bound dimers of DIMP and DMMP was performed at both locations with fixed-wavelength 10.6 μm $CO_2$ lasers. At UF, powers ranged from 0.8 to 2 watts depending on the sample and the alignment of the laser. DIMP and DMMP were irradiated for 0.6 seconds so that little or no dimer was detected with either molecule. At FOM, DIMP required irradiation with the $CO_2$ laser attenuated to 4 watts for 0.5 seconds and DMMP required irradiation with the $CO_2$ laser attenuated to 8 watts for 0.5 seconds to eliminate proton-bound dimers.

A Linos OS 4000 OPO laser was used at UF to generate an infrared spectrum ranging from 2.7 to 2.9 μm (3430 to 3700 cm$^{-1}$) for DIMP. This OPO laser is equipped with a continuous wave (cw) neodymium yttrium aluminum garnet pump laser and a periodically poled lithium niobate crystal for generating different wavelengths. Because of the low power of the OPO laser (maximum powers were about 40 mW because only one of the outputted light beams was properly aimed into the cell at the time these experiments were performed), preliminary “heating” of the molecules with the $CO_2$ laser was required to bring the molecule to the dissociation threshold. To do so, the molecule (DIMP) was given enough $CO_2$ laser irradiation to initiate fragmentation of the monomer

(a fragment appeared with 1 to 2 percent of the abundance of protonated monomer). After this point, the protonated DIMP monomers were irradiated for an additional 4 seconds with the OPO laser. It should be noted that production of fragments with beyond 1-2 percent of the abundance of the monomer was OPO wavelength dependent and was not observed unless DIMP was undergoing a vibrational mode transition. The OPO laser was not powerful enough at that time to dissociate DMMP.

FELIX was used to generate infrared spectra ranging in the wavelength range from 6.25 to 17.8 μm (560 to ~1600$cm^{-1}$). The laser was operated at 5 Hz, achieving maximum powers of 250 mW (50 mJ per macropulse). After preliminary dissociation of their proton-bound dimers with either SORI-CID or irradiation from a $CO_2$ laser, protonated DIMP monomers were irradiated by FELIX for 3 seconds and protonated DMMP monomers were irradiated for 5 seconds.

**FT-ICR MS at UF**

Studies at UF were performed with a Bruker Daltonics (Billerica, MA) BioApex II 4.7 T FT-ICR MS. Daily tuning of ion focusing optics and mass calibration were performed with electrospray ionization (ESI) using ESI Tuning Mix (Agilent Technologies, Palo Alto, CA). Voltages of -3500 to -4000 V were applied to the entrance electrode of the glass capillary for ESI (the spray needle was held at ground potential). After tuning, in preparation for the DART analyses, the capillary voltage was dropped to -1100 V and the hexapole accumulation time was raised to 2 to 4 seconds depending on the sample. The spray shield used for the ESI was replaced with the flared capillary extender and the DART source was aimed directly at the inlet for analyses. All other parameters of the FT-ICR MS were left unchanged.

After ionization and injection of protonated DIMP dimers into the ICR cell, several

steps occurred to create an IRMPD action spectrum. First, ions were irradiated with the $CO_2$ laser to dissociate the proton-bound dimers and to preliminarily energize the molecule. Next, the protonated monomer was isolated in the cell with a swept frequency ejection pulse to eliminate all other ions. Last, the protonated monomer was irradiated with the OPO laser. This process was repeated for wavelengths between 2.7 to 2.9 μm (3430 to 3700 $cm^{-1}$). The experiment was repeated with DMMP with various times for each lasing event, but an IR spectrum was not generated due to inadequate fragmentation. Five mass spectral scans were averaged at each wavelength.

**FT-ICR MS at the FOM Institute**

A custom-built 4.7 T FT-ICR MS was used for experiments at the FOM Institute.[153] Tuning was done daily with a Waters Z-spray electrospray source using 18-crown-6 and arginine solutions. After tuning, the ESI source housing and sprayer were removed and the DART source was aimed directly at the skimmer inlet for all DART experiments (pictured in Figure 7-4 a.). Ions were accumulated in the hexapole for 5 to 6 seconds prior to transport into the ICR cell. Proton-bound analyte dimers were dissociated prior to IR spectral acquisition using either a $CO_2$ laser or SORI-CID in the ICR cell to produce protonated monomers for both of the species.

After ionization and injection of protonated DIMP or DMMP dimers into the ICR cell, several steps occurred to create an IRMPD action spectrum. First, ions were dissociated either by irradiation with the $CO_2$ laser or with SORI-CID. After $CO_2$ irradiation, the ions were allowed to cool for one second. Next, the protonated monomer was isolated in the cell with a stored waveform inverse Fourier transform (SWIFT) pulse. Last, the protonated monomer was irradiated with infrared photons produced by FELIX. This process was repeated for wavelengths between 6.25 to 17.8

μm (560 to ~1600cm$^{-1}$). Four mass spectral scans were averaged at each wavelength.

**Sample Introduction**

Two methods of sample introduction were used in these studies. For general tests to determine that the instrument was working properly, the tapered ends of glass pipettes were dipped into sample solutions and held in place in the region between the DART source and the mass spectrometer inlets by hand. For IRMPD studies, samples were syringe-infused into the DART gas flow at flow rates of 5-15 μL/min depending on signal stability. This sample introduction configuration allowed samples to be introduced for hours at a time. The sampling configuration is pictured in Figure 7-4 b.

**Density Functional Theory Calculations**

Density functional theory (DFT) calculations were used to compute theoretical IR spectra of the two molecules to elucidate the location of protonation. Prior to DFT calculations, conformations of the molecules were generated in the Hyperchem software suite.[154] Conformations were further optimized with the Gaussian 03 software suite.[155] Initial calculations were performed by Dr. Cesar Contreras using (B3LYP/6-31G(d )) method and basis set. Because the level of theory used in these calculations was determined to be too low, Dr. Jan Szczepanski performed additional calculations using the (MPW1PW91/6-311++G(d,p) functional and basis set.

## Results and Discussion

**DFT Calculations**

The lowest energy structures of DIMP-A, where the ionizing proton is attached to the phosphonyl oxygen, and DIMP-B, where the proton is attached to the singly-bonded oxygen, calculated with (B3LYP/6-31G(d)) and (MPW1PW91/6-311++G(d,p), are given in Figure 7-5. Both levels of theory indicated that DIMP-A was at least 22 kcal/mol

lower in energy than DIMP-B. An elongated (broken in appearance) bond between the proton-bound singly-bonded oxygen atom and the connecting carbon atom was generated with both levels of theory. If the ionizing proton was attaching to this location, the observed destabilization could be a driving force for the second fragmentation mechanism displayed in Figure 7-9 b., which will be discussed below. The appearance of double bonds between the phosphorous and the singly bonded oxygens when the proton is bound to the phosphonyl oxygen as in Figure 7-5 a. indicates increased stabilization of those bonds (not actually double bonds). A similar effect was seen with DMMP when the ionizing proton was attached to the phosphonyl oxygen (Figure 7-6). The results of the spectral calculations will be presented in conjunction with the experimental IRMPD spectral results.

**DIMP and DMMP Fragmentation**

Mass spectra of DIMP and DMMP dissociated with a $CO_2$ laser are given in Figure 7-7. Further irradiation with the OPO laser tuned to 3643 $cm^{-1}$ for 4 seconds was used to generate the DIMP spectrum (Figure 7-7 a.) and a short (1 second), high-power (12.5 W) irradiation event with the $CO_2$ laser was used to generate the fragments in the DMMP spectrum (Figure 7-7 b.). As mentioned previously, no additional fragmentation was obtained by irradiating DMMP with the OPO laser. Regardless of the dissociation method, the same fragments were consistently seen with each molecule. The daughter ion assignments are based on exact mass.

Protonated DMMP underwent a loss of methanol to yield one daughter ion with a mass of 93. A fragmentation mechanism of DMMP is given in Figure 7-8. Snyder et al. gave evidence of this mechanism by using chemical ionization with a deuterium oxide reagent gas to ionize the molecule.[156] Upon CID in a triple quadrupole mass

spectrometer, the $[M+D]^+$ ions were fragmented to produce species with m/z 93. The authors stated that this result demonstrated that the added $D^+$ cation was not retained during fragmentation and instead was part of the leaving methanol group (containing a singly-bonded oxygen atom).[156] It should be noted that twice as much power was required to dissociate the DMMP dimers as the DIMP dimers in these experiments. Likewise, fragmentation with FELIX required 5 seconds of unattenuated irradiation compared to 3 seconds with DIMP.

The fragmentation of DIMP was more complicated. Daughter ions with masses of 97 and 139 corresponding to neutral propylene losses were primarily detected. Very low abundances of m/z 79, corresponding to the loss of a water molecule from the m/z 97 ion, were also seen occasionally. These three fragments were also reported by Johnson et al. while using DIMP as a model compound in a study comparing the triple quadrupole to the quadrupole ion trap.[157] Two fragmentation mechanisms that involve sequential dissociations are presented in Figure 7-9. The first is fairly simple, but requires the participation of another molecule ("X") or part of the leaving group for donation of a proton in each step. The second mechanism was proposed by Snyder et al. and involves two McLafferty-like rearrangement steps to produce each of the daughter ions.[158,159] The loss of water from the m/z 97 ion follows. The first mechanism may favor protonation on the phosphonyl oxygen and the second mechanism supports protonation on one of the singly bonded oxygen atoms.

**Preliminary dissociation of DIMP and sample flow rate concerns**

Two methods were used to dissociate the proton-bound DIMP dimer into protonated monomers. The first method was SORI-CID. A comparison of a mass

spectrum of DIMP without and with SORI-CID is given in Figure 7-10. As shown in Figure 7-11, the quantity of dimer present after the SORI event appeared to be related to the sample introduction flow rate. As a result, both an abundant dimer and a large degree of monomer fragmentation could be observed simultaneously. This was believed to be due to an uneven distribution ion temperatures in the cell, resulting in fragmentation of some monomers while other dimer species were still dissociating into monomers. After an acceptable flow rate was found, stored waveform inverse Fourier transform (SWIFT) pulses were used to eliminate the fragments and remaining proton-bound dimer following the SORI process. One FELIX IRMPD spectrum (one round of acquiring spectra while the molecule was irradiated over a range of wavelengths) of DIMP was acquired with SORI-CID preliminary dissociation. All other IRMPD spectra (both with FELIX and the OPO laser) were acquired with preliminary dissociation occurring via irradiation with a $CO_2$ laser. Little or no preliminary monomer fragmentation was seen when the $CO_2$ laser was used prior to irradiation with FELIX. A one second cooling period was included between the two irradiation events to allow equilibration of the ions' internal energies.

**IRMPD Spectra**

IRMPD spectra were generated by collecting mass spectra while protonated monomer ions were irradiated with an infrared laser whose output could be tuned over wavelengths in a given range. Fragmentation yield (F.Y.) was plotted as a function of wavenumber to generate each spectrum. Data points on the IRMPD graphs were determined by dividing the sum of the abundances of the fragments produced by the chosen protonated molecule by the sum of the fragments' and parent abundances, as shown in equation 7.1.

$$F.Y. = \Sigma(\text{Fragment Abundances}) / \Sigma(\text{Parent + Fragment Abundances}) \quad (7.1)$$

**OH region of the DIMP IRMPD spectrum (3400 – 3700 $cm^{-1}$)**

The OPO laser was used to interrogate the OH region of the IRMPD spectrum of DIMP. Upon inspection of the IRMPD spectral results, one narrow absorption band with its maximum at 3644 $cm^{-1}$ was observed. Though observation of a single peak was in agreement with the calculated spectra using either level of theory, determining which calculated spectrum was most similar the experimental spectrum was not possible. DFT-calculated vibrational frequencies are known to vary from the frequencies observed experimentally. Because the shift in frequencies is generally uniform throughout a region of the spectrum, a scaling factor is applied to the calculated values.[160] Generally, with (MPW1PW91/6-311++G(d,p), the experimental spectrum was closest to the spectrum calculated for DIMP-B, whether the scaling factor applied to the calculated frequencies was 0.97, 0.98, or 1 (Figure 7-12 a.). Still, even greater scaling factors (i.e. multiplication of the calculated frequencies by a factor 0.96 or lower) have been applied to this region of the spectrum.[161] For spectra generated with (B3LYP/6-31G(d)), the calculated spectra could be shifted to align the experimental peak to match either structure, depending on the scaling factor (Figure 7-12 b.). To further complicate the matter, Correia et al. stated that reliable scaling factors are unavailable for molecules containing a phosphorous group.[162] This uncertainty and a general absence of other features in the spectrum led to the conclusion that this region was not diagnostic for DIMP and that the fingerprint region (below 1600 $cm^{-1}$) should be examined at the FELIX facility. Further efforts to examine DMMP with the OPO laser were suspended for this reason.

**Fingerprint region of the DIMP IRMPD spectrum (500 – 1600 $cm^{-1}$)**

Comparisons of the calculated IRMPD spectra ((MPW1PW91/6-311++G(d,p)) and the IRMPD action spectrum generated with FELIX are given in Figure 7-13. All comparisons and assignments of vibrations will be made between the experimental spectrum and the spectra calculated with (MPW1PW91/6-311++G(d,p) theory. Table 7-1 (next page) lists dominant peaks from the experimental spectra and spectra generated with FELIX irradiation as well as some vibrational assignments.

The experimental spectrum was very noisy and broad between 850 and 1200 $cm^{-1}$, a region that likely corresponds to P-OR and P=O stretches. However, the highest maximum of this conglomeration occurred experimentally at 1055 $cm^{-1}$. The highest peaks in the lower energy, DIMP-A, and the higher energy, DIMP-B, calculated spectra were positioned at 1053 and 1006 $cm^{-1}$ respectively. With all features considered, a marginally better correlation between the experimental spectrum and the DIMP-A spectrum was present from about 860 to 930 $cm^{-1}$ and the DIMP-A feature at 1120 $cm^{-1}$ may have also contributed to the broadened region right of the maximum at 1055 $cm^{-1}$. The distinctive features between 1300 and 1500 $cm^{-1}$ may be attributed to P-$CH_3$ bends but have overlapping peaks with both structures' calculated spectra. The experimental low frequency peak at 697 $cm^{-1}$ was broad enough that it might be attributed to contributions from either structure.

With a visual comparison and a frequency-to-frequency comparison, the agreement between the experimental IRMPD spectrum generated with DIMP using FELIX as the light source and the DIMP-A calculated spectrum was fairly convincing. This corresponded to attachment of the ionizing proton to the phosphonyl oxygen. However, several spectral features and the occasional appearance of the m/z 79

fragment ion indicated that a population of DIMP ions with the ionizing proton bound to a singly-bonded oxygen could not be ruled out. With these pieces of information, it seemed possible that both species were present in the ICR cell, though there was probably a greater population of phosphonyl oxygen-protonated DIMP species.

**Fingerprint region of the DMMP IRMPD spectrum (500 – 1600 $cm^{-1}$)**

Comparisons of the calculated IRMPD spectra ((MPW1PW91/6-311++G(d,p)) and the IRMPD action spectrum generated with FELIX are given in Figure 7-13. Only three distinct features were detected in the experimental IRMPD spectrum of DMMP. The observed absence of features was probably due to the drastically smaller extent of IRMPD fragmentation for DMMP when irradiated; thus, a smaller difference in the fragment-to-total ion abundance ratio was observed at any given point than with the other analyte, DIMP. The highest peak in this spectrum (1095 $cm^{-1}$) is similar in position to that observed with DIMP and, again, it more closely corresponds to lower-energy structure, with the ionizing proton bound to the phosphonyl oxygen (DMMP-A). The region from 750 to 970 $cm^{-1}$ has no real definition and no conclusions can be drawn from it except that P-OR and P=O stretches were observed (which would be expected with DMMP-A or DMMP-B). The experimental peak with its maximum at 1315 $cm^{-1}$ is bracketed by a calculated DMMP-B peak, whose frequency is 1305 $cm^{-1}$, and a DMMP-A peak, whose frequency is 1327 $cm^{-1}$. The peak's relative height is more similar to the DMMP-B peak at 1305 $cm^{-1}$, though generally intensity is considered less important in IRMPD spectra than frequency.[142]

With respect to the most dominant absorption band, it appears that the theoretical DMMP-A spectrum may agree somewhat better with the experimental spectrum than the theoretical DMMP-B spectrum. However, due to the broadness

throughout it, it is difficult to draw conclusions from the experimental IRMPD spectrum of DMMP other than, again, it appears there may have been a mixture of DMMP-A and DMMP-B in the ICR cell.

## Conclusion

The coupling of a DART source to an FT-ICR MS to perform IRMPD studies was demonstrated for the first time. A novel sample introduction method (for DART-MS) involving syringe injection was employed that allowed analyte ions to be produced and detected for extended periods of time. Though used to generate IRMPD spectra in this application, the syringe introduction technique could also be very useful in situations where it would be desirable to average many spectra for signal-to-noise improvements. Based on IRMPD spectral comparisons and the observed daughter ions, it was concluded that a population of DIMP had an ionizing proton bound to the singly-bonded oxygen, as previously implied in the literature.[158] However, because the IRMPD action spectrum most closely corresponded with the calculated spectra of the lower energy structure, it was concluded that a greater population of DIMP ions had an ionizing proton bound to the phosphonyl oxygen atom. Because it is a more energetically stable structure that requires more imputed energy for fragmentation, little information was gained in performing IRMPD with DMMP. It was concluded that, again, a mixture of the structures was present, though an inference was not made about the relative proportions of the two species.

Table 7-1. Frequencies corresponding to dominant absorption bands in the experimental and calculated IRMPD spectra of DIMP.

| Dominant Bands | | | | |
|---|---|---|---|---|
| Experimental ($cm^{-1}$) | DIMP-A[a] ($cm^{-1}$) | DIMP-B[a] ($cm^{-1}$) | Best Match[b] | Vibrational assignment[c] |
| | | 557 | - | |
| 654 | 658 | 671 | A | |
| 697 | 708 | 695 | B | |
| 789 | 776 | 764 | A | *v*POO |
| 866 | 864 | | A | |
| 881 | 886 | 882 | Both | |
| 916-965 | 923 | | B | *v*C-C, *v*POH, *δ*POH |
| | | 1006 | Swamped | *v*POH, *δ*POH, *v*POC |
| | 1040 | | A/Swamped | *v*POH, *δ*POH, *v*POC |
| 1053 | 1055 | 1068 | A | *v*POH, *δ*POH, *v*POC |
| | 1096 | | Swamped | |
| 1110 | 1121 | | A | |
| | | 1130 | Swamped | |
| | | 1175 | Swamped | |
| 1264 | | 1263 | B | *v*POC, *δ*$CH_3$P |
| 1282 | | | - | |
| | | 1311 | - | |
| 1318 | 1325 | 1327 | Both | *δ*$CH_3$P |
| | | 1368 | - | |
| 1393 | 1390 | 1397 | Both | *δ*COH, *δ*C-H |
| 1448 | 1465 | 1466 | Both | |

a. The (MPW1PW91/6-311++G(d,p) theory was used to calculate these frequencies. DIMP-A is the lower energy structure, with the ionizing proton bound to the phosponyl oxygen. DIMP-B is the higher energy structure, with the ionizing proton bound to the singly-bonded oxygen atom.

b. Refers to the structure (DIMP-A or DIMP-B) whose theoretical spectrum best matches the experimental spectrum at the corresponding frequency range.

c. Vibrational absorption band assignments are based on reports by Correia et. al. and Brunol et al. Stretches are denoted with "*v*" and deformations are denoted with "*δ*". [162,163]

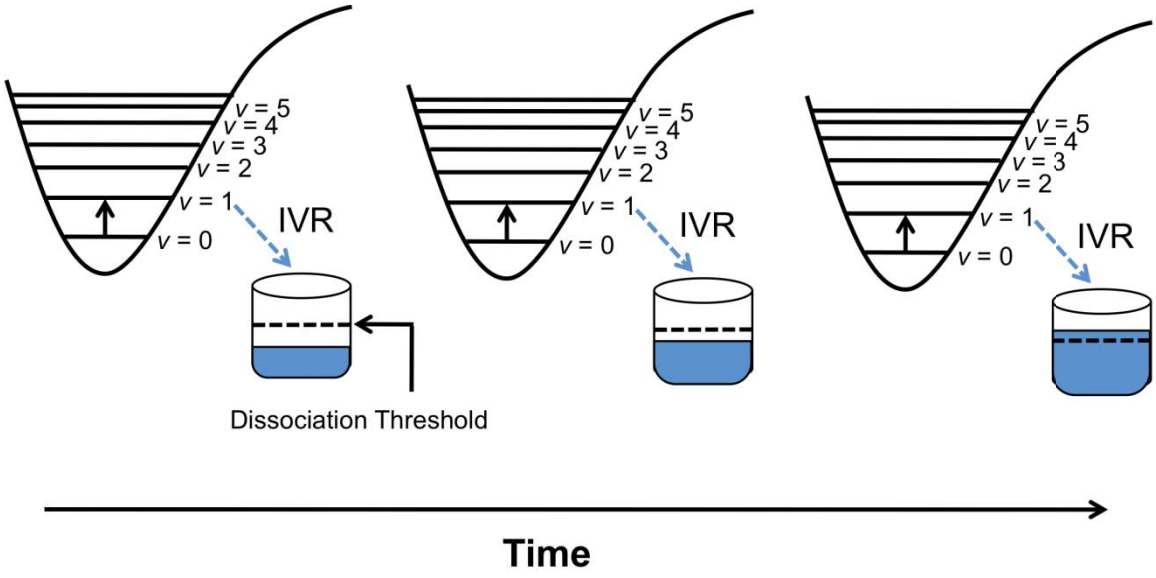


Figure 7-1. Depiction of the IRMPD mechanism in polyatomic molecules or ions. The energy of each absorbed photon is distributed to other vibrational modes in a molecule through intermolecular vibrational energy redistribution. The process is repeated until a dissociation threshold is reached, which results in fragmentation of the molecule or ion. This figure is adapted from a report by Polfer et al.[141]

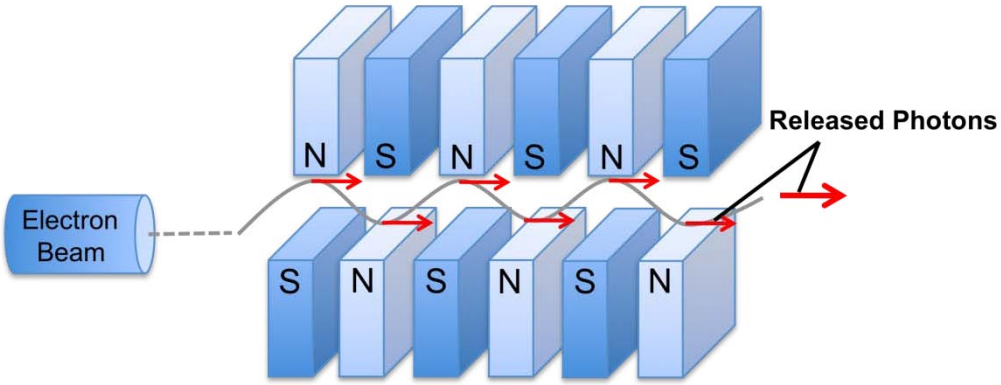


Figure 7-2. Schematic diagram of an undulator used to generate radiation in a free electron laser. Free electrons oscillate through a series of oppositely poled magnets. Infrared photons are released each time the electron path changes directions. Figure adapted from report by Oepts et al.[147]

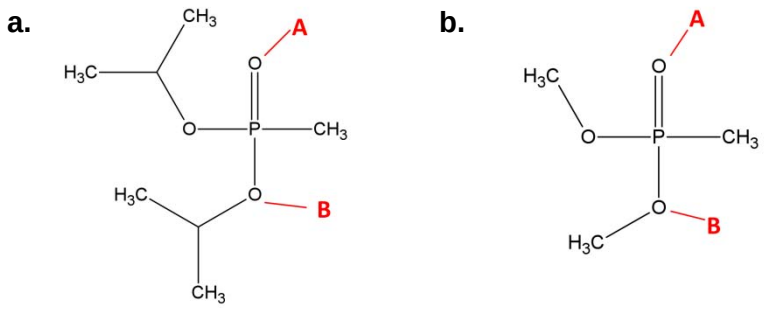


Figure 7-3. Structures and possible protonation sites of (a.) DIMP and (b.) DMMP.

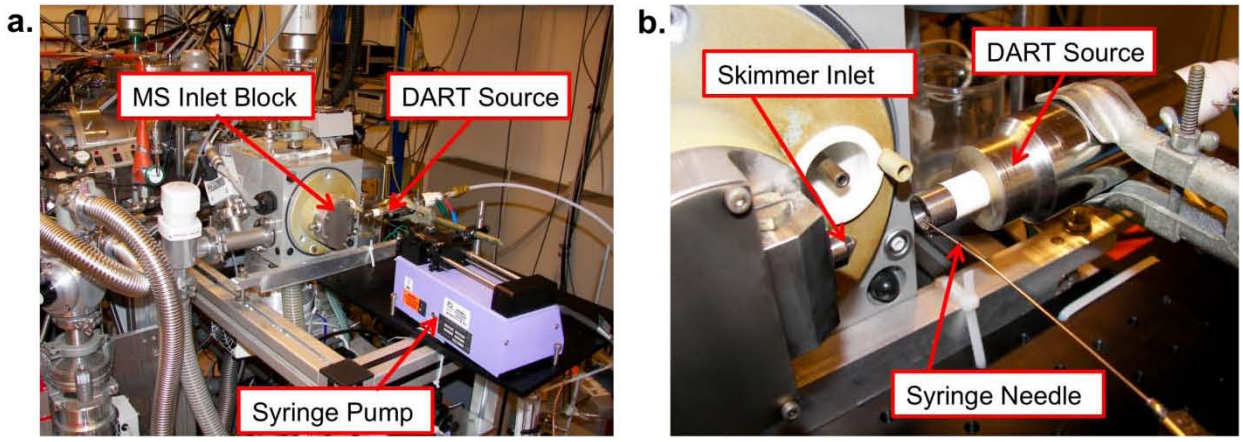


Figure 7-4. Photographs of the DART source interfaced to the FT-ICR MS at the FOM Institute. A zoomed-out photo (a.) shows that a syringe pump was used for sample introduction and the syringe needle can be seen in the close-up photograph (b.).

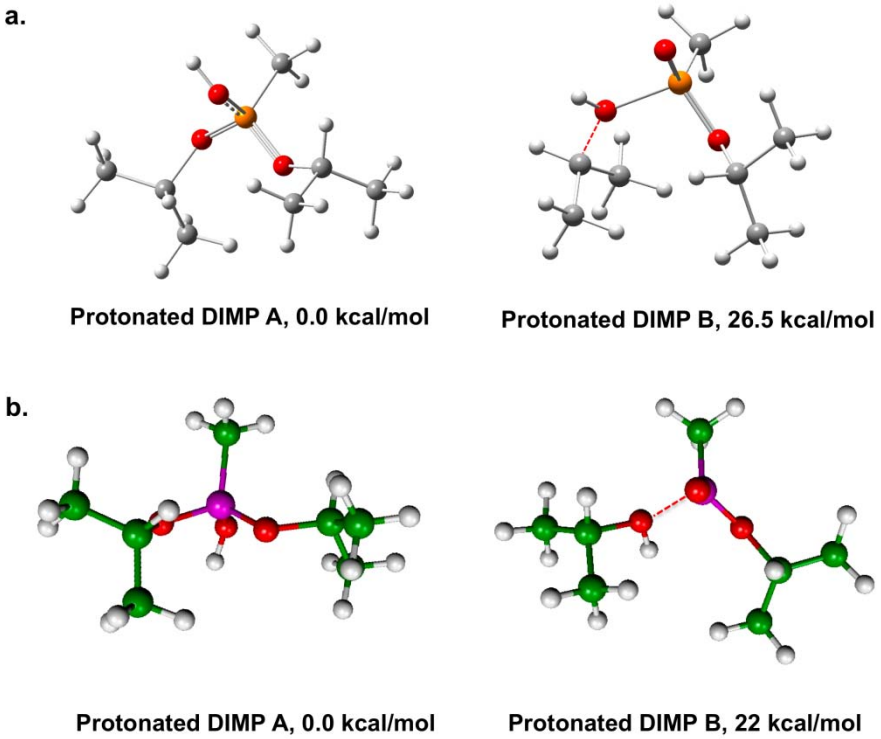


Figure 7-5. Lowest energy conformations of the possible protonated DIMP structures. These structures were generated with (a.) (MPW1PW91/6-311++G(d,p) theory and (b.) (B3LYP/6-31G(d)) theory.

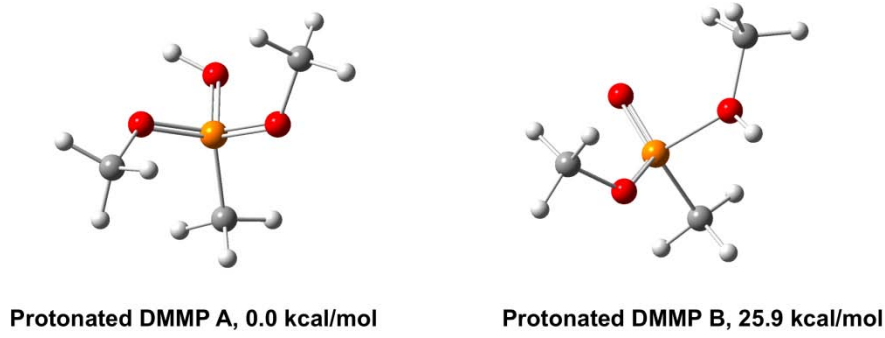


Figure 7-6. Lowest-energy conformations of the possible protonated DMMP structures. These structures were generated with (MPW1PW91/6-311++G(d,p) theory.

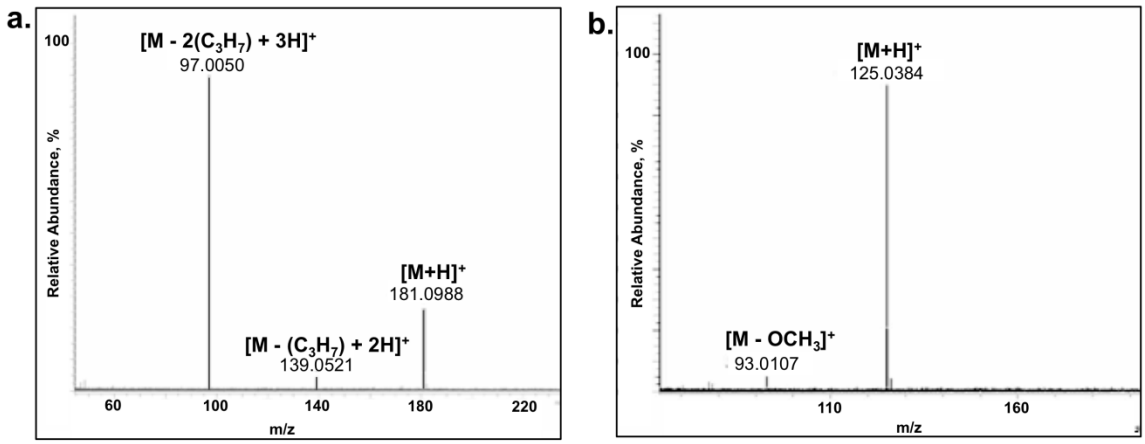


Figure 7-7. Mass spectra showing fragmentation of (a.) DIMP and (b.) DMMP.

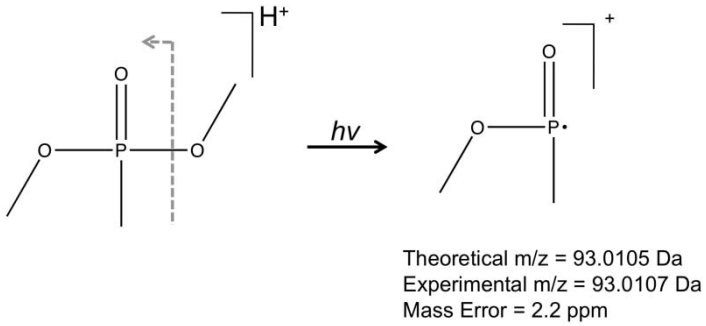


Figure 7-8. Simplified fragmentation mechanism of DMMP. The dashed arrow denotes the proposed location of fragmentation upon irradiation.

**a.** Mechanism 1

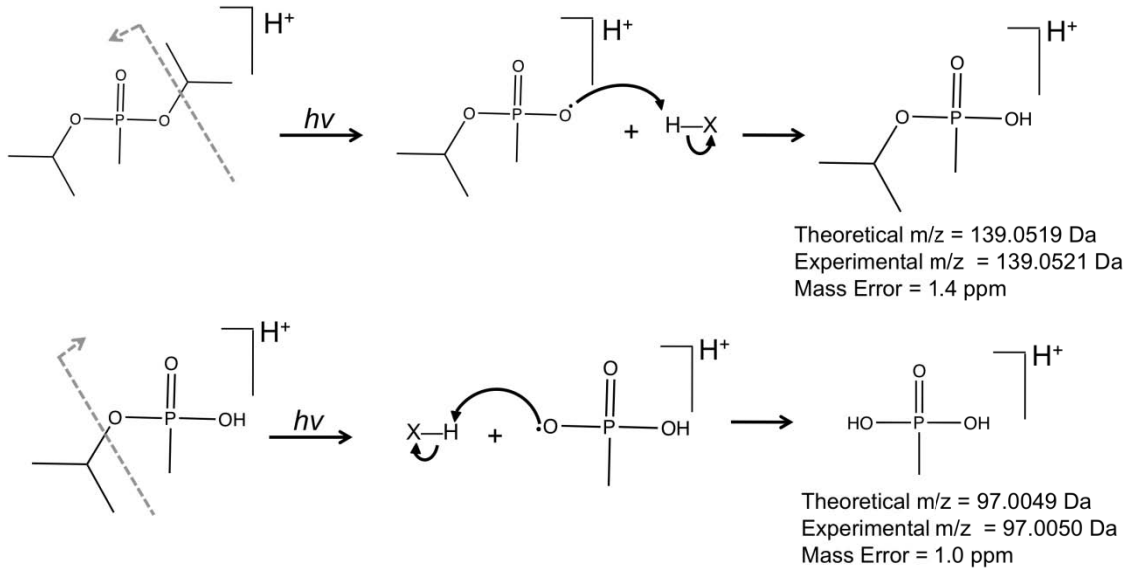


**b.** Mechanism 2

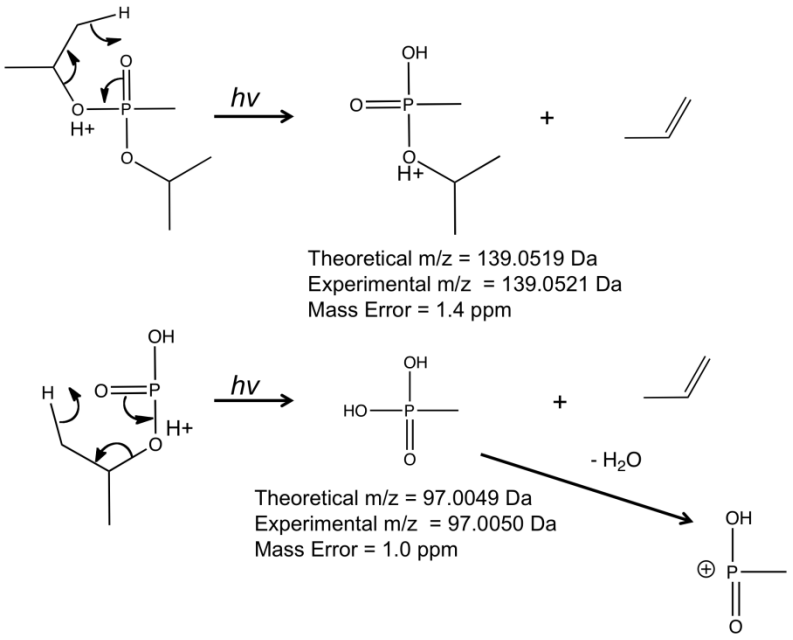


Figure 7-9. Proposed fragmentation mechanisms of DIMP. The proposed mechanisms involve (a.) retrieval of a proton from another molecule or part of DIMP after fragmentation and (b.) a McLafferty-like rearrangement. The dashed arrow denotes the proposed location of fragmentation upon irradiation.

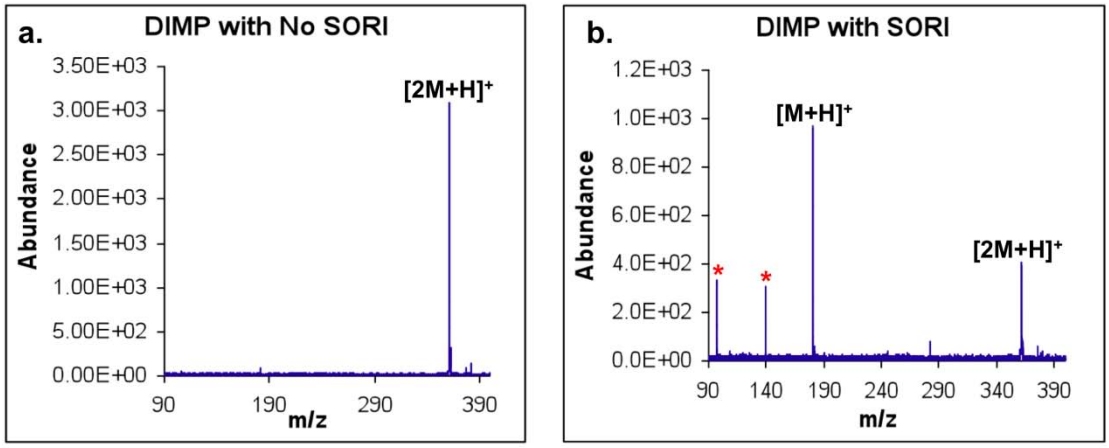


Figure 7-10. Comparison of DIMP mass spectra acquired (a.) without SORI-CID and (b.) with SORI-CID. Fragment ions are marked with (*).

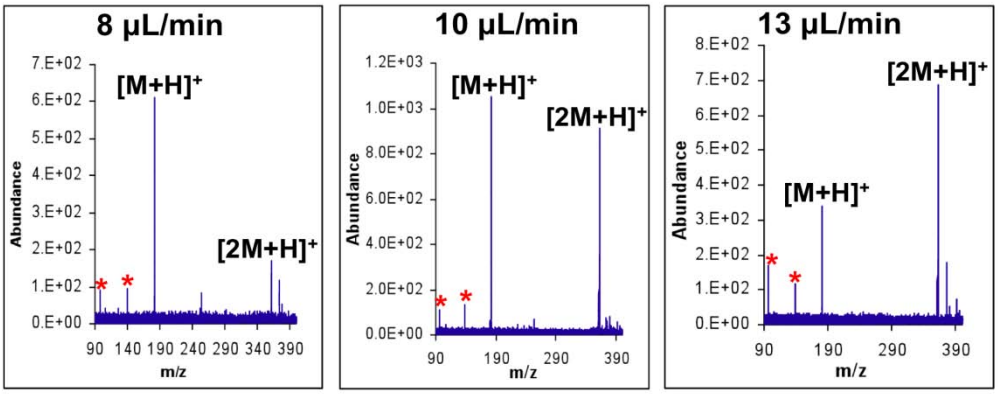


Figure 7-11. SORI-CID mass spectra acquired with DIMP solution introduced at various flow rates. The sample flow rates are listed at the top of each mass spectrum.

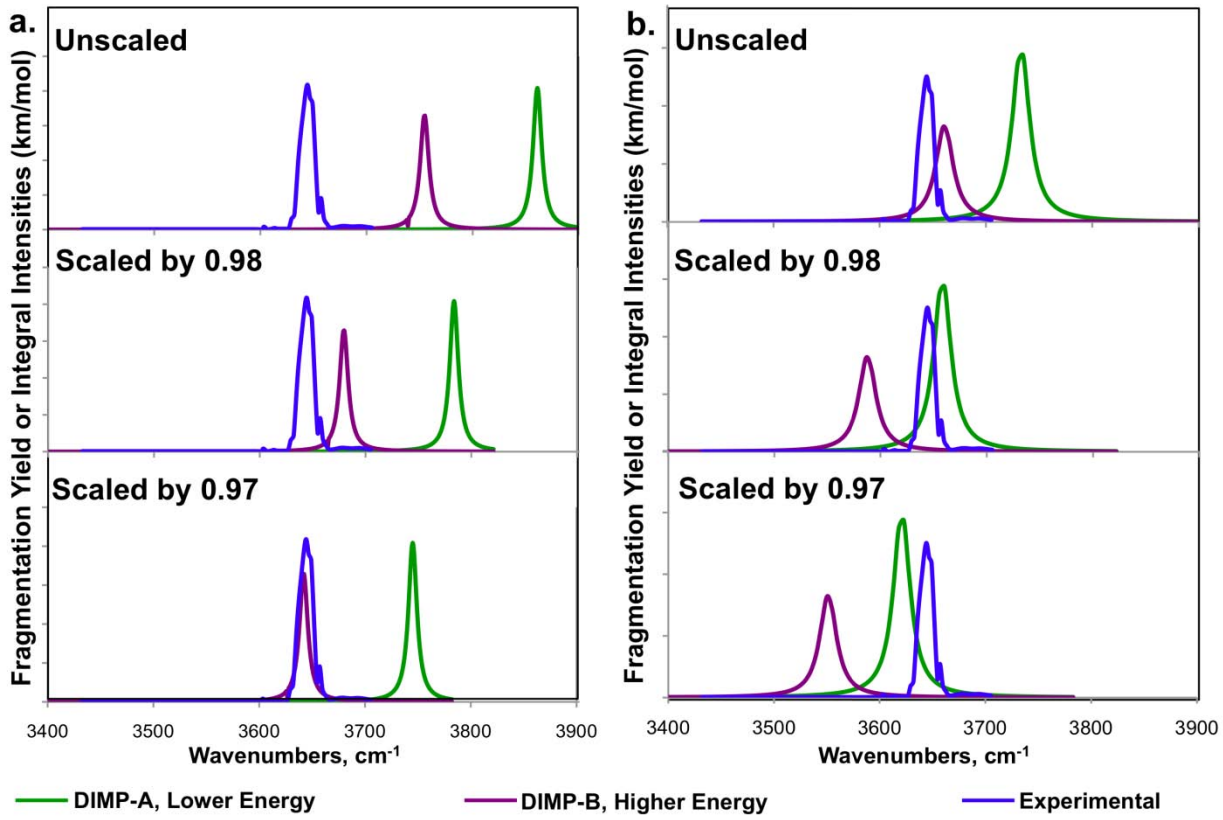


Figure 7-12. IRMPD spectrum of DIMP acquired in the OH region overlapped with spectra calculated by (a.) (MPW1PW91/6-311++G(d,p) theory and (b.) (B3LYP/6-31G(d)) theory.

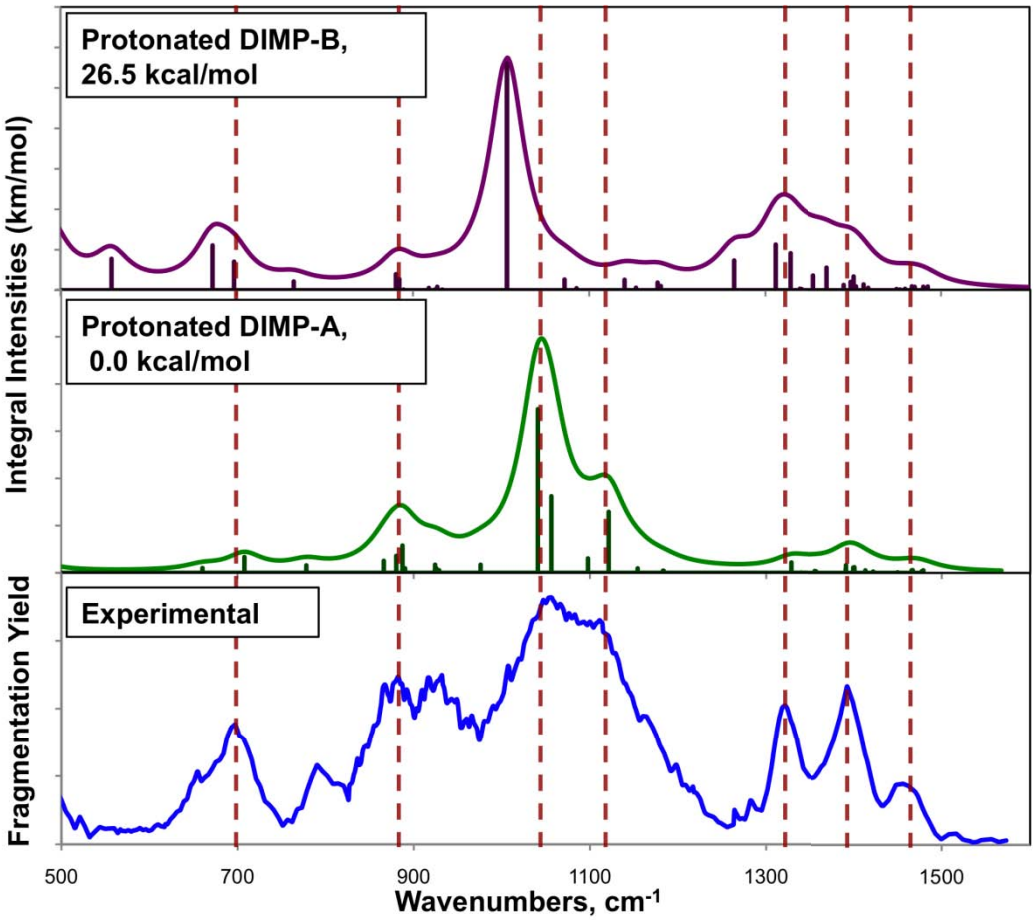


Figure 7-13. Comparison of experimental and calculated IRMPD spectra of DIMP. Dashed lines are included to highlight similarities between the experimental and calculated spectra. A 0.98 scaling factor was used in the theoretical spectra.

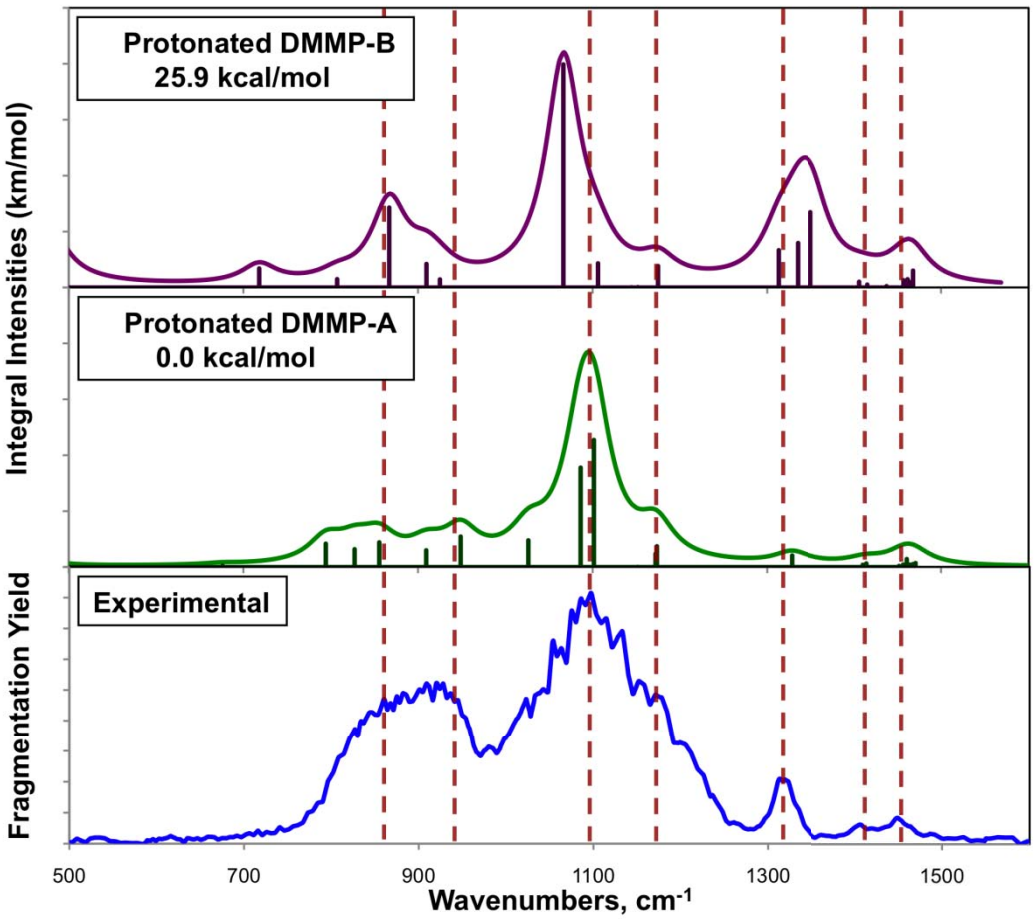


Figure 7-14. Comparison of experimental and calculated IRMPD spectra of DMMP. Dashed lines are included to highlight similarities between the experimental and calculated spectra.

# CHAPTER 8
# CONCLUSIONS AND FUTURE DIRECTIONS

## Summary of Presented Work

Many different aspects of Direct Analysis in Real Time ionization for mass spectrometry were studied. A custom-built DART source was used for a number of different applications. Fundamental studies increased understanding of the mechanisms important in DART ionization. A novel coupling of the custom-built DART source to multiple FTMS instruments took advantage of the ultrahigh resolving power capabilities and the extended trapping capabilities of FT-ICR MS.

An inexpensive custom-built DART source was fabricated and studied. The source was optimized and low-picogram detection limits were achieved with several analytes. The DART source was applied to a number of different applications with little or no sample preparation. These experiments demonstrated the wide utility of DART as a surface ionization technique and that the custom-built DART source could be used in the same manner as the commercial DART source. These studies showed that DART-MS is particularly suitable for compound identification and rapid screening experiments.

The effects of analyte substrate, matrix, and surrounding environment were explored. Little difference was seen between molecules desorbed from glass or metal, but substrate roughness was important in the analysis of solids. The ability to analyze alternative substrates such as sand, soil, and concrete was established and showed that preliminary extraction or purification may be warranted at times. Suppression effects were observed when analytes of interest were spiked into complex matrices. The possibility of modifying ionization characteristics and even expanding DART capabilities was demonstrated with the addition of dopants to the sampling region.

The mechanistic factors governing DART sensitivity were systematically studied. The importance of proton affinity (both of the analyte and other compounds in its vicinity) in analyte sensitivity and detectability was demonstrated. Self-protonation was definitively shown to be operative in DART ionization even though it had not been discussed previously in the DART literature. The source enclosure experiments introduced doubt to the widely held belief that Penning ionization is a dominant analyte ionization mechanism in helium DART. In all cases, the pathways of DART ionization appeared to fall into the class of mechanisms operative in atmospheric pressure chemical ionization (charge exchange, proton transfer, etc.).

Its compact design allowed the custom-built DART source to be interfaced to several different FT-ICR instruments. The utility of ultrahigh resolving power afforded by FT-ICR MS was demonstrated by analyzing isobaric compounds and by distinguishing $^{13}C$ molecular ion isotopes and $[M+H]^+$ species of different polycyclic aromatic hydrocarbons. Infrared multiple photon dissociation was applied for spectroscopic structural determination of DART-ionized molecules.

## Future Studies

As illustrated in the above summary, the work presented in this dissertation covered a wide range of topics involving DART ionization. Further expansion of any one of these areas is possible. Though not discussed in this dissertation, nitrogen was also employed as a desorption/ionization gas with a commercial DART source in additional studies. In the future, argon should also be explored as a desorption gas because it is cheaper than helium and produces relatively high-energy metastable species (11.55 eV).[164] A few more ideas that were either actually implemented to some degree during with this work or that were just dreamed of are presented below.

## Applications

### Crude oil analysis

An analysis of crude oil with DART-FT-ICR MS was presented in Chapter 6. In this proof-of-concept study, the ions' intensities and distribution were less than desirable. Future work in this area should include optimization of the sampling conditions and ambient environment about the DART source. To start, future researchers should find the optimal sample flow using a syringe pump, syringe needle position, and gas temperature. It may be beneficial to explore spray creation as venue for transporting the oil to the gas phase. Next, dopants should be explored to enhance ionization. Addition of ammonium hydroxide vapors may promote adduct formation. Addition of a volatile acid vapor, such as acetic acid, may enhance ionization of low-proton affinity compounds. One may also consider adding dopants directly to the crude oil sample to ensure that interaction occurs between the analyte molecules and the dopants. Taking these steps should allow better desorption and ionization of the crude oil sample, thus generating mass spectra with more abundant ion signals spanning a wider range of masses.

### Reaction monitoring

A couple of studies claiming to perform reaction monitoring with DART have been reported.[38,165] Neither of these studies presented a "real time" analysis of the reaction mixtures because each involved sample retrieval prior to analysis. Real time reaction monitoring is possible and has been accomplished in the mass spectrometry laboratory where the research reported in this dissertation was done. With a couple of gas lines (one inserted in a reaction mixture and one leading from the container's headspace to the DART source sampling region) and a flow of nitrogen, gas-phase reaction products

were monitored in real time as they were produced. Generation of a spray of the liquid in a reaction mixture for analyzing less volatile components could be accomplished with a peristaltic pump and a nebulizer. Though these studies could be somewhat cumbersome to implement, the information they could provide would be invaluable and novel. This could be a very rewarding project for a new graduate student.

**Polycyclic aromatic hydrocarbons**

Studies from Chapters 5 and 6 demonstrated that the distribution of PAH ions could be modified by adjusting the position of the sample relative to the DART source. There is interest in this class of molecules because they are believed to be responsible for spectral observations in interstellar clouds.[166,167] As generation of protonated PAH species has been an "experimental challenge,"[168] DART may be a suitable ionization source for IRMPD studies of these molecules. Conversely, IRMPD studies of DART-ionized PAH molecules may provide information on their formation. Though several mechanisms are possible, the work reported here did not experimentally show how all molecular ions and protonated species are formed during analyses with DART (particularly those that do not appear to have interacted with ambient water clusters). For example, Vala et al. and others have presented evidence that these molecules undergo proton ejection.[169-171] The reported studies with deuterated anthracene (Chapter 5) also support this hypothesis. Spectroscopic investigations could shed light on this subject.

**TSA security swabs**

An interesting project suitable for an undergraduate researcher is analysis of the swabs used by the Transportation Security Administration (TSA) at airports to collect samples for their ion mobility spectrometers (IMS). Though widely used across the

nation for airport security, a common complaint about IMS instruments is their false positive rate.[172,173] DART-MS could either provide a highly specific alternative to IMS without sacrificing rapidity or it could complement IMS detection systems. In either case, it would be interesting to determine how DART-MS compares to traditional IMS systems for the analysis of drugs, explosives, and chemical warfare agents from swabs used to wipe surfaces like the inside of luggage or shoe soles.

**Continued Mechanism Studies**

**Source enclosure experiments.** At the conclusion of the mechanism studies presented in Chapter 5, the source enclosure studies indicated the possibility of additional mechanisms occurring in lieu of (or maybe in combination with) Penning ionization. A direction future researchers should take with this is to repeat the enclosure studies with varying amounts of other "external" gases. In particular, an experiment should be done where helium and nitrogen mixtures are introduced to determine if there is a correlation (possibly an inverse relationship) between the amount of helium and the signal abundance. This will determine if the helium itself is hindering ionization or if another mechanism is operative. Other inert atomic gases such as argon should also be introduced externally to determine if the loss of signal is the result of collisional de-excitation between helium atoms prior to interaction with the analytes (helium and argon do not have various vibrational modes to contain and distribute internal energy like bimolecular gases). If ion signals are detected, collisional de-excitation is not the answer.

**Combination Ionization Sources**

Though the minute size of the DART source used in this work simplified transfer to various other mass spectrometers, it can also allow the device to be easily combined

with other ionization sources for multi-mode operation. All multi-mode ionization sources are designed with a goal of broadening the range of capabilities of one or both ionization sources (possibly synergistically). This goal may be achieved by providing more efficient sample introduction (e.g. enhanced desorption) with one source followed by ionization with another source or by creating multiple venues for analyte ionization.

**Laser desorption-DART**

The DART source was originally built to serve as an atmospheric pressure chemical ionization (APCI) source that would be inserted into an atmospheric pressure matrix-assisted laser desorption ionization source (MALDI) to create a combined laser desorption/APCI source. This coupling was intended to broaden the range of analytes ionizable by desorption ionization on porous silicon (DIOS). The benefits of this combination source would be two-fold. First, adding reagent ions to the source region atmosphere would provide more opportunities for desorbed materials to ionize, thus improving the sensitivity of DIOS (or MALDI). Second and derived from the first benefit, identification of the neutral species desorbed during the DIOS process might be possible, perhaps providing greater insight into the ionization mechanism(s) of DIOS. There was too little time to implement laser desorption-DART ("LD-DART") in the current work. However, because all of the necessary components (a DART source and a MALDI source) are already housed in the Powell laboratory at UF, a few simple modifications to the respective sources could make the implementation and application of LD-DART a fruitful project for a future graduate student.

**DART combined with other ionization sources**

Other ionization sources could also be coupled with the DART source to enhance analysis capabilities. For example, it would be fairly simple to direct the DART gas

stream through an electrospray ionization (ESI) nebulizer in place of nitrogen. By doing so, analytes exiting a high performance liquid chromatograph could be ionized both by ESI and APCI without modifying the geometry of the ESI spray head (as is the case with the current ESI/APCI multimode source).

Another possibility that was explored for a while in conjunction with the current work was DART-atmospheric pressure photoionization (DART-APPI). This source was implemented by replacing the nebulizer in an APPI source with the DART source. This combination allowed low-proton affinity analytes such as naphthalene to be desorbed without solvents and ionized by photon absorption. A similar idea that essentially combined desorption electrospray ionization (DESI) with APPI was reported by Haapala in 2007, but required solvents. Further method development would be necessary to take DART-APPI from an idea to a versatile ambient ionization technique.

## General Conclusion

Research with and about Direct Analysis in Real Time ionization is still in the early stages. Though many different topic areas utilizing the custom-built UF DART source were covered in this thesis, many more areas remain unexplored. Because of its simplicity and wide applicability, the use of DART-MS as a powerful analytical tool will continue to grow.

LIST OF REFERENCES


(1) Cody, R. B.; Laramee, J. A.; Durst, H. D. Anal. Chem . 2005 , 77 , 2297.

(2) Watson, J. T. Introduction to Mass Spectrom etry ; 3rd Ed.; Lipincott-Raven Publishers: Philadelphia, PA, 1997.

(3) KiviEtelatalo, E.; Kostiainen, O.; Kokko, M. J. Chrom . A. 1997 , 787 , 205.

(4) Helmig, D.; Greenberg, J. P. J. Chrom . A. 1994 , 677 , 123.

(5) Nanita, S. C.; Pentz, A. M.; Grant, J.; Vogl, E.; Devine, T. J.; Henze, R. M. Anal. Chem. 2009 , 81 , 797.

(6) Augusti, D. V.; Carazza, F.; Augusti, R.; Tao, W. A.; Cooks, R. G. Anal. Chem . 2002 , 74 , 3458.

(7) Nicol, G.; Sunner, J.; Kebarle, P. Int. J. Mass Spectrom . Ion Pr oc . 1988 , 84 , 135.

(8) Wang, H. Y.; Zhang, X.; Guo, Y. L.; Lu, L. J. Am. Soc . Mass Spectr om. 2005 , 16 , 1561.

(9) Tolmachev, A. V.; Udseth, H. R.; Smith, R. D. Anal. Chem . 2000 , 72 , 970.

(10) de Hoffmann, E.; Stroobant, V. Mass Spectrom etry : Principles and Applications ; John Wiley & Sons, Ltd.: West Sussex, England, 2007.

(11) Yamashita, M.; Fenn, J. B. J. Phys. Chem. 1984 , 88 , 4451.

(12) Wilm, M. S.; Mann, M. Int. J . Mass Spectrom . 1994 , 136 , 167.

(13) Rockwood, A. L.; Busman, M.; Smith, R. D. Int. J . Mass Spectrom . 1991 , 111 , 103.

(14) Cech, N. B.; Krone, J. R.; Enke, C. G. Anal. Chem . 2001 , 73 , 208.

(15) Gaskell, S. J. J Mass Spectrom . 1997 , 32 , 677.

(16) Takats, Z.; Wiseman, J. M.; Gologan, B.; Cooks, R. G. Science . 2004 , 306 , 471.

(17) Steiner, R. R.; Larson, R. L. J. Forens . Sci. 2009 , 54 , 617.

(18) Jackson, A. U.; Werner, S. R.; Talaty, N.; Song, Y.; Campbell, K.; Cooks, R. G.; Morgan, J. A. Anal. Biochem. 2008 , 375 , 272.

(19) Talaty, N.; Takats, Z.; Cooks, R. G. Analyst . 2005 , 130 , 1624.

(20) Haefliger, O. P.; Jeckelmann, N. Rap. Commun . Mass Spectrom . 2007 , 21 , 1361.

(21) Shiea, J.; Huang, M. Z.; Hsu, H. J.; Lee, C. Y.; Yuan, C. H.; Beech, I.; Sunner, J. Rap. Commun. Mass Spectrom . 2005 , 19 , 3701.

(22) Sampson, J. S.; Hawkridge, A. M.; Muddiman, D. C. J. Am. Soc . Mass Spectr om. 2006 , 17 , 1712.

(23) Nemes, P.; Vertes, A. Anal. Chem . 2007 , 79 , 8098.

(24) Haapala, M.; Pol, J.; Saarela, V.; Arvola, V.; Kotiaho, T.; Ketola, R. A.; Franssila, S.; Kauppila, T. J.; Kostiainen, R. Anal. Chem . 2007 , 79 , 7867.

(25) McEwen, C. N.; McKay, R. G.; Larsen, B. S. Anal. Chem . 2005 , 77 , 7826.

(26) Takats, Z.; Cotte-Rodriguez, I.; Talaty, N.; Chen, H. W.; Cooks, R. G. Chem. Commun . 2005 , 1950.

(27) Venter, A.; Nefliu, M.; Cooks, R. G. TRAC-Trends in Anal. Chem. 2008 , 27 , 284.

(28) Van Berkel, G. J.; Pasilis, S. P.; Ovchinnikova, O. J. Mass Spectrom . 2008 , 43 , 1161.

(29) Harris, G. A.; Nyadong, L.; Fernandez, F. M. Analyst . 2008 , 133 , 1297.

(30) Nyadong, L.; Galhena, A. S.; Fernandez, F. M. Anal. Chem . 2009 , 81 , 7788.

(31) Kertesz, V.; Ford, M. J.; Van Berkel, G. J. Anal. Chem . 2005 , 77 , 7183.

(32) Cotte-Rodriguez, I.; Takats, Z.; Talaty, N.; Chen, H. W.; Cooks, R. G. Anal. Chem . 2005 , 77 , 6755.

(33) Haddad, R.; Sparrapan, R.; Eberlin, M. N. Rap. Commun. Mass Spectrom . 2006 , 20 , 2901.

(34) Na, N.; Zhao, M. X.; Zhang, S. C.; Yang, C. D.; Zhang, X. R. J. Am. Soc . Mass Spectr om. 2007 , 18 , 1859.

(35) Chen, H.; Yang, S.; Wortmann, A.; Zenobi, R. Ang. Chemie -Intl. Ed . 2007 , 46 , 7591.

(36) Andrade, F. J.; Shelley, J. T.; Wetzel, W. C.; Webb, M. R.; Gamez, G.; Ray, S. J.; Hieftje, G. M. Anal. Chem . 2008 , 80 , 2646.

(37) Harper, J. D.; Charipar, N. A.; Mulligan, C. C.; Zhang, X. R.; Cooks, R. G.; Ouyang, Z. Anal. Chem . 2008 , 80 , 9097.

(38) Smith, N. J.; Domin, M. A.; Scott, L. T. Org. Let t. 2008 , 10 , 3493.

(39) Van Berkel, G. J.; Kertesz, V.; Koeplinger, K. A.; Vavrek, M.; Kong, A. N. T. J. Mass Spectrom . 2008 , 43 , 500.

(40) Shelley, J. T.; Ray, S. J.; Hieftje, G. M. Anal. Chem . 2008 , 80 , 8308.

(41) Rezenom, Y. H.; Dong, J.; Murray, K. K. Analyst . 2008 , 133 , 226.

(42) Martinez-Lozano, P.; Rus, J.; de la Mora, G. F.; Hernandez, M.; de la Mora, J. F. J. Am. Soc. Mass Spectr om. 2009 , 20 , 287.

(43) Faubert, D.; Paul, G. J. C.; Giroux, J.; Bertrand, M. J. Int. J. Mass Spectrom . 1993 , 124 , 69.

(44) Hiraoka, K.; Fujimaki, S.; Kambara, S.; Furuya, H.; Okazaki, S. Rap. Commun . Mass Spectrom . 2004 , 18 , 2323.

(45) McLuckey, S. A.; Glish, G. L.; Asano, K. G.; van Berkel, G. J. Anal. Chem . 1988 , 60 , 2312.

(46) ISI Web of Science. database, (accessed November, 2009)

(47) "The DART MS Discussion Board." Google Groups . http://groups.google.com/group/dart-mass-spectrometer-users. (accessed September 2009)

(48) Cody, R. B. Anal. Chem . 2009 , 81 , 1101.

(49) Harris, G. A.; Fernandez, F. M. Anal. Chem. 2009 , 81 , 322.

(50) Nilles, J. M.; Connell, T. R.; Durst, H. D. Anal. Chem. 2009 , 81 , 6744.

(51) Grange, A. H. Environ. Forens. 2008 , 9 , 127.

(52) Grange, A. H. Environ. Forens. 2008 , 9 , 137.

(53) Grange, A. H. Environ. Foren s; 2009 , 10 , 183.

(54) Yu, S. X.; Crawford, E.; Tice, J.; Musselman, B.; Wu, J. T. Anal. Chem . 2009 , 81 , 193.

(55) Shelley, J. T.; Wiley, J. S.; Chan, G. C. Y.; Schilling, G. D.; Ray, S. J.; Hieftje, G. M. J. Am. Soc . Mass Spectr om. 2009 , 20 , 837.

(56) Fridman, A. A.; Kennedy, L. A. Plasma Ph ysics and Engineering ; Taylor & Frances: Abingdon, Oxford, UK, 2004.

(57) Penning, F. M. Naturwissenschaften 1927 , 15 , 818.

(58) Searcy, J. Q.; Fenn, J. B. J. Chem. Phys. 1976 , 64 , 1861.

(59) Harrison, R. G.; Aplin, K. L. Atmos . Res. 2007 , 85 , 199.

(60) Goebbert, D. J.; Wenthold, P. G. Eur. J. Mass Spectrom . 2004 , 10 , 837.

(61) Schurek, J.; Vaclavik, L.; Hooijerink, H.; Lacina, O.; Poustka, J.; Sharman, M.; Caldow, M.; Nielen, M. W. F.; Hajslova, J. Anal. Chem . 2008 , 80 , 9567.

(62) Cooks, R. G.; Ast, T.; Pradeep, T.; Wysocki, V. Acc. Chem . Res. 1994 , 27 , 316.

(63) Harrison, A. G. Chemical Ionization Mass Spectrom etry; 2nd Ed.; CRC Press: Boca Raton, FL, 1992.

(64) Rummel, J. L.; McKenna, A. M.; Tipton, J. D.; Marshall, A. G.; Eyler, J. R.; Powell, D. H. Proc . 56th ASMS Conf . Mass Spectrom . and Allied Topics . Denver, CO, 2008.

(65) Song, L. G.; Dykstra, A. B.; Yao, H. F.; Bartmess, J. E. J. Am. Soc . Mass Spectr om. 2009 , 20 , 42.

(66) NIST Chemistry Webbook. http://webbook.nist.gov/chemistry. (accessed January-November 2009)

(67) Bell, K. L.; Dalgarno, A.; Kingston, A. E. J. Phys. B Atom. Molec. Phys. 1968 , 1 , 18.

(68) Good, A.; Durden, D. A.; Kebarle, P. J. Chem. Phys. 1970 , 52 , 222.

(69) Visser, R. J.; Baggerman, J. A. G.; Poppelaars, J. P. J.; Collart, E. J. H. J App. Phys. 1992 , 71 , 5792.

(70) Kauppila, T. J.; Kotiaho, T.; Kostiainen, R.; Bruins, A. P. J. Am. Soc . Mass Spectr om. 2004 , 15 , 203.

(71) Issaq, H. J.; Van, Q. N.; Waybright, T. J.; Muschik, G. M.; Veenstra, T. D. J. Sep. Sci. 2009 , 32 , 2183.

(72) Zhao, Y. P.; Lam, M.; Wu, D. L.; Mak, R. Rap. Commun. Mass Spectrom . 2008 , 22 , 3217.

(73) Banerjee, S.; Madhusudanan, K. P.; Khanuja, S. P. S.; Chattopadhyay, S. K. Biomed. Chrom . 2008 , 22 , 250.

(74) Yew, J. Y.; Cody, R. B.; Kravitz, E. A. Proc. Nat. Acad. Sci. 2008 , 105 , 7135.

(75) Newton, P. N.; Fernandez, F. M.; Plancon, A.; Mildenhall, D. C.; Green, M. D.; Ziyong, L.; Christophel, E. M.; Phanouvong, S.; Howells, S.; McIntosh, E.; Laurin, P.; Blum, N.; Hampton, C. Y.; Faure, K.; Nyadong, L.; Soong, C. W. R.; Santoso, B.; Zhiguang, W.; Newton, J.; Palmer, K. Plos . Med. 2008 , 5 , 209.

(76) Nyadong, L.; Harris, G. A.; Balayssac, S.; Galhena, A. S.; Malet-Martino, M.; Martino, R.; Parry, R. M.; Wang, M. D. M.; Fernandez, F. M.; Gilard, V. Anal. Chem . 2009 , 81 , 4803.

(77) Jones, R. W.; Cody, R. B.; McClelland, J. F. J. Forens. Sci. 2006 , 51 , 915.

(78) Coates, C. M.; Coticone, S.; Barreto, P. D.; Cobb, A. E.; Cody, R. B.; Barreto, J. C. J. Foren s. Ident. 2008 , 58 , 8.

(79) Laramee, J. A.; Durst, H. D.; Connell, T. R.; Nilles, J. M. Am. Lab. 2008 , 40 , 16.

(80) Laramee, J. A.; Durst, H. D.; Nilles, J. M.; Connell, T. R. Am. Lab . 2009 , 41 , 24.

(81) Kpegba, K.; Spadaro, T.; Cody, R. B.; Nesnas, N.; Olson, J. A. Anal. Chem. 2007 , 79 , 5479.

(82) Vaclavik, L.; Cajka, T.; Hrbek, V.; Hajslova, J. Anal. Chim. Acta . 2009 , 645 , 56.

(83) Vail, T. M.; Jones, P. R.; Sparkman, O. D. J. Anal. Toxicol. 2007 , 31 , 304.

(84) Morlock, G.; Ueda, Y. J. Chrom . A. 2007 , 1143 , 243.

(85) Alpmann, A.; Morlock, G. J. Sep . Sci . 2008 , 31 , 71.

(86) Dytkiewitz, E.; Morlock, G. E. J. AOAC. Intl. 2008 , 91 , 1237.

(87) Na, N.; Zhao, M.X.; Zhang, S.C.; Yang, C.D.; Zhang, X.R.; J. Am. Soc. Mass Spectrom. 2007 , 18 , 1859.

(88) Ratcliffe, L. V.; Rutten, F. J. M.; Barrett, D. A.; Whitmore, T.; Seymour, D.; Greenwood, C.; Aranda-Gonzalvo, Y.; Robinson, S.; McCoustra, M. Anal. Chem . 2007 , 79 , 6094.

(89) Andrade, F. J.; Wetzel, W. C.; Chan, G. C. Y.; Webb, M. R.; Gamez, G.; Ray, S. J.; Hieftje, G. M. J. Anal. Atom. Spectrom . 2006 , 21 , 1175.

(90) Marshall, A. G.; Hendrickson, C. L. Ann. Rev . Anal. Chem. 2008 , 1 , 579.

(91) Russell, D. H.; Edmondson, R. D. J. Mass Spectrom . 1997 , 32 , 263.

(92) Perry, R. H.; Hu, Q. Z.; Salazar, G. A.; Cooks, R. G.; Noll, R. J. J. Am. Soc . Mass Spectr om. 2009 , 20 , 1397.

(93) Tipton, J. D.; Carter, J. D.; Mathias, J. D.; Emmett, M. R.; Fanucci, G. E.; Marshall, A. G. Anal. Chem . 2009 , 81 , 7611.

(94) Stoll, N.; Schmidt, E.; Thurow, K. J. Am. Soc . Mass Spectr om. 2006 , 17 , 1692.

(95) Mamyrin, B. A. Int. J . Mass Spectrom . 2001 , 206 , 251.

(96) Guilhaus, M.; Mlynski, V.; Selby, D. Rap. Commun. Mass Spectrom . 1997 , 11 , 951.

(97) Mamyrin, B. A.; Karataev, V. I.; Shmikk, D. V.; Zagulin, V. A. Zhurnal Eksperimentalnoi I Teoreticheskoi Fiziki . 1973 , 64 , 82.

(98) Guilhaus, M.; Selby, D.; Mlynski, V. Mass . Spectrom . Rev . 2000 , 19 , 65.

(99) "TOF Course Module 1: Instrumental and Software Overview," Agilent Technologies Wilmington, DE, 2006. p 3.

(100) Marshall, A. G.; Hendrickson, C. L.; Jackson, G. S. Mas s Spectrom . Rev . 1998 , 17 , 1.

(101) Marshall, A. G.; Hendrickson, C. L.; Ernmett, M. R.; Rodgers, R. P.; Blakney, G. T.; Nilsson, C. L. Eur . J. Mass Spectrom . 2007 , 13 , 57.

(102) Marshall, A. G.; Hendrickson, C. L. Int. J . Mass Spectrom . 2002 , 215 , 16.

(103) Schaub, T. M.; Hendrickson, C. L.; Horning, S.; Quinn, J. P.; Senko, M. W.; Marshall, A. G. Anal. Chem . 2008 , 80 , 3985.

(104) Wu, S.; Zhang, K.; Kaiser, N. K.; Bruce, J. E. J. Am. Soc . Mass Spectr om. 2006 , 17 , 772.

(105) Long, G. L.; Winefordner, J. D. Anal. Chem . 1983 , 55 , 3.

(106) Kusai, A.; Kiyotaka, K.; Kobayashi, M.; Vargas, D. Proc. 55 th ASMS Conf. Mass Spectrom. and Allied Topics. Indianapolis, IN, 2007.

(107) Benton, M.; Rowell, F.; Sundar, L.; Jan, M. Surf. Interfac. Anal. 2009 , n/a.

(108) Oyler, J.; Darwin, W. D.; Cone, E. J. J. Anal. Toxicol. 1996 , 20 , 213.

(109) Sleeman, R.; Burton, R.; Carter, J.; Roberts, D.; Hulmston, P. Anal. Chem . 2000 , 72 , 397A.

(110) Jenkins, A. J. Forens. Sci . Int. 2001 , 121 , 189.

(111) Carter, J. F.; Sleeman, R.; Parry, J. Forens. Sci. Int. 2003 , 132 , 106.

(112) Frederick, K. A.; Pertaub, R.; Kam, N. W. S. Spec. Lett. 2004 , 37 , 301.

(113) Zuo, Y. G.; Zhang, K.; Wu, J. P.; Rego, C.; Fritz, J. J. Sep. Sci. 2008 , 31 , 2444.

(114) IonSense, Inc. www.ionsense.com (accessed November, 2009)

(115) Schlosser, G.; Pocsfalvi, G.; Huszar, E.; Malorni, A.; Hudecz, F. J. Mass Spectrom . 2005 , 40 , 1590.

(116) Huang, Y. F.; Chang, H. T. Anal. Chem . 2006 , 78 , 1485.

(117) Mallet, C. R.; Lu, Z. L.; Mazzeo, J. R. Rap. Commun. Mass Spectrom . 2004 , 18 , 49.

(118) King, R.; Bonfiglio, R.; Fernandez-Metzler, C.; Miller-Stein, C.; Olah, T. J. Am. Soc . Mass Spectr om. 2000 , 11 , 942.

(119) Tang, L.; Kebarle, P. Anal. Chem . 1991 , 63 , 2709.

(120) Wang, F.; Ma, S. G.; Zhang, D. X.; Cooks, R. G. J. Phys . Chem . A. 1998 , 102 , 2988.

(121) Rudewicz, P.; Munson, B. Anal. Chem . 1986 , 58 , 2903.

(122) Danzer, K. Analytical Chemistry: Theoretical and Metrological Fundamentals ; Springer: New York, NY, 2006.

(123) Kawai, Y.; Yamaguchi, S.; Okada, Y.; Takeuchi, K.; Yamauchi, Y.; Ozawa, S.; Nakai, H. Chem . Phys . Lett. 2003 , 377 , 69.

(124) Schmidt, M. W.; Baldridge, K. K.; Boatz, J. A.; Elbert, S. T.; Gordon, M. S.; Jensen, J. H.; Koseki, S.; Matsunaga, N.; Nguyen, K. A.; Su, S. J.; Windus, T. L.; Dupuis, M.; Montgomery, J. A. J. Comp . Chem . 1993 , 14 , 1347.

(125) Gordon, M. S.; Schmidt, A. Theory and Applications of Computational Chemistry: the first forty years ; Elsevier: Amsterdam, 2005.

(126) Stanton, J. F.; Gauss, J.; Watts, J. D.; Nooijen, M.; Oliphant, N.; Perera, S. A.; Szalay, P. G.; Lauderdale, W. J.; Kucharski, S. A.; Gwaltney, S. R.; Beck, S.; A., B.; Bernholdt, D. E.; Baeck, K. K.; Rozyczko, P.; Sekino, H.; Hober, C.; Bartlett, R. J. ACES II.: Gainesville, FL.

(127) Rummel, J. L.; Eyler, J. R.; Powell, D. H. Proc. 55 th ASMS Conf. Mass Spectrom. and Allied Topics. Indianapolis, IN, 2007.

(128) Senko, M. W.; Canterbury, J. D.; Guan, S. H.; Marshall, A. G. Rap. Commun. Mass Spectrom . 1996 , 10 , 1839.

(129) Senko, M. W.; Hendrickson, C. L.; PasaTolic, L.; Marto, J. A.; White, F. M.; Guan, S. H.; Marshall, A. G. Rap. Commun . Mass Spectrom . 1996 , 10 , 1824.

(130) Sinclair, W. B. The Grapefruit: Its Composition, Physiology, and Products ; ANR Publications: Oakland, CA, 1972.

(131) Guo, L. Q.; Yamazoe, Y. Acta Pharmacol. Sinica . 2004 , 25 , 129.

(132) Marshall, A. G.; Rodgers, R. P. Acc. Chem . Res . 2004 , 37 , 53.

(133) Fernandez, F. M.; Cody, R. B.; Green, M. D.; Hampton, C. Y.; McGready, R.; Sengaloundeth, S.; White, N. J.; Newton, P. N. Chem. M ed . C hem . 2006 , 1, 702.

(134) Kawamura, M.; Kikura-Hanajiri, R.; Goda, Y. Yakugaku Zasshi -J Pharm . Soc . Japan . 2009 , 129 , 719.

(135) Maleknia, S. D.; Vail, T. M.; Cody, R. B.; Sparkman, D. O.; Bell, T. L.; Adams, M. A. Rap . Commun . Mass Spectrom . 2009 , 23 , 2241.

(136) Wenthold, P. G.; Wierschke, S. G.; Nash, J. J.; Squires, R. R. J. Am. Chem . Soc . 1994 , 116 , 7378.

(137) Zhang, H. Y.; Grubb, M.; Wu, W.; Josephs, J.; Humphreys, W. G. Anal. Chem . 2009 , 81 , 2695.

(138) Peterman, S. M.; Mulholland, J. J. J. Am. Soc . Mass Spectr om. 2006 , 17 , 168.

(139) Gergov, M.; Nokua, P.; Vuori, E.; Qjanpera, I. Forens. Sci. Int. 2009 , 186 , 36.

(140) Eyler, J. R. Mass Spectrom . Rev . 2009 , 28 , 448.

(141) Polfer, N. C.; Oomens, J. Mass Spectrom . Rev . 2009 , 28 , 468.

(142) Oomens, J.; Sartakov, B. G.; Meijer, G.; von Helden, G. Int. J . Mass Spectrom . 2006 , 254 , 1.

(143) Laskin, J.; Futrell, J. J. Phys . Chem . A. 2000 , 104 , 5484.

(144) Laskin, J.; Byrd, M.; Futrell, J. Int. J . Mass Spectrom . 2000 , 196 , 285.

(145) Heeren, R. M. A.; Kleinnijenhuis, A. J.; McDonnell, L. A.; Mize, T. H. Anal. Bioanal . Chem . 2004 , 378 , 1048.

(146) Lehmann, K. K.; Scoles, G.; Pate, B. H. Ann. Rev. Phys. Chem. 1994 , 45 , 241.

(147) Oepts, D.; van Dermeer, A. F. G.; van Amersfoort, P. W. Infr. Phys . Tech. 1995 , 36 , 297.

(148) Duarte, F. J. Tunable Laser Applications ; 2nd Ed.; CRC Press: New York, NY, 2009. pp. 29-30.

(149) Bartelt-Hunt, S. L.; Knappe, D. R. U.; Barlaz, M. A. CRC Crit. Rev. Environ. Sci Tech. 2008 , 38 , 112.

(150) Singer, B. C.; Hodgson, A. T.; Destaillats, H.; Hotchi, T.; Revzan, K. L.; Sextro, R. G. Environ. Sci. Tech. 2005 , 39 , 3203.

(151) Mangun, C. L.; Yue, Z. R.; Economy, J.; Maloney, S.; Kemme, P.; Cropek, D. Chem. Mat . 2001 , 13 , 2356.

(152) Yue, Z. G.; Mangun, C.; Economy, J.; Kemme, P.; Cropek, D.; Maloney, S. Environ. Sci. Tech. 2001, 35, 2844.

(153) Valle, J. J.; Eyler, J. R.; Oomens, J.; Moore, D. T.; van der Meer, A. F. G.; von Helden, G.; Meijer, G.; Hendrickson, C. L.; Marshall, A. G.; Blakney, G. T. Rev. Sci. Inst. 2005, 76. 023103.

(154) Hyperchem(TM) Profession al, 7.51 Ed., Hypercube, Inc.: Gainesville, FL.

(155) Frisch, M. J.; Trucks, G. W.; Schlegel, H. B.; Scuseria, G. E.; Robb, M. A.; Cheeseman, J. R.; Montgomery, J. A.; Vreven, T.; Kudin, K. N.; Burant, J. C.; Millam, J. M.; Iyengar, S. S.; Tomasi, J.; Barone, V.; Mennucci, B.; Cossi, M.; Scalmani, G.; Rega, N.; Petersson, G. A.; Nakatsuji, H.; Hada, M.; Ehara, M.; Toyota, K.; Fukuda, R.; Hasegawa, J.; Ishida, M.; Nakajima, T.; Honda, Y.; Kitao, O.; Nakai, H.; Klene, M.; Li, X.; Knox, J. E.; Hratchian, H. P.; Cross, J. B.; Bakken, V.; Adamo, C.; Jaramillo, J.; Gomperts, R.; Stratmann, R. E.; Yazyev, O.; Austin, A. J.; Cammi, R.; Pomelli, C.; Ochterski, J. W.; Ayala, P. Y.; Morokuma, K.; Voth, G. A.; Salvador, P.; Dannenberg, J. J.; Zakrzewski, V. G.; Dapprich, S.; Daniels, A. D.; Strain, M. C.; Farkas, O.; Malick, D. K.; Rabuck, A. D.; Raghavachari, K.; Foresman, J. B.; Ortiz, J. V.; Cui, Q.; Baboul, A. G.; Clifford, S.; Cioslowski, J.; Stefanov, B. B.; Liu, G.; Liashenko, A.; Piskorz, P.; Komaromi, I.; Martin, R. L.; Fox, D. J.; Keith, T.; Al-Laham, M. A.; Peng, C. Y.; Nanayakkara, A.; Challacombe, M.; Gill, P. M. W.; Johnson, B.; Chen, W.; Wong, M. W.; Gonzalez, C.; Pople, J. A.; D.02 ed. ed.; Gaussian 03, Gaussian, Inc.: Wallingford, CT, 2004.

(156) Snyder, A. P.; Harden, C. S. Org. Mass Spectrom. 1990, 25, 53.

(157) Johnson, J. V.; Yost, R. A.; Kelley, P. E.; Bradford, D. C. Anal. Chem. 1990, 62, 2162.

(158) Snyder, A. P.; Harden, C. S. Org. Mass Spectrom. 1990, 25, 301.

(159) McLafferty, F. W. Anal. Chem. 1959, 31, 82.

(160) Scott, A. P.; Radom, L. J. Phys. Chem. 1996, 100, 16502.

(161) Wong, M. W. Chem. Phys. Lett. 1996, 256, 391.

(162) Correia, C. F.; Balaj, P. O.; Scuderi, D.; Maitre, P.; Ohanessian, G. J. Am. Chem. Soc. 2008, 130, 3359.

(163) Brunol, E.; Berger, F.; Fromm, A.; Planade, R. Sensors and Actuators B - Chemical, 2006, 120, 35.

(164) Moore, S. Chemosphere. 2002, 49, 121.

(165) Petucci, C.; Diffendal, J.; Kaufman, D.; Mekonnen, B.; Terefenko, G.; Musselman, B. Anal. Chem . 2007 , 79 , 5064.

(166) Leger, A.; Puget, J. L. Astron. Astrophys. 1984 , 137 , L5.

(167) Allamandola, L. J.; Tielens, A. G. G. M.; Barker, J. R. Astrophy s. J. 1985 , 290 , L25.

(168) Knorke, H.; Langer, J.; Oomens, J.; Dopfer, O. Astron . Astrophys . 2009 , 706 . L66.

(169) Vala, M.; Szczepanski, J.; Oomens, J.; Steill, J. D. J. Am. Chem. Soc. 2009 , 131 , 5784.

(170) Hirama, M.; Tokosumi, T.; Ishida, T.; Aihara, J. Chem. Phys. 2004 , 305 , 307.

(171) Jolibois, F.; Klotz, A.; Gadea, F. X.; Joblin, C. Astron. Astrophys. 2005 , 444 , 629.

(172) Kanu, A. B.; Hill, H. H. Talanta . 2007 , 73 , 692.

(173) Matz, L. M.; Tornatore, P. S.; Hill, H. H. Talanta . 2001 , 54 , 171.

# BIOGRAPHICAL SKETCH

Julia Diane Laney Rummel was born on October 2, 1981 and grew up in Livermore, Kentucky. In 2000, she matriculated at Eastern Kentucky University (EKU) to study forensic chemistry. While at EKU, Julia was encouraged to participate in a Research Experience for Undergraduates (REU) program and to consider graduate school. After doing an REU at the University of Florida (UF) and later doing an internship at the North Carolina State Bureau of Investigation Crime Laboratory in drug chemistry, Julia was convinced she should attend graduate school. In the fall of 2004, after receiving her Bachelor's of Science in forensic chemistry, Julia started graduate work at UF. She worked under Dr. David Powell and Dr. John Eyler doing research on the ambient ionization technique, Direct Analysis in Real Time. In 2006, she married Ian Rummel. In December of 2009, Julia will graduate with a doctorate in analytical chemistry.